

Formulation and Calculation of Isoparametric Finite Element Matrices

5.1 INTRODUCTION

A very important phase of a finite element solution is the calculation of the finite element matrices. In Chapter 4 we discussed the formulation and calculation of generalized coordinate finite element models. The aim in the presentation of the generalized coordinate finite elements was primarily to enhance our understanding of the finite element method. We have already pointed out that in most practical analyses the use of isoparametric finite elements is more effective. For the original developments of these elements, see I. C. Taig [A] and B. M. Irons [A, B].

Our objective in this chapter is to present the formulation of isoparametric finite elements and describe effective implementations. In the derivation of generalized coordinate finite element models, we used local element coordinate systems x, y, z and assumed the element displacements $u(x, y, z)$, $v(x, y, z)$, and $w(x, y, z)$ (and in the case of mixed methods also the element stress and strain variables) in the form of polynomials in x, y , and z with undetermined constant coefficients α_i, β_i , and $\gamma_i, i = 1, 2, \dots$, identified as generalized coordinates. It was not possible to associate a priori a physical meaning with the generalized coordinates; however, on evaluation we found that the generalized coordinates determining the displacements are linear combinations of the element nodal point displacements. The principal idea of the isoparametric finite element formulation is to achieve the relationship between the element displacements at any point and the element nodal point displacements directly through the use of *interpolation functions* (also called *shape functions*). This means that the transformation matrix A^{-1} [see (4.57)] is not evaluated; instead, the element matrices corresponding to the required degrees of freedom are obtained directly.

5.2 ISOPARAMETRIC DERIVATION OF BAR ELEMENT STIFFNESS MATRIX

Consider the example of a bar element to illustrate the procedure of an isoparametric stiffness formulation. In order to simplify the explanation, assume that the bar lies in the global X -coordinate axis, as shown in Fig. 5.1. The first step is to relate the actual global coordinates X to a *natural coordinate system* with variable r , $-1 \leq r \leq 1$ (Fig. 5.1). This transformation is given by

$$X = \frac{1}{2}(1 - r)X_1 + \frac{1}{2}(1 + r)X_2 \quad (5.1)$$

or

$$X = \sum_{i=1}^2 h_i X_i \quad (5.2)$$

where $h_1 = \frac{1}{2}(1 - r)$ and $h_2 = \frac{1}{2}(1 + r)$ are the interpolation or shape functions. Note that (5.2) establishes a unique relationship between the coordinates X and r on the bar.

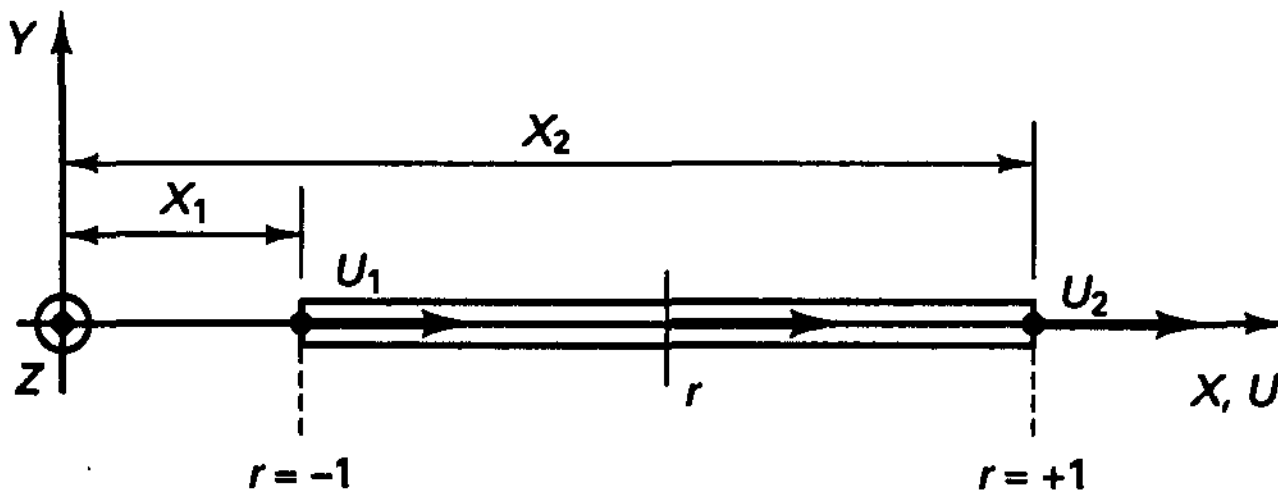


Figure 5.1 Element in global and natural coordinate system

The bar global displacements are expressed in the same way as the global coordinates:

$$U = \sum_{i=1}^2 h_i U_i \quad (5.3)$$

where in this case a linear displacement variation is specified. *The interpolation of the element coordinates and element displacements using the same interpolation functions, which are defined in a natural coordinate system, is the basis of the isoparametric finite element formulation.*

For the calculation of the element stiffness matrix we need to find the element strains $\epsilon = dU/dX$. Here we use

$$\epsilon = \frac{dU}{dr} \frac{dr}{dX} \quad (5.4)$$

where, from (5.3),

$$\frac{dU}{dr} = \frac{U_2 - U_1}{2} \quad (5.5)$$

and using (5.2), we obtain

$$\frac{dX}{dr} = \frac{X_2 - X_1}{2} = \frac{L}{2} \quad (5.6)$$

where L is the length of the bar. Hence, as expected, we have

$$\epsilon = \frac{U_2 - U_1}{L} \quad (5.7)$$

The strain-displacement transformation matrix corresponding to (4.32) is therefore

$$\mathbf{B} = \frac{1}{L} \begin{bmatrix} -1 & 1 \end{bmatrix} \tag{5.8}$$

In general, the strain-displacement transformation matrix is a function of the natural coordinates, and we therefore evaluate the stiffness matrix volume integral in (4.33) by integrating over the natural coordinates. Following this general procedure, although in this example it is not necessary, we have

$$\mathbf{K} = \frac{AE}{L^2} \int_{-1}^1 \begin{bmatrix} -1 \\ 1 \end{bmatrix} \begin{bmatrix} -1 & 1 \end{bmatrix} J dr \tag{5.9}$$

where the bar area A and modulus of elasticity E have been assumed constant and J is the Jacobian relating an element length in the global coordinate system to an element length in the natural coordinate system; i.e.,

$$dX = J dr \tag{5.10}$$

From (5.6) we have
$$J = \frac{L}{2} \tag{5.11}$$

Then, evaluating (5.9), we obtain the well-known matrix

$$\mathbf{K} = \frac{AE}{L} \begin{bmatrix} 1 & -1 \\ -1 & 1 \end{bmatrix} \tag{5.12}$$

As stated in the introduction, the isoparametric formulation avoids the construction of the transformation matrix \mathbf{A}^{-1} . In order to compare this formulation with the generalized coordinate formulation, we need to solve from (5.1) for r and then substitute for r into (5.3). We obtain

$$r = \frac{X - [(X_1 + X_2)/2]}{L/2} \tag{5.13}$$

and then
$$U = \alpha_0 + \alpha_1 X \tag{5.14}$$

where

$$\left. \begin{aligned} \alpha_0 &= \frac{1}{2}(U_1 + U_2) - \frac{X_1 + X_2}{2L}(U_2 - U_1) \\ \alpha_1 &= \frac{1}{L}(U_2 - U_1) \end{aligned} \right\} \tag{5.15}$$

or
$$\boldsymbol{\alpha} = \begin{bmatrix} \frac{1}{2} + \frac{X_1 + X_2}{2L} & \frac{1}{2} - \frac{X_1 + X_2}{2L} \\ -\frac{1}{L} & \frac{1}{L} \end{bmatrix} \mathbf{U} \tag{5.16}$$

where
$$\boldsymbol{\alpha}^T = [\alpha_0 \quad \alpha_1]; \quad \mathbf{U}^T = [U_1 \quad U_2] \tag{5.17}$$

and the matrix relating $\boldsymbol{\alpha}$ to \mathbf{U} in (5.16) is \mathbf{A}^{-1} . It should be noted that in this example the generalized coordinates α_0 and α_1 relate the global element displacement to the global element coordinate [see (5.14)].

5.3 FORMULATION OF CONTINUUM ELEMENTS

For a continuum finite element, it is in most cases effective to calculate directly the element matrices corresponding to the global degrees of freedom. However, we shall first present the formulation of the matrices that correspond to the element local degrees of freedom because additional considerations may be necessary when the element matrices that correspond to the global degrees of freedom are calculated directly (see Section 5.3.4). In the following we consider the derivation of the element matrices of straight truss elements; two-dimensional plane stress, plane strain, and axisymmetric elements; and three-dimensional elements that all have a variable number of nodes. Typical elements are shown in Fig. 5.2.

We direct our discussion to the calculation of displacement-based finite element matrices. However, the same procedures are also used in the calculation of the element matrices of mixed formulations, and in particular of the displacement/pressure-based formulations for incompressible analysis, as briefly discussed in Section 5.3.5.

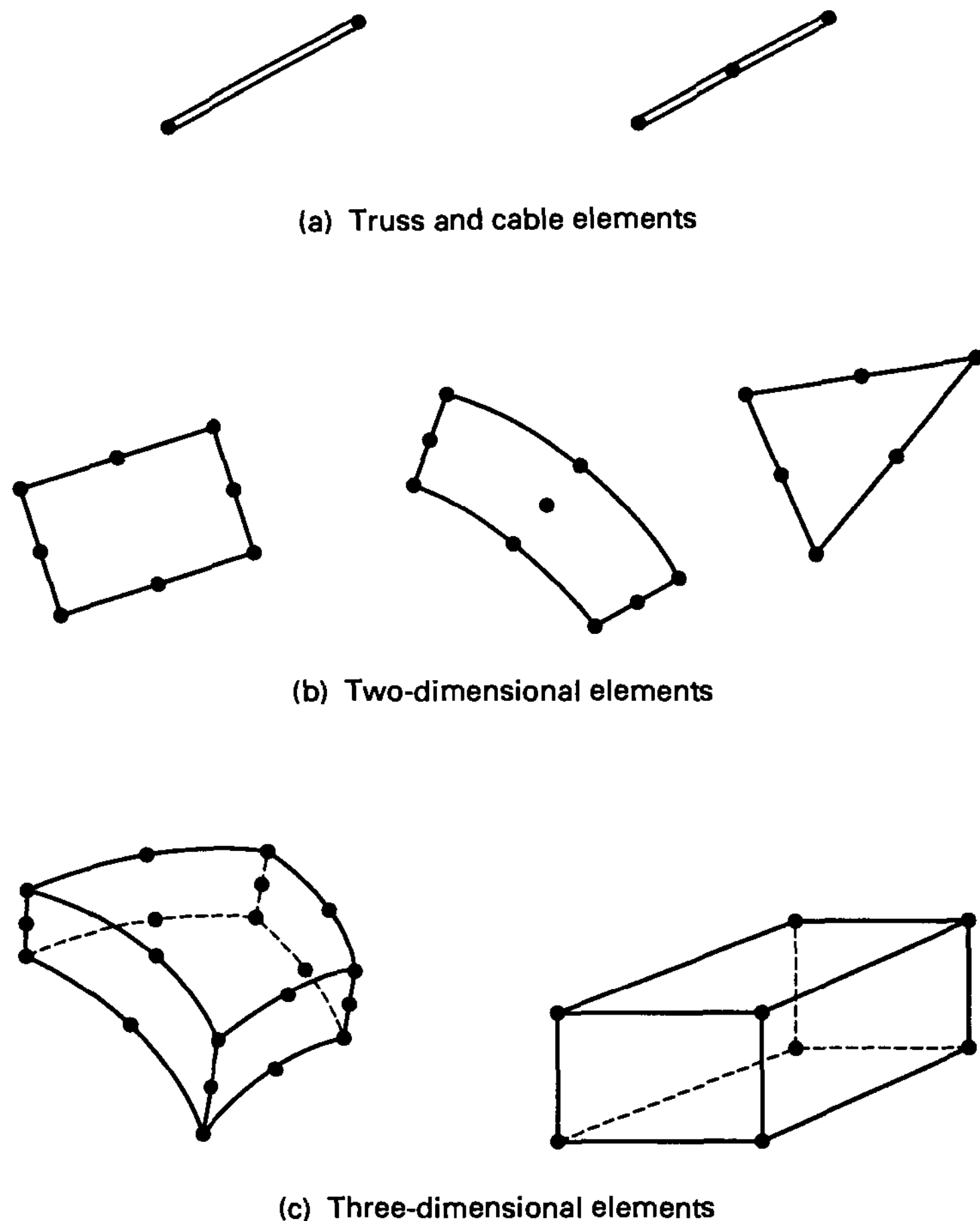


Figure 5.2 Some typical continuum elements

5.3.1 Quadrilateral Elements

The basic procedure in the isoparametric finite element formulation is to express the element coordinates and element displacements in the form of interpolations using the natural coordinate system of the element. This coordinate system is one-, two-, or three-dimensional, depending on the dimensionality of the element. The formulation of the element matrices is the same whether we deal with a one, two-, or three-dimensional element. For this reason we use in the following general presentation the equations of a three-dimensional element. However, the one- and two-dimensional elements are included by simply using only the relevant coordinate axes and the appropriate interpolation functions.

Considering a general three-dimensional element, the coordinate interpolations are

$$x = \sum_{i=1}^q h_i x_i; \quad y = \sum_{i=1}^q h_i y_i; \quad z = \sum_{i=1}^q h_i z_i \quad (5.18)$$

where $x, y,$ and z are the coordinates at any point of the element (here local coordinates) and $x_i, y_i, z_i, i = 1, \dots, q,$ are the coordinates of the q element nodes. The interpolation functions h_i are defined in the natural coordinate system of the element, which has variables $r, s,$ and t that each vary from -1 to $+1$. For one- or two-dimensional elements, only the relevant equations in (5.18) would be employed, and the interpolation functions would depend only on the natural coordinate variables r and $r, s,$ respectively.

The unknown quantities in (5.18) are so far the interpolation functions h_i . The fundamental property of the interpolation function h_i is that its value in the natural coordinate system is unity at node i and zero at all other nodes. Using these conditions, the functions h_i corresponding to a specific nodal point layout could be solved for in a systematic manner. However, it is convenient to construct them by inspection, which is demonstrated in the following simple example.

EXAMPLE 5.1: Construct the interpolation functions corresponding to the three-node truss element in Fig. E5.1.

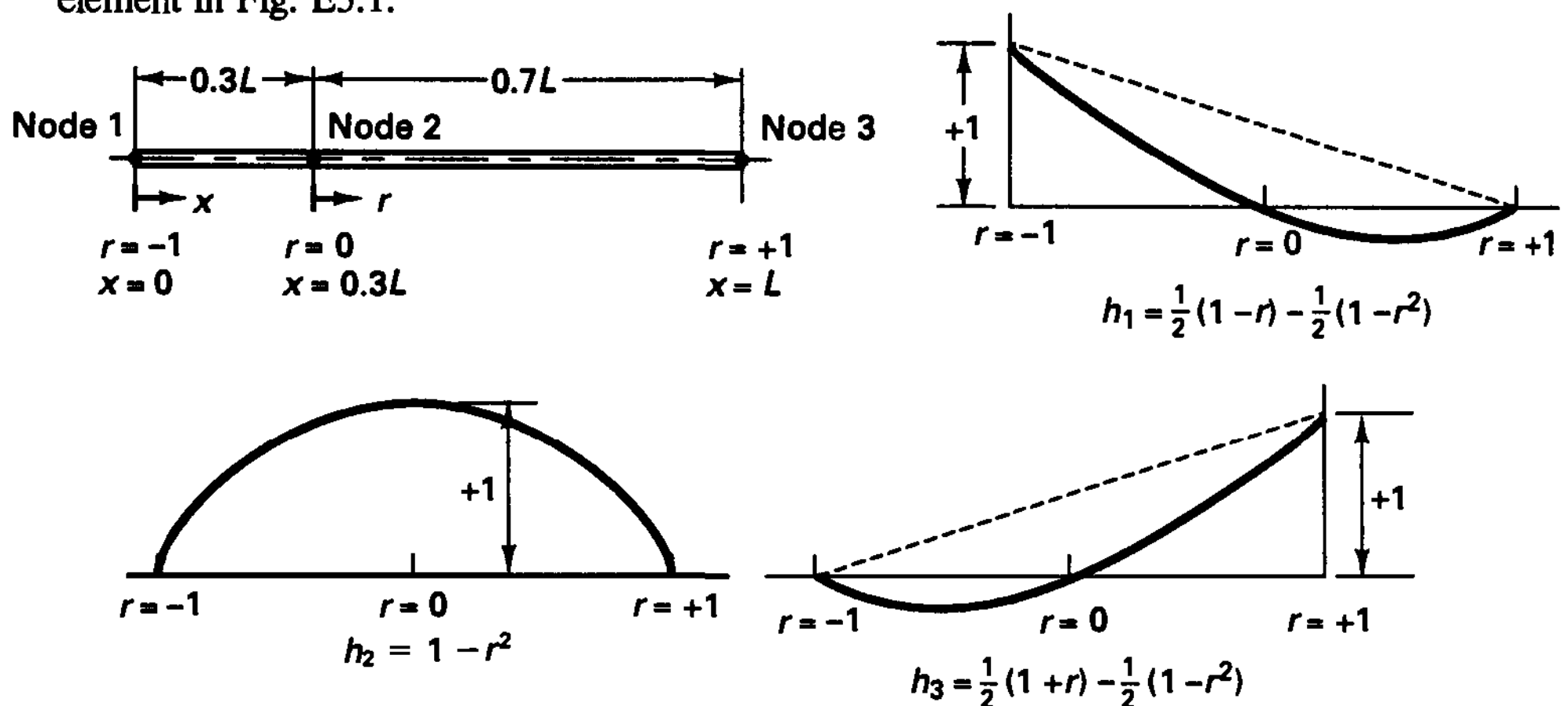
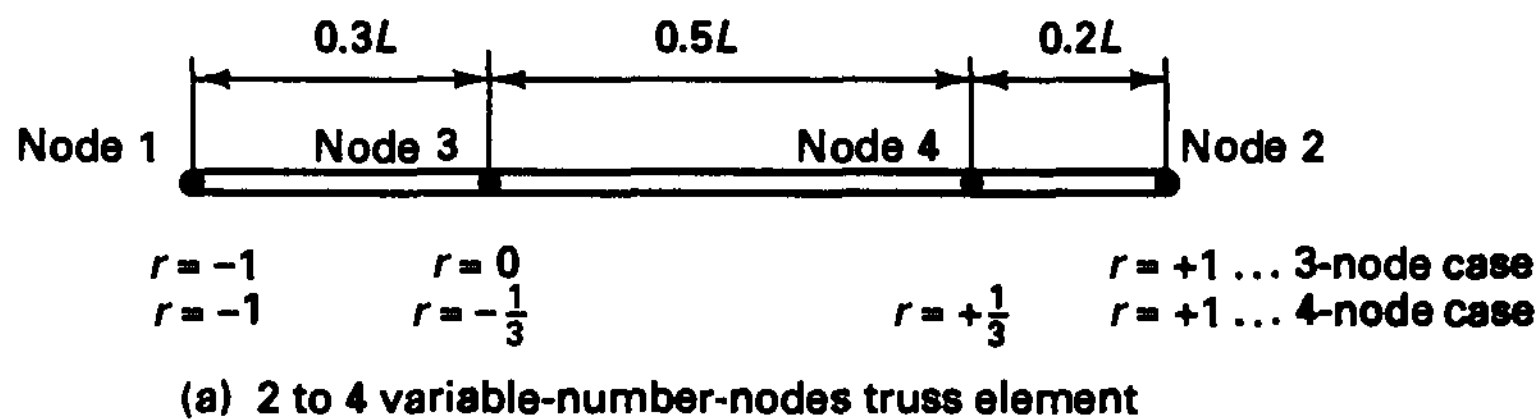


Figure E5.1 One-dimensional interpolation functions of a truss element

A first observation is that for the three-node truss element we want interpolation polynomials that involve r^2 as the highest power of r ; in other words, the interpolation functions shall be parabolas. The function h_2 can thus be constructed without much effort. Namely, the parabola that satisfies the conditions to be equal to zero at $r = \pm 1$ and equal to 1 at $r = 0$ is given by $(1 - r^2)$. The other two interpolation functions h_1 and h_3 are constructed by superimposing a linear function and a parabola. Consider the interpolation function h_3 . Using $\frac{1}{2}(1 + r)$, the conditions that the function shall be zero at $r = -1$ and 1 at $r = +1$ are satisfied. To ensure that h_3 is also zero at $r = 0$, we need to use $h_3 = \frac{1}{2}(1 + r) - \frac{1}{2}(1 - r^2)$. The interpolation function h_1 is obtained in a similar manner.

The procedure used in Example 5.1 of constructing the final required interpolation functions suggests an attractive formulation of an element with a variable number of nodes. This formulation is achieved by constructing first the interpolations corresponding to a basic two-node element. The addition of another node then results in an additional interpolation function and a correction to be applied to the already existing interpolation functions. Figure 5.3 gives the interpolation functions of the one-dimensional element considered in Example 5.1, with an additional fourth node possible. As shown, the element can have from two to four nodes. We should note that nodes 3 and 4 are now interior nodes because nodes 1 and 2 are used to define the two-node element.

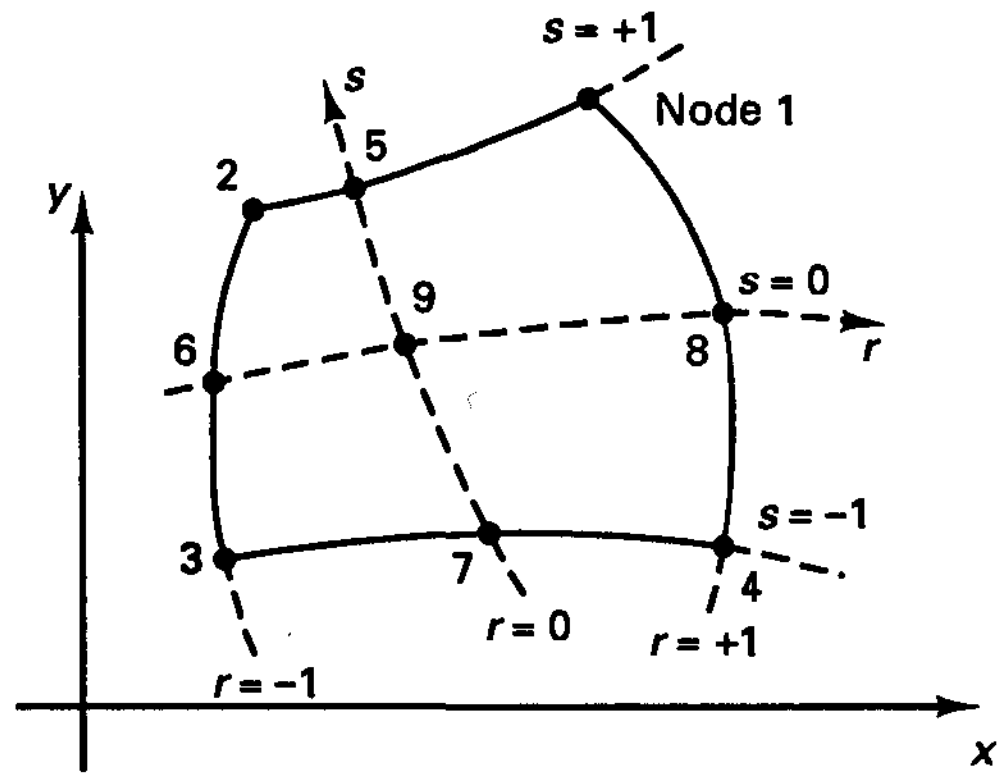


	Include only if node 3 is present	Include only if nodes 3 and 4 are present
$h_1 = \frac{1}{2}(1 - r)$	$-\frac{1}{2}(1 - r^2)$	$+\frac{1}{16}(-9r^3 + r^2 + 9r - 1)$
$h_2 = \frac{1}{2}(1 + r)$	$-\frac{1}{2}(1 - r^2)$	$+\frac{1}{16}(9r^3 + r^2 - 9r - 1)$
$h_3 = (1 - r^2)$		$+\frac{1}{16}(27r^3 + 7r^2 - 27r - 7)$
$h_4 = \frac{1}{16}(-27r^3 - 9r^2 + 27r + 9)$		

(b) Interpolation functions

Figure 5.3 Interpolation functions of two to four variable-number-nodes one-dimensional element

This procedure of constructing the element interpolation functions for one-dimensional analysis can be directly generalized for use in two and three dimensions. Figure 5.4 shows the interpolation functions of a four to nine variable-number-nodes two-dimensional element, and Fig. 5.5 gives the interpolation functions for three-dimensional 8- to 20-node elements. The two- and three-dimensional interpolations have been established in a manner analogous to the one-dimensional interpolations, where the basic functions used are, in fact, those already employed in Fig. 5.3. We consider in Figs. 5.4 and 5.5 at most parabolic interpolation, but variable-number-nodes elements with interpolations of higher order could be derived in an analogous way.



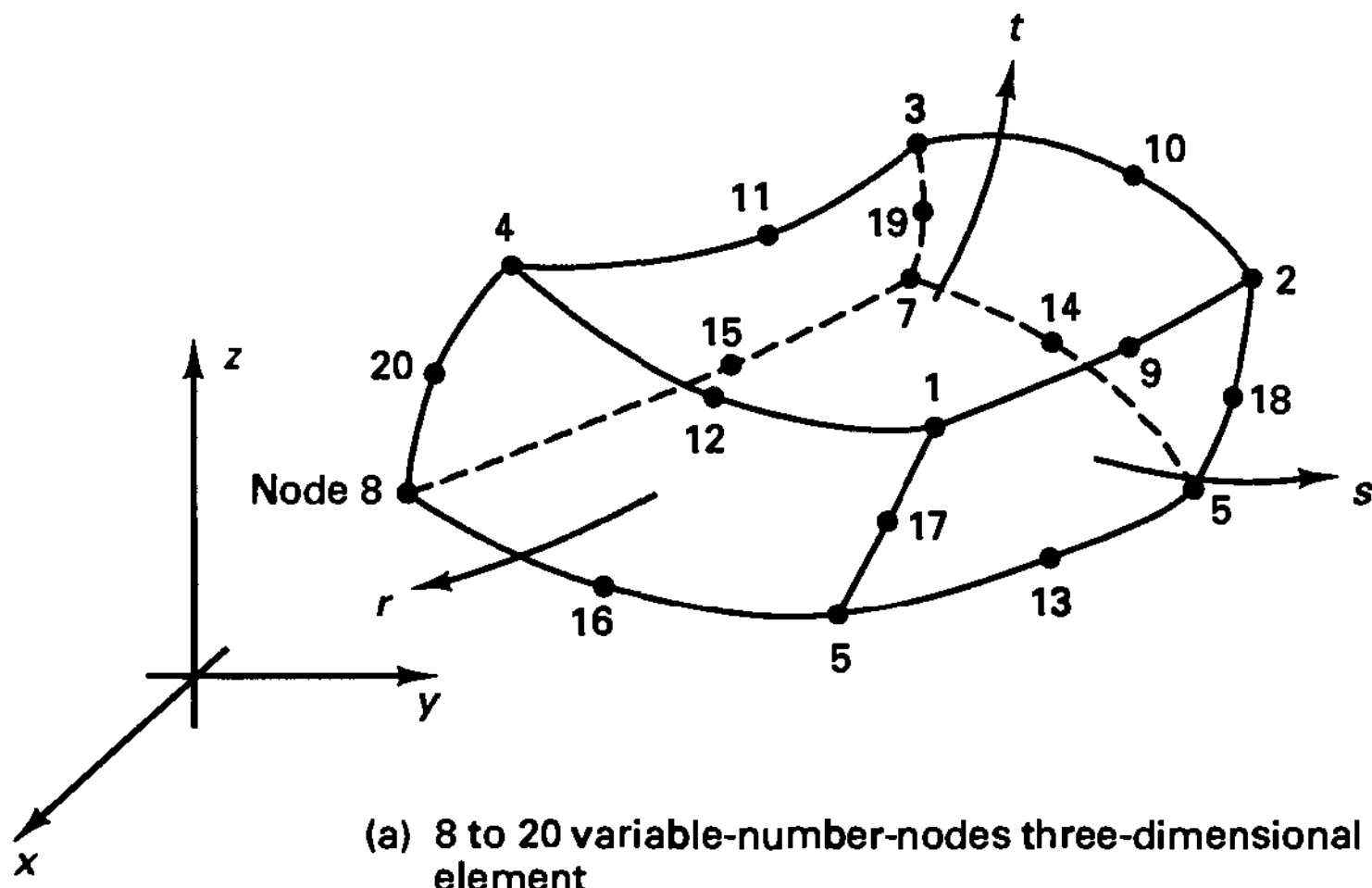
(a) 4 to 9 variable-number-nodes two-dimensional element

Include only if node i is defined

	$i = 5$	$i = 6$	$i = 7$	$i = 8$	$i = 9$
$h_1 = \frac{1}{4}(1+r)(1+s)$	$-\frac{1}{2}h_5$			$-\frac{1}{2}h_8$	$-\frac{1}{4}h_9$
$h_2 = \frac{1}{4}(1-r)(1+s)$	$-\frac{1}{2}h_5$	$-\frac{1}{2}h_6$			$-\frac{1}{4}h_9$
$h_3 = \frac{1}{4}(1-r)(1-s)$		$-\frac{1}{2}h_6$	$-\frac{1}{2}h_7$		$-\frac{1}{4}h_9$
$h_4 = \frac{1}{4}(1+r)(1-s)$			$-\frac{1}{2}h_7$	$-\frac{1}{2}h_8$	$-\frac{1}{4}h_9$
$h_5 = \frac{1}{2}(1-r^2)(1+s)$					$-\frac{1}{2}h_9$
$h_6 = \frac{1}{2}(1-s^2)(1-r)$					$-\frac{1}{2}h_9$
$h_7 = \frac{1}{2}(1-r^2)(1-s)$					$-\frac{1}{2}h_9$
$h_8 = \frac{1}{2}(1-s^2)(1+r)$					$-\frac{1}{2}h_9$
$h_9 = (1-r^2)(1-s^2)$					

(b) Interpolation functions

Figure 5.4 Interpolation functions of four to nine variable-number-nodes two-dimensional element



(a) 8 to 20 variable-number-nodes three-dimensional element

Figure 5.5 Interpolation functions of eight to twenty variable-number-nodes three-dimensional element

$$\begin{aligned}
 h_1 &= g_1 - (g_9 + g_{12} + g_{17})/2 & h_6 &= g_6 - (g_{13} + g_{14} + g_{18})/2 \\
 h_2 &= g_2 - (g_9 + g_{10} + g_{18})/2 & h_7 &= g_7 - (g_{14} + g_{15} + g_{19})/2 \\
 h_3 &= g_3 - (g_{10} + g_{11} + g_{19})/2 & h_8 &= g_8 - (g_{15} + g_{16} + g_{20})/2 \\
 h_4 &= g_4 - (g_{11} + g_{12} + g_{20})/2 & h_j &= g_j \text{ for } j = 9, \dots, 20 \\
 h_5 &= g_5 - (g_{13} + g_{16} + g_{17})/2
 \end{aligned}$$

$g_i = 0$ if node i is not included; otherwise,

$$g_i = G(r, r_i) G(s, s_i) G(t, t_i)$$

$$\begin{aligned}
 G(\beta, \beta_i) &= \frac{1}{2} (1 + \beta_i \beta) \text{ for } \beta_i = \pm 1 \\
 G(\beta, \beta_i) &= (1 - \beta^2) \text{ for } \beta_i = 0
 \end{aligned}
 \quad ; \beta = r, s, t$$

(b) Interpolation functions

Figure 5.5 (continued)

The attractiveness of the elements in Figs. 5.3 to 5.5 lies in that the elements can have any number of nodes between the minimum and the maximum. Also, triangular elements can be formed (see Section 5.3.2). However, in general, to obtain maximum accuracy, the variable-number-nodes elements should be as nearly rectangular (in three-dimensional analysis, rectangular in each local plane) as possible and the noncorner nodes should, in general, be located at their natural coordinate positions; e.g., for the nine-node two-dimensional element the intermediate side nodes should, in general, be located at the midpoints between the corner nodes and the ninth node should be at the center of the element (for some exceptions see Section 5.3.2, and for more details on these observations, see Section 5.3.3).

Considering the geometry of the two- and three-dimensional elements in Figs. 5.4 and 5.5 we note that by means of the coordinate interpolations in (5.18), the elements can have, without any difficulty, curved boundaries. This is an important advantage over the generalized coordinate finite element formulation. Another important advantage is the ease with which the element displacement functions can be constructed.

In the *isoparametric* formulation the element displacements are interpolated in the same way as the geometry; i.e., we use

$$\boxed{u = \sum_{i=1}^q h_i u_i; \quad v = \sum_{i=1}^q h_i v_i; \quad w = \sum_{i=1}^q h_i w_i} \tag{5.19}$$

where u , v , and w are the local element displacements at any point of the element and u_i , v_i , and w_i , $i = 1, \dots, q$, are the corresponding element displacements at its nodes. Therefore, it is assumed that to each nodal point coordinate necessary to describe the geometry of the element, there corresponds one nodal point displacement.¹

To be able to evaluate the stiffness matrix of an element, we need to calculate the strain-displacement transformation matrix. The element strains are obtained in terms of

¹ In addition to the isoparametric elements, there are *subparametric* elements, for which the geometry is interpolated to a lower degree than the displacements (see end of this section) and *superparametric* elements for which the reverse is applicable (see Section 5.4).

derivatives of element displacements with respect to the local coordinates. Because the element displacements are defined in the natural coordinate system using (5.19), we need to relate the x, y, z derivatives to the r, s, t derivatives, where we realize that (5.18) is of the form

$$x = f_1(r, s, t); \quad y = f_2(r, s, t); \quad z = f_3(r, s, t) \tag{5.20}$$

where f_i denotes “function of.” The inverse relationship is

$$r = f_4(x, y, z); \quad s = f_5(x, y, z); \quad t = f_6(x, y, z) \tag{5.21}$$

We require the derivatives $\partial/\partial x, \partial/\partial y,$ and $\partial/\partial z,$ and it seems natural to use the chain rule in the following form:

$$\frac{\partial}{\partial x} = \frac{\partial}{\partial r} \frac{\partial r}{\partial x} + \frac{\partial}{\partial s} \frac{\partial s}{\partial x} + \frac{\partial}{\partial t} \frac{\partial t}{\partial x} \tag{5.22}$$

with similar relationships for $\partial/\partial y$ and $\partial/\partial z.$ However, to evaluate $\partial/\partial x$ in (5.22), we need to calculate $\partial r/\partial x, \partial s/\partial x,$ and $\partial t/\partial x,$ which means that the explicit inverse relationships in (5.21) would need to be evaluated. These inverse relationships are, in general, difficult to establish explicitly, and it is necessary to evaluate the required derivatives in the following way. Using the chain rule, we have

$$\begin{bmatrix} \frac{\partial}{\partial r} \\ \frac{\partial}{\partial s} \\ \frac{\partial}{\partial t} \end{bmatrix} = \begin{bmatrix} \frac{\partial x}{\partial r} & \frac{\partial y}{\partial r} & \frac{\partial z}{\partial r} \\ \frac{\partial x}{\partial s} & \frac{\partial y}{\partial s} & \frac{\partial z}{\partial s} \\ \frac{\partial x}{\partial t} & \frac{\partial y}{\partial t} & \frac{\partial z}{\partial t} \end{bmatrix} \begin{bmatrix} \frac{\partial}{\partial x} \\ \frac{\partial}{\partial y} \\ \frac{\partial}{\partial z} \end{bmatrix} \tag{5.23}$$

or, in matrix notation,

$$\frac{\partial}{\partial \mathbf{r}} = \mathbf{J} \frac{\partial}{\partial \mathbf{x}} \tag{5.24}$$

where \mathbf{J} is the *Jacobian operator* relating the natural coordinate derivatives to the local coordinate derivatives. We should note that the Jacobian operator can easily be found using (5.18). We require $\partial/\partial \mathbf{x}$ and use

$$\frac{\partial}{\partial \mathbf{x}} = \mathbf{J}^{-1} \frac{\partial}{\partial \mathbf{r}} \tag{5.25}$$

which requires that the inverse of \mathbf{J} exists. This inverse exists provided that there is a one-to-one (i.e., unique) correspondence between the natural and the local coordinates of the element, as expressed in (5.20) and (5.21). In most formulations the one-to-one correspondence between the coordinate systems (i.e., to each $r, s,$ and t there corresponds only one $x, y,$ and z) is obviously given, such as for the elements in Figs. 5.3 to 5.5. However, in cases where the element is much distorted or folds back upon itself, as in Fig. 5.6, the unique relation between the coordinate systems does not exist (see also Section 5.3.2 for singularities in the Jacobian transformation, Example 5.17).

Using (5.19) and (5.25), we evaluate $\partial u/\partial x, \partial u/\partial y, \partial u/\partial z, \partial v/\partial x, \dots, \partial w/\partial z$ and can therefore construct the strain-displacement transformation matrix $\mathbf{B},$ with

$$\boldsymbol{\epsilon} = \mathbf{B} \hat{\mathbf{u}} \tag{5.26}$$

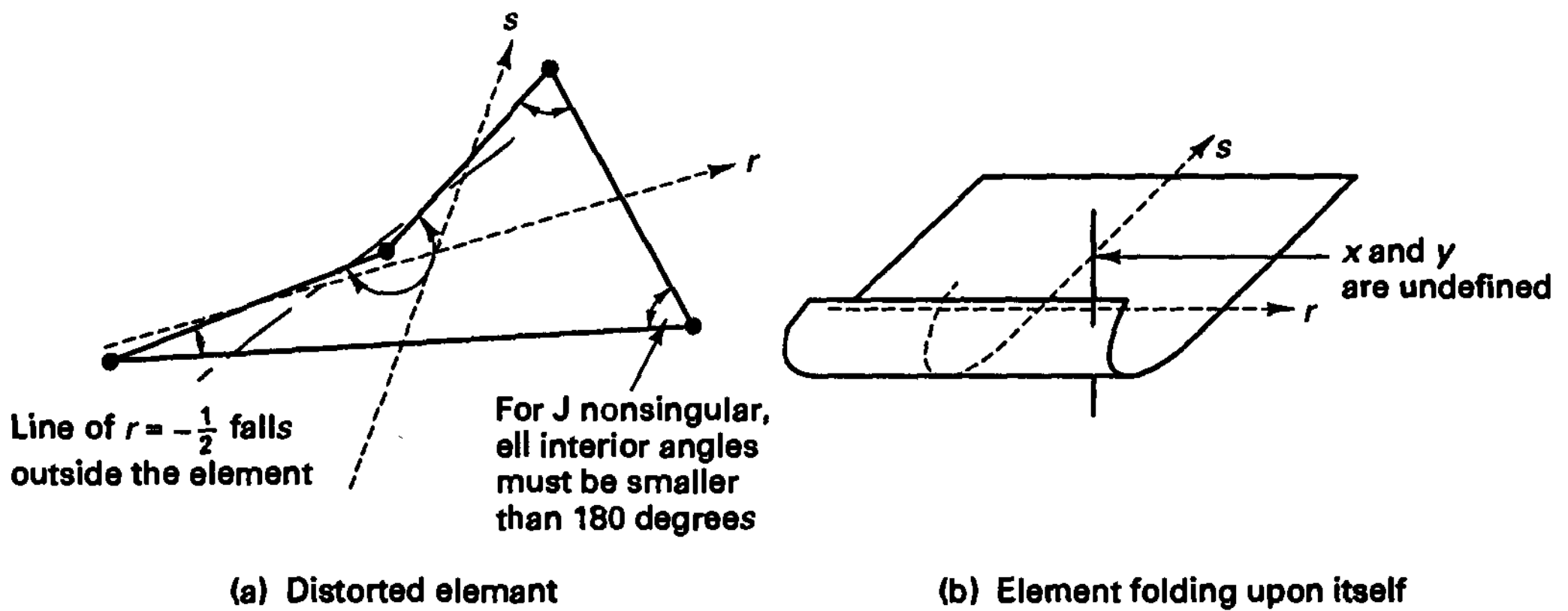


Figure 5.6 Elements with possible singular Jacobian

where $\hat{\mathbf{u}}$ is a vector listing the element nodal point displacements of (5.19), and we note that \mathbf{J} affects the elements in \mathbf{B} . The element stiffness matrix corresponding to the local element degrees of freedom is then

$$\mathbf{K} = \int_V \mathbf{B}^T \mathbf{C} \mathbf{B} dV \tag{5.27}$$

We should note that the elements of \mathbf{B} are functions of the natural coordinates r , s , and t . Therefore, the volume integration extends over the natural coordinate volume, and the volume differential dV need also be written in terms of the natural coordinates. In general, we have

$$dV = \det \mathbf{J} dr ds dt \tag{5.28}$$

where $\det \mathbf{J}$ is the determinant of the Jacobian operator in (5.24) (see Exercise 5.6).

An explicit evaluation of the volume integral in (5.27) is, in general, not effective, particularly when higher-order interpolations are used or the element is distorted. Therefore, numerical integration is employed. Indeed, numerical integration must be regarded as an integral part of isoparametric element matrix evaluations. The details of the numerical integration procedures are described in Section 5.5, but the process can briefly be summarized as follows. First, we write (5.27) in the form

$$\mathbf{K} = \int_V \mathbf{F} dr ds dt \tag{5.29}$$

where $\mathbf{F} = \mathbf{B}^T \mathbf{C} \mathbf{B} \det \mathbf{J}$ and the integration is performed in the natural coordinate system of the element. As stated above, the elements of \mathbf{F} depend on r , s , and t , but the detailed functional relationship is usually not calculated. Using numerical integration, the stiffness matrix is now evaluated as

$$\mathbf{K} = \sum_{i,j,k} \alpha_{ijk} \mathbf{F}_{ijk} \tag{5.30}$$

where \mathbf{F}_{ijk} is the matrix \mathbf{F} evaluated at the point (r_i, s_j, t_k) , and α_{ijk} is a given constant that depends on the values of r_i , s_j , and t_k . The sampling points (r_i, s_j, t_k) of the function and the

corresponding weighting factors α_{ijk} are chosen to obtain maximum accuracy in the integration. Naturally, the integration accuracy can increase as the number of sampling points is increased.

The purpose of this brief outline of the numerical integration procedure was to complete the description of the general isoparametric formulation. The relative simplicity of the formulation may already be noted. It is the simplicity of the element formulation and the efficiency with which the element matrices can actually be evaluated in a computer that has drawn much attention to the development of the isoparametric and related elements.

The formulation of the element mass matrix and load vectors is now straightforward. Namely, writing the element displacements in the form

$$\mathbf{u}(r, s, t) = \mathbf{H}\hat{\mathbf{u}} \tag{5.31}$$

where \mathbf{H} is a matrix of the interpolation functions, we have, as in (4.34) to (4.37),

$$\mathbf{M} = \int_V \rho \mathbf{H}^T \mathbf{H} dV \tag{5.32}$$

$$\mathbf{R}_B = \int_V \mathbf{H}^T \mathbf{f}^B dV \tag{5.33}$$

$$\mathbf{R}_S = \int_S \mathbf{H}^{sT} \mathbf{f}^S dS \tag{5.34}$$

$$\mathbf{R}_I = \int_V \mathbf{B}^T \boldsymbol{\tau}^I dV \tag{5.35}$$

These matrices are evaluated using numerical integration, as indicated for the stiffness matrix \mathbf{K} in (5.30). In the evaluation we need to use the appropriate function \mathbf{F} . To calculate the body force vector \mathbf{R}_B we use $\mathbf{F} = \mathbf{H}^T \mathbf{f}^B \det \mathbf{J}$, for the surface force vector we use $\mathbf{F} = \mathbf{H}^{sT} \mathbf{f}^S \det \mathbf{J}^S$, for the initial stress load vector we use $\mathbf{F} = \mathbf{B}^T \boldsymbol{\tau}^I \det \mathbf{J}$, and for the mass matrix we have $\mathbf{F} = \rho \mathbf{H}^T \mathbf{H} \det \mathbf{J}$.

This formulation was for one-, two-, or three-dimensional elements. We shall now consider some specific cases and demonstrate the details of the calculation of element matrices.

EXAMPLE 5.2: Derive the displacement interpolation matrix \mathbf{H} , strain-displacement interpolation matrix \mathbf{B} , and Jacobian operator \mathbf{J} for the three-node truss element shown in Fig. E5.2.

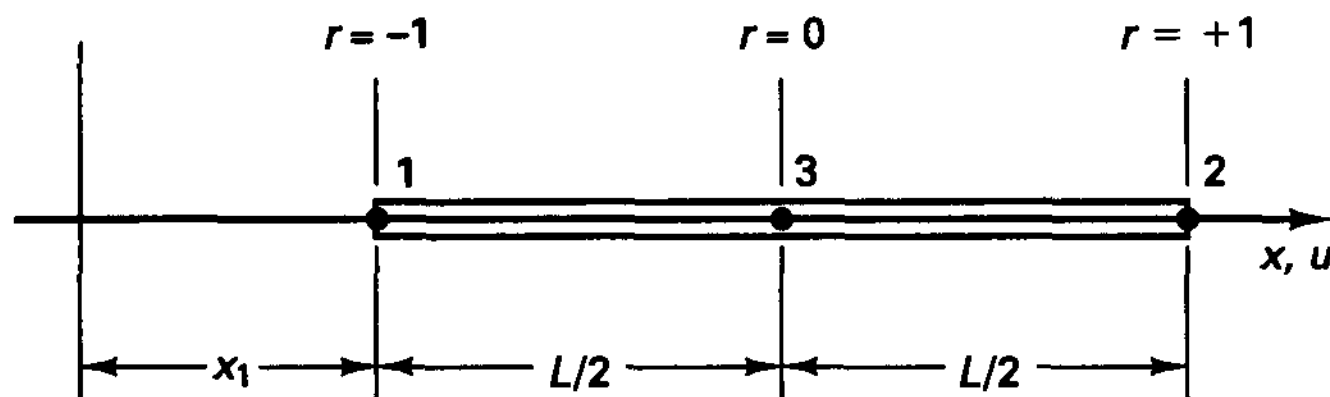


Figure E5.2 Truss element with node 3 at center of element

The interpolation functions of the element were given in Fig. E5.1. Thus, we have

$$\mathbf{H} = \left[-\frac{r}{2}(1 - r) \quad \frac{r}{2}(1 + r) \quad (1 - r^2) \right] \tag{a}$$

The strain-displacement matrix \mathbf{B} is obtained by differentiation of \mathbf{H} with respect to r and premultiplying the result by the inverse of the Jacobian operator,

$$\mathbf{B} = \mathbf{J}^{-1} \begin{bmatrix} (-\frac{1}{2} + r) & (\frac{1}{2} + r) & -2r \end{bmatrix} \quad (b)$$

To evaluate \mathbf{J} formally we use

$$x = -\frac{r}{2}(1-r)x_1 + \frac{r}{2}(1+r)(x_1 + L) + (1-r^2)\left(x_1 + \frac{L}{2}\right)$$

hence,
$$x = x_1 + \frac{L}{2} + \frac{L}{2}r \quad (c)$$

where we may note that because node 3 is at the center of the truss, x is interpolated linearly between nodes 1 and 2. The same result would be obtained using only nodes 1 and 2 for the geometry interpolation. Using now the relation in (c), we have

$$\mathbf{J} = \begin{bmatrix} L \\ 2 \end{bmatrix} \quad (d)$$

and
$$\mathbf{J}^{-1} = \begin{bmatrix} 2 \\ L \end{bmatrix}; \quad \det \mathbf{J} = \frac{L}{2}$$

With the relations in (a) to (d), we can now evaluate all finite element matrices and vectors given in (5.27) to (5.35).

EXAMPLE 5.3: Establish the Jacobian operator \mathbf{J} of the two-dimensional elements shown in Fig. E5.3.

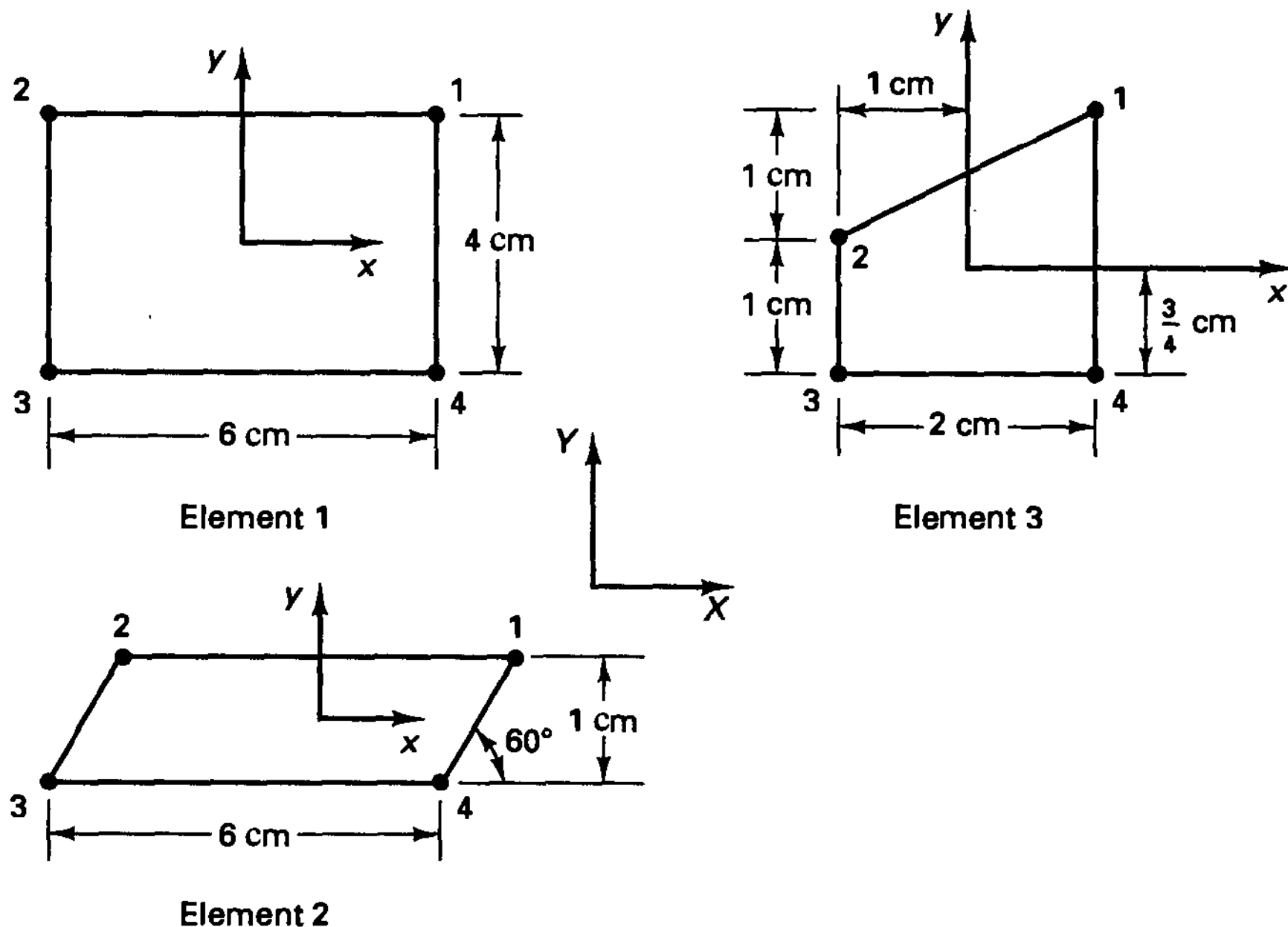


Figure E5.3 Some two-dimensional elements

The Jacobian operator is the same for the global X, Y and the local x, y coordinate systems. For convenience we therefore use the local coordinate systems. Substituting into (5.18) and (5.23) using the interpolation functions given in Fig. 5.4, we obtain for element 1:

$$x = 3r; \quad y = 2s$$

$$\mathbf{J} = \begin{bmatrix} 3 & 0 \\ 0 & 2 \end{bmatrix}$$

Similarly, for element 2, we have

$$\begin{aligned} x &= \frac{1}{4}\{(1+r)(1+s)[3 + 1/(2\sqrt{3})] + (1-r)(1+s)[-3 - 1/(2\sqrt{3})]) \\ &\quad + (1-r)(1-s)[-3 + 1/(2\sqrt{3})]) + (1+r)(1-s)[3 - 1/(2\sqrt{3})])\} \\ y &= \frac{1}{4}\{(1+r)(1+s)(\frac{1}{2}) + (1-r)(1+s)(\frac{1}{2}) + (1-r)(1-s)(-\frac{1}{2}) \\ &\quad + (1+r)(1-s)(-\frac{1}{2})\} \end{aligned}$$

and hence,

$$\mathbf{J} = \begin{bmatrix} 3 & 0 \\ \frac{1}{2\sqrt{3}} & \frac{1}{2} \end{bmatrix}$$

Also, for element 3,

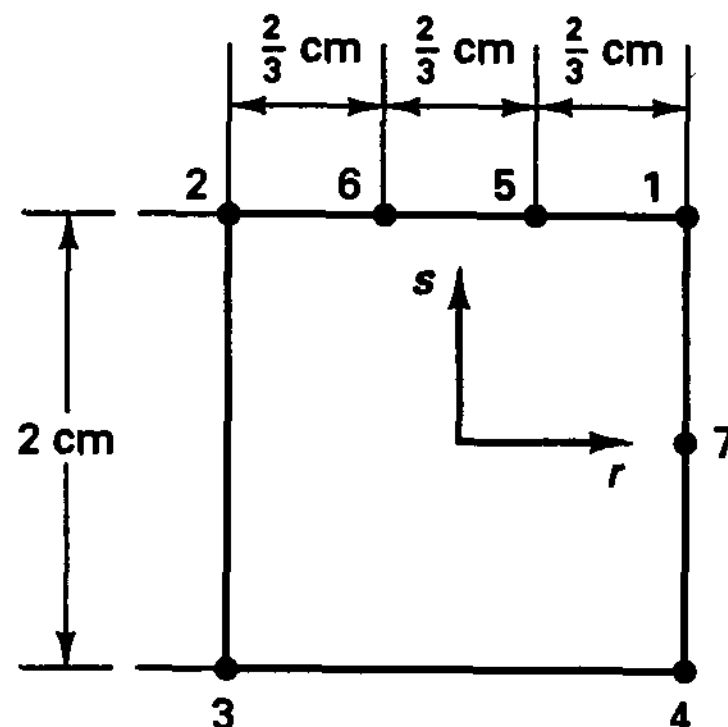
$$\begin{aligned} x &= \frac{1}{4}[(1+r)(1+s)(1) + (1-r)(1+s)(-1) + (1-r)(1-s)(-1) \\ &\quad + (1+r)(1-s)(+1)] \\ y &= \frac{1}{4}[(1+r)(1+s)(\frac{5}{4}) + (1-r)(1+s)(\frac{1}{4}) + (1-r)(1-s)(-\frac{3}{4}) \\ &\quad + (1+r)(1-s)(-\frac{3}{4})] \end{aligned}$$

therefore,

$$\mathbf{J} = \frac{1}{4} \begin{bmatrix} 4 & (1+s) \\ 0 & (3+r) \end{bmatrix}$$

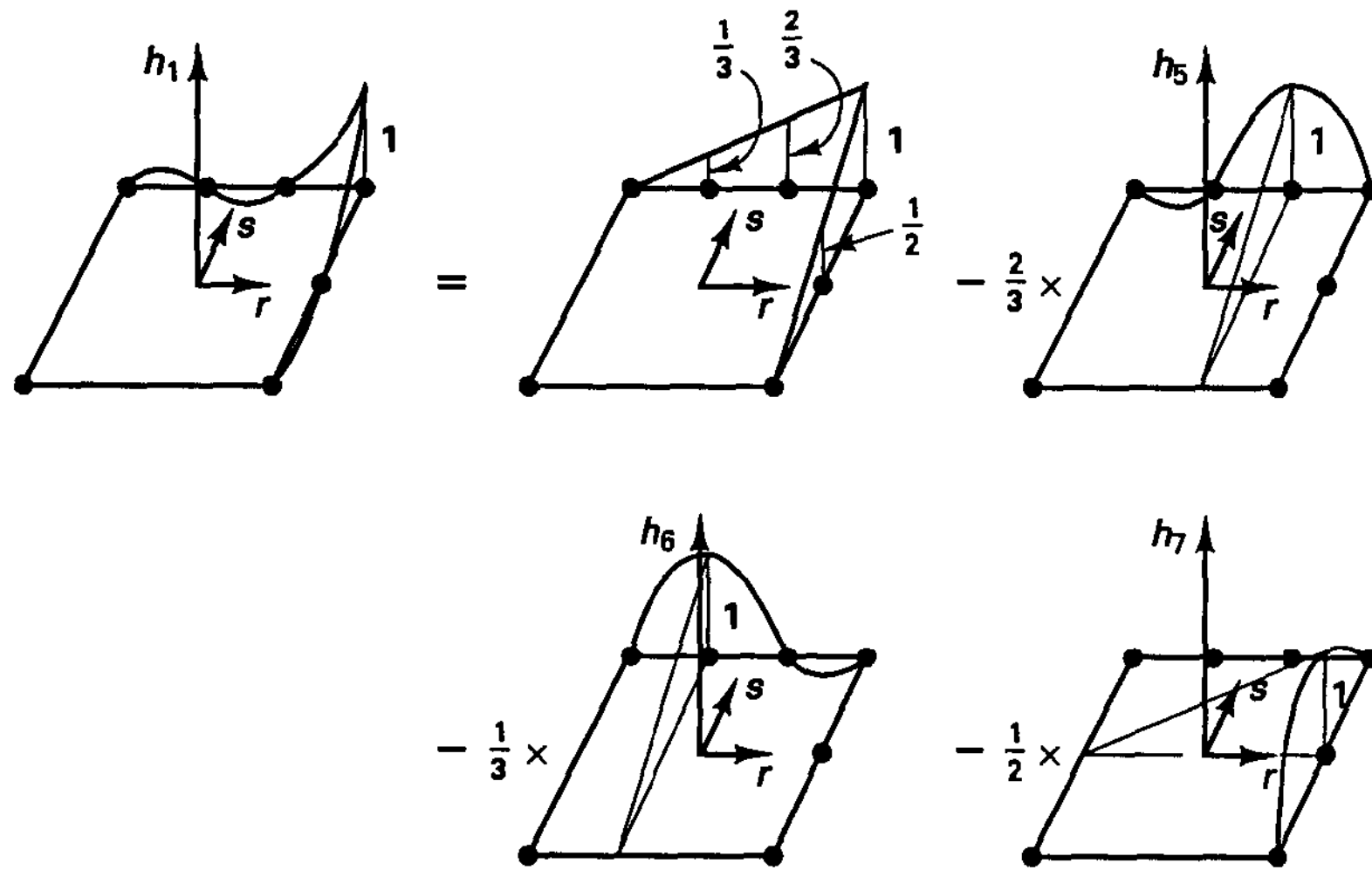
We may recognize that the Jacobian operator of a 2×2 square element is the identity matrix, and that the entries in the operator \mathbf{J} of a general element express the amount of distortion from that 2×2 square element. Since the distortion is constant at any point (r, s) of elements 1 and 2, the operator \mathbf{J} is constant for these elements.

EXAMPLE 5.4: Establish the interpolation functions of the two-dimensional element shown in Fig. E5.4.



(a)

Figure E5.4 A seven-node element



(b) Construction of h_1

Figure E5.4 (continued)

The individual functions are obtained by combining the basic linear, parabolic, and cubic interpolations corresponding to the r and s directions. Thus, using the functions in Figure 5.3, we obtain

$$\begin{aligned}
 h_5 &= \left[\frac{1}{16}(-27r^3 - 9r^2 + 27r + 9) \right] \left[\frac{1}{2}(1 + s) \right] \\
 h_6 &= \left[(1 - r^2) + \frac{1}{16}(27r^3 + 7r^2 - 27r - 7) \right] \left[\frac{1}{2}(1 + s) \right] \\
 h_2 &= \left[\frac{1}{2}(1 - r) - \frac{1}{2}(1 - r^2) + \frac{1}{16}(-9r^3 + r^2 + 9r - 1) \right] \left[\frac{1}{2}(1 + s) \right] \\
 h_3 &= \frac{1}{4}(1 - r)(1 - s) \\
 h_7 &= \frac{1}{2}(1 - s^2)(1 + r) \\
 h_4 &= \frac{1}{4}(1 + r)(1 - s) - \frac{1}{2}h_7 \\
 h_1 &= \frac{1}{4}(1 + r)(1 + s) - \frac{2}{3}h_5 - \frac{1}{3}h_6 - \frac{1}{2}h_7
 \end{aligned}$$

where h_1 is constructed as indicated in an oblique/aerial view in Fig. E5.4.

EXAMPLE 5.5: Derive the expressions needed for the evaluation of the stiffness matrix of the isoparametric four-node finite element in Fig. E5.5. Assume plane stress or plane strain conditions.

Using the interpolation function $h_1, h_2, h_3,$ and h_4 defined in Fig. 5.4, the coordinate interpolation given in (5.18) is, for this element,

$$\begin{aligned}
 x &= \frac{1}{4}(1 + r)(1 + s)x_1 + \frac{1}{4}(1 - r)(1 + s)x_2 + \frac{1}{4}(1 - r)(1 - s)x_3 + \frac{1}{4}(1 + r)(1 - s)x_4 \\
 y &= \frac{1}{4}(1 + r)(1 + s)y_1 + \frac{1}{4}(1 - r)(1 + s)y_2 + \frac{1}{4}(1 - r)(1 - s)y_3 + \frac{1}{4}(1 + r)(1 - s)y_4
 \end{aligned}$$

The displacement interpolation given in (5.19) is

$$\begin{aligned}
 u &= \frac{1}{4}(1 + r)(1 + s)u_1 + \frac{1}{4}(1 - r)(1 + s)u_2 + \frac{1}{4}(1 - r)(1 - s)u_3 + \frac{1}{4}(1 + r)(1 - s)u_4 \\
 v &= \frac{1}{4}(1 + r)(1 + s)v_1 + \frac{1}{4}(1 - r)(1 + s)v_2 + \frac{1}{4}(1 - r)(1 - s)v_3 + \frac{1}{4}(1 + r)(1 - s)v_4
 \end{aligned}$$

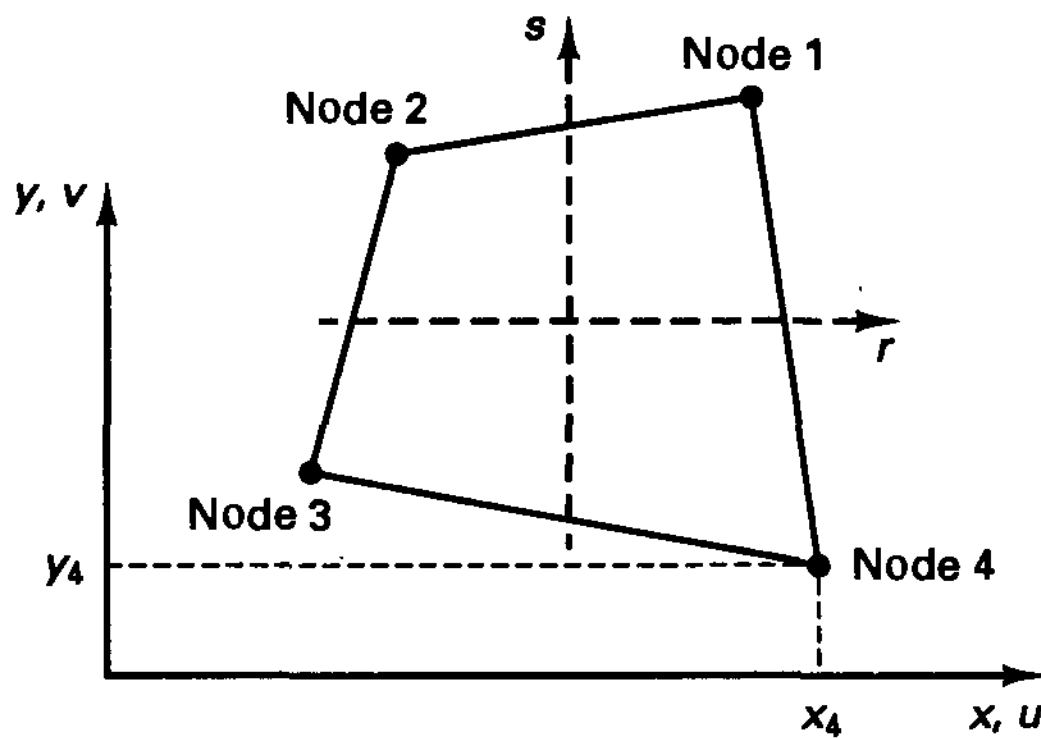


Figure E5.5 Four-node two-dimensional element

The element strains are given by

$$\boldsymbol{\epsilon}^T = [\epsilon_{xx} \quad \epsilon_{yy} \quad \gamma_{xy}]$$

where

$$\epsilon_{xx} = \frac{\partial u}{\partial x}; \quad \epsilon_{yy} = \frac{\partial v}{\partial y}; \quad \gamma_{xy} = \frac{\partial u}{\partial y} + \frac{\partial v}{\partial x}$$

To evaluate the displacement derivatives, we need to evaluate (5.23):

$$\begin{bmatrix} \frac{\partial}{\partial r} \\ \frac{\partial}{\partial s} \end{bmatrix} = \begin{bmatrix} \frac{\partial x}{\partial r} & \frac{\partial y}{\partial r} \\ \frac{\partial x}{\partial s} & \frac{\partial y}{\partial s} \end{bmatrix} \begin{bmatrix} \frac{\partial}{\partial x} \\ \frac{\partial}{\partial y} \end{bmatrix} \quad \text{or} \quad \frac{\partial}{\partial \mathbf{r}} = \mathbf{J} \frac{\partial}{\partial \mathbf{x}}$$

where

$$\frac{\partial x}{\partial r} = \frac{1}{4}(1+s)x_1 - \frac{1}{4}(1+s)x_2 - \frac{1}{4}(1-s)x_3 + \frac{1}{4}(1-s)x_4$$

$$\frac{\partial x}{\partial s} = \frac{1}{4}(1+r)x_1 + \frac{1}{4}(1-r)x_2 - \frac{1}{4}(1-r)x_3 - \frac{1}{4}(1+r)x_4$$

$$\frac{\partial y}{\partial r} = \frac{1}{4}(1+s)y_1 - \frac{1}{4}(1+s)y_2 - \frac{1}{4}(1-s)y_3 + \frac{1}{4}(1-s)y_4$$

$$\frac{\partial y}{\partial s} = \frac{1}{4}(1+r)y_1 + \frac{1}{4}(1-r)y_2 - \frac{1}{4}(1-r)y_3 - \frac{1}{4}(1+r)y_4$$

Therefore, for any value r and s , $-1 \leq r \leq +1$ and $-1 \leq s \leq +1$, we can form the Jacobian operator \mathbf{J} by using the expressions shown for $\partial x/\partial r$, $\partial x/\partial s$, and $\partial y/\partial r$, $\partial y/\partial s$. Assume that we evaluate \mathbf{J} at $r = r_i$ and $s = s_j$ and denote the operator by \mathbf{J}_{ij} and its determinant by $\det \mathbf{J}_{ij}$. Then we have

$$\begin{bmatrix} \frac{\partial}{\partial x} \\ \frac{\partial}{\partial y} \end{bmatrix}_{\text{at } r=r_i, s=s_j} = \mathbf{J}_{ij}^{-1} \begin{bmatrix} \frac{\partial}{\partial r} \\ \frac{\partial}{\partial s} \end{bmatrix}_{\text{at } r=r_i, s=s_j}$$

To evaluate the element strains we use

$$\begin{aligned} \frac{\partial u}{\partial r} &= \frac{1}{4}(1+s)u_1 - \frac{1}{4}(1+s)u_2 - \frac{1}{4}(1-s)u_3 + \frac{1}{4}(1-s)u_4 \\ \frac{\partial u}{\partial s} &= \frac{1}{4}(1+r)u_1 + \frac{1}{4}(1-r)u_2 - \frac{1}{4}(1-r)u_3 - \frac{1}{4}(1+r)u_4 \\ \frac{\partial v}{\partial r} &= \frac{1}{4}(1+s)v_1 - \frac{1}{4}(1+s)v_2 - \frac{1}{4}(1-s)v_3 + \frac{1}{4}(1-s)v_4 \\ \frac{\partial v}{\partial s} &= \frac{1}{4}(1+r)v_1 + \frac{1}{4}(1-r)v_2 - \frac{1}{4}(1-r)v_3 - \frac{1}{4}(1+r)v_4 \end{aligned}$$

Therefore,

$$\begin{bmatrix} \frac{\partial u}{\partial x} \\ \frac{\partial u}{\partial y} \end{bmatrix}_{\substack{\text{at } r=r_i \\ s=s_j}} = \frac{1}{4} \mathbf{J}_{ij}^{-1} \begin{bmatrix} 1+s_j & 0 & -(1+s_j) & 0 & -(1-s_j) & 0 & 1-s_j & 0 \\ 1+r_i & 0 & 1-r_i & 0 & -(1-r_i) & 0 & -(1+r_i) & 0 \end{bmatrix} \hat{\mathbf{u}} \quad (\text{a})$$

and

$$\begin{bmatrix} \frac{\partial v}{\partial x} \\ \frac{\partial v}{\partial y} \end{bmatrix}_{\substack{\text{at } r=r_i \\ s=s_j}} = \frac{1}{4} \mathbf{J}_{ij}^{-1} \begin{bmatrix} 0 & 1+s_j & 0 & -(1+s_j) & 0 & -(1-s_j) & 0 & 1-s_j \\ 0 & 1+r_i & 0 & 1-r_i & 0 & -(1-r_i) & 0 & -(1+r_i) \end{bmatrix} \hat{\mathbf{u}} \quad (\text{b})$$

where

$$\hat{\mathbf{u}}^T = [u_1 \quad v_1 \quad u_2 \quad v_2 \quad u_3 \quad v_3 \quad u_4 \quad v_4]$$

Evaluating the relations in (a) and (b), we can establish the strain-displacement transformation matrix at the point (r_i, s_j) ; i.e., we obtain

$$\boldsymbol{\epsilon}_{ij} = \mathbf{B}_{ij} \hat{\mathbf{u}}$$

where the subscripts i and j indicate that the strain-displacement transformation is evaluated at the point (r_i, s_j) . For example, if $x = r, y = s$ (i.e., the stiffness matrix of a square element is required that has side lengths equal to 2), the Jacobian operator is the identity matrix, and hence

$$\mathbf{B}_{ij} = \frac{1}{4} \begin{bmatrix} 1+s_j & 0 & -(1+s_j) & 0 & -(1-s_j) & 0 & 1-s_j & 0 \\ 0 & 1+r_i & 0 & 1-r_i & 0 & -(1-r_i) & 0 & -(1+r_i) \\ 1+r_i & 1+s_j & 1-r_i & -(1+s_j) & -(1-r_i) & -(1-s_j) & -(1+r_i) & 1-s_j \end{bmatrix}$$

The matrix \mathbf{F}_{ij} in (5.30) is now simply

$$\mathbf{F}_{ij} = \mathbf{B}_{ij}^T \mathbf{C} \mathbf{B}_{ij} \det \mathbf{J}_{ij}$$

where the material property matrix \mathbf{C} is given in Table 4.3. In the case of plane stress or plane strain conditions, we integrate in the r, s plane and assume that the function \mathbf{F} is constant through the thickness of the element. The stiffness matrix of the element is therefore

$$\mathbf{K} = \sum_{i,j} t_{ij} \alpha_{ij} \mathbf{F}_{ij}$$

where t_{ij} is the thickness of the element at the sampling point (r_i, s_j) ($t_{ij} = 1.0$ in plane strain analysis). With the matrices \mathbf{F}_{ij} as given and the weighting factors α_{ij} available, the required stiffness matrix can readily be evaluated.

For the actual implementation it should be noted that in the evaluation of \mathbf{J}_{ij} and of the matrices defining the displacement derivatives in (a) and (b), only the eight possible derivatives of the interpolation functions h_1, \dots, h_4 are required. Therefore, it is expedient to calculate these derivatives corresponding to the point (r_i, s_j) once at the start of the evaluation of \mathbf{B}_{ij} and use them whenever they are required.

It should also be realized that considering the specific point (r_i, s_j) , the relations in (a) and (b) may be written, respectively, as

$$\left. \begin{aligned} \frac{\partial u}{\partial x} &= \sum_{i=1}^4 \frac{\partial h_i}{\partial x} u_i \\ \frac{\partial u}{\partial y} &= \sum_{i=1}^4 \frac{\partial h_i}{\partial y} u_i \end{aligned} \right\} \quad (c)$$

and

$$\left. \begin{aligned} \frac{\partial v}{\partial x} &= \sum_{i=1}^4 \frac{\partial h_i}{\partial x} v_i \\ \frac{\partial v}{\partial y} &= \sum_{i=1}^4 \frac{\partial h_i}{\partial y} v_i \end{aligned} \right\} \quad (d)$$

Hence, we have

$$\mathbf{B} = \begin{bmatrix} \frac{\partial h_1}{\partial x} & 0 & \frac{\partial h_2}{\partial x} & 0 & \frac{\partial h_3}{\partial x} & 0 & \frac{\partial h_4}{\partial x} & 0 \\ 0 & \frac{\partial h_1}{\partial y} & 0 & \frac{\partial h_2}{\partial y} & 0 & \frac{\partial h_3}{\partial y} & 0 & \frac{\partial h_4}{\partial y} \\ \frac{\partial h_1}{\partial y} & \frac{\partial h_1}{\partial x} & \frac{\partial h_2}{\partial y} & \frac{\partial h_2}{\partial x} & \frac{\partial h_3}{\partial y} & \frac{\partial h_3}{\partial x} & \frac{\partial h_4}{\partial y} & \frac{\partial h_4}{\partial x} \end{bmatrix} \quad (e)$$

where it is implied that in (c) and (d), the derivatives are evaluated at point (r_i, s_j) , and therefore in (e), we have, in fact, the matrix \mathbf{B}_{ij} .

EXAMPLE 5.6: Derive the expressions needed for the evaluation of the mass matrix of the element considered in Example 5.5.

The mass matrix of the element is given by

$$\mathbf{M} = \sum_{i,j} \alpha_{ij} t_{ij} \mathbf{F}_{ij}$$

where

$$\mathbf{F}_{ij} = \rho_{ij} \mathbf{H}_{ij}^T \mathbf{H}_{ij} \det \mathbf{J}_{ij}$$

and \mathbf{H}_{ij} is the displacement interpolation matrix. The displacement interpolation functions for u and v of the four-node element have been given in Example 5.5, and we have

$$\mathbf{H}_{ij} = \frac{1}{4} \begin{bmatrix} (1+r_i)(1+s_j) & 0 & (1-r_i)(1+s_j) & 0 \\ 0 & (1+r_i)(1+s_j) & 0 & (1-r_i)(1+s_j) \\ (1-r_i)(1-s_j) & 0 & (1+r_i)(1-s_j) & 0 \\ 0 & (1-r_i)(1-s_j) & 0 & (1+r_i)(1-s_j) \end{bmatrix}$$

The determinant of the Jacobian matrix, $\det \mathbf{J}_{ij}$, was given in Example 5.5, and ρ_{ij} is the mass density at the sampling point (r_i, s_j) . Therefore, all required variables for the evaluation of the mass matrix have been defined.

EXAMPLE 5.7: Derive the expressions needed for the evaluation of the body force vector \mathbf{R}_B and the initial stress vector \mathbf{R}_I of the element considered in Example 5.5.

These vectors are obtained using the matrices \mathbf{H}_{ij} , \mathbf{B}_{ij} , and \mathbf{J}_{ij} defined in Examples 5.5 and 5.6; i.e., we have

$$\mathbf{R}_B = \sum_{i,j} \alpha_{ij} t_{ij} \mathbf{H}_{ij}^T \mathbf{f}_{ij}^B \det \mathbf{J}_{ij}$$

$$\mathbf{R}_I = \sum_{i,j} \alpha_{ij} t_{ij} \mathbf{B}_{ij}^T \boldsymbol{\tau}_{ij} \det \mathbf{J}_{ij}$$

where \mathbf{f}_{ij}^B and $\boldsymbol{\tau}_{ij}$ are the body force vector and initial stress vector evaluated at the integration sampling points.

EXAMPLE 5.8: Derive the expressions needed in the calculation of the surface force vector \mathbf{R}_S when the element edge 1-2 of the four-node isoparametric element considered in Example 5.5 is loaded as shown in Fig. E5.8.

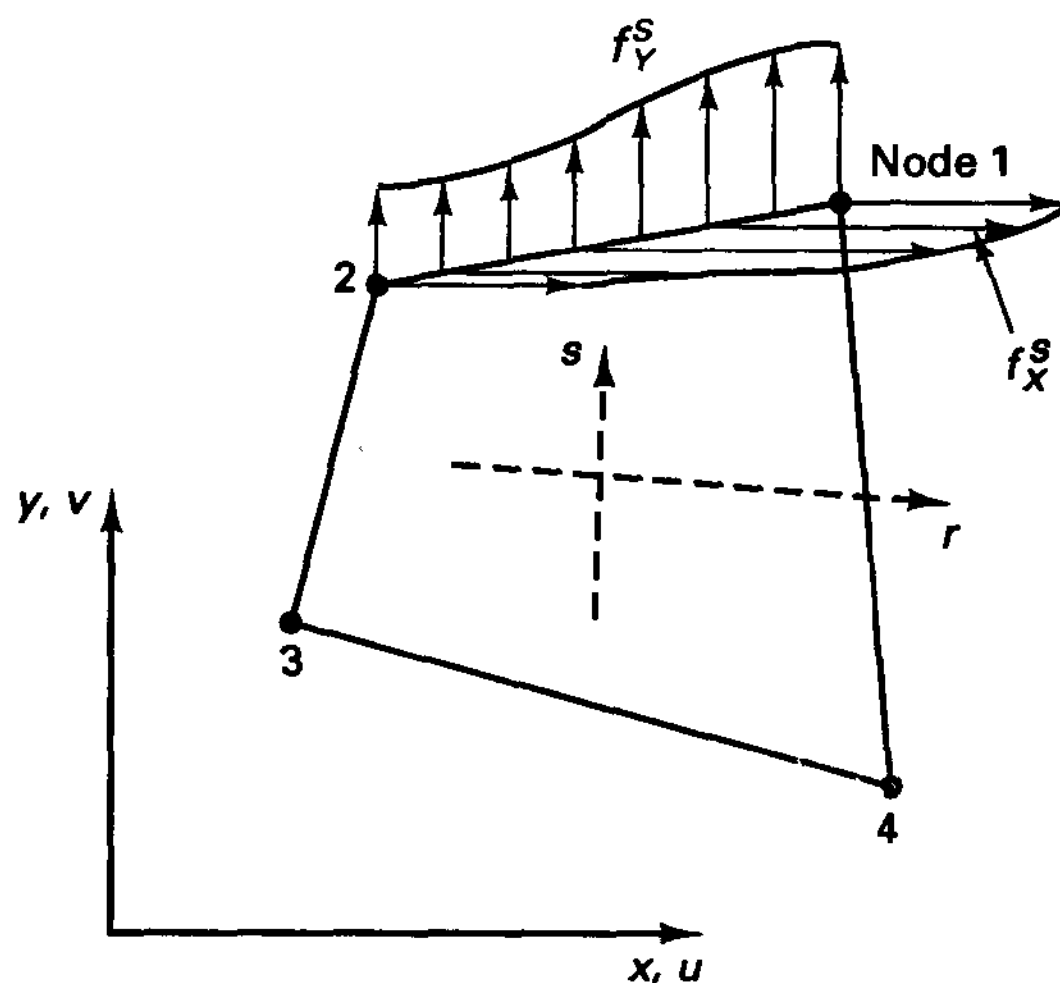


Figure E5.8 Traction distribution along edge 1-2 of a four-node element

The first step is to establish the displacement interpolations. Since $s = +1$ at the edge 1-2, we have, using the interpolation functions given in Example 5.5,

$$u^s = \frac{1}{2}(1 + r)u_1 + \frac{1}{2}(1 - r)u_2$$

$$v^s = \frac{1}{2}(1 + r)v_1 + \frac{1}{2}(1 - r)v_2$$

Hence, to evaluate \mathbf{R}_S in (5.34) we can use

$$\mathbf{H}^s = \begin{bmatrix} \frac{1}{2}(1 + r) & 0 & \frac{1}{2}(1 - r) & 0 & 0 & 0 & 0 & 0 & 0 \\ 0 & \frac{1}{2}(1 + r) & 0 & \frac{1}{2}(1 - r) & 0 & 0 & 0 & 0 & 0 \end{bmatrix}$$

and

$$\mathbf{f}^s = \begin{bmatrix} f_x^s \\ f_y^s \end{bmatrix}$$

where f_x^s and f_y^s are the x and y components of the applied surface force. These components may have been given as a function of r .

For the evaluation of the integral in (5.34), we also need the differential surface area dS expressed in the r, s natural coordinate system. If t_r is the thickness, $dS = t_r dl$, where dl is a differential length,

$$dl = \det \mathbf{J}^s dr; \quad \det \mathbf{J}^s = \left[\left(\frac{\partial x}{\partial r} \right)^2 + \left(\frac{\partial y}{\partial r} \right)^2 \right]^{1/2}$$

But the derivatives $\partial x/\partial r$ and $\partial y/\partial r$ have been given in Example 5.5. Using $s = +1$, we have, in this case,

$$\frac{\partial x}{\partial r} = \frac{x_1 - x_2}{2}, \quad \frac{\partial y}{\partial r} = \frac{y_1 - y_2}{2}$$

Although the vector \mathbf{R}_s could in this case be evaluated in a closed-form solution (provided that the functions used in \mathbf{f}^s are simple), in order to keep generality in the program that calculates \mathbf{R}_s , it is expedient to use numerical integration. This way, variable-number-nodes elements can be implemented in an elegant manner in one program. Thus, using the notation defined in this section, we have

$$\mathbf{R}_s = \sum_i \alpha_i t_{ri} \mathbf{F}_i$$

$$\mathbf{F}_i = \mathbf{H}_i^{sT} \mathbf{f}_i^s \det \mathbf{J}_i^s$$

It is noted that in this case only one-dimensional numerical integration is required because s is not a variable.

EXAMPLE 5.9: Explain how the expressions given in Examples 5.5 to 5.7 need be modified when the element considered is an axisymmetric element.

In this case two modifications are necessary. First, we consider 1 radian of the structure. Hence, the thickness to be employed in all integrations is that corresponding to 1 radian, which means that at an integration point the thickness is equal to the radius at that point:

$$t_{ij} = \sum_{k=1}^4 h_k \Big|_{r_i, s_j} x_k \quad (a)$$

Second, it is recognized that also circumferential strains and stresses are developed (see Table 4.2). Hence, the strain-displacement matrix must be augmented by one row for the hoop strain u/R ; i.e., we have

$$\mathbf{B} = \begin{bmatrix} \dots & & & & \dots \\ \frac{h_1}{t} & 0 & \frac{h_2}{t} & 0 & \frac{h_3}{t} & 0 & \frac{h_4}{t} & 0 \\ \dots & & & & \dots \end{bmatrix} \quad (b)$$

where the first three rows have already been defined in Example 5.5 and t is equal to the radius. To obtain the strain-displacement matrix at integration point (i, j) we use (a) to evaluate t and substitute into (b).

EXAMPLE 5.10: Calculate the nodal point forces of the four-node axisymmetric finite element shown in Fig. E5.10 when the element is subjected to centrifugal loading.

Here we want to evaluate

$$\mathbf{R}_B = \int_V \mathbf{H}^T \mathbf{f}^B dV$$

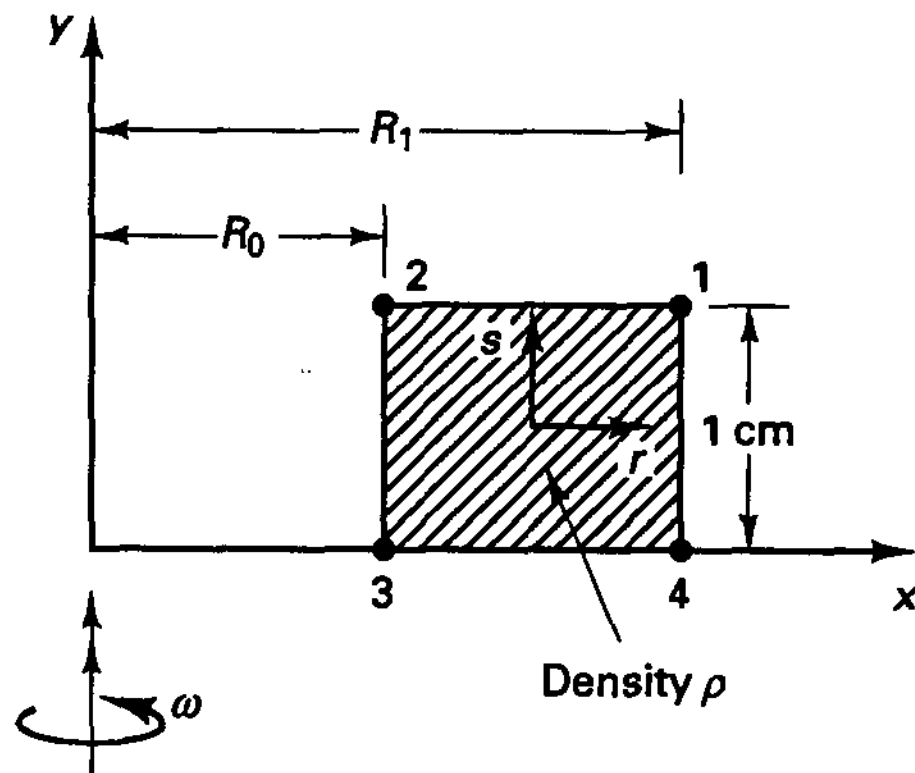


Figure E5.10 Four-node axisymmetric element rotating at angular velocity ω (rad/sec)

where

$$f_x^B = \rho\omega^2 R; \quad f_y^B = 0$$

$$R = \frac{1}{2}(1 - r)R_0 + \frac{1}{2}(1 + r)R_1$$

$$\mathbf{H} = \begin{bmatrix} h_1 & 0 & h_2 & 0 & h_3 & 0 & h_4 & 0 \\ 0 & h_1 & 0 & h_2 & 0 & h_3 & 0 & h_4 \end{bmatrix}; \quad \mathbf{J} = \begin{bmatrix} \frac{R_1 - R_0}{2} & 0 \\ 0 & \frac{1}{2} \end{bmatrix}$$

and the h_i are defined in Fig. 5.4. Also, considering 1 radian,

$$dV = \det \mathbf{J} \, dr \, ds \, R = \left(\frac{R_1 - R_0}{4} \right) dr \, ds \left(\frac{R_1 + R_0}{2} + \frac{R_1 - R_0}{2} r \right)$$

Hence,

$$\mathbf{R}_B = \frac{\rho\omega^2(R_1 - R_0)}{64} \int_{r=-1}^{+1} \int_{s=-1}^{+1} \begin{bmatrix} (1+r)(1+s) & 0 \\ 0 & (1+r)(1+s) \\ (1-r)(1+s) & 0 \\ 0 & (1-r)(1+s) \\ (1-r)(1-s) & 0 \\ 0 & (1-r)(1-s) \\ (1+r)(1-s) & 0 \\ 0 & (1+r)(1-s) \end{bmatrix} [(R_1 + R_0) + (R_1 - R_0)r]^2 \begin{bmatrix} 1 \\ 0 \end{bmatrix} dr \, ds$$

If we let $A = R_1 + R_0$ and $B = R_1 - R_0$, we have

$$\mathbf{R}_B = \frac{\rho\omega^2 B}{64} \begin{bmatrix} \frac{2}{3}(6A^2 + 4AB + 2B^2) \\ 0 \\ \frac{2}{3}(6A^2 - 4AB + 2B^2) \\ 0 \\ \frac{2}{3}(6A^2 - 4AB + 2B^2) \\ 0 \\ \frac{2}{3}(6A^2 + 4AB + 2B^2) \\ 0 \end{bmatrix}$$

EXAMPLE 5.11: The four-node plane stress element shown in Fig. E5.11 is subjected to the given temperature distribution. If the temperature corresponding to the stress-free state is θ_0 , evaluate the nodal point forces to which the element must be subjected so that there are no nodal point displacements.

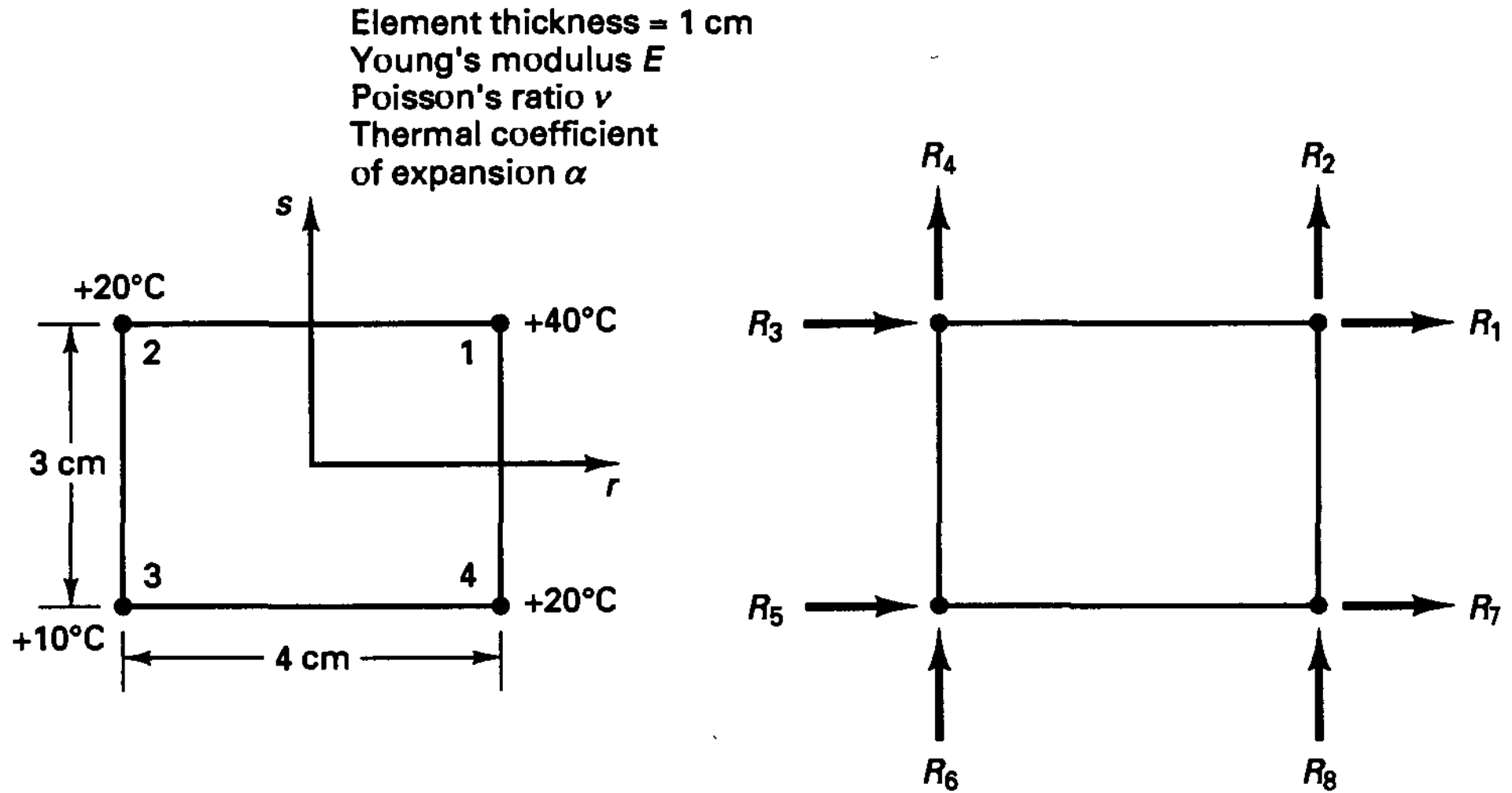


Figure E5.11 Nodal point forces due to initial temperature distribution

In this case we have for the total stresses, due to total strains ϵ and thermal strains ϵ^{th} ,

$$\tau = C(\epsilon - \epsilon^{th}) \tag{a}$$

where $\epsilon_{xx}^{th} = \alpha(\theta - \theta_0)$, $\epsilon_{yy}^{th} = \alpha(\theta - \theta_0)$, $\gamma_{xy}^{th} = 0$. If the nodal point displacements are zero, we have $\epsilon = 0$, and the stresses due to the thermal strains can be thought of as initial stresses. Thus, the nodal point forces are

$$R_i = \int_V B^T \tau^I dV$$

$$\tau^I = -\frac{E\alpha}{1-\nu^2} \begin{bmatrix} 1 & \nu & 0 \\ \nu & 1 & 0 \\ 0 & 0 & \frac{1-\nu}{2} \end{bmatrix} \begin{bmatrix} 1 \\ 1 \\ 0 \end{bmatrix} \left\{ \left(\sum_{i=1}^4 h_i \theta_i \right) - \theta_0 \right\}$$

and the h_i are the interpolation functions defined in Fig. 5.4. Also,

$$J = \begin{bmatrix} 2 & 0 \\ 0 & 1.5 \end{bmatrix}; \quad J^{-1} = \begin{bmatrix} \frac{1}{2} & 0 \\ 0 & \frac{2}{3} \end{bmatrix}; \quad \det J = 3$$

$$B = \begin{bmatrix} \frac{1+s}{8} & 0 & -\frac{1+s}{8} & 0 & -\frac{1-s}{8} & 0 & \frac{1-s}{8} & 0 \\ 0 & \frac{1+r}{6} & 0 & \frac{1-r}{6} & 0 & -\frac{1-r}{6} & 0 & -\frac{1+r}{6} \\ \frac{1+r}{6} & \frac{1+s}{8} & \frac{1-r}{6} & -\frac{1+s}{8} & -\frac{1-r}{6} & -\frac{1-s}{8} & -\frac{1+r}{6} & \frac{1-s}{8} \end{bmatrix}$$

Hence,

$$\mathbf{R}_T = \int_{-1}^{+1} \int_{-1}^{+1} \begin{bmatrix} \frac{1+s}{8} & 0 & \frac{1+r}{6} \\ 0 & \frac{1+r}{6} & \frac{1+s}{8} \\ -\frac{1+s}{8} & 0 & \frac{1-r}{6} \\ 0 & \frac{1-r}{6} & -\frac{1+s}{8} \\ -\frac{1-s}{8} & 0 & -\frac{1-r}{6} \\ 0 & -\frac{1-r}{6} & -\frac{1-s}{8} \\ \frac{1-s}{8} & 0 & -\frac{1+r}{6} \\ 0 & -\frac{1+r}{6} & \frac{1-s}{8} \end{bmatrix} \begin{bmatrix} 1+\nu \\ 1+\nu \\ 0 \end{bmatrix} \frac{E\alpha}{1-\nu^2} [2.5(s+3)(r+3) - \theta_0] 3 \, dr \, ds$$

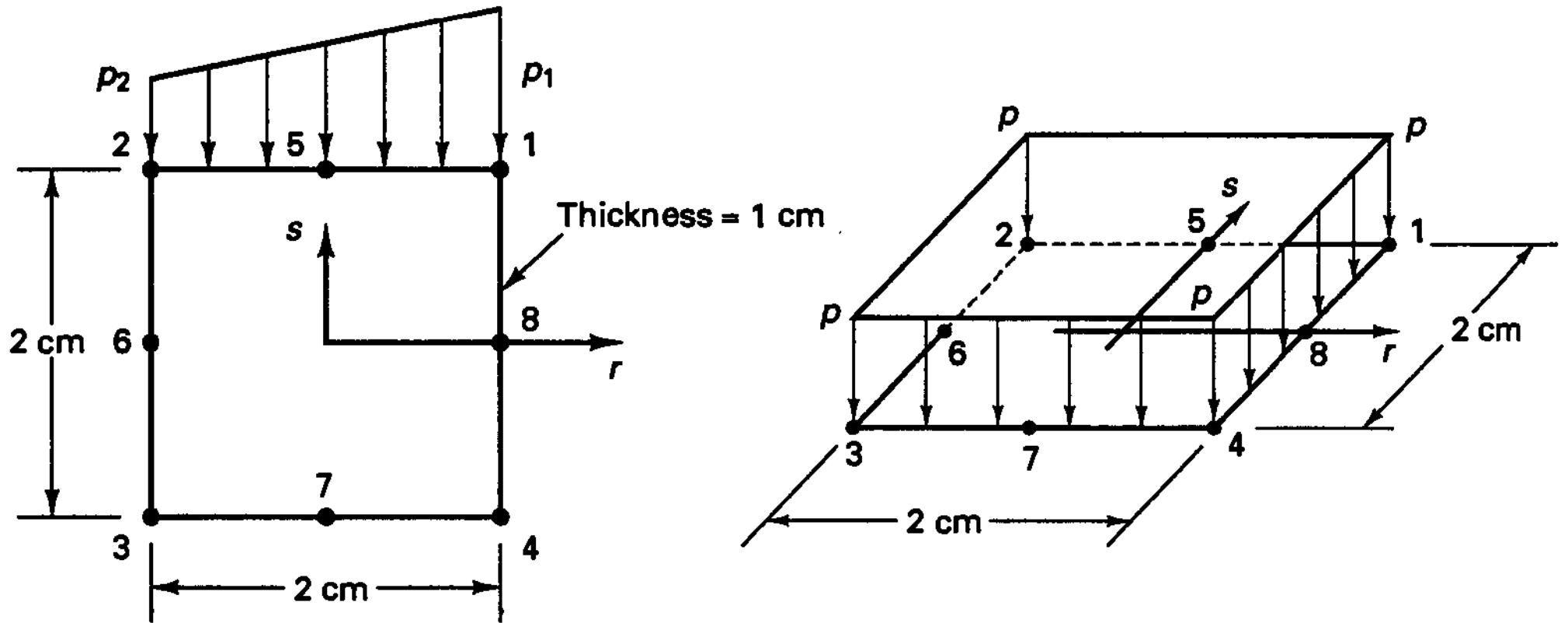
$$\mathbf{R}_T = -\frac{E\alpha}{(1-\nu)} \begin{bmatrix} 37.5 - 1.5\theta_0 \\ 50 - 2\theta_0 \\ -37.5 + 1.5\theta_0 \\ 40 - 2\theta_0 \\ -30 + 1.5\theta_0 \\ -40 + 2\theta_0 \\ +30 - 1.5\theta_0 \\ -50 + 2\theta_0 \end{bmatrix}$$

The calculation of the initial stress force vector as performed here is a typical step in a thermal stress analysis. In a complete thermal stress analysis the temperatures are calculated as described in Section 7.2, the element load vectors due to the thermal effects are evaluated as illustrated in this example, and the solution of the equilibrium equations (4.17) of the complete element assemblage then yields the nodal point displacements. The element total strains ϵ are evaluated from the nodal point displacements and then, using (a), the final element stresses are calculated.

EXAMPLE 5.12: Consider the elements in Fig. E5.12. Evaluate the consistent nodal point forces corresponding to the surface loading (assuming that the nodal point forces are positive when acting in the direction of the pressure).

Here we want to evaluate

$$\mathbf{R}_S = \int_S \mathbf{H}^T \mathbf{f}^S \, dS$$



(a) Two-dimensional element subjected to linearly varying pressure along one side

(b) Flat surface of three-dimensional element subjected to constant pressure p

Figure E5.12 Two- and three-dimensional elements subjected to pressure loading

Consider first the two-dimensional element. Since $s = +1$ at the edge 1-2, we have, using the interpolation functions for the eight-node element (see Fig. 5.4),

$$h_s = \frac{1}{2}(1 - r^2)(1 + s)|_{s=+1} = 1 - r^2$$

$$h_1 = \frac{1}{4}(1 + r)(1 + s)(r + s - 1)|_{s=+1} = \frac{1}{2}r(1 + r)$$

$$h_2 = \frac{1}{4}(1 - r)(1 + s)(s - r - 1)|_{s=+1} = -\frac{1}{2}r(1 - r)$$

which are equal to the interpolation functions of the three-node bar in Fig. E5.2. Hence

$$\begin{bmatrix} u^s \\ v^s \end{bmatrix} = \begin{bmatrix} \frac{1}{2}r(1 + r) & 0 & -\frac{1}{2}r(1 - r) & 0 & (1 - r^2) & 0 \\ 0 & \frac{1}{2}r(1 + r) & 0 & -\frac{1}{2}r(1 - r) & 0 & (1 - r^2) \end{bmatrix} \begin{bmatrix} u_1 \\ v_1 \\ u_2 \\ v_2 \\ u_s \\ v_s \end{bmatrix}$$

Also,
$$\mathbf{f}^s = \begin{bmatrix} f_r^s \\ f_s^s \end{bmatrix} = \begin{bmatrix} 0 \\ \frac{1}{2}(1 + r)p_1 + \frac{1}{2}(1 - r)p_2 \end{bmatrix}; \quad \det \mathbf{J}^s = 1$$

Hence,

$$\mathbf{R}_s = \int_{-1}^{+1} \frac{t}{2} \begin{bmatrix} r(1 + r) & 0 \\ 0 & r(1 + r) \\ -r(1 - r) & 0 \\ 0 & -r(1 - r) \\ 2(1 - r^2) & 0 \\ 0 & 2(1 - r^2) \end{bmatrix} \frac{1}{2} \begin{bmatrix} 0 \\ (1 + r)p_1 + (1 - r)p_2 \end{bmatrix} dr$$

$$\mathbf{R}_s = \frac{1}{3} \begin{bmatrix} 0 \\ p_1 \\ 0 \\ p_2 \\ 0 \\ 2(p_1 + p_2) \end{bmatrix} \tag{a}$$

For the three-dimensional element we proceed similarly. Since the surface is flat and the loading is normal to it, only the nodal point forces normal to the surface are nonzero [see also (a)]. Also, by symmetry, we know that the forces at nodes 1, 2, 3, 4 and 5, 6, 7, 8 are equal, respectively. Using the interpolation functions of Fig. 5.4, we have for the force at node 1,

$$R_1 = p \int_{-1}^{+1} \int_{-1}^{+1} \frac{1}{4} (1+r)(1+s)(r+s-1) dr ds = -\frac{1}{3} p$$

and for the force at node 5,

$$R_5 = p \int_{-1}^{+1} \int_{-1}^{+1} \frac{1}{2} (1-r^2)(1+s) dr ds = \frac{4}{3} p$$

The total pressure loading on the surface is $4p$, which, as a check, is equal to the sum of all the nodal point forces. However, it should be noted that the consistent nodal point forces at the corners of the element act in the direction opposite that of the pressure!

EXAMPLE 5.13: Calculate the deflection u_A of the structural model shown in Fig. E5.13.

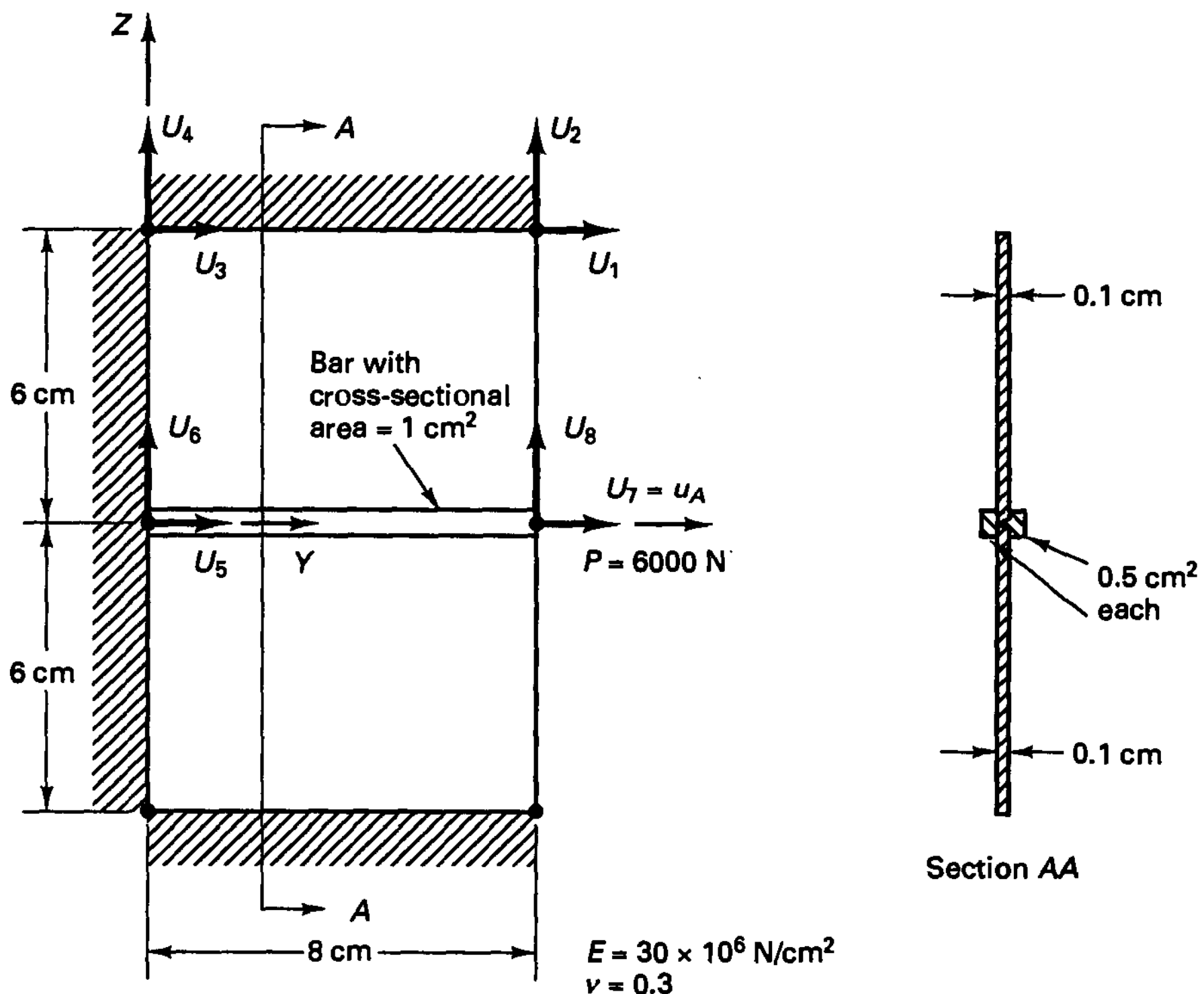


Figure E5.13 A simple structural model

Because of the symmetry and boundary conditions, we need to evaluate only the stiffness coefficient corresponding to u_A . Here we have for the four-node element,

$$\mathbf{J} = \begin{bmatrix} 4 & 0 \\ 0 & 3 \end{bmatrix}; \quad \mathbf{B} = \frac{1}{48} \begin{bmatrix} \dots & 3(1-s) & \dots \\ \dots & 0 & \dots \\ \dots & -4(1+r) & \dots \end{bmatrix}$$

$$k_{77} = \int_{-1}^{+1} \int_{-1}^{+1} \left(\frac{1}{48}\right)^2 \frac{E}{1-\nu^2} [3(1-s) \mid 0 \mid -4(1+r)] \begin{bmatrix} 3(1-s) \\ 3\nu(1-s) \\ -2(1-\nu)(1+r) \end{bmatrix} (12)(0.1) dr ds$$

or $k_{77} = 1,336,996.34 \text{ N/cm}$

Also, the stiffness of the truss is AE/L , or

$$k = \frac{(1)(30 \times 10^6)}{8} = 3,750,000 \text{ N/cm}$$

Hence $k_{\text{total}} = 6.424 \times 10^6 \text{ N/cm}$

and $u_A = 9.34 \times 10^{-4} \text{ cm}$

EXAMPLE 5.14: Consider the five-node element in Fig. E5.14. Evaluate the consistent nodal point forces corresponding to the stresses given.

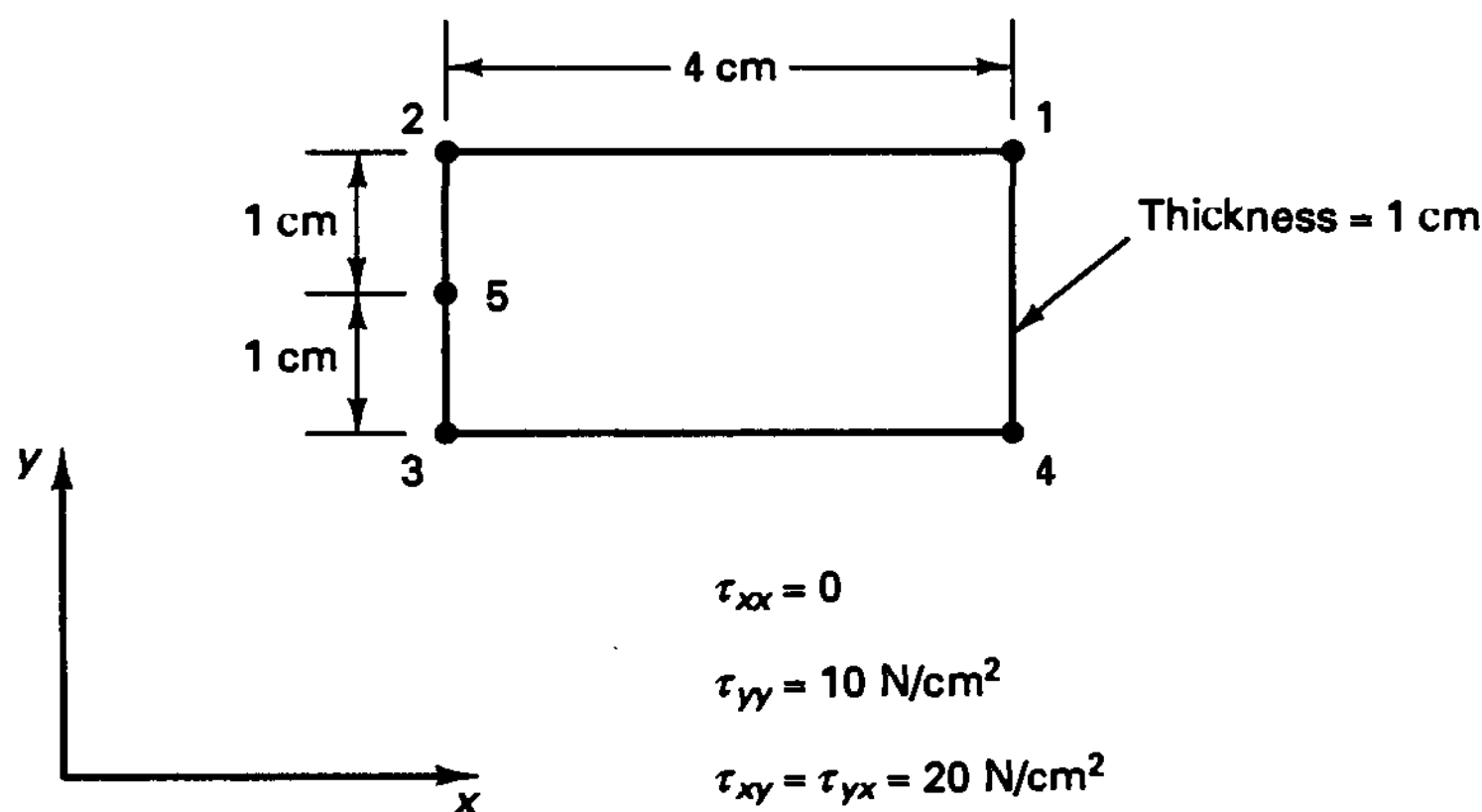


Figure E5.14 Five-node element with stresses given

Using the interpolation functions in Fig. 5.4, we can evaluate the strain-displacement matrix of the element:

$$\mathbf{B} = \frac{1}{8} \begin{bmatrix} (1+s) & 0 & -s(1+s) & 0 & s(1-s) \\ 0 & 2(1+r) & 0 & 2(1-r)(1+2s) & 0 \\ 2(1+r) & (1+s) & 2(1-r)(1+2s) & -s(1+s) & -2(1-r)(1-2s) \\ 0 & (1-s) & 0 & -2(1-s^2) & 0 \\ -2(1-r)(1-2s) & 0 & -2(1+r) & 0 & -8(1-r)s \\ s(1-s) & -2(1+r) & (1-s) & -8(1-r)s & -2(1-s^2) \end{bmatrix}$$

where we used
$$\mathbf{J} = \begin{bmatrix} 2 & 0 \\ 0 & 1 \end{bmatrix}$$

The required nodal point forces can now be evaluated using (5.35); hence,

$$\mathbf{R}_I = \int_{-1}^{+1} \int_{-1}^{+1} \mathbf{B}^T \begin{bmatrix} 0 \\ 10 \\ 20 \end{bmatrix} (2) dr ds$$

which gives

$$\mathbf{R}_I^T = [40 \quad 40 \quad 40 \quad \frac{40}{3} \quad -40 \quad -\frac{80}{3} \quad -40 \quad 0 \quad 0 \quad -\frac{80}{3}]$$

It should be noted that the forces in this vector are also equal to the nodal point consistent forces that correspond to the (constant) surface tractions, which are in equilibrium with the internal stresses given in Fig. E.5.14.

Earlier we mentioned briefly the possible use of *subparametric* elements: here the geometry is interpolated to a lower degree than the displacements. In the above examples, the nodes corresponding to the higher-order interpolation functions (nodes 5 and higher for the two-dimensional elements) were always placed at their “natural” positions so that the Jacobian matrix would be the same if, for the geometry interpolation, only the “basic” lower-order functions were used. Hence, in this case the subparametric two-dimensional element, using only the four corner nodes for the interpolation of the geometry, gives the same element matrices as the isoparametric element. For instance, in Example 5.14, the Jacobian matrix \mathbf{J} would be the same using only the basic four-node interpolation functions, and hence the vector \mathbf{R}_I for the subparametric element (using the four corner nodes for the geometry interpolation and the five nodes for the displacement interpolation) would be the same as for the isoparametric five-node element.

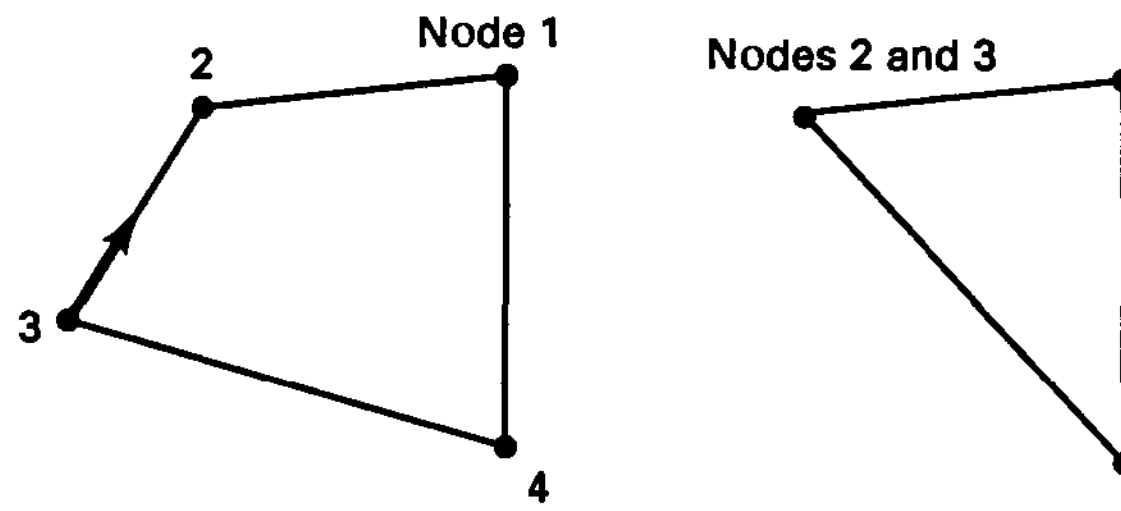
However, while the use of subparametric elements decreases somewhat the computational effort, such use also limits the generality of the finite element discretization and in addition complicates the solution procedures considerably in geometrically nonlinear analysis (where the new geometry of an element is obtained by adding the displacements to the previous geometry; see Chapter 6).

5.3.2 Triangular Elements

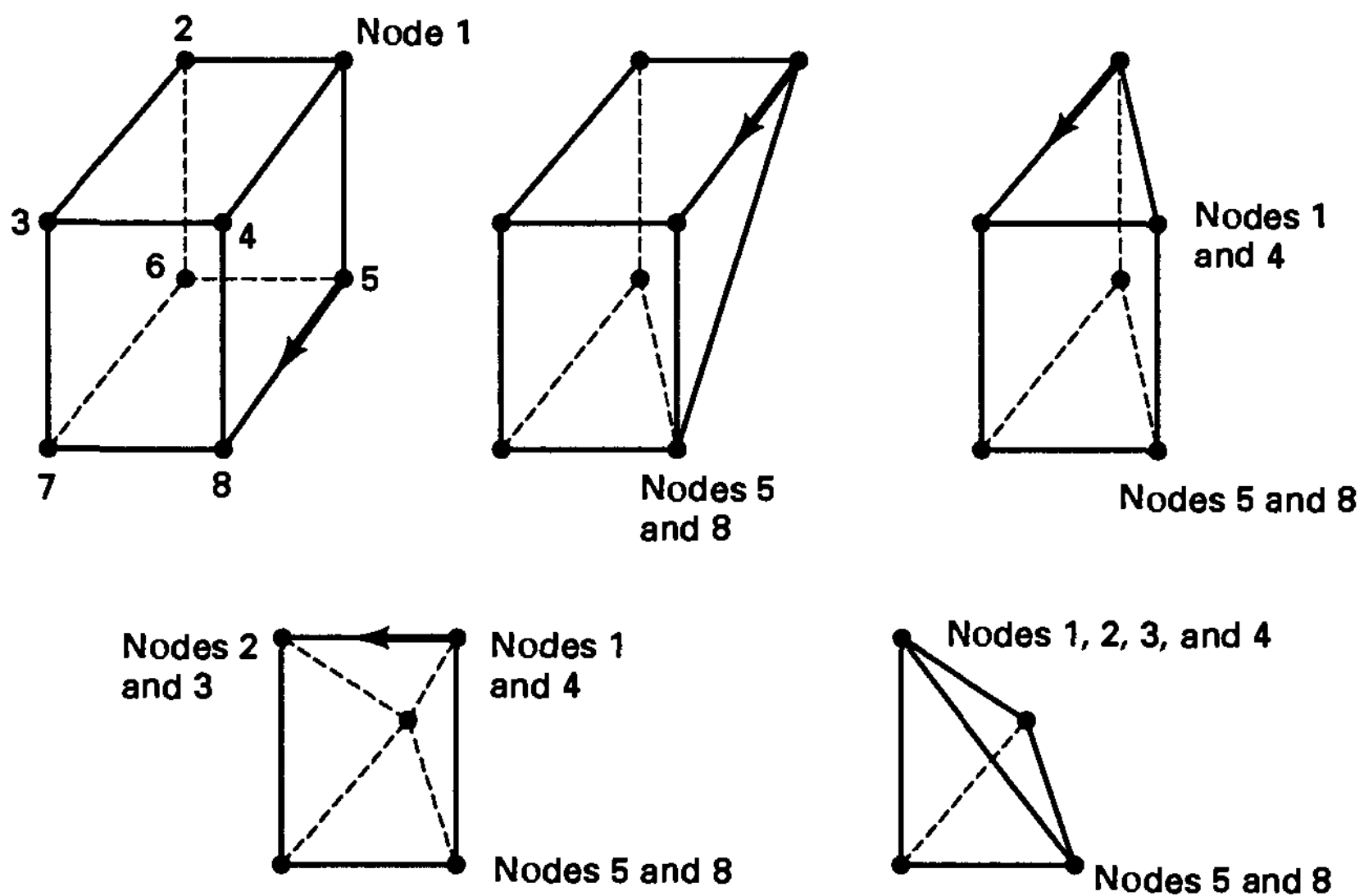
In the previous section we discussed quadrilateral isoparametric elements that can be used to model very general geometries. However, in some cases the use of triangular or wedge elements may be attractive. Triangular elements can be formulated using different approaches, which we briefly discuss in this section.

Triangular Elements Formulated by Collapsing Quadrilateral Elements

Since the elements discussed in Section 5.3.1 can be distorted, as shown for example in Fig. 5.2, a natural way of generating triangular elements appears to be to simply distort the basic quadrilateral element into the required triangular form (see Fig. 5.7). This is achieved in practice by assigning the same global node to two corner nodes of the element. We demonstrate this procedure in the following example.



(a) Degeneration of 4-node to 3-node two-dimensional element



(b) Degenerate forms of 8-node three-dimensional element

Figure 5.7 Degenerate forms of four- and eight-node elements of Figs. 5.4 and 5.5

EXAMPLE 5.15: Show that by collapsing the side 1-2 of the four-node quadrilateral element in Fig. E5.15 a constant strain triangle is obtained.

Using the interpolation functions of Fig. 5.4, we have

$$x = \frac{1}{4}(1 + r)(1 + s)x_1 + \frac{1}{4}(1 - r)(1 + s)x_2 + \frac{1}{4}(1 - r)(1 - s)x_3 + \frac{1}{4}(1 + r)(1 - s)x_4$$

$$y = \frac{1}{4}(1 + r)(1 + s)y_1 + \frac{1}{4}(1 - r)(1 + s)y_2 + \frac{1}{4}(1 - r)(1 - s)y_3 + \frac{1}{4}(1 + r)(1 - s)y_4$$

Thus, using the conditions $x_1 = x_2$ and $y_1 = y_2$, we obtain

$$x = \frac{1}{2}(1 + s)x_2 + \frac{1}{4}(1 - r)(1 - s)x_3 + \frac{1}{4}(1 + r)(1 - s)x_4$$

$$y = \frac{1}{2}(1 + s)y_2 + \frac{1}{4}(1 - r)(1 - s)y_3 + \frac{1}{4}(1 + r)(1 - s)y_4$$

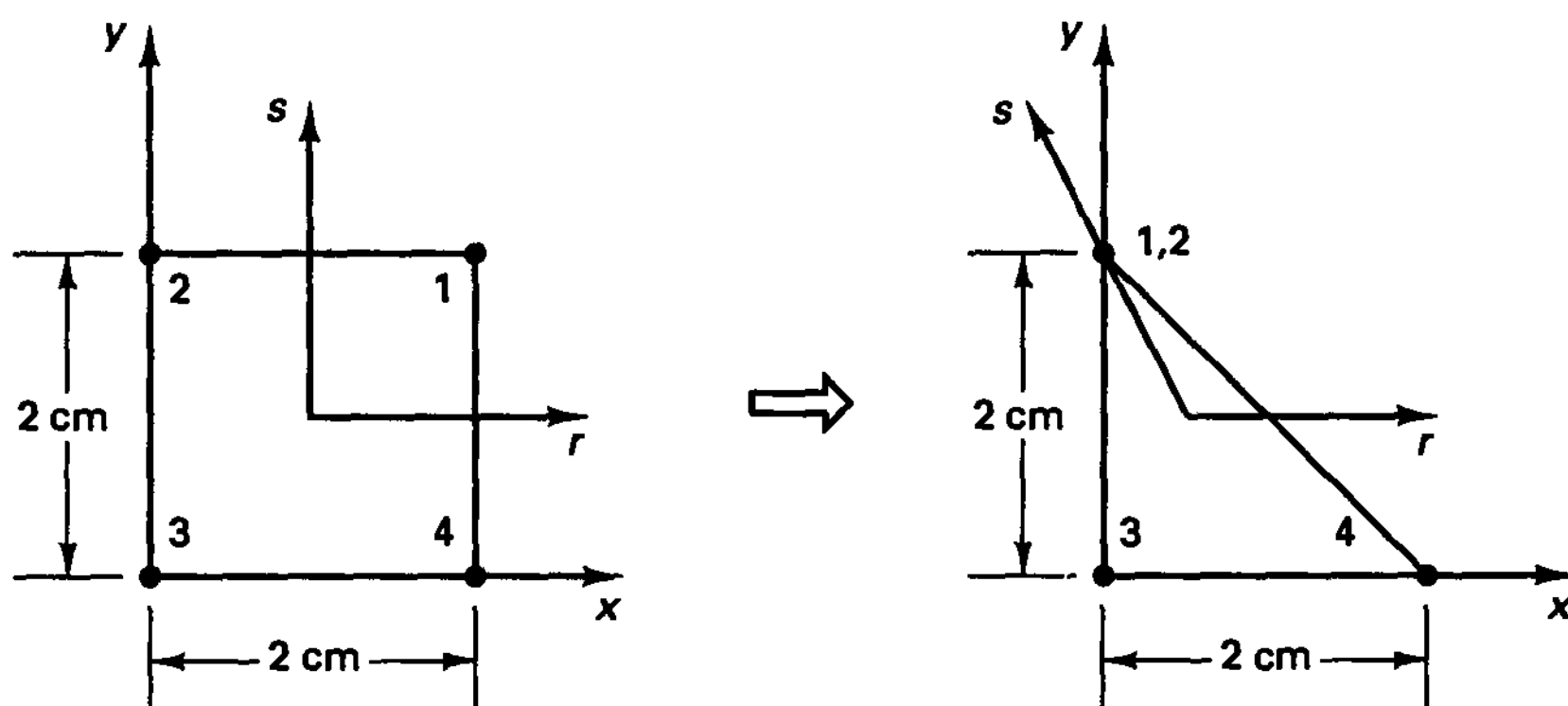


Figure E5.15 Collapsing a plane stress four-node element to a triangular element

and hence with the nodal coordinates given in Fig. E5.15,

$$x = \frac{1}{2}(1 + r)(1 - s)$$

$$y = 1 + s$$

It follows that

$$\begin{aligned} \frac{\partial x}{\partial r} &= \frac{1}{2}(1 - s) & \frac{\partial y}{\partial r} &= 0 \\ \frac{\partial x}{\partial s} &= -\frac{1}{2}(1 + r) & \frac{\partial y}{\partial s} &= 1 \end{aligned}; \quad \mathbf{J} = \frac{1}{2} \begin{bmatrix} (1 - s) & 0 \\ -(1 + r) & 2 \end{bmatrix}; \quad \mathbf{J}^{-1} = \begin{bmatrix} \frac{2}{1 - s} & 0 \\ \frac{1 + r}{1 - s} & 1 \end{bmatrix}$$

Using the isoparametric assumption, we also have

$$u = \frac{1}{2}(1 + s)u_2 + \frac{1}{4}(1 - r)(1 - s)u_3 + \frac{1}{4}(1 + r)(1 - s)u_4$$

$$v = \frac{1}{2}(1 + s)v_2 + \frac{1}{4}(1 - r)(1 - s)v_3 + \frac{1}{4}(1 + r)(1 - s)v_4$$

$$\frac{\partial u}{\partial r} = -\frac{1}{4}(1 - s)u_3 + \frac{1}{4}(1 - s)u_4; \quad \frac{\partial v}{\partial r} = -\frac{1}{4}(1 - s)v_3 + \frac{1}{4}(1 - s)v_4$$

$$\frac{\partial u}{\partial s} = \frac{1}{2}u_2 - \frac{1}{4}(1 - r)u_3 - \frac{1}{4}(1 + r)u_4; \quad \frac{\partial v}{\partial s} = \frac{1}{2}v_2 - \frac{1}{4}(1 - r)v_3 - \frac{1}{4}(1 + r)v_4$$

$$\begin{bmatrix} \frac{\partial}{\partial x} \\ \frac{\partial}{\partial y} \end{bmatrix} = \mathbf{J}^{-1} \begin{bmatrix} \frac{\partial}{\partial r} \\ \frac{\partial}{\partial s} \end{bmatrix}$$

Hence,

$$\begin{bmatrix} \frac{\partial u}{\partial x} \\ \frac{\partial u}{\partial y} \end{bmatrix} = \begin{bmatrix} \frac{2}{1 - s} & 0 \\ \frac{1 + r}{1 - s} & 1 \end{bmatrix} \begin{bmatrix} 0 & 0 & -\frac{1}{4}(1 - s) & 0 & \frac{1}{4}(1 - s) & 0 \\ \frac{1}{2} & 0 & -\frac{1}{4}(1 - r) & 0 & -\frac{1}{4}(1 + r) & 0 \end{bmatrix} \begin{bmatrix} u_2 \\ v_2 \\ u_3 \\ v_3 \\ u_4 \\ v_4 \end{bmatrix}$$

and

$$\begin{bmatrix} \frac{\partial u}{\partial x} \\ \frac{\partial u}{\partial y} \end{bmatrix} = \begin{bmatrix} 0 & 0 & -\frac{1}{2} & 0 & \frac{1}{2} & 0 \\ \frac{1}{2} & 0 & -\frac{1}{2} & 0 & 0 & 0 \end{bmatrix} \begin{bmatrix} u_2 \\ \vdots \\ u_4 \\ v_4 \end{bmatrix}$$

Similarly,

$$\begin{bmatrix} \frac{\partial v}{\partial x} \\ \frac{\partial v}{\partial y} \end{bmatrix} = \begin{bmatrix} 0 & 0 & 0 & -\frac{1}{2} & 0 & \frac{1}{2} \\ 0 & \frac{1}{2} & 0 & -\frac{1}{2} & 0 & 0 \end{bmatrix} \begin{bmatrix} u_2 \\ \vdots \\ u_4 \\ v_4 \end{bmatrix}$$

So we obtain

$$\boldsymbol{\epsilon} = \begin{bmatrix} 0 & 0 & -\frac{1}{2} & 0 & \frac{1}{2} & 0 \\ 0 & \frac{1}{2} & 0 & -\frac{1}{2} & 0 & 0 \\ \frac{1}{2} & 0 & -\frac{1}{2} & -\frac{1}{2} & 0 & \frac{1}{2} \end{bmatrix} \begin{bmatrix} u_2 \\ v_2 \\ u_3 \\ v_3 \\ u_4 \\ v_4 \end{bmatrix}$$

For any values of $u_2, v_2, u_3, v_3,$ and u_4, v_4 the strain vector is constant and independent of r, s . Thus, the triangular element is a constant strain triangle.

In the preceding example we considered only one specific case. However, using the same approach it is apparent that collapsing any one side of a four-node plane stress or plane strain element will always result in a constant strain triangle.

In considering the process of collapsing an element side, it is interesting to note that in the formulation used in Example 5.15 the matrix \mathbf{J} is singular at $s = +1$, but that this singularity disappears when the strain-displacement matrix is calculated. A practical consequence is that if in a computer program the general formulation of the four-node element is employed to generate a constant strain triangle (as in Example 5.15), the stresses should not be calculated at the two local nodes that have been assigned the same global node. (Since the stresses are constant throughout the element, they are conveniently evaluated at the center of the element, i.e., at $r = 0, s = 0$.)

The same procedure can also be employed in three-dimensional analysis in order to obtain, from the basic eight-node element, wedge or tetrahedral elements. The procedure is illustrated in Fig. 5.7 and in the following example.

EXAMPLE 5.16: Show that the three-dimensional tetrahedral element generated in Fig. E5.16 from the eight-node three-dimensional brick element is a constant strain element.

Here we proceed as in Example 5.15. Thus, using the interpolation functions of the brick element (see Fig. 5.5) and substituting the nodal point coordinates of the tetrahedron, we obtain

$$x = \frac{1}{4}(1 + r)(1 - s)(1 - t)$$

$$y = \frac{1}{2}(1 + s)(1 - t)$$

$$z = 1 + t$$

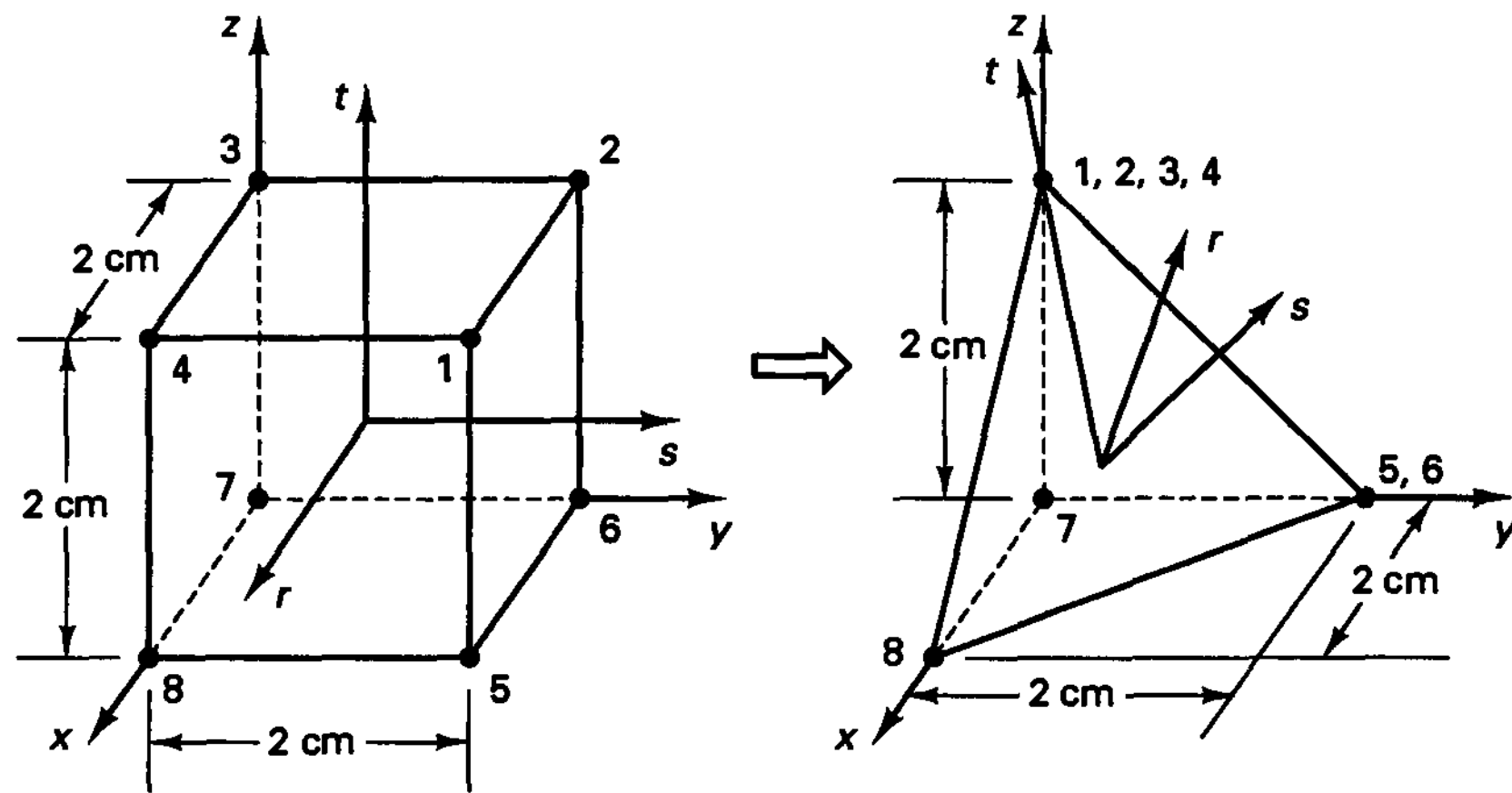


Figure E5.16 Collapsing an eight-node brick element into a tetrahedral element

Hence,

$$\mathbf{J} = \begin{bmatrix} \frac{1}{4}(1-s)(1-t) & 0 & 0 \\ -\frac{1}{4}(1+r)(1-t) & \frac{1}{2}(1-t) & 0 \\ -\frac{1}{4}(1+r)(1-s) & -\frac{1}{2}(1+s) & 1 \end{bmatrix};$$

$$\mathbf{J}^{-1} = \begin{bmatrix} \frac{4}{(1-s)(1-t)} & 0 & 0 \\ \frac{2(1+r)}{(1-s)(1-t)} & \frac{2}{1-t} & 0 \\ \frac{2(1+r)}{(1-s)(1-t)} & \frac{1+s}{1-t} & 1 \end{bmatrix} \tag{a}$$

Using the same interpolation functions for u , and the conditions that $u_1 = u_2 = u_3 = u_4$ and $u_5 = u_6$, we obtain

$$u = h_4^* u_4 + h_5^* u_5 + h_7^* u_7 + h_8^* u_8$$

with

$$h_4^* = \frac{1}{2}(1+t); \quad h_5^* = \frac{1}{4}(1+s)(1-t);$$

$$h_7^* = \frac{1}{8}(1-r)(1-s)(1-t); \quad h_8^* = \frac{1}{8}(1+r)(1-s)(1-t)$$

Similarly, we also have

$$v = h_4^* v_4 + h_5^* v_5 + h_7^* v_7 + h_8^* v_8$$

$$w = h_4^* w_4 + h_5^* w_5 + h_7^* w_7 + h_8^* w_8$$

Evaluating now the derivatives of the displacements u , v , and w with respect to r , s , and t , and using \mathbf{J}^{-1} of (a), we obtain

$$\begin{bmatrix} \frac{\partial u}{\partial x} \\ \frac{\partial v}{\partial y} \\ \frac{\partial w}{\partial z} \\ \frac{\partial u}{\partial y} + \frac{\partial v}{\partial x} \\ \frac{\partial v}{\partial z} + \frac{\partial w}{\partial y} \\ \frac{\partial u}{\partial z} + \frac{\partial w}{\partial x} \end{bmatrix} = \begin{bmatrix} 0 & 0 & 0 & 0 & 0 & 0 & -\frac{1}{2} & 0 & 0 & \frac{1}{2} & 0 & 0 \\ 0 & 0 & 0 & 0 & \frac{1}{2} & 0 & 0 & -\frac{1}{2} & 0 & 0 & 0 & 0 \\ 0 & 0 & \frac{1}{2} & 0 & 0 & 0 & 0 & 0 & -\frac{1}{2} & 0 & 0 & 0 \\ 0 & 0 & 0 & \frac{1}{2} & 0 & 0 & -\frac{1}{2} & -\frac{1}{2} & 0 & 0 & \frac{1}{2} & 0 \\ 0 & \frac{1}{2} & 0 & 0 & 0 & \frac{1}{2} & 0 & -\frac{1}{2} & -\frac{1}{2} & 0 & 0 & 0 \\ \frac{1}{2} & 0 & 0 & 0 & 0 & 0 & -\frac{1}{2} & 0 & -\frac{1}{2} & 0 & 0 & \frac{1}{2} \end{bmatrix} \begin{bmatrix} u_4 \\ v_4 \\ w_4 \\ \dots \\ u_5 \\ v_5 \\ w_5 \\ \dots \\ u_7 \\ v_7 \\ w_7 \\ \dots \\ u_8 \\ v_8 \\ w_8 \end{bmatrix}$$

Hence, the strains are constant for any nodal point displacements, which means that the element can represent only constant strain conditions.

The process of collapsing an element side, or in three-dimensional analysis a number of element sides, may directly yield a desired element, but when higher-order two- or three-dimensional elements are employed, some special considerations may be necessary regarding the interpolation functions used. Specifically, when the lower-order elements displayed in Fig. 5.7 are employed, spatially isotropic triangular and wedge elements are automatically generated, but this is not necessarily the case when using higher-order elements.

As an example, we consider the six-node triangular two-dimensional element obtained by collapsing one side of an eight-node element as shown in Fig. 5.8. If the triangular element has sides of equal length, we may want the element to be spatially isotropic; i.e.,

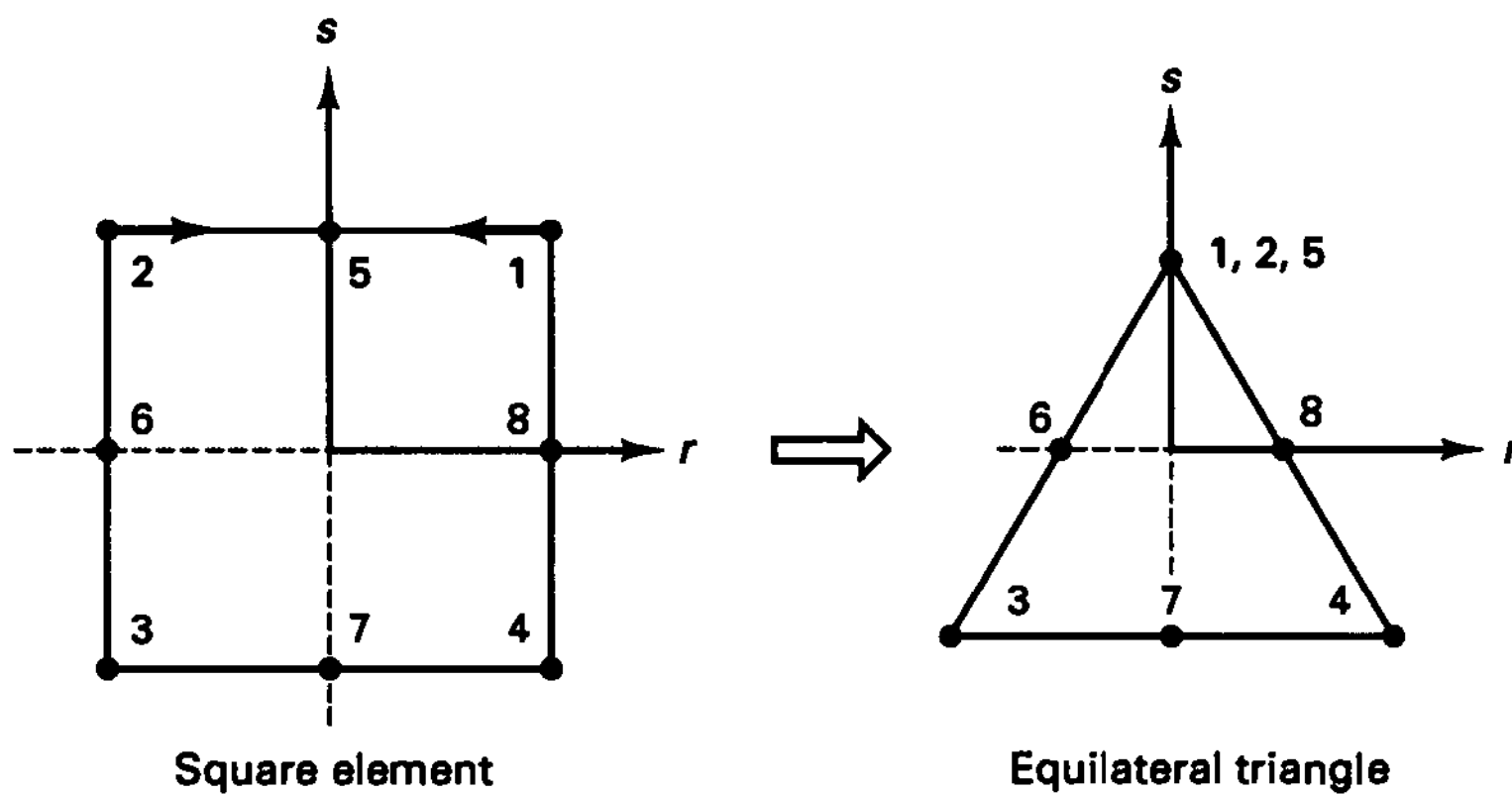


Figure 5.8 Collapsing an eight-node element into a triangle

we may wish the internal element displacements u and v to vary in the same manner for each corner nodal displacement and each midside nodal displacement, respectively. However, the interpolation functions that are generated for the triangle when the side 1-2-5 of the square is simply collapsed do not fulfill the requirement that we should be able to change the numbering of the vertices without a change in the displacement assumptions. In order to fulfill this requirement, corrections need be applied to the interpolation functions of the nodes 3, 4, and 7 to obtain the final interpolations h_i^* of the triangular element (see Exercise 5.25),

$$\begin{aligned}
 h_1^* &= \frac{1}{2}(1 + s) - \frac{1}{2}(1 - s^2) \\
 h_3^* &= \frac{1}{4}(1 - r)(1 - s) - \frac{1}{4}(1 - s^2)(1 - r) - \frac{1}{4}(1 - r^2)(1 - s) + \Delta h \\
 h_4^* &= \frac{1}{4}(1 + r)(1 - s) - \frac{1}{4}(1 - r^2)(1 - s) - \frac{1}{4}(1 - s^2)(1 + r) + \Delta h \\
 h_6^* &= \frac{1}{2}(1 - s^2)(1 - r) \\
 h_7^* &= \frac{1}{2}(1 - r^2)(1 - s) - 2\Delta h \\
 h_8^* &= \frac{1}{2}(1 - s^2)(1 + r)
 \end{aligned} \tag{5.36}$$

where we added the appropriate interpolations given in Fig. 5.4 and

$$\Delta h = \frac{(1 - r^2)(1 - s^2)}{8} \tag{5.37}$$

Thus, to generate higher-order triangular elements by collapsing sides of square elements, it may be necessary to apply a correction to the interpolation functions used.

Triangular Elements in Fracture Mechanics

In the preceding considerations, we assumed that a spatially isotropic element was desirable because the element was to be employed in a finite element assemblage used to predict a somewhat homogeneous stress field. However, in some cases, very specific stress variations are to be predicted, and in such analyses a spatially nonisotropic element may be more effective. One area of analysis in which specific spatially nonisotropic elements are employed is the field of fracture mechanics. Here it is known that specific stress singularities exist at crack tips, and for the calculation of stress intensity factors or limit loads, the use of finite elements that contain the required stress singularities can be effective. Various elements of this sort have been designed, but very simple and attractive elements can be obtained by distorting the higher-order isoparametric elements (see R. D. Henshell and K. G. Shaw [A] and R. S. Barsoum [A, B]). Figure 5.9 shows two-dimensional isoparametric elements that have been employed with much success in linear and nonlinear fracture mechanics because they contain the $1/\sqrt{R}$ and $1/R$ strain singularities, respectively. We should note that these elements have the interpolation functions given in (5.36) but with $\Delta h = 0$. The same node-shifting and side-collapsing procedures can also be employed with higher-order three-dimensional elements in order to generate the required singularities. We demonstrate the procedure of node shifting to generate a strain singularity in the following example.

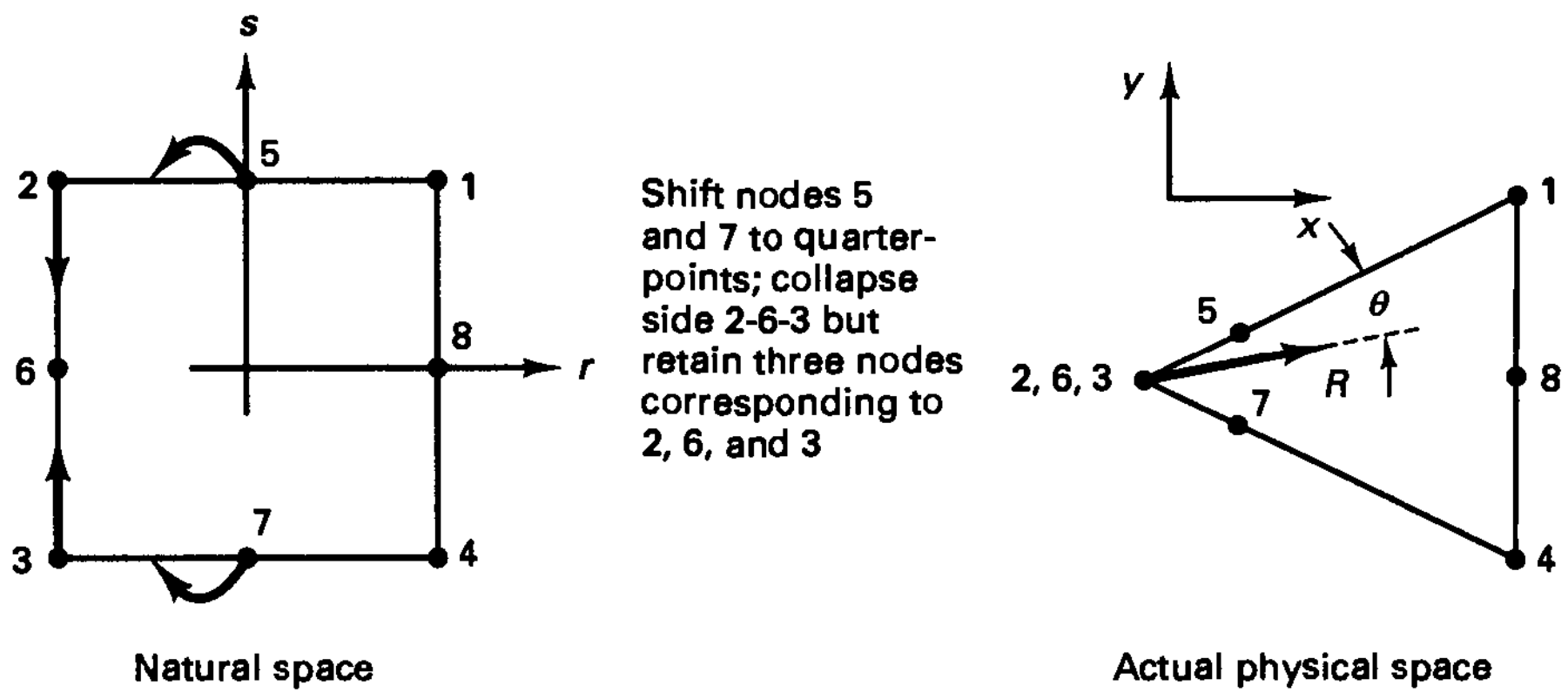
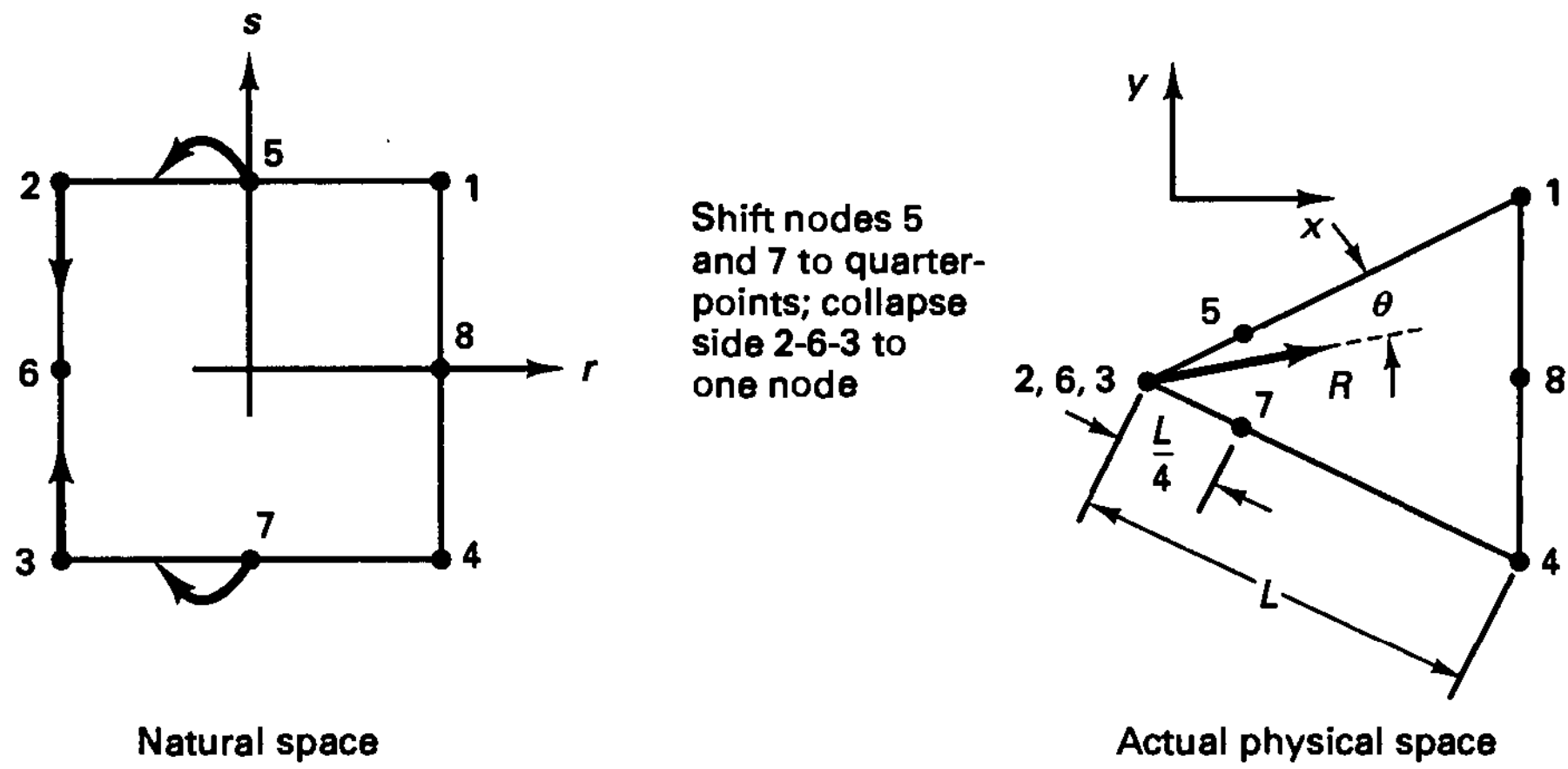
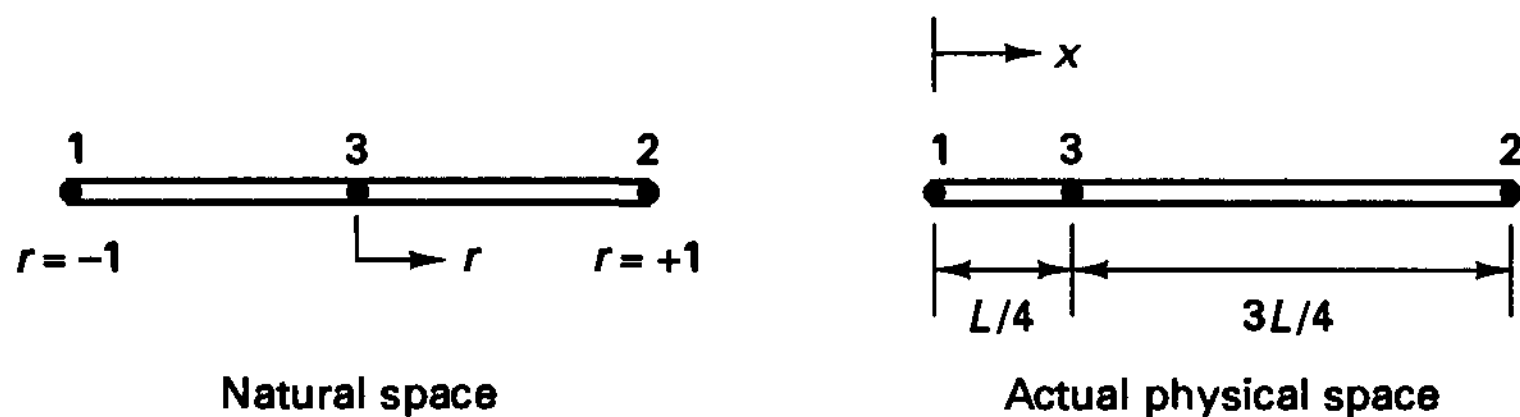


Figure 5.9 Two-dimensional distorted (quarter point) isoparametric elements useful in fracture mechanics. Strain singularities are within the element for any angle θ . [Note that in (a) the one node (2-6-3) has two degrees of freedom, and that in (b) nodes 2, 3, and 6 each have two degrees of freedom.]

EXAMPLE 5.17: Consider the three-node truss element in Fig. E5.17. Show that when node 3 is specified to be at the quarter-point, the strain has a singularity of $1/\sqrt{x}$ at node 1.



We have already considered a three-node truss in Example 5.2. Proceeding as before, we now have

$$x = \frac{r}{2}(1+r)L + (1-r^2)\frac{L}{4}$$

or

$$x = \frac{L}{4}(1+r)^2 \tag{a}$$

Hence,

$$\mathbf{J} = \left[\frac{L}{2} + \frac{r}{2}L \right]$$

and the strain-displacement matrix is [using (b) in Example 5.2]

$$\mathbf{B} = \left[\frac{1}{L/2 + rL/2} \right] \left[\left(-\frac{1}{2} + r \right) \quad \left(\frac{1}{2} + r \right) \quad -2r \right] \tag{b}$$

To show the $1/\sqrt{x}$ singularity we need to express r in terms of x . Using (a), we have

$$r = 2\sqrt{\frac{x}{L}} - 1$$

Substituting this value for r into (b), we obtain

$$\mathbf{B} = \left[\left(\frac{2}{L} - \frac{3}{2\sqrt{L}} \frac{1}{\sqrt{x}} \right) \quad \left(\frac{2}{L} - \frac{1}{2\sqrt{L}} \frac{1}{\sqrt{x}} \right) \quad \left(\frac{2}{\sqrt{L}} \frac{1}{\sqrt{x}} - \frac{4}{L} \right) \right]$$

Hence at $x = 0$ the quarter-point element in Fig. E5.17 has a strain singularity of order $1/\sqrt{x}$.

Triangular Elements by Area Coordinates

Although the procedure of distorting a rectangular isoparametric element to generate a triangular element can be effective in some cases as discussed above, triangular elements (and in particular spatially isotropic elements) can be constructed directly by using area coordinates. For the triangle in Fig. 5.10, the position of a typical interior point P with coordinates x and y is defined by the area coordinates

$$L_1 = \frac{A_1}{A}; \quad L_2 = \frac{A_2}{A}; \quad L_3 = \frac{A_3}{A} \tag{5.38}$$

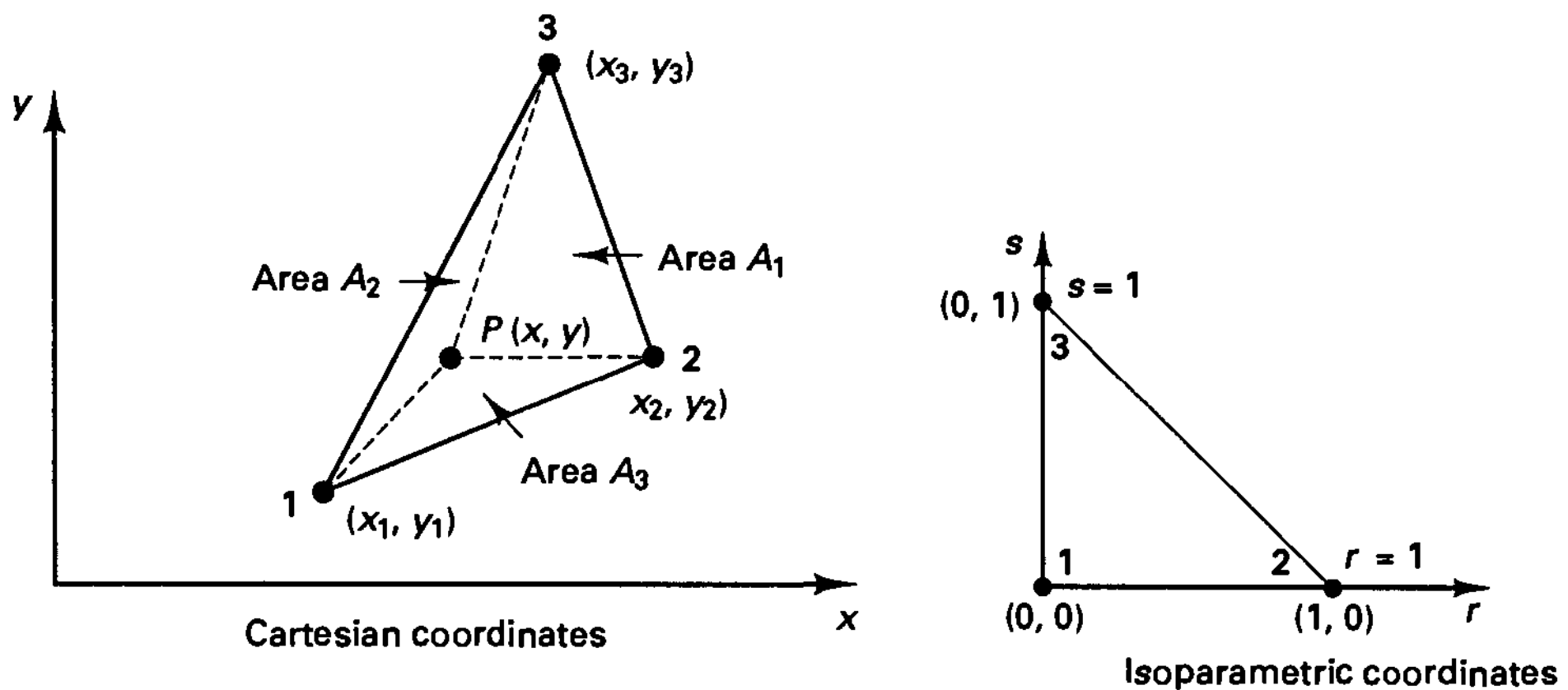


Figure 5.10 Description of three-node triangle

where the areas $A_i, i = 1, 2, 3$, are defined in the figure and A is the total area of the triangle. Thus, we also have

$$L_1 + L_2 + L_3 = 1 \tag{5.39}$$

Since element strains are obtained by taking derivatives with respect to the Cartesian coordinates, we need a relation that gives the area coordinates in terms of the coordinates x and y . Here we have

$$x = L_1x_1 + L_2x_2 + L_3x_3 \tag{5.40}$$

$$y = L_1y_1 + L_2y_2 + L_3y_3 \tag{5.41}$$

because these relations hold at points 1, 2, and 3 and x and y vary linearly in between. Using (5.39) to (5.41), we have

$$\begin{bmatrix} 1 \\ x \\ y \end{bmatrix} = \begin{bmatrix} 1 & 1 & 1 \\ x_1 & x_2 & x_3 \\ y_1 & y_2 & y_3 \end{bmatrix} \begin{bmatrix} L_1 \\ L_2 \\ L_3 \end{bmatrix} \tag{5.42}$$

which gives
$$L_i = \frac{1}{2A} (a_i + b_i x + c_i y); \quad i = 1, 2, 3$$

where

$$\begin{aligned} 2A &= x_1y_2 + x_2y_3 + x_3y_1 - y_1x_2 - y_2x_3 - y_3x_1 \\ a_1 &= x_2y_3 - x_3y_2; & a_2 &= x_3y_1 - x_1y_3; & a_3 &= x_1y_2 - x_2y_1 \\ b_1 &= y_2 - y_3; & b_2 &= y_3 - y_1; & b_3 &= y_1 - y_2 \\ c_1 &= x_3 - x_2; & c_2 &= x_1 - x_3; & c_3 &= x_2 - x_1 \end{aligned} \tag{5.43}$$

As must have been expected, these L_i are equal to the interpolation functions of a constant strain triangle. Thus, in summary we have for the three-node triangular element in Fig. 5.10,

$$\begin{aligned} u &= \sum_{i=1}^3 h_i u_i; & x &\equiv \sum_{i=1}^3 h_i x_i \\ v &= \sum_{i=1}^3 h_i v_i; & y &\equiv \sum_{i=1}^3 h_i y_i \end{aligned} \tag{5.44}$$

where $h_i = L_i, i = 1, 2, 3$, and the h_i are functions of the coordinates x and y .

Using the relations in (5.44), the various finite element matrices of (5.27) to (5.35) can be directly evaluated. However, just as in the formulation of the quadrilateral elements (see Section 5.3.1), in practice, it is frequently expedient to use a natural coordinate space in order to describe the element coordinates and displacements. Using the natural coordinate system shown in Fig. 5.10, we have

$$h_1 = 1 - r - s; \quad h_2 = r; \quad h_3 = s \tag{5.45}$$

and the evaluation of the element matrices now involves a Jacobian transformation. Furthermore, all integrations are carried out over the natural coordinates; i.e., the r integrations go from 0 to 1 and the s integrations go from 0 to $(1 - r)$.

EXAMPLE 5.18: Using the isoparametric natural coordinate system in Fig. 5.10, establish the displacement and strain-displacement interpolation matrices of a three-node triangular element with

$$\begin{aligned} x_1 &= 0; & x_2 &= 4; & x_3 &= 1 \\ y_1 &= 0; & y_2 &= 0; & y_3 &= 3 \end{aligned}$$

In this case we have, using (5.44),

$$\begin{aligned} x &= 4r + s \\ y &= 3s \end{aligned}$$

Hence, using (5.23),

$$\mathbf{J} = \begin{bmatrix} 4 & 0 \\ 1 & 3 \end{bmatrix}$$

and

$$\frac{\partial}{\partial \mathbf{x}} = \frac{1}{12} \begin{bmatrix} 3 & 0 \\ -1 & 4 \end{bmatrix} \frac{\partial}{\partial \mathbf{r}}$$

It follows that

$$\mathbf{H} = \begin{bmatrix} (1 - r - s) & 0 & \vdots & r & 0 & \vdots & s & 0 \\ 0 & (1 - r - s) & \vdots & 0 & r & \vdots & 0 & s \end{bmatrix}$$

and

$$\mathbf{B} = \frac{1}{12} \begin{bmatrix} -3 & 0 & \vdots & 3 & 0 & \vdots & 0 & 0 \\ 0 & -3 & \vdots & 0 & -1 & \vdots & 0 & 4 \\ -3 & -3 & \vdots & -1 & 3 & \vdots & 4 & 0 \end{bmatrix}$$

By analogy to the formulation of higher-order quadrilateral elements, we can also directly formulate higher-order triangular elements. Using the natural coordinate system in Fig. 5.10, which reduces to

$$L_1 = 1 - r - s; \quad L_2 = r; \quad L_3 = s \tag{5.46}$$

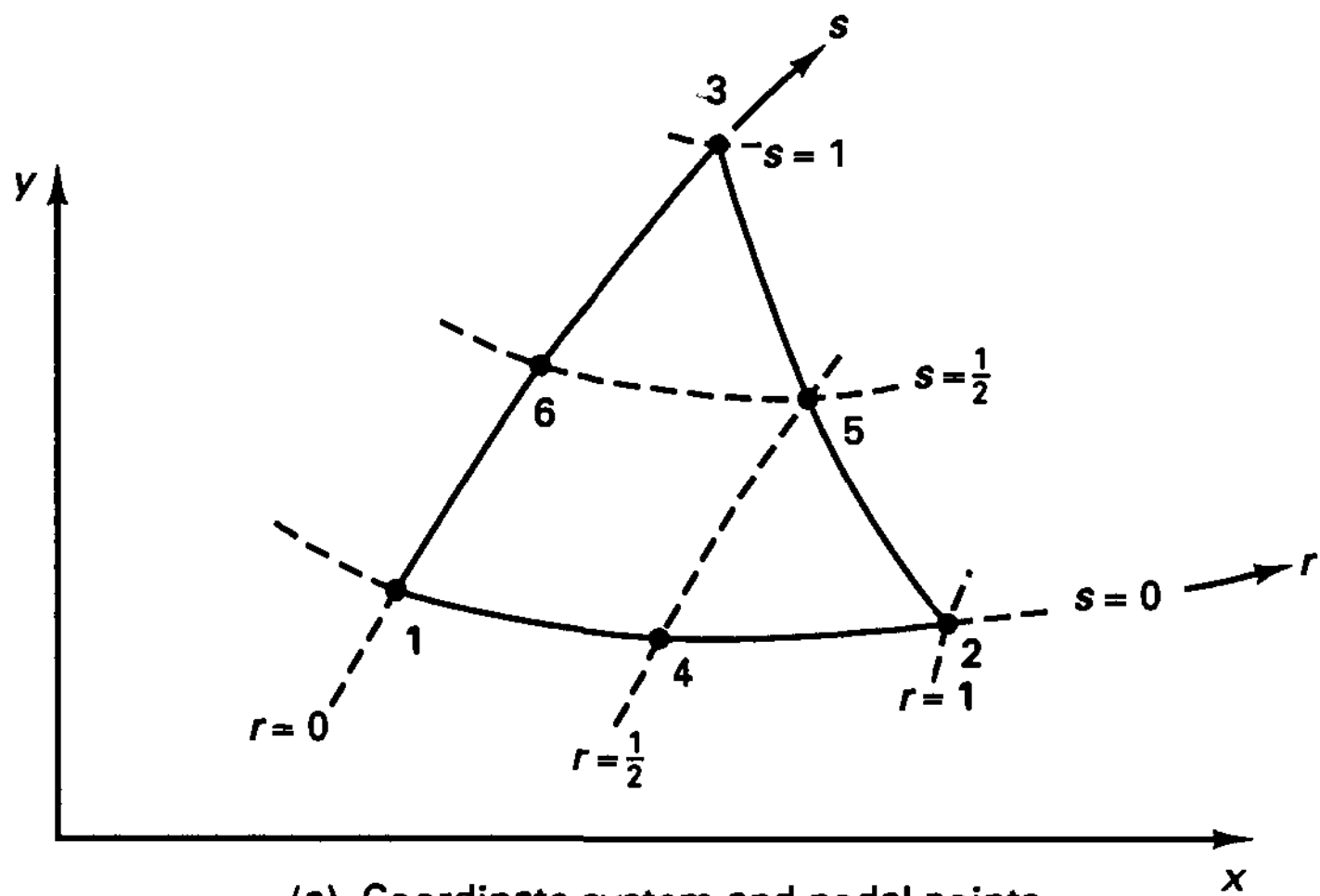
where the L_i are the area coordinates of the “unit triangle,” the interpolation functions of a 3 to 6 variable-number-nodes element are given in Fig. 5.11. These functions are constructed in the usual way, namely, h_i must be unity at node i and zero at all other nodes (see Example 5.1).² The interpolation functions of still higher-order triangular elements are obtained in a similar manner. Then the “cubic bubble function” $L_1L_2L_3$ is also employed.

Using this approach we can now also directly construct the interpolation functions of three-dimensional tetrahedral elements. First, we note that in analogy to (5.46) we now employ *volume coordinates*

$$\begin{aligned} L_1 &= 1 - r - s - t; & L_2 &= r \\ L_3 &= s; & L_4 &= t \end{aligned} \tag{5.47}$$

where we may check that $L_1 + L_2 + L_3 + L_4 = 1$. The L_i in (5.47) are the interpolation functions of the four-node element in Fig. 5.12 in its natural space. The interpolation

²It is interesting to note that the functions of the six-node triangle in Fig. 5.11 are exactly those given in (5.36), provided the variables r and s in Fig. 5.11 are replaced by $\frac{1}{4}(1 + r)(1 - s)$ and $\frac{1}{2}(1 + s)$, respectively, in order to account for the different natural coordinate systems. Hence, the correction Δh in (5.36) can be evaluated from the functions in Fig. 5.11.



(a) Coordinate system and nodal points

Include only if node i is defined

		$i = 4$	$i = 5$	$i = 6$
$h_1 =$	$1 - r - s$	$-\frac{1}{2} h_4$	$-\frac{1}{2} h_6$
$h_2 =$	r	$-\frac{1}{2} h_4$	$-\frac{1}{2} h_5$	
$h_3 =$	s	$-\frac{1}{2} h_5$	$-\frac{1}{2} h_6$
$h_4 =$	$4r(1 - r - s)$			
$h_5 =$	$4rs$			
$h_6 =$	$4s(1 - r - s)$			

(b) Interpolation functions

Figure 5.11 Interpolation functions of three to six variable-number-nodes two-dimensional triangle

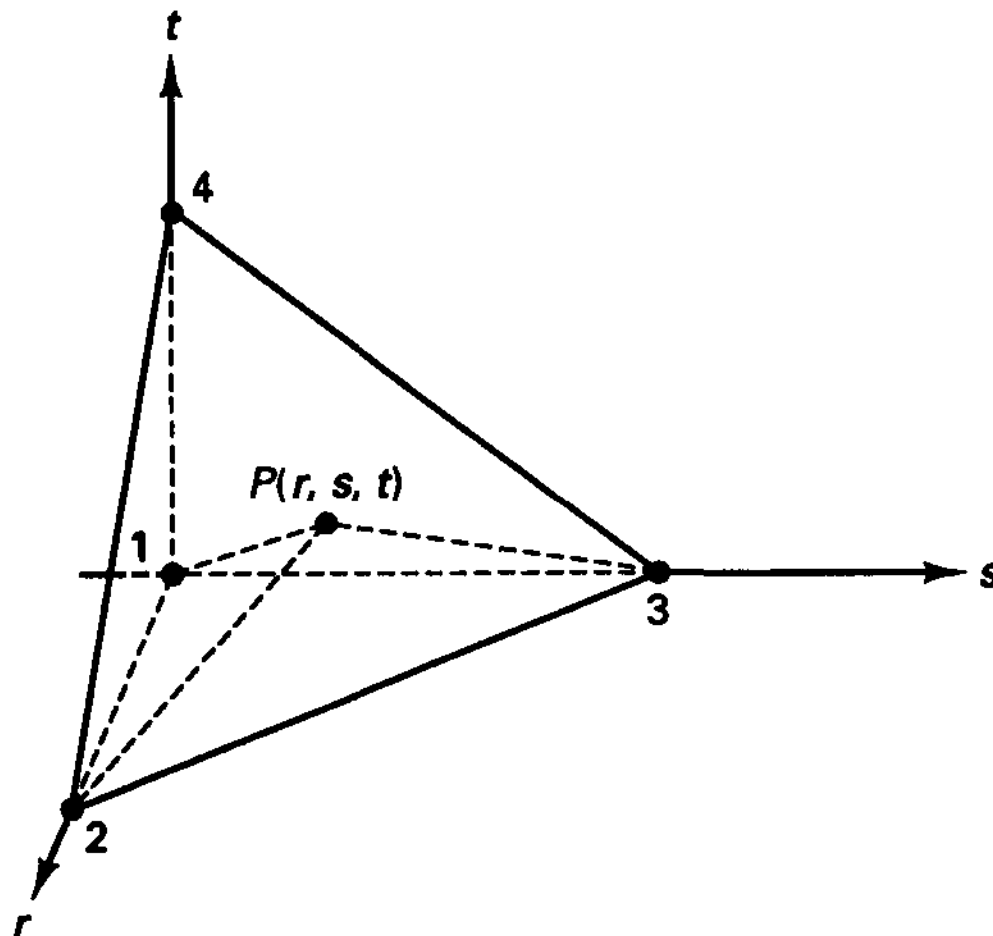
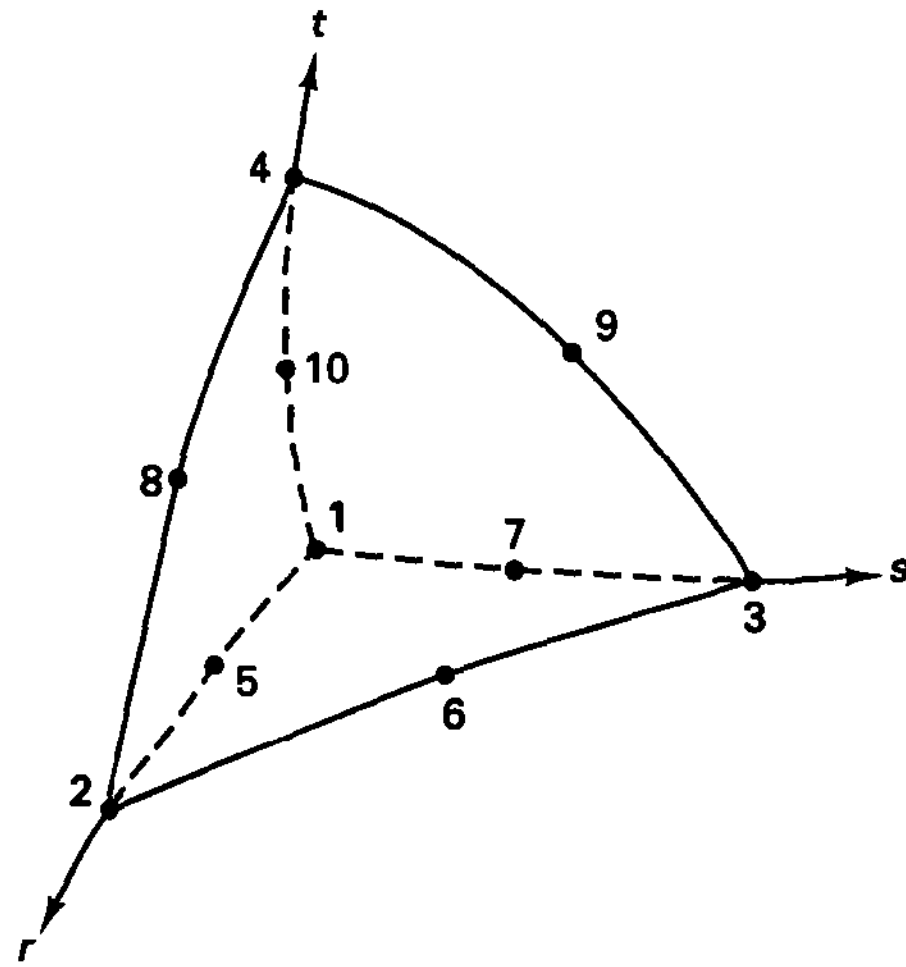


Figure 5.12 Natural coordinate system of tetrahedral element



(a) Coordinate system and nodal points

Include only if node i is defined

	$i = 5$	$i = 6$	$i = 7$	$i = 8$	$i = 9$	$i = 10$
$h_1 = 1 - r - s - t$	$-\frac{1}{2} h_5$		$-\frac{1}{2} h_7$			$-\frac{1}{2} h_{10}$
$h_2 = r$	$-\frac{1}{2} h_5$	$-\frac{1}{2} h_6$		$-\frac{1}{2} h_8$		
$h_3 = s$		$-\frac{1}{2} h_6$	$-\frac{1}{2} h_7$		$-\frac{1}{2} h_9$	
$h_4 = t$				$-\frac{1}{2} h_8$	$-\frac{1}{2} h_9$	$-\frac{1}{2} h_{10}$
$h_5 = 4r(1 - r - s - t)$						
$h_6 = 4rs$						
$h_7 = 4s(1 - r - s - t)$						
$h_8 = 4rt$						
$h_9 = 4st$						
$h_{10} = 4t(1 - r - s - t)$						

(b) Interpolation functions

Figure 5.13 Interpolation functions of four to ten variable-number-nodes three-dimensional tetrahedral element

functions of a 4 to 10 three-dimensional variable-number-nodes element are given in Fig. 5.13.

To evaluate the element matrices, it is necessary to include the Jacobian transformation as given in (5.24) and to perform the r integrations from 0 to 1, the s integrations from 0 to $(1 - r)$, and the t integrations from 0 to $(1 - r - s)$. As for the quadrilateral elements, these integrations are carried out effectively in general analysis using numerical integration, but the integration rules employed are different from those used for quadrilateral elements (see Section 5.5.4).

EXAMPLE 5.19: The triangular element shown in Fig. E5.19 is subjected to the body force vector \mathbf{f}^B per unit volume. Calculate the consistent nodal point load vector.

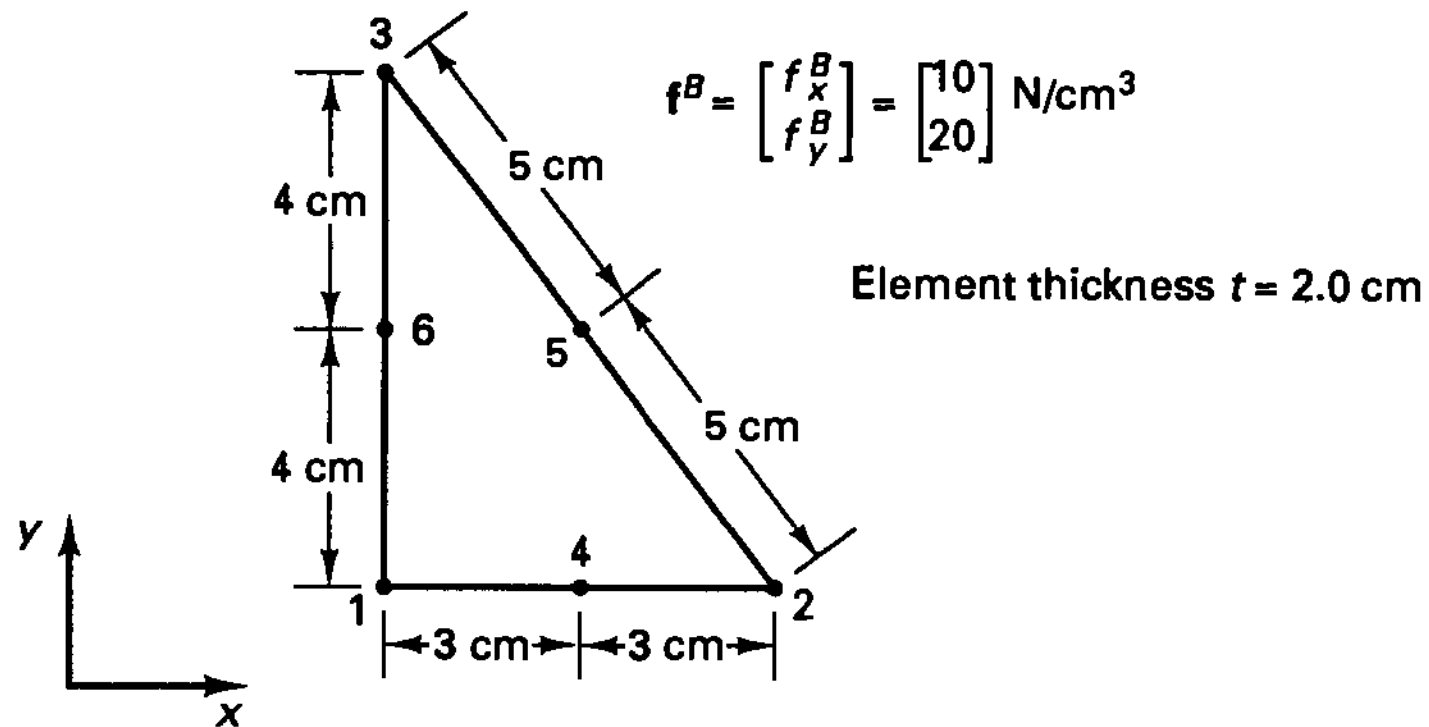


Figure E5.19 Six-node triangular element

Let us use the displacement vector

$$\hat{\mathbf{u}}^T = [u_1 \quad v_1 \quad u_2 \quad v_2 \quad u_3 \quad v_3 \quad \dots \quad v_6]$$

Hence, the load vector corresponding to the applied body force loading is

$$\mathbf{R}_B = \int_V \begin{bmatrix} h_1 & f_x^B \\ h_1 & f_y^B \\ \vdots & \vdots \\ h_6 & f_y^B \end{bmatrix} dV$$

We have

$$\mathbf{J} = \begin{bmatrix} 6 & 0 \\ 0 & 8 \end{bmatrix}$$

and note that the Jacobian matrix is diagonal and constant and that $\det \mathbf{J}$ is equal to twice the area of the triangle. The integrations involve the following term for node i :

$$f_i = \int_{r=0}^1 \int_{s=0}^{1-r} h_i t \det \mathbf{J} \, ds \, dr$$

which gives $f_1 = f_2 = f_3 = 0$, whereas $f_4 = f_5 = f_6 = (t/6) \det \mathbf{J}$. Hence, we obtain

$$\mathbf{R}_B^T = [0 \quad \dots \quad 0 \quad 160 \quad 320 \quad 160 \quad 320 \quad 160 \quad 320] \quad (\text{a})$$

with the consistent nodal forces at the corner nodes equal to zero. Note that the total applied load is of course statically equivalent to the nodal forces listed in (a).

5.3.3 Convergence Considerations

We discussed in Section 4.3 the requirements for monotonic convergence of a finite element discretization. Since isoparametric elements are used very widely, let us address some key issues of convergence specifically for these elements.

Basic Requirements for Convergence

The two requirements for monotonic convergence are that the elements (or the mesh) must be compatible and complete.

To investigate the compatibility of an element assemblage, we need to consider each edge, or rather face, between adjacent elements. For compatibility it is necessary that the coordinates and the displacements of the elements at the common face be the same. We note that for the elements considered here, the coordinates and displacements on an element face are determined only by nodes and nodal degrees of freedom on that face. Therefore, compatibility is satisfied if the elements have the same nodes on the common face and the coordinates and displacements on the common face are in each element defined by the same interpolation functions.

Examples of adjacent elements that do and do not preserve compatibility are shown in Fig. 5.14.

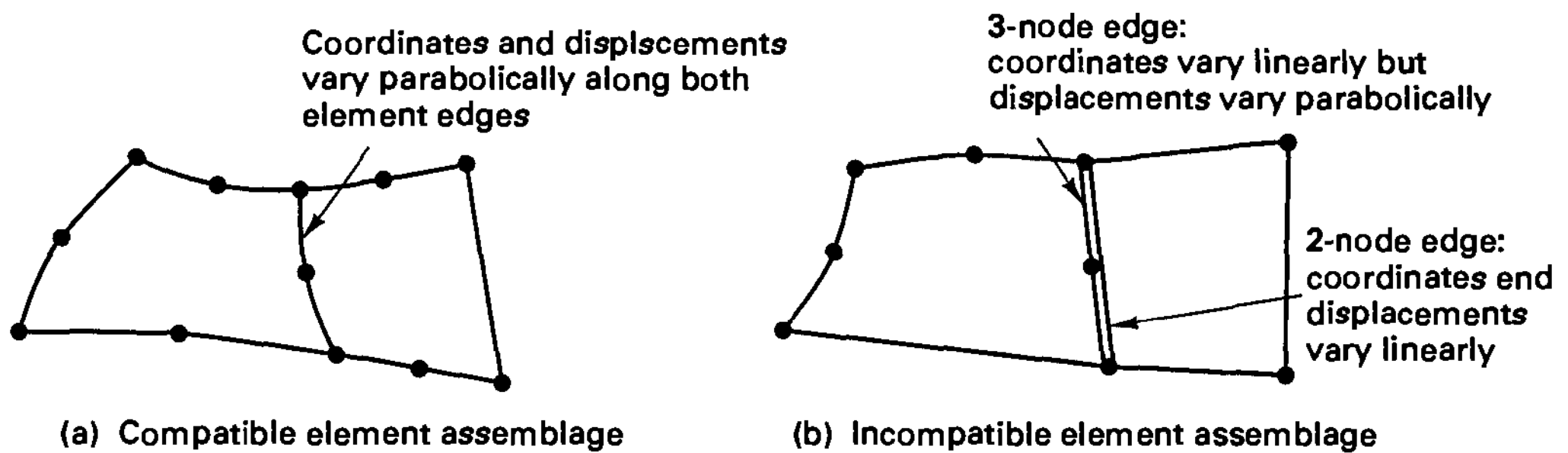


Figure 5.14 Compatible and incompatible two-dimensional element assemblage

In practice, mesh grading is frequently necessary (see Section 4.3), and the isoparametric elements show particular flexibility in achieving compatible graded meshes (see Fig. 5.15).

Completeness requires that the rigid body displacements and constant strain states be possible. One way to investigate whether these criteria are satisfied for an isoparametric element is to follow the considerations given in Section 4.3.2. However, we now want to obtain more insight into the specific conditions that pertain to the isoparametric formulation of a continuum element. For this purpose we consider in the following discussion a three-dimensional continuum element because the one- and two-dimensional elements can be regarded as special cases of these three-dimensional considerations. For the rigid body and constant strain states to be possible, the following displacements defined in the local element coordinate system must be contained in the isoparametric formulation

$$\left. \begin{aligned} u &= a_1 + b_1x + c_1y + d_1z \\ v &= a_2 + b_2x + c_2y + d_2z \\ w &= a_3 + b_3x + c_3y + d_3z \end{aligned} \right\} \quad (5.48)$$

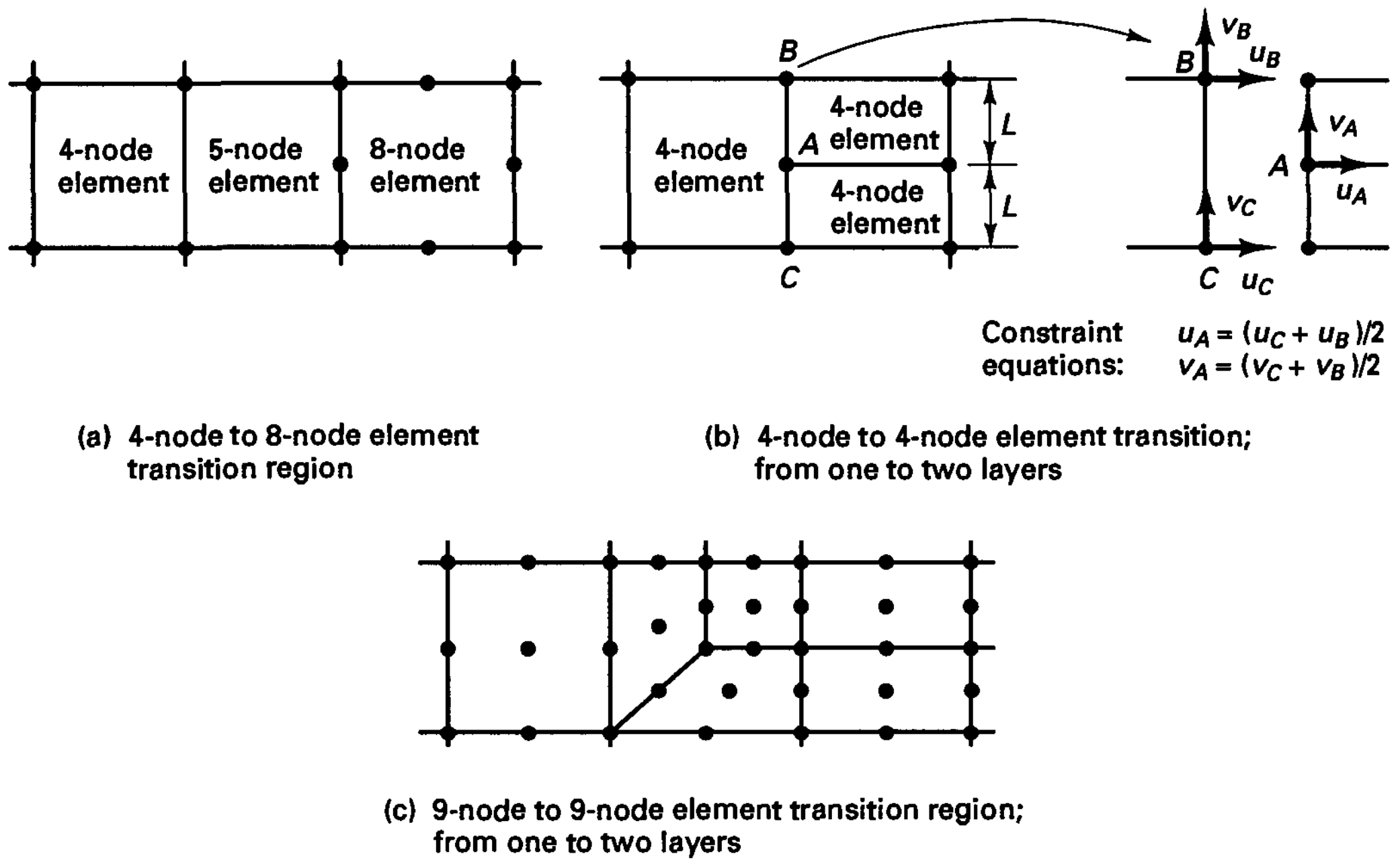


Figure 5.15 Some transitions with compatible element layouts

where the $a_j, b_j, c_j,$ and $d_j, j = 1, 2, 3,$ are constants. The nodal point displacements corresponding to this displacement field are

$$\left. \begin{aligned} u_i &= a_1 + b_1 x_i + c_1 y_i + d_1 z_i \\ v_i &= a_2 + b_2 x_i + c_2 y_i + d_2 z_i \\ w_i &= a_3 + b_3 x_i + c_3 y_i + d_3 z_i \end{aligned} \right\} \quad (5.49)$$

where $i = 1, \dots, q$ and $q =$ number of nodes.

The test for completeness is now as follows: show that the displacements in (5.48) are *in fact* obtained *within* the element when the element nodal point displacements are given by (5.49). In other words, we should find that with the nodal point displacements in (5.49), the displacements *within* the element are actually those given in (5.48).

In the isoparametric formulation we have the displacement interpolation

$$u = \sum_{i=1}^q h_i u_i; \quad v = \sum_{i=1}^q h_i v_i; \quad w = \sum_{i=1}^q h_i w_i$$

which, using (5.49), reduces to

$$\left. \begin{aligned} u &= a_1 \sum_{i=1}^q h_i + b_1 \sum_{i=1}^q h_i x_i + c_1 \sum_{i=1}^q h_i y_i + d_1 \sum_{i=1}^q h_i z_i \\ v &= a_2 \sum_{i=1}^q h_i + b_2 \sum_{i=1}^q h_i x_i + c_2 \sum_{i=1}^q h_i y_i + d_2 \sum_{i=1}^q h_i z_i \\ w &= a_3 \sum_{i=1}^q h_i + b_3 \sum_{i=1}^q h_i x_i + c_3 \sum_{i=1}^q h_i y_i + d_3 \sum_{i=1}^q h_i z_i \end{aligned} \right\} \quad (5.50)$$

Since in the isoparametric formulation the coordinates are interpolated in the same way as the displacements, we can use (5.18) to obtain from (5.50),

$$\left. \begin{aligned} u &= a_1 \sum_{i=1}^q h_i + b_1 x + c_1 y + d_1 z \\ v &= a_2 \sum_{i=1}^q h_i + b_2 x + c_2 y + d_2 z \\ w &= a_3 \sum_{i=1}^q h_i + b_3 x + c_3 y + d_3 z \end{aligned} \right\} \quad (5.51)$$

The displacements defined in (5.51), however, are the same as those given in (5.48), provided that for any point in the element,

$$\sum_{i=1}^q h_i = 1 \quad (5.52)$$

The relation in (5.52) is the condition on the interpolation functions for the completeness requirements to be satisfied. We may note that (5.52) is certainly satisfied at the nodes of an element because the interpolation function h_i has been constructed to be unity at node i with all other interpolation functions $h_j, j \neq i$, being zero at that node; but in order that an isoparametric element be properly constructed, the condition must be satisfied for all points in the element.

In the preceding discussion, we considered a three-dimensional continuum element, but the conclusions are also directly applicable to the other isoparametric continuum element formulations. For the one- or two-dimensional continuum elements we simply include only the appropriate displacement and coordinate interpolations in the relations (5.48) to (5.52). We demonstrate the convergence considerations in the following example.

EXAMPLE 5.20: Investigate whether the requirements for monotonic convergence are satisfied for the variable-number-nodes elements in Figs. 5.4 and 5.5.

Compatibility is maintained between element edges in two-dimensional analysis and element faces in three-dimensional analysis, provided that the same number of nodes is used on connecting element edges and faces. A typical compatible element layout is shown in Fig. 5.14(a).

The second requirement for monotonic convergence is the completeness condition. Considering first the basic four-node two-dimensional element, we recognize that the arguments leading to the condition in (5.52) are directly applicable, provided that only the x and y coordinates and u and v displacements are considered.

Evaluating $\sum_{i=1}^4 h_i$ for the element, we find

$$\frac{1}{4}(1+r)(1+s) + \frac{1}{4}(1-r)(1+s) + \frac{1}{4}(1-r)(1-s) + \frac{1}{4}(1+r)(1-s) = 1$$

Hence, the basic four-node element is complete. We now study the interpolation functions given in Fig. 5.4 for the variable-number-nodes element and find that the total contribution that is added to the basic four-node interpolation functions is always zero for whichever additional node is included. Hence, any one of the possible elements defined by the variable number of nodes in Fig. 5.4 is complete. The proof for the three-dimensional elements in Fig. 5.5 is carried out in an analogous manner.

It follows therefore that the variable-number-nodes continuum elements satisfy the requirements for monotonic convergence.

Order of Convergence, the Effect of Element Distortions

The basic requirements for monotonic convergence, namely, compatibility and completeness, are satisfied by the isoparametric elements, as discussed above, when these elements are of general (but admissible) geometric shape. Therefore, the elements always have the capability to represent the rigid body modes and constant strain states, and convergence is guaranteed.

We discussed in Section 4.3.5 the rates of convergence of sequences of finite element discretizations with the assumptions that the elements are based on polynomial expansions and that uniform meshes of elements with characteristic dimension h are used. For the discussion we used the Pascal triangle to display which polynomial terms are present in various elements. The complete polynomial of highest order in the Pascal triangle determines the order of convergence. Let this degree (now for r, s, t) be k . Then if the exact solution \mathbf{u} is sufficiently smooth and uniform meshes are used, the rate of convergence of the finite element solution \mathbf{u}_h is given by [see (4.102)]

$$\|\mathbf{u} - \mathbf{u}_h\|_1 \leq c h^k \quad (5.53)$$

where k is the order of convergence. The constant c is independent of h but depends on the exact solution of the mathematical model and the material properties.

In general practical finite element analysis, the exact solution of the mathematical model is not smooth (e.g., because of rapid load variations, changes in material properties), and with uniform meshes the order of convergence is much reduced. Therefore, mesh grading must be employed with fine discretizations in regions of nonsmooth stress distributions and coarse discretizations in the other regions. The meshes will therefore be nonuniform and based on geometrically distorted elements using, for example, in two-dimensional analysis general quadrilateral and triangular elements; see Fig. 5.16 for an example of a nine-node quadrilateral element.

The aim in such mesh constructions is then to use meshes in which the density of solution error is (nearly) constant over the domain considered and to use *regular* meshes.³ When regular meshes are used, the rate of convergence is still given by a form such as (5.53) [see (4.101c)], namely,

$$\|\mathbf{u} - \mathbf{u}_h\|_1^2 \leq c \sum_m h_m^{2k} \|\mathbf{u}\|_{k+1,m}^2$$

where h_m denotes the largest dimension of element m (see Fig. 5.16). We note that, in essence, in this relation the interpolation errors over all elements are added to obtain the total interpolation error, which then gives us the usual bound on the actual error of the solution.

The (nearly) constant density of solution error can of course be achieved, in general, only by proper mesh grading and adaptive mesh refinement because the mesh to be used depends on the exact (and unknown) solution. In practice, a refinement of a mesh is constructed on the basis of local error estimates computed from the solution just obtained (with a coarser mesh).

³In referring to a "regular mesh," we always mean "a mesh from a sequence of meshes that is regular."

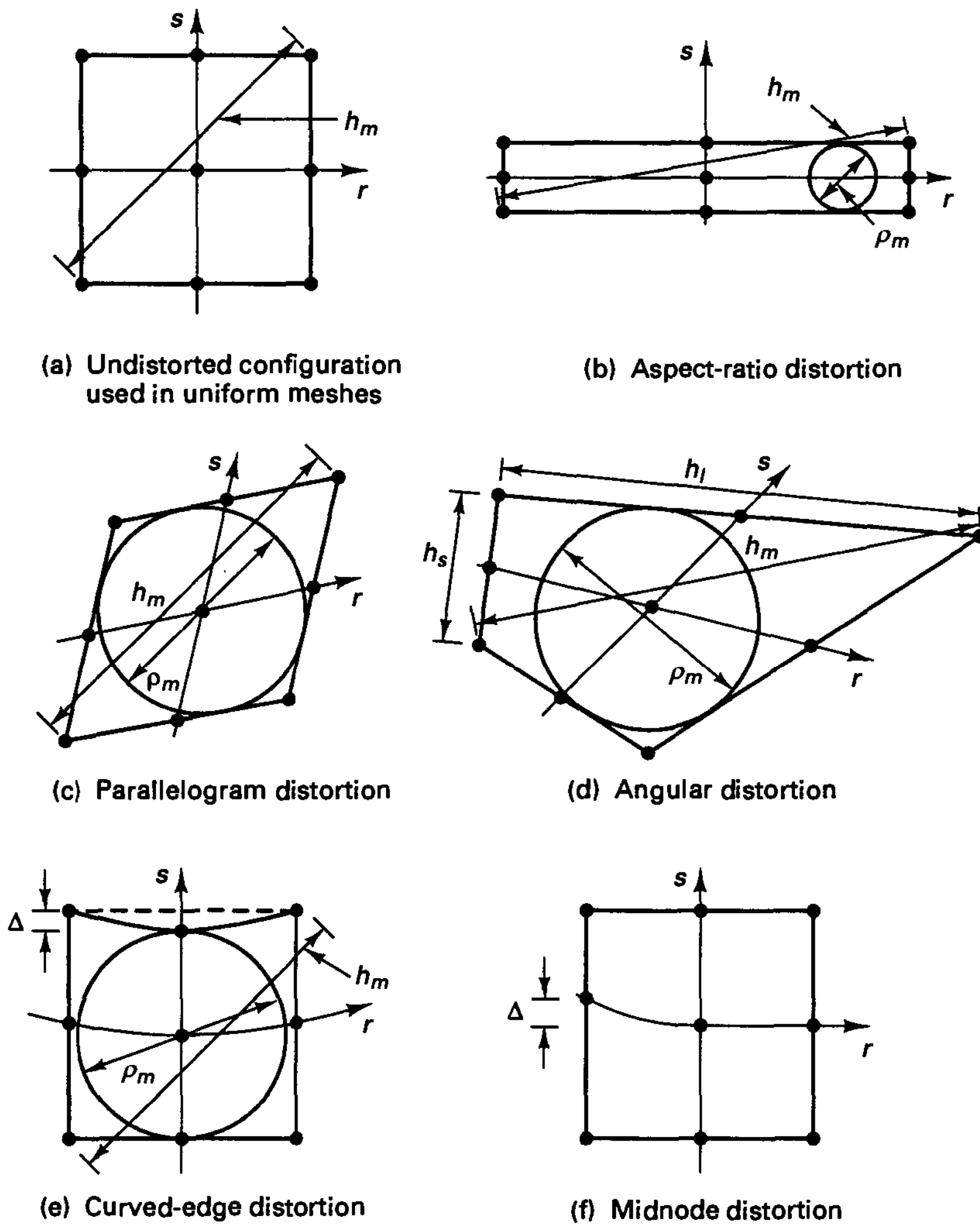


Figure 5.16 Classification of element distortions for the 9-node two-dimensional element; all midside and interior nodes are placed at their “natural” positions for cases (a) to (e). The value of Δ should be smaller than h_m^2 for (5.53) to be applicable. An actual distortion in practice would be a combination of those shown.

To introduce a measure of mesh regularity, the element geometric parameter σ_m , is used,

$$\sigma_m = \frac{h_m}{\rho_m}$$

where h_m is the largest dimension and ρ_m is the diameter of the largest circle (or sphere) that can be inscribed in element m (see Fig. 5.16). A sequence of meshes is *regular* if $\sigma_m \leq \sigma_0$ for all elements m and meshes used, where σ_0 is a fixed positive value. In addition, when using meshes of quadrilateral elements in two-dimensional analysis and hexahedral ele-

ments in three-dimensional analysis, we also require that for each element the ratio of the largest to the smallest side lengths (h_l/h_s in Fig. 5.16) is smaller than a reasonable positive number. These conditions prevent excessive aspect ratios and geometric distortions of the elements. Referring to Fig. 5.16, the elements in (b), (c), and in particularly (d) are used extensively in regular meshes.⁴

The above described mesh grading can in general be achieved with straight-sided elements, and the noncorner nodes can usually be placed at their natural positions (i.e., at the physical x, y, z locations in proportion to the r, s, t distances from the corner nodes); and the most typically used element in Fig. 5.16 is the quadrilateral in Fig. 5.16(d). However, when curved boundaries need to be modeled, the element sides will also be curved [see Fig. 5.16(e)], and we must ask what effect all these geometric distortions will have on the order of convergence.

Whereas the cases in Figs. 5.16(a) to (e) are used extensively in mesh designs, we note that the element distortion shown in Fig. 5.16(f) is avoided, unless specific stress effects need to be modeled, such as in fracture mechanics [where even larger distortions than those shown in Fig. 5.16(f) are used; see Fig. 5.9]. However, the distortion in Fig. 5.16(f) may also arise in geometrically nonlinear analysis.

P. G. Ciarlet and P. -A. Raviart [A] and P. G. Ciarlet [A] have shown in their mathematical analyses that the order of convergence of a sequence of regular meshes with straight element sides is still given as in (5.53) (even though, for example, in two-dimensional analysis, general straight-sided quadrilaterals are used instead of square elements) *and* that the order of convergence is also still given as in (5.53) with curved element sides and when the noncorner nodes are not placed at their natural positions provided these distortions are small, measured on the size of the element. For the element in Fig. 5.16 the distortions must be $o(h^2)$. The element distortions due to curved sides and due to interior nodes not placed at their natural positions must therefore be small, *and* in the refinement process the distortions must decrease much faster than the element size. The order of convergence in (5.53) is reached directly when the exact solution \mathbf{u} is smooth, whereas when the exact solution is nonsmooth, mesh grading is necessary (to fulfill the requirement that the density of solution error be (almost) constant over the solution domain). We present some solutions to illustrate a few of these results in Section 5.5.5 (see Fig. 5.39).⁵

Of course, the actual accuracy attained with a given mesh is also determined by the constant c in (5.53). This constant depends on the specific elements used (all with the complete polynomial of degree k) and also on the geometric distortions of the elements. We should note that if the constant is large, the order of convergence may be of little interest because the h^k term may decrease the error sufficiently only at very small values of h .

These remarks pertain to the order of convergence reached when element sizes are small. However, interesting observations also pertain to a study of the predictive capability of elements when the element sizes are large. Namely, element geometric distortions can affect the general predictive capabilities to a significant degree.

⁴In addition, we can also define a sequence of meshes that is *quasi-uniform*. In such sequence we also have, in addition to the regularity condition that the ratio of the maximum h_m encountered in the mesh over the minimum h_m encountered in that same mesh remains for all meshes below a reasonable positive number. Hence, whereas regularity allows that the ratio of element sizes becomes any value, quasi-uniformity restricts the relative sizes that are permitted. Therefore, the error measure in (4.101c) is also valid when a quasi-uniform sequence of meshes is used.

⁵These solutions are given in Section 5.5.5 because the element matrices of the distorted elements are evaluated using numerical integration and the effect of the numerical integration error must also be considered.

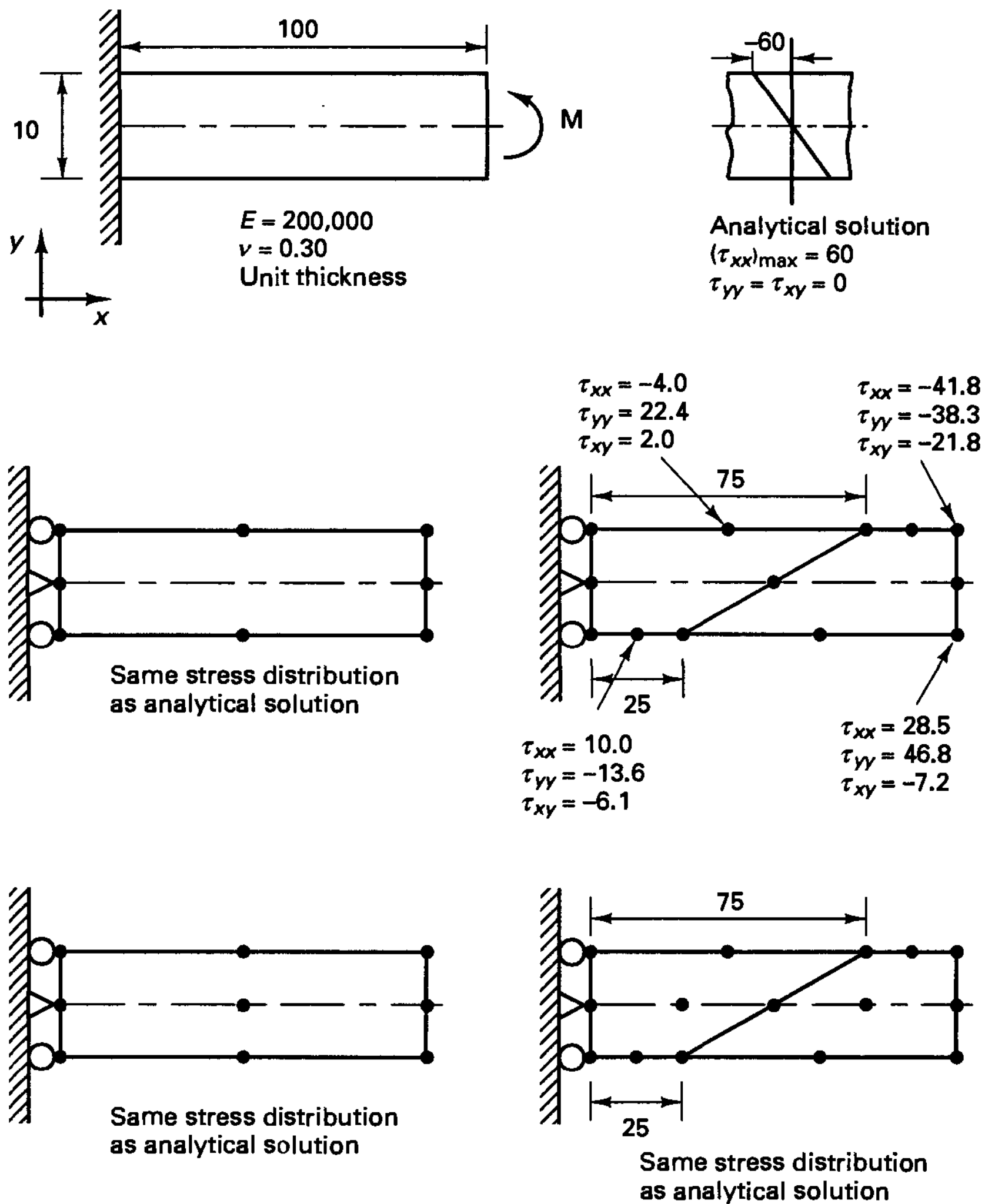


Figure 5.17 Example demonstrating effect of element distortions on predictive capability of elements

As an example to demonstrate a possible loss of predictive capability when an isoparametric element is geometrically distorted, consider the results given in Fig. 5.17. The single undistorted eight-node element gives the exact (beam theory) solution for the beam bending problem. However, when two elements of distorted shape are used, significant solution errors are obtained. On the other hand, when the same problem is analyzed with nine-node elements, the mesh of two distorted elements gives the correct result.

This example shows that in coarse meshes the stress predictive capability of certain elements can be significantly affected by element geometric distortions. Since, in practice, frequently rather coarse meshes are used and complete convergence studies are not performed, surely it is preferable to use those elements that are least sensitive to element geometric distortions.

On studying the cause of loss of predictive capability, we find that this effect is due to the elements no longer being able to represent the same order of polynomials in the physical coordinates x, y, z after the geometric distortion as they did without the distortion. For example, the general quadrilateral nine-node element, shown in Fig. 5.16(d), is able to represent the x^2, xy, y^2 displacement variations *exactly*, whereas the corresponding eight-node quadrilateral element is not able to do so. Hence, the general quadrilateral eight-node element does not contain the quadratic terms in the Pascal triangle of the physical coordinates.

This observation explains the results in Fig. 5.17, and an investigation into this phenomenon for widely used elements and common distortions is of general interest. In such a study, we can measure the loss of predictive capability by identifying which terms in the physical coordinates of the Pascal triangle can no longer be represented exactly, (see N. S. Lee and K. J. Bathe [A]).

Let us consider the two-dimensional element in Fig. 5.16 as an example. For elements with undistorted configurations or with aspect ratio distortions only, the physical coordinates x, y are linearly related to the isoparametric coordinates r, s ; i.e., we have $x = c_1 r$, $y = c_2 s$, where c_1 and c_2 are constants. Hence, the Pascal triangle terms in physical coordinates are simply the r, s terms obtained from the interpolation functions h_i replaced by x and y , respectively.

The effects of the parallelogram, general angular, and curved edge distortions shown in Figs. 5.16(c) to (e) can be studied by establishing the physical coordinate variations for these specific cases with the coordinate interpolations (5.18) and then asking what polynomial terms in x and y are contained in the r, s polynomial terms of the displacement variations given in (5.19) (see Example 5.21).

Table 5.1 summarizes the results obtained in such a study for two-dimensional quadrilateral elements (see N. S. Lee and K. J. Bathe [A]). The first column in Table 5.1 gives the terms in the Pascal triangle when the element is undistorted or is subjected to an aspect ratio or parallelogram distortion only. The terms below the dashed line are present only when the element is undistorted, or subjected only to an aspect ratio distortion, *and* also unrotated. Table 5.1 in particular shows that a general angular distortion significantly affects the predictive capability of 8- and 12-node elements; i.e., with such distortions the elements can represent only linear displacement variations in x and y *exactly*, whereas the 9- and 16-node elements can in distorted form still represent the parabolic and cubic displacement fields *exactly*.

On the other hand, curved edge distortions reduce the order of displacement polynomials that can be represented *exactly* for all the elements considered in Table 5.1, and indeed with such distortions only the biquartic 25-node element can still represent the parabolic displacement field exactly.

While the information given in Table 5.1 shows clearly that the Lagrangian elements are preferable to the 8- and 12-node elements in terms of predictive capability, of course, we also need to recall that the Lagrangian elements are computationally slightly more expensive, and for fine meshes the order of convergence is identical [although the constant c in (5.53) is different].

We demonstrate the procedure of analysis to obtain the information given in Table 5.1 in the following example.

TABLE 5.1 Polynomial displacement fields in physical coordinates that can be solved exactly by various elements in their undistorted and distorted configurations†

Type of element	Fields for undistorted configuration, aspect ratio and/or parallelogram distortions		Angular distortion	Quadratic curved-edge distortion
	Additional fields if also unrotated			
8-node element	$\begin{array}{c} 1 \\ x \ y \\ x^2 \ xy \ y^2 \\ \hline x^2y \ xy^2 \end{array}$		$\begin{array}{c} 1 \\ x \ y \end{array}$	$\begin{array}{c} 1 \\ x \ y \end{array}$
12-node element	$\begin{array}{c} 1 \\ x \ y \\ x^2 \ xy \ y^2 \\ x^3 \ x^2y \ xy^2 \ y^3 \\ \hline x^3y \ xy^3 \end{array}$		$\begin{array}{c} 1 \\ x \ y \end{array}$	$\begin{array}{c} 1 \\ x \ y \end{array}$
9-node Lagrangian element	$\begin{array}{c} 1 \\ x \ y \\ x^2 \ xy \ y^2 \\ \hline x^2y \ xy^2 \\ x^2y^2 \end{array}$		$\begin{array}{c} 1 \\ x \ y \\ x^2 \ xy \ y^2 \end{array}$	$\begin{array}{c} 1 \\ x \ y \end{array}$
16-node Lagrangian element	$\begin{array}{c} 1 \\ x \ y \\ x^2 \ xy \ y^2 \\ x^3 \ x^2y \ xy^2 \ y^3 \\ \hline x^3y \ x^2y^2 \ xy^3 \\ x^3y^2 \ x^2y^3 \\ x^3y^3 \end{array}$		$\begin{array}{c} 1 \\ x \ y \\ x^2 \ xy \ y^2 \\ x^3 \ x^2y \ xy^2 \ y^3 \end{array}$	$\begin{array}{c} 1 \\ x \ y \end{array}$
25-node Lagrangian element	$\begin{array}{c} 1 \\ x \ y \\ x^2 \ xy \ y^2 \\ x^3 \ x^2y \ xy^2 \ y^3 \\ x^4 \ x^3y \ x^2y^2 \ xy^3 \ y^4 \\ \hline x^4y \ x^3y^2 \ x^2y^3 \ xy^4 \\ x^4y^2 \ x^3y^3 \ x^2y^4 \\ x^4y^3 \ x^3y^4 \\ x^4y^4 \end{array}$		$\begin{array}{c} 1 \\ x \ y \\ x^2 \ xy \ y^2 \\ x^3 \ x^2y \ xy^2 \ y^3 \\ x^4 \ x^3y \ x^2y^2 \ xy^3 \ y^4 \end{array}$	$\begin{array}{c} 1 \\ x \ y \\ x^2 \ xy \ y^2 \end{array}$

† Two-dimensional quadrilateral elements are considered.

EXAMPLE 5.21: Consider the general angularly distorted eight-node element in Fig. E5.21. Evaluate the Pascal triangle terms in x, y for this element.

The physical coordinate variations are obtained by using the interpolation functions in Fig. 5.4, which give for this element with its midside nodes placed halfway between the corner nodes,

$$x = \gamma_1 + \gamma_2 r + \gamma_3 s + \gamma_4 rs \tag{a}$$

$$y = \delta_1 + \delta_2 r + \delta_3 s + \delta_4 rs \tag{b}$$

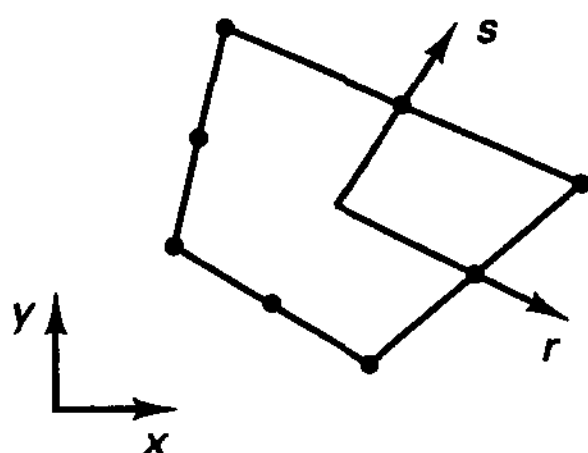


Figure E5.21 Eight-node isoparametric element, with angular distortion

with $\gamma_1, \dots, \gamma_4$ and $\delta_1, \dots, \delta_4$ constants. We use (a) and (b) to identify which x and y terms are contained in the displacement interpolations

$$u = \sum_{i=1}^8 h_i u_i \quad (c)$$

$$v = \sum_{i=1}^8 h_i v_i \quad (d)$$

where the h_i are again those in Fig. 5.4.

Consider the u -displacement interpolation. The constant and x and y terms in (a) and (b) are clearly contained in (c) because (c) interpolates u in terms of the functions $(1, r, s, r^2, rs, s^2, r^2s, rs^2)$ multiplied by constants. We discussed this fact earlier when considering the requirements for convergence.

However, if we next consider the term x^2 , we notice that the term r^2s^2 [obtained by squaring the right-hand side of (a)] is not present in (c). Similarly, the terms xy , y^2 , x^2y , and xy^2 are not present in the displacement interpolation (c).

The analysis for the v -displacement interpolation is of course identical. Hence, when an eight-node isoparametric element is subjected to a general angular distortion, the predictive capability is diminished in that quadratic displacement variations in x and y can no longer be represented exactly (see Table 5.1).

This analysis also shows that the quadratic displacement variations in x and y are retained when the nine-node displacement-based element is subjected to the same angular distortions. These conclusions explain the results shown in Fig. 5.16.

5.3.4 Element Matrices in Global Coordinate System

So far we have considered the calculation of isoparametric element matrices that correspond to local element degrees of freedom. In the evaluation we used local element coordinates x , y , and z , whichever were applicable, and local element degrees of freedom u_i , v_i , and w_i . However, we may note that for the two-dimensional element considered in Examples 5.5 to 5.7 the element matrices could have been evaluated using the global coordinate variables X and Y , and the global nodal point displacements U_i and V_i . Indeed, in the calculations presented, the x and y local coordinates and u and v local displacement components simply needed to be replaced by the X and Y global coordinates and U and V global displacement components, respectively. In such cases the matrices then would correspond directly to the global displacement components.

In general, the calculation of the element matrices should be carried out in the global coordinate system, using global displacement components if the number of natural coordinate variables is equal to the number of global variables. Typical examples are two-dimensional elements defined in a global plane and the three-dimensional element in

Fig. 5.5. In these cases the Jacobian operator in (5.24) is a square matrix, which can be inverted as required in (5.25), and the element matrices correspond directly to the global displacement components.

In cases where the order of the global coordinate system is higher than the order of the natural coordinate system, it is usually most expedient to calculate first the element matrices in the local coordinate system and corresponding to local displacement components. Afterward, the matrices must be transformed in the usual manner to the global displacement system. Examples are the truss element or the plane stress element when they are oriented arbitrarily in three-dimensional space. However, alternatively, we may include the transformation to the global displacement components directly in the formulation. This is accomplished by introducing a transformation that expresses in the displacement interpolation the local nodal point displacements in terms of the global components.

EXAMPLE 5.22: Evaluate the element stiffness matrix of the truss element in Fig. E5.22 using directly global nodal point displacements.

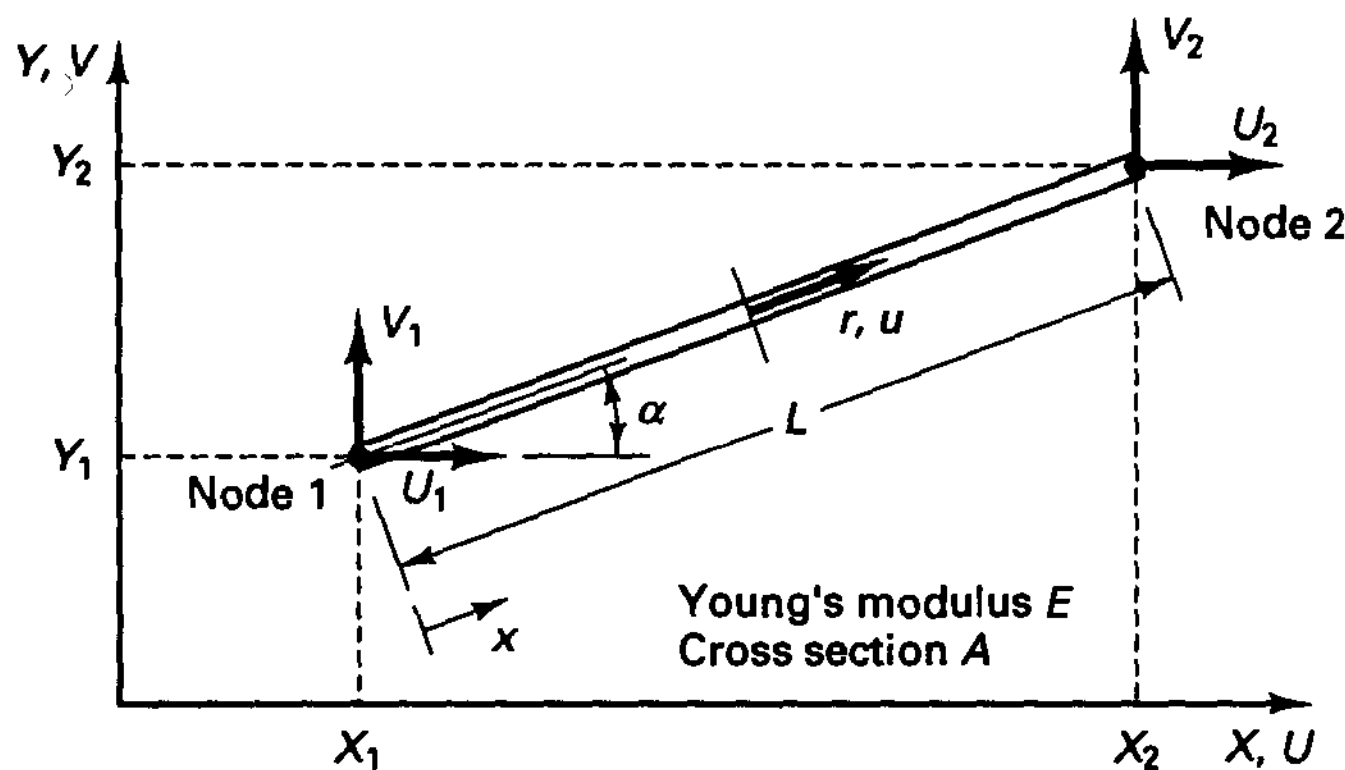


Figure E5.22 Truss element in global coordinate system

The stiffness matrix of the element is given in (5.27); i.e.,

$$\mathbf{K} = \int_V \mathbf{B}^T \mathbf{C} \mathbf{B} dV$$

where \mathbf{B} is the strain-displacement matrix and \mathbf{C} is the stress-strain matrix. For the truss element considered we have

$$u = [\cos \alpha \quad \sin \alpha] \begin{bmatrix} \frac{1}{2}(1 - r)U_1 + \frac{1}{2}(1 + r)U_2 \\ \frac{1}{2}(1 - r)V_1 + \frac{1}{2}(1 + r)V_2 \end{bmatrix}$$

Then, using $\epsilon = \partial u / \partial x$, expressed in the natural coordinate system as $\epsilon = (2/L) \partial u / \partial r$ (see Section 5.2), we can write the strain-displacement transformation corresponding to the displacement vector $\mathbf{U}^T = [U_1 \quad V_1 \quad U_2 \quad V_2]$ as

$$\mathbf{B} = \frac{1}{L} [\cos \alpha \quad \sin \alpha \quad \cos \alpha \quad \sin \alpha] \begin{bmatrix} -1 & & & \\ & -1 & & \text{zeros} \\ & & 1 & \\ \text{zeros} & & & 1 \end{bmatrix}$$

Also, as given in Section 5.2, we have

$$dV = \frac{AL}{2} dr \quad \text{and} \quad \mathbf{C} = E$$

Substituting the relations for \mathbf{B} , \mathbf{C} , and dV and evaluating the integral, we obtain

$$\mathbf{K} = \frac{AE}{L} \begin{bmatrix} \cos^2 \alpha & \cos \alpha \sin \alpha & -\cos^2 \alpha & -\cos \alpha \sin \alpha \\ \sin \alpha \cos \alpha & \sin^2 \alpha & -\sin \alpha \cos \alpha & -\sin^2 \alpha \\ -\cos^2 \alpha & -\cos \alpha \sin \alpha & \cos^2 \alpha & \cos \alpha \sin \alpha \\ -\sin \alpha \cos \alpha & -\sin^2 \alpha & \sin \alpha \cos \alpha & \sin^2 \alpha \end{bmatrix}$$

5.3.5 Displacement/Pressure Based Elements for Incompressible Media

We discussed in Section 4.4.3 the fact that pure displacement-based elements are not effective for the analysis of incompressible (or almost incompressible) media and introduced two displacement/pressure formulations. In the u/p formulation, the pressure is interpolated individually for each element and can (in the almost incompressible case) be statically condensed out prior to the element matrix assemblage, whereas in the u/p -c formulation the element pressures are defined by nodal variables which, as for the displacements, pertain to adjacent elements. Various effective elements of these formulations were given (see Tables 4.6 and 4.7) and discussed (see Section 4.5).

As for the pure displacement-based elements, we assumed in Chapter 4 that the displacement and pressure interpolation matrices are constructed using the generalized coordinate approach. However, it is now apparent that these matrices can be obtained directly using the isoparametric formulation.

In the u/p formulation, we use the same coordinate and displacement interpolations for an element as in the pure displacement formulation [see (5.18) and (5.19)], and we interpolate the pressure using

$$p = p_0 + p_1 r + p_2 s + p_3 t + \dots \quad (5.54)$$

where $p_0, p_1, p_2, p_3, \dots$ are the pressure parameters to be calculated and $r, s,$ and t are the isoparametric coordinates. Of course, as an alternative, we could also interpolate the pressure using

$$p = p_0 + p_1 x + p_2 y + p_3 z + \dots$$

where $x, y,$ and z are the usual Cartesian coordinates.

In the u/p -c formulation we also use the displacement and coordinate interpolations as in the pure displacement formulation, and

$$p = \sum_{i=1}^{q_p} \tilde{h}_i \hat{p}_i \quad (5.55)$$

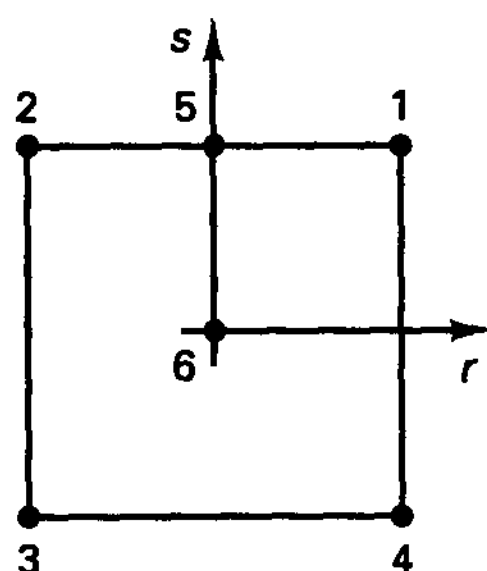
where the $\tilde{h}_i, i = 1, \dots, q_p$ are the nodal point pressure interpolation functions and the \hat{p}_i are the unknown nodal pressures. We note that the \tilde{h}_i are different from the h_i which are used for the displacement and coordinate interpolations. For example, for the 9/4-c two-dimensional element, the displacement and coordinate interpolations are the functions

corresponding to the nine element nodes in Table 5.4, whereas the \tilde{h}_i are the functions corresponding to the four element corner nodes.

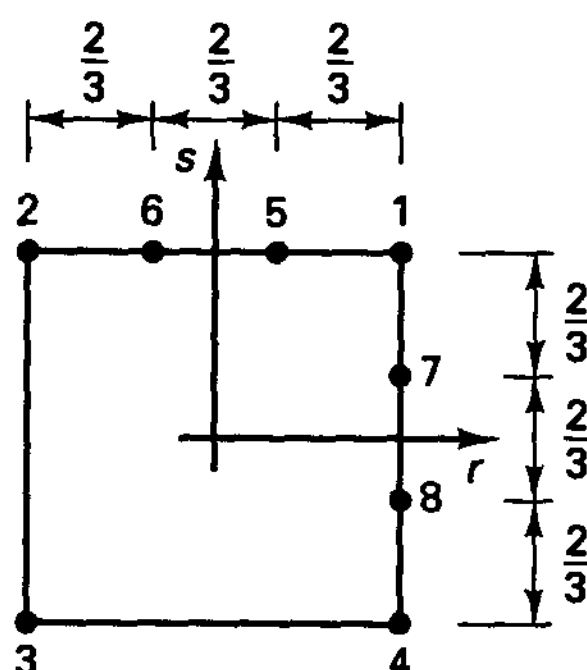
In practice, the isoparametric formulation of the u/p and $u/p-c$ elements is effective because the generality of nonrectangular and curved elements is then also available (see Fig. 4.21 and T. Sussman and K. J. Bathe [A, B]).

5.3.6 Exercises

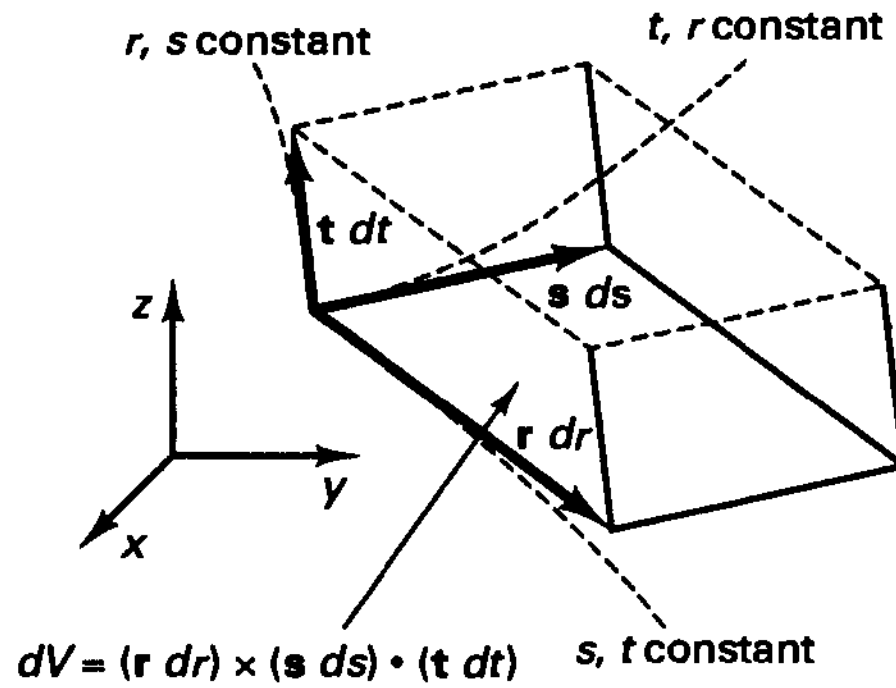
- 5.1. Use the procedure in Example 5.1 to prove that the functions in Fig. 5.3 for the four-node truss element are correct.
- 5.2. Use the procedure in Example 5.1 to prove that the functions in Fig. 5.4 for the two-dimensional element are correct.
- 5.3. Use the functions in Fig. 5.4 to construct the interpolation functions of the six-node element shown. Plot the interpolation functions in an oblique/aerial view (as in Example 5.4).



- 5.4. Prove that the construction of the interpolation functions in Fig. 5.5 gives the correct functions for the three-dimensional element.
- 5.5. Determine the interpolation function h_i for the element shown for use in a compatible finite element mesh.



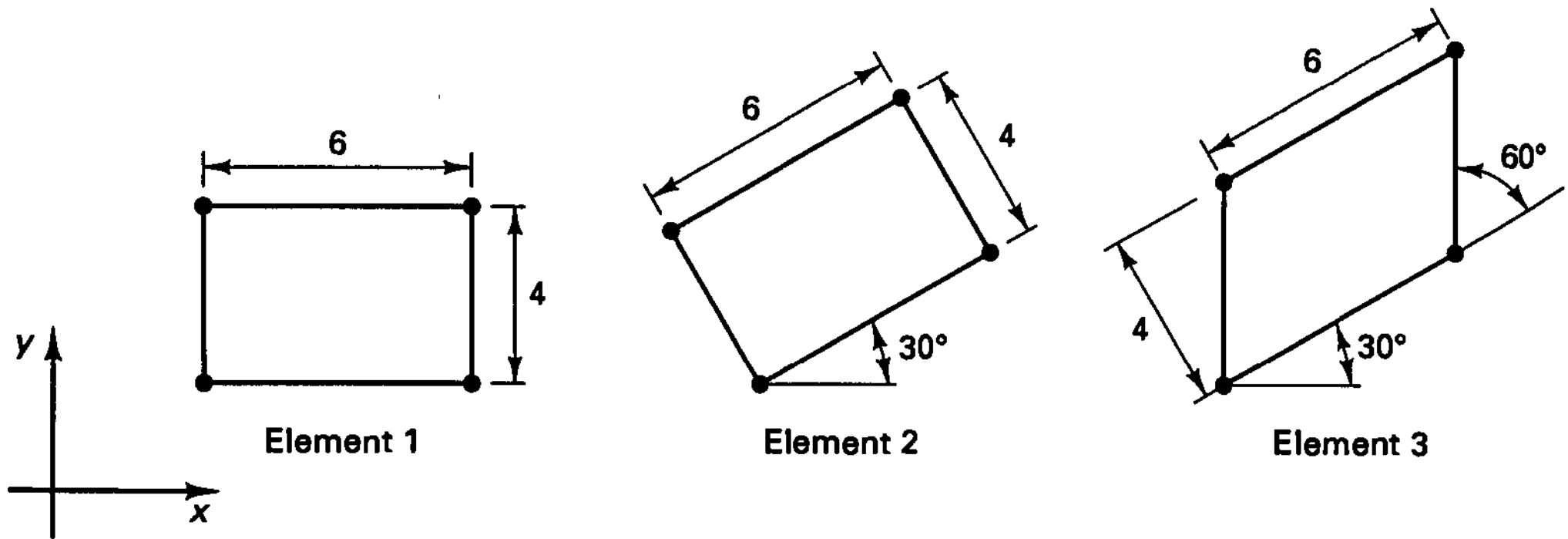
- 5.6. In the computation of isoparametric element matrices, the integration is performed over the natural coordinates r, s, t , which requires the transformation (5.28). Derive this transformation using the elementary volume $dV = (\mathbf{r} \, dr) \times (\mathbf{s} \, ds) \cdot (\mathbf{t} \, dt)$ shown.



Here the vectors r, s, t are given by

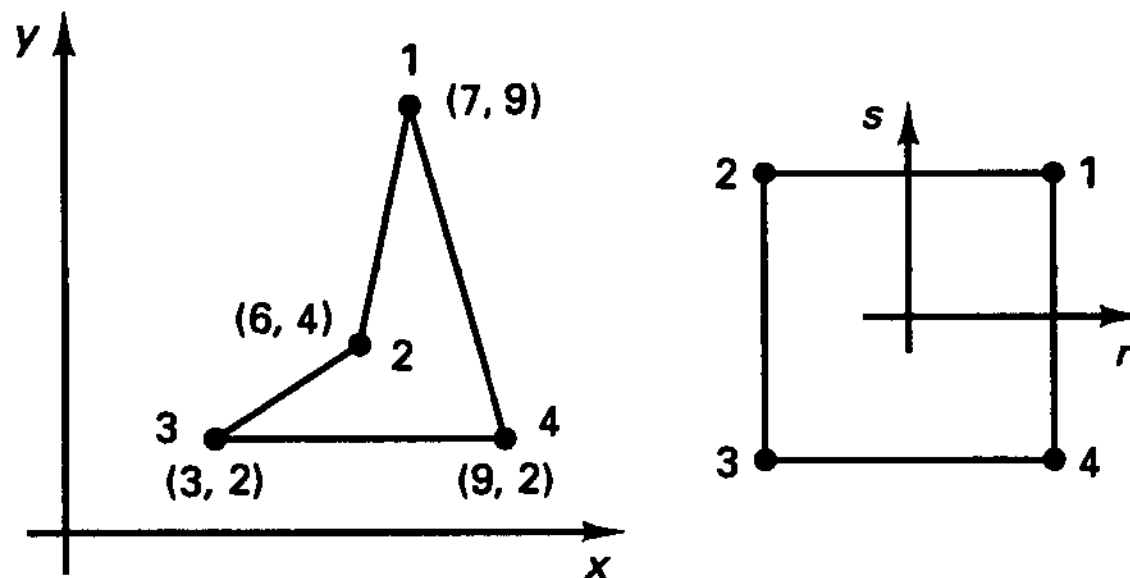
$$\mathbf{r} = \begin{bmatrix} \frac{\partial x}{\partial r} \\ \frac{\partial y}{\partial r} \\ \frac{\partial z}{\partial r} \end{bmatrix}; \quad \mathbf{s} = \begin{bmatrix} \frac{\partial x}{\partial s} \\ \frac{\partial y}{\partial s} \\ \frac{\partial z}{\partial s} \end{bmatrix}; \quad \mathbf{t} = \begin{bmatrix} \frac{\partial x}{\partial t} \\ \frac{\partial y}{\partial t} \\ \frac{\partial z}{\partial t} \end{bmatrix}$$

5.7. Evaluate the Jacobian matrices for the following four-node elements.

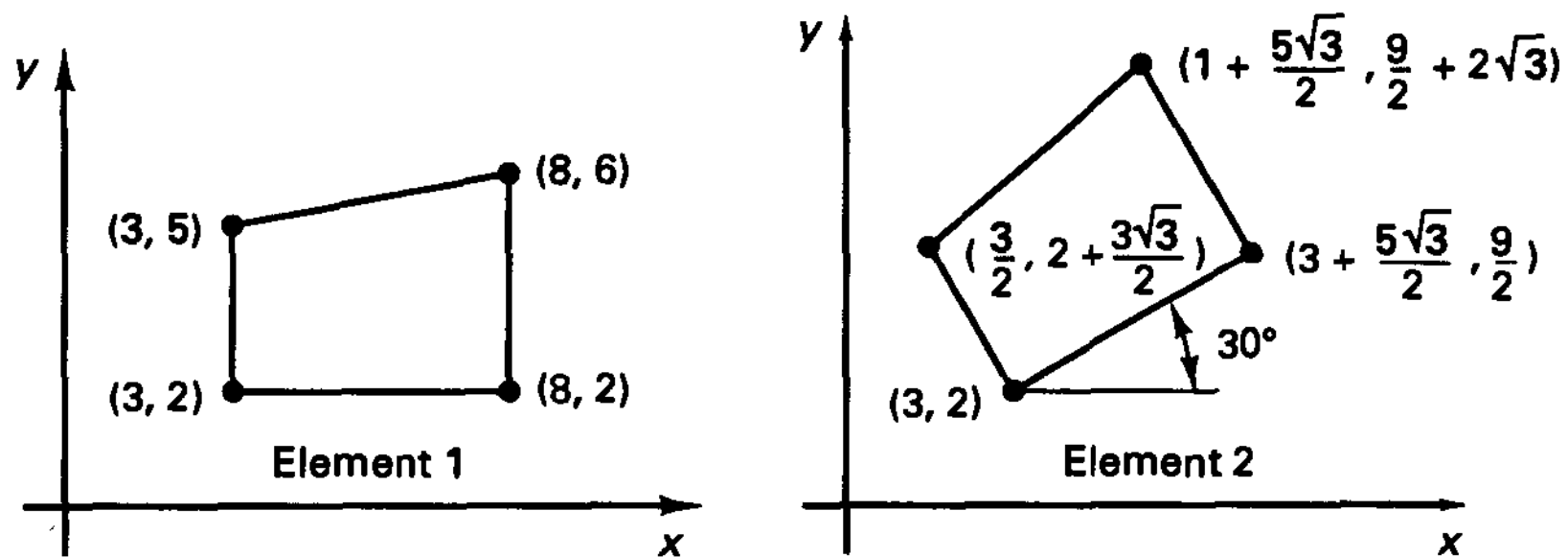


Show explicitly that the Jacobian matrices of elements 2 and 3 contain a rotation matrix representing a 30-degree rotation.

5.8. Calculate the Jacobian matrix of the element shown for all r, s . Identify the values of r, s for which the Jacobian matrix is singular.



5.9. Evaluate the Jacobian matrices J for the following four-node elements.



Show how the Jacobian matrix J of element 2 can be obtained by applying a rotation matrix to the Jacobian matrix J of element 1. Give this rotation matrix.

5.10. Consider the isoparametric elements given by

(a) Case 1:

$$x = \sum_{i=1}^8 h_i x_i; \quad x_1 = 12, x_2 = 4, x_3 = 4, x_4 = 12, x_5 = 9, x_6 = 5, x_7 = 8, x_8 = 11$$

$$y = \sum_{i=1}^8 h_i y_i; \quad y_1 = 12, y_2 = 8, y_3 = 2, y_4 = 2, y_5 = 8, y_6 = 5, y_7 = 1, y_8 = 7$$

(b) Case 2:

$$x = \sum_{i=1}^6 h_i^* x_i; \quad x_1 = 8, x_2 = 2, x_3 = 1, x_4 = 9, x_5 = 5, x_6 = 5$$

$$y = \sum_{i=1}^6 h_i^* y_i; \quad y_1 = 10, y_2 = 8, y_3 = 3, y_4 = 1, y_5 = 9, y_6 = 2$$

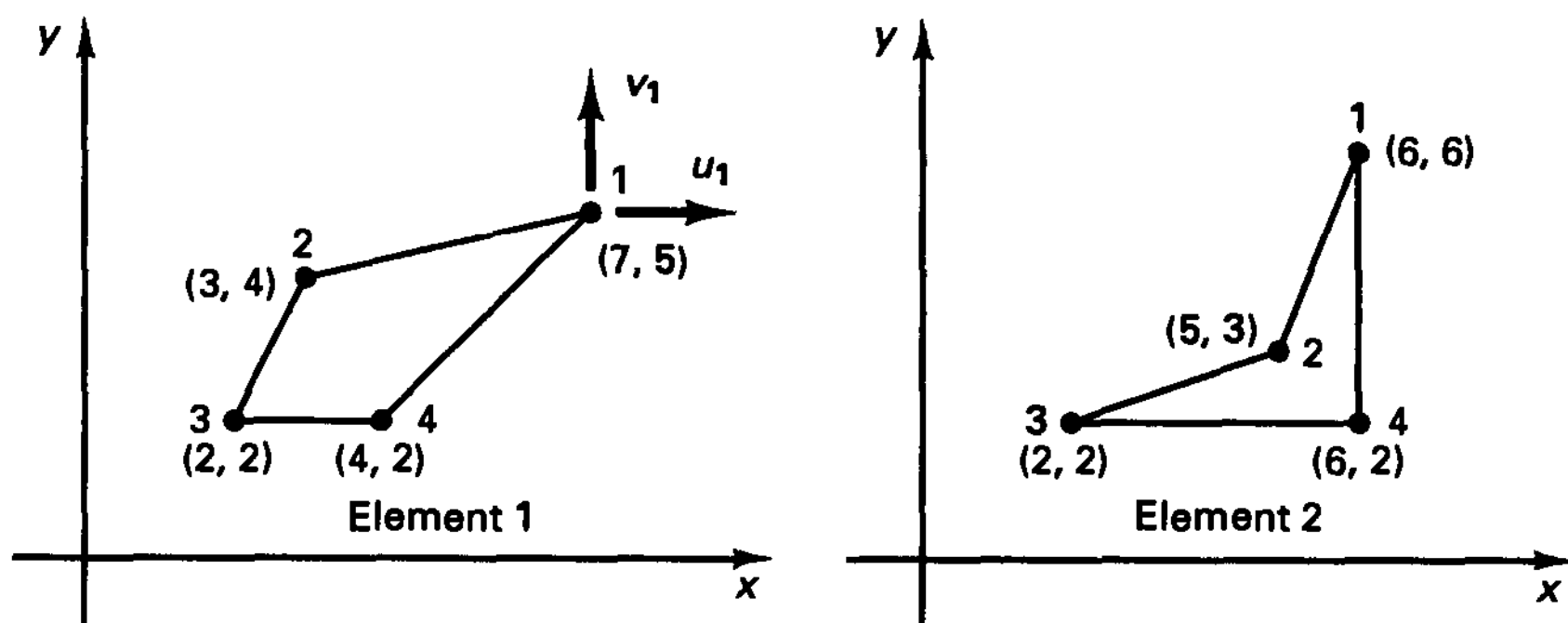
Draw the elements accurately on graph paper and show the physical locations of the lines $r = \frac{1}{2}$, $r = -\frac{1}{4}$, $s = \frac{3}{4}$, and $s = -\frac{1}{3}$ for each case. (You may also write a small program to perform this task.)

5.11. Consider the isoparametric finite elements shown. Sketch the following for each element.

(a) The lines, s as the variable and constant $r = -\frac{2}{3}, -\frac{1}{3}, 0, \frac{1}{3}, \frac{2}{3}$.

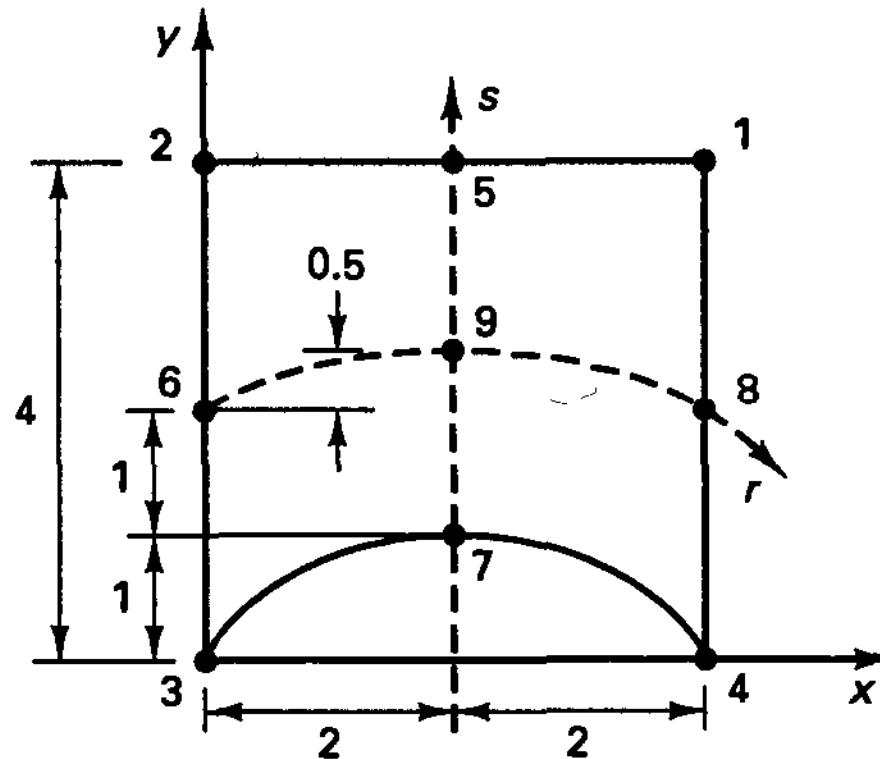
(b) The lines, r as the variable and constant $s = -\frac{2}{3}, -\frac{1}{3}, 0, \frac{1}{3}, \frac{2}{3}$.

(c) The determinant of the Jacobian over element 1 (in an oblique aerial view).

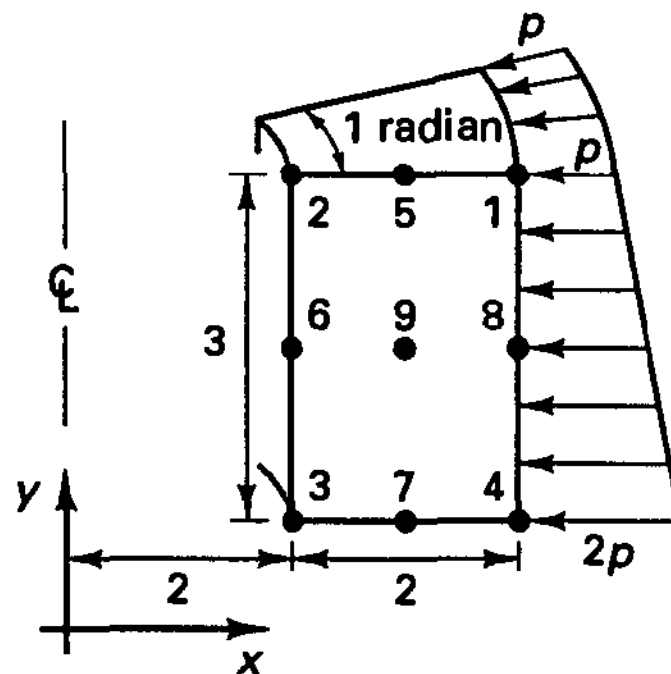


5.12. Prove that for any parallelogram-shaped isoparametric element the Jacobian determinant is constant. Also, prove that the Jacobian determinant always varies with r and/or s whenever the element is not square, rectangular, or parallelogram-shaped.

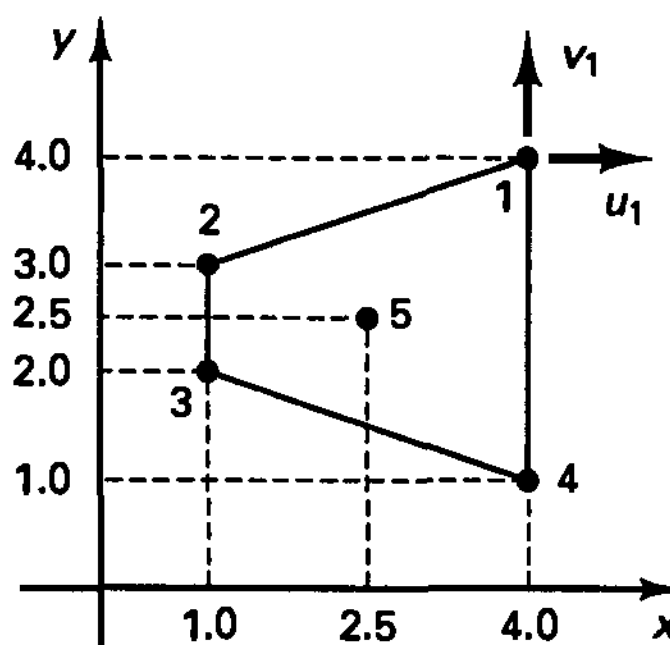
5.13. Consider the isoparametric element shown. Calculate the coordinates x, y of any point in the element as a function of r, s and establish the Jacobian matrix.



5.14. Calculate the nodal point forces corresponding to the surface loading on the axisymmetric element shown (consider 1 radian).



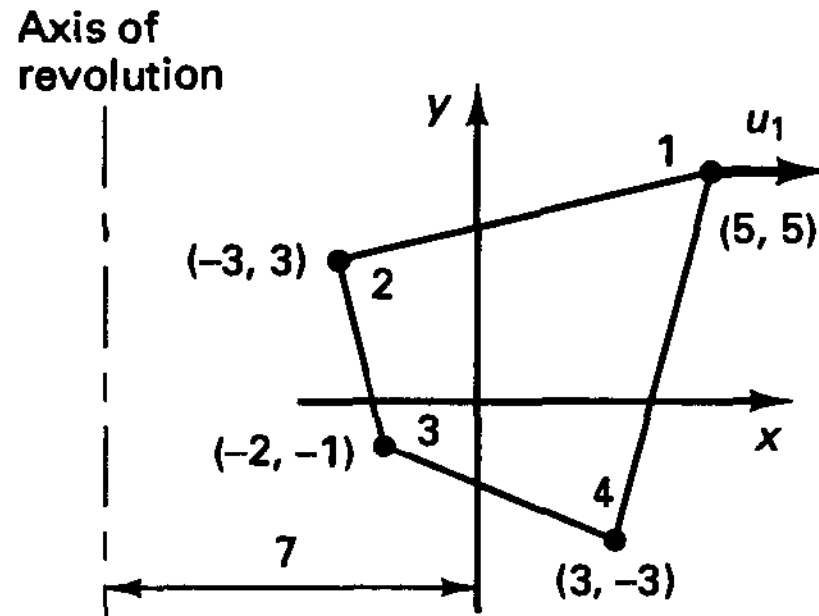
5.15. Consider the five-node plane strain isoparametric element shown.
 (a) Evaluate appropriate interpolation functions $h_i, i = 1$ to 5.
 (b) Evaluate the column in the strain-displacement matrix corresponding to the displacement u_1 at the point $x = 2.5, y = 2.5$.



5.16. Consider the isoparametric axisymmetric two-dimensional finite element shown.

(a) Construct the Jacobian matrix \mathbf{J} .

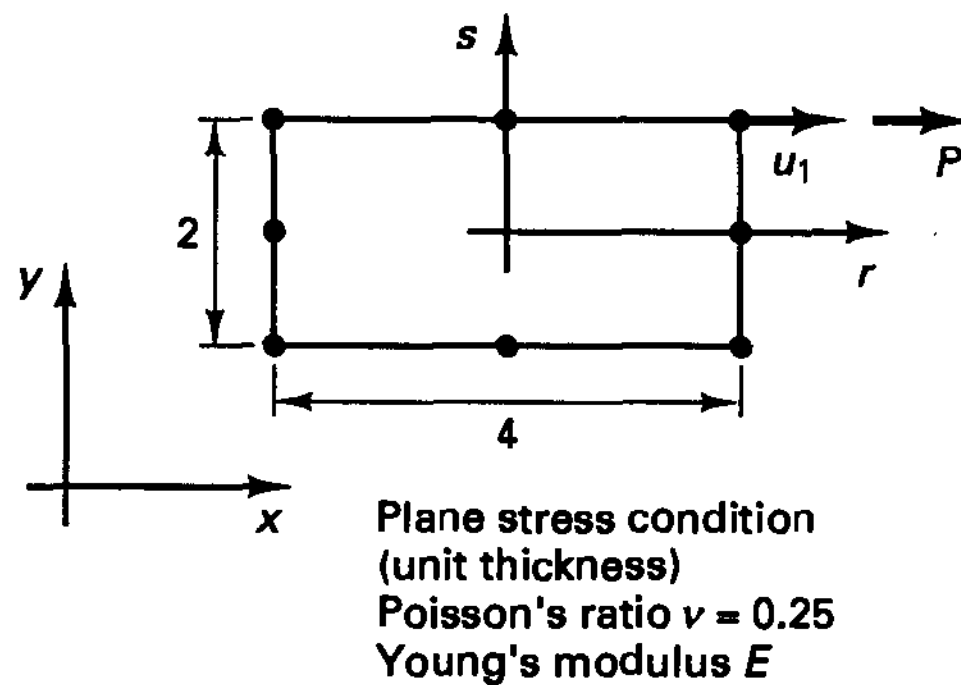
(b) Give an analytical expression of the column in the strain-displacement matrix $\mathbf{B}(r, s)$ that corresponds to the displacement u_1 .



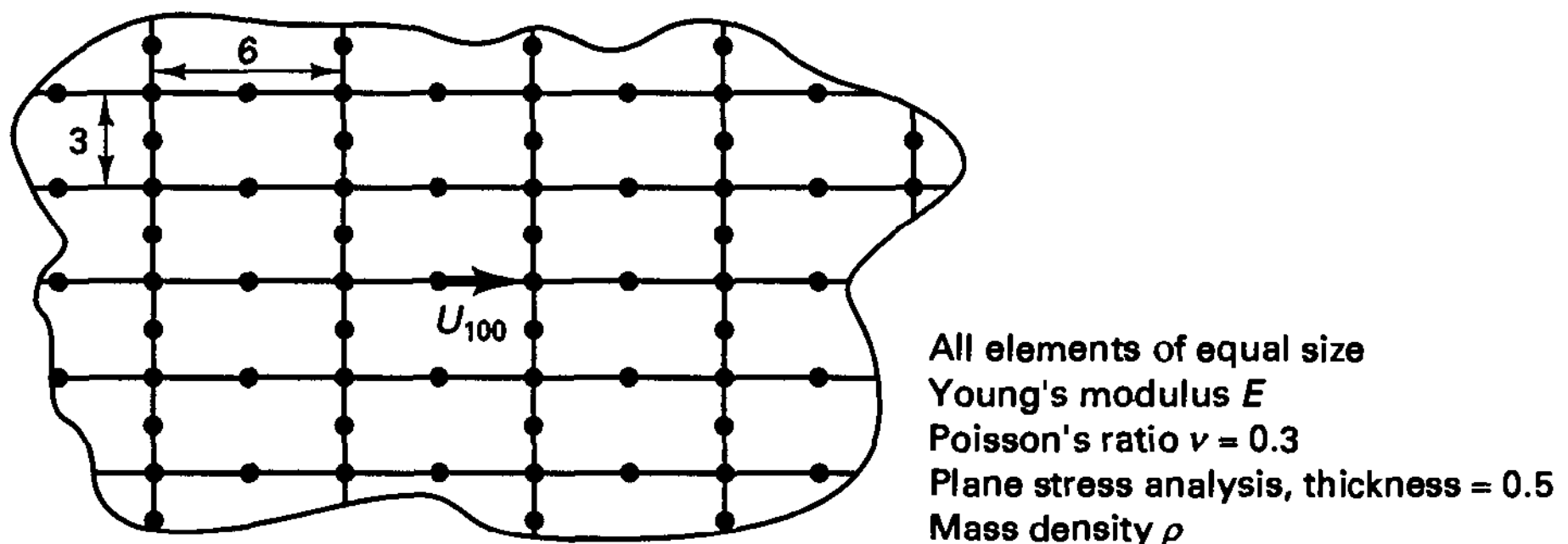
5.17. The eight-node isoparametric element shown has all its nodal point displacements constrained to zero except for u_1 . The element is subjected to a concentrated load P into u_1 .

(a) Calculate and sketch the displacements corresponding to P .

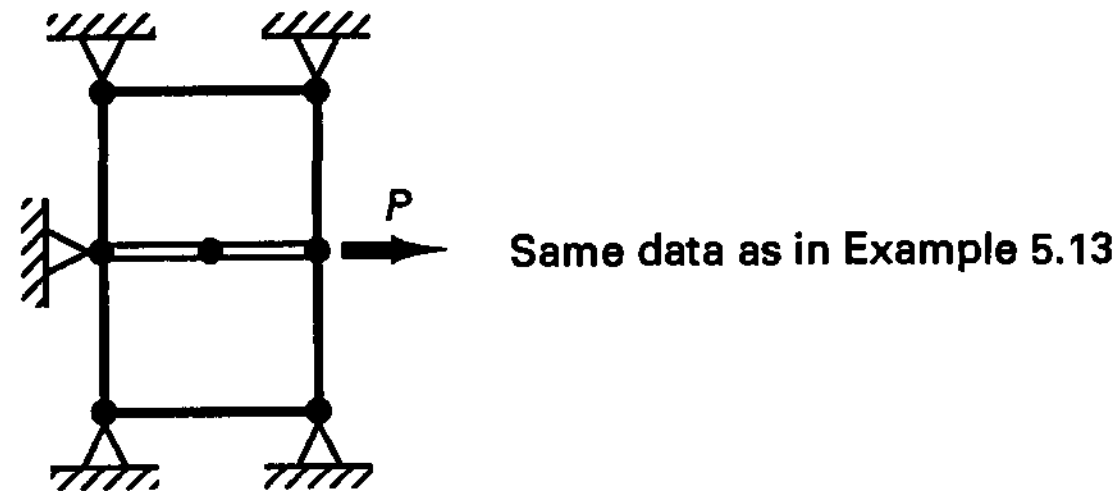
(b) Sketch all element stresses corresponding to the deformed configuration. Use an oblique/aerial view for your sketches.



5.18. The eight-node element assemblage shown is used in a finite element analysis. Calculate the diagonal elements of the stiffness matrix and consistent mass matrix corresponding to the degree of freedom U_{100} .

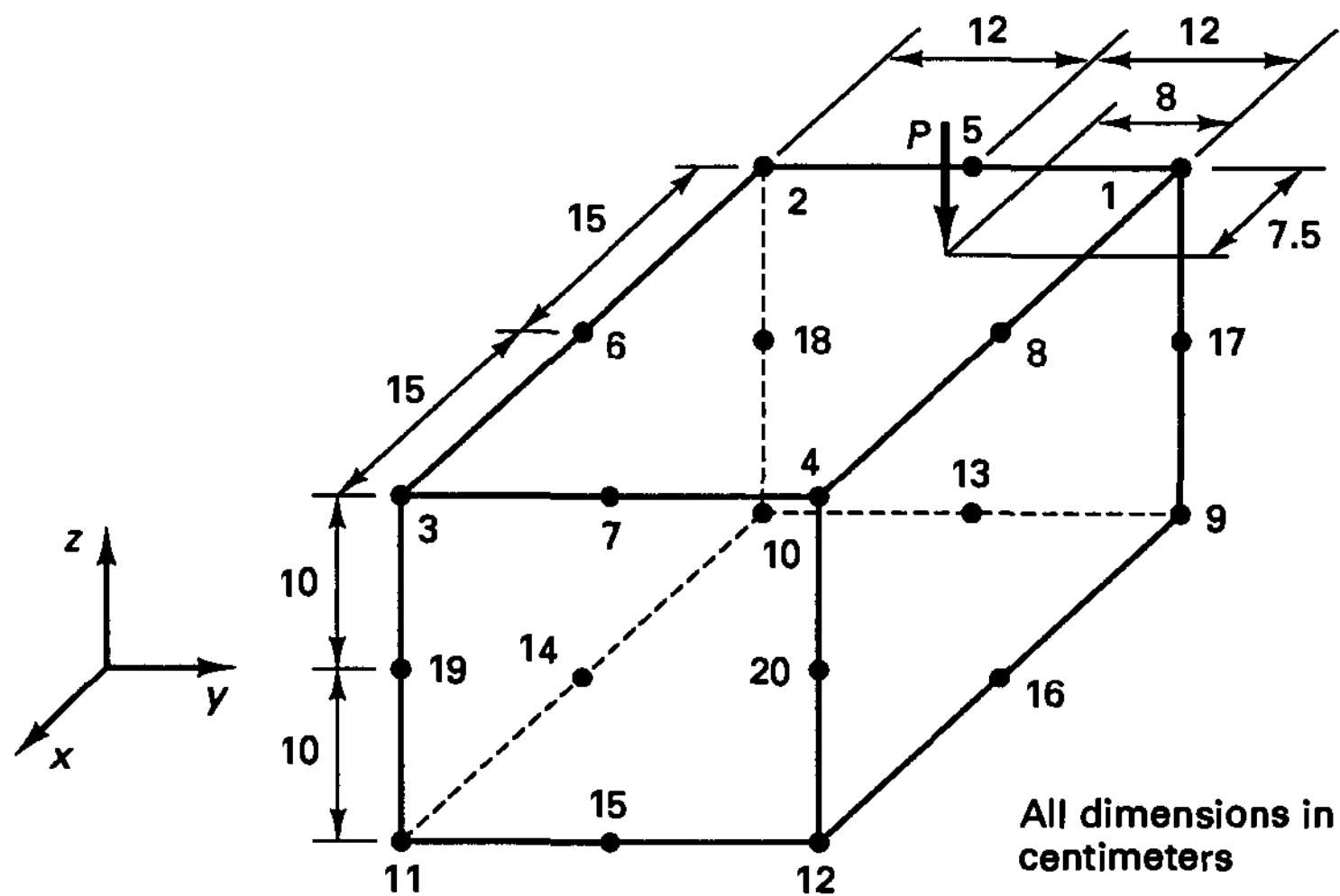


5.19. The problem in Example 5.13 is modeled by two five-node plane stress elements and one three-node bar element:



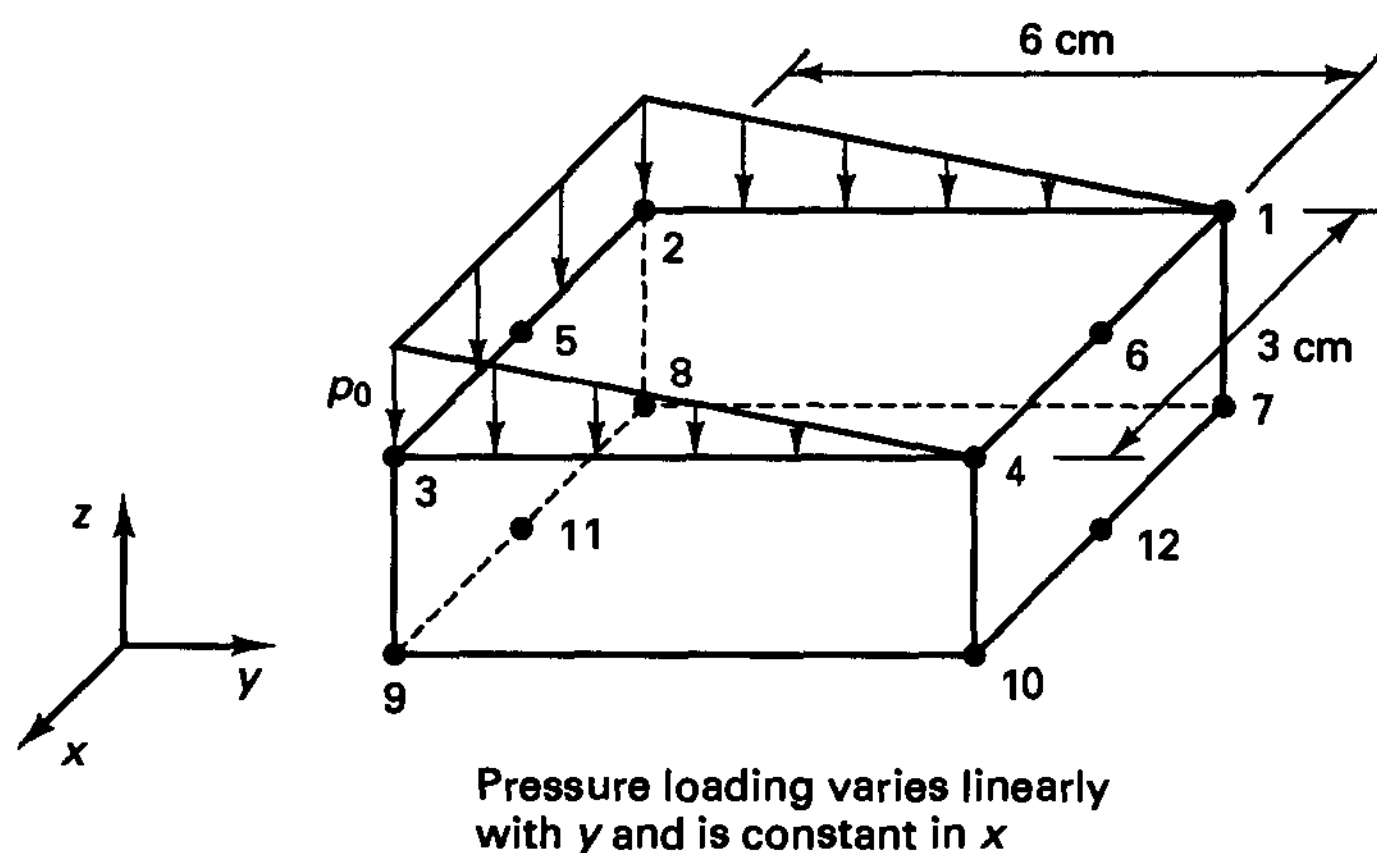
- (a) Establish in detail all matrices used in the formulation of the governing equilibrium equations but do not perform any integrations.
- (b) Assume that you have evaluated the unknown nodal point displacements. Present graphically in an oblique/aerial view all displacements and stresses in the elements.

5.20. The 20-node brick element shown is loaded by a concentrated load at the location indicated. Calculate the consistent nodal point loads.

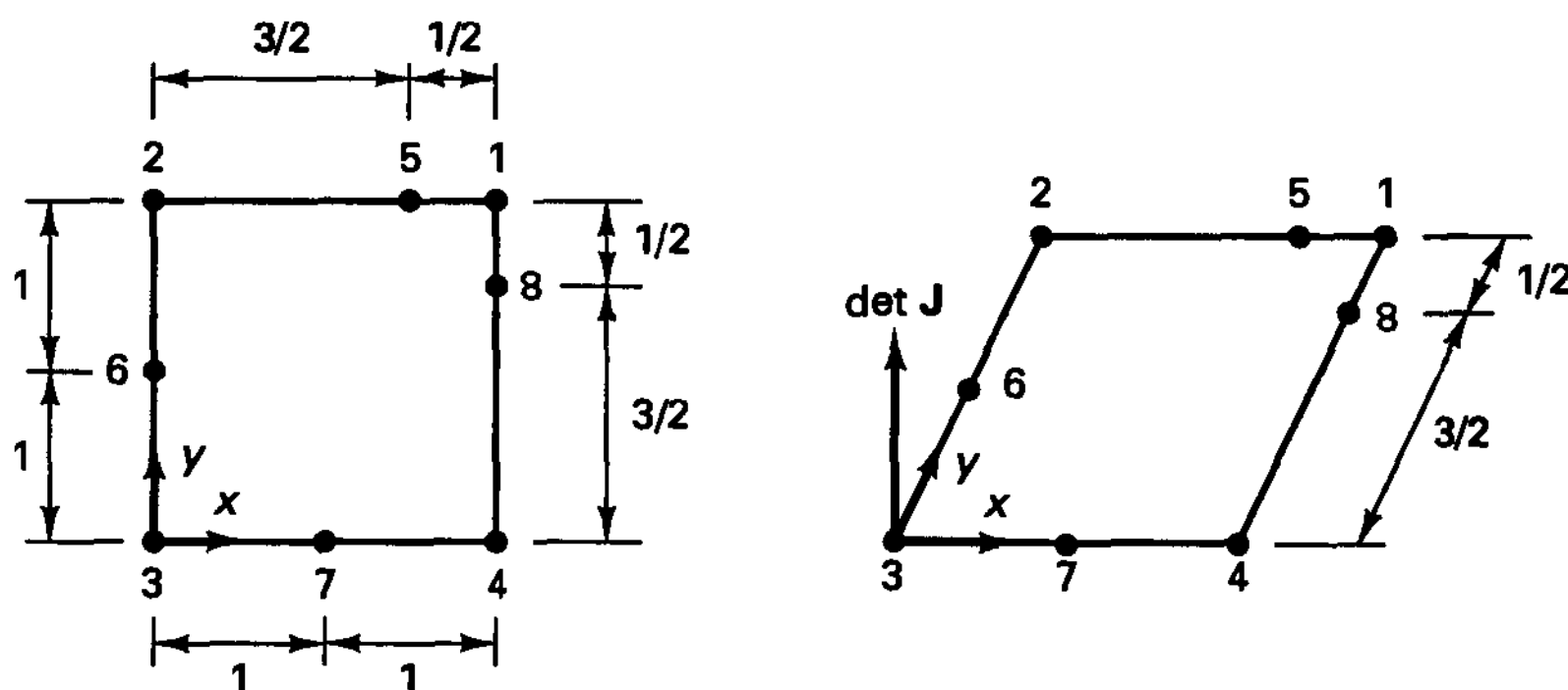


5.21. The element in Exercise 5.20 is to be used in dynamic analysis. Construct a reasonable lumped mass matrix of the element; use $\rho = 7.8 \times 10^{-3} \text{ kg/cm}^3$.

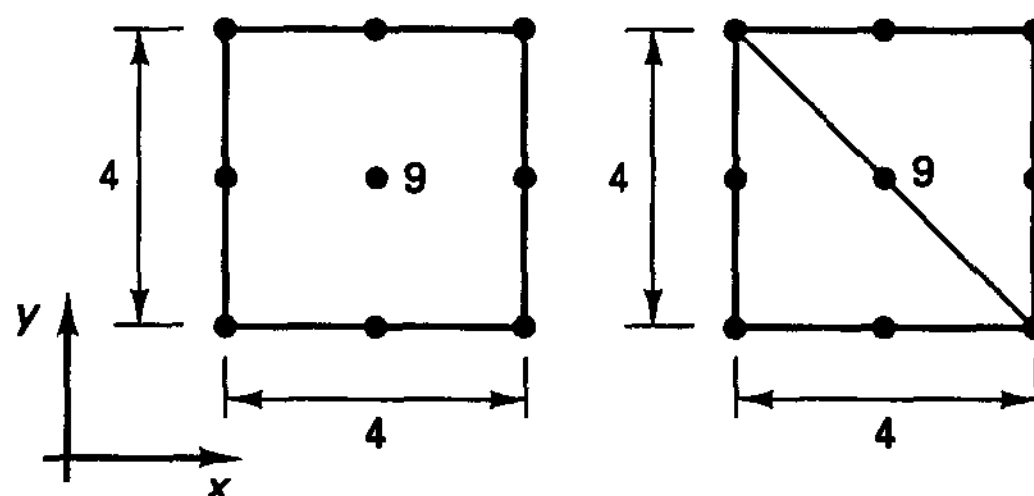
5.22. The 12-node three-dimensional element shown is loaded with the pressure loading indicated. Calculate the nodal point consistent load vector for nodes 1, 2, 7, and 8.



5.23. Evaluate the Jacobian matrix J of the following element as a function of r, s and plot $\det J$ "over" the element (in our oblique/aerial view).

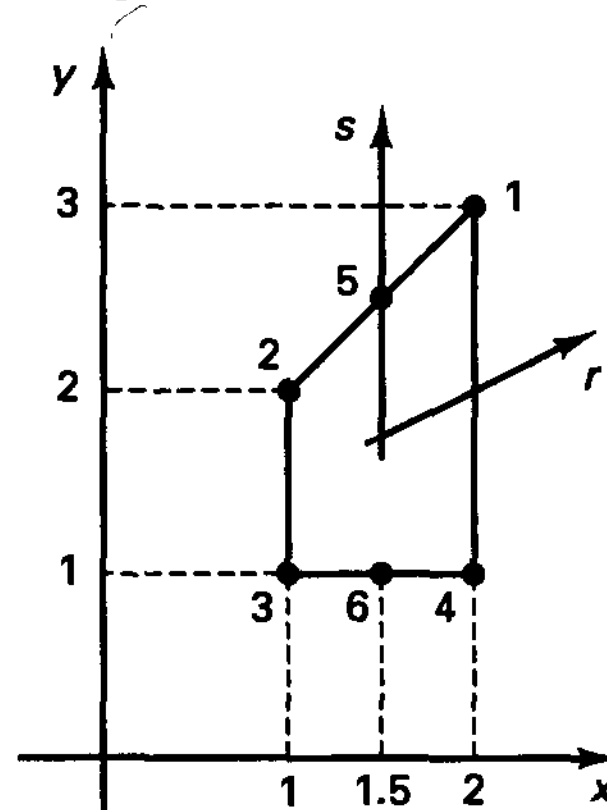


5.24. Plot, for node 9, the displacement interpolation functions and their x -derivatives for the nine-node element and the assemblage of two six-node triangles (formed using the interpolation functions in Fig. 5.11).

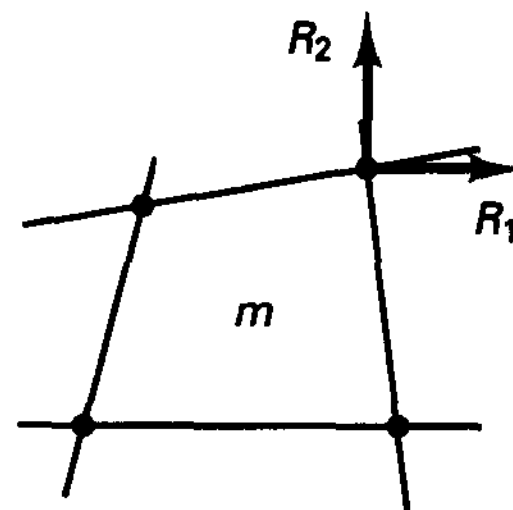


5.25. Prove that the interpolation functions in (5.36), with Δh defined in (5.37), define the same displacement assumptions as the functions in Fig. 5.11 (note that the origins of the coordinates used in the two formulations are different).

- 5.26. Collapse a 20-node brick element into a spatially isotropic 10-node tetrahedron (use the collapsing of sides in Fig. E5.16). Determine the correction that must be applied to the interpolation function h_{16} of the brick element in order to obtain the displacement assumption h_6 of the tetrahedron (given in Fig. 5.13).
- 5.27. Consider the six-node isoparametric plane strain finite element shown.



- (a) Construct the interpolation functions, $h_i(r, s)$, $i = 1, \dots, 6$, of the element.
- (b) Prove in detail that this finite element does (or does not) satisfy all convergence requirements when used in a compatible finite element assemblage.
- 5.28. Consider a general isoparametric four-node element used in an assemblage of elements as shown.



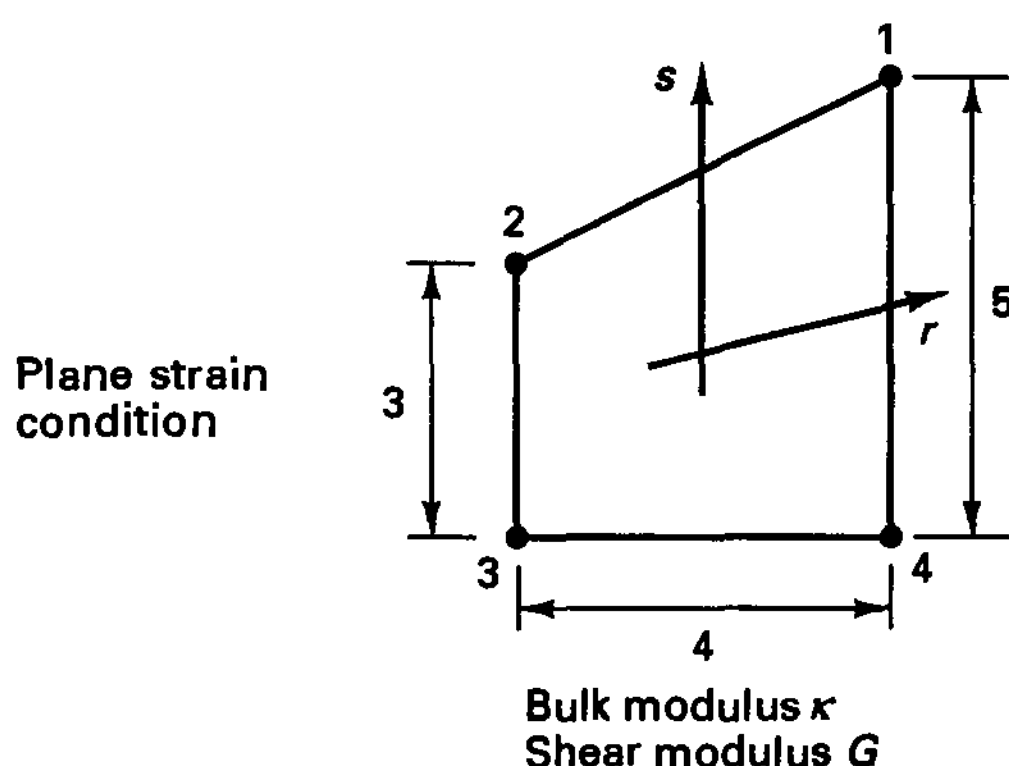
Either plane strain or plane stress condition

- (a) Prove that the nodal point forces defined as

$$\mathbf{F}^{(m)} = \int_{V^{(m)}} \mathbf{B}^{(m)T} \boldsymbol{\tau}^{(m)} dV^{(m)}$$

are in equilibrium for element m , where $\boldsymbol{\tau}^{(m)} = \mathbf{CB}^{(m)}\mathbf{U}$ has been calculated.

- (b) Show that the sum of the nodal point forces at each node is in equilibrium with the applied external loads R_i (including the reactions). (*Hint*: Refer to Section 4.2.1, Fig. 4.2.)
- 5.29. Consider Table 5.1 and the case of angular distortion. Prove that the terms listed for the 12- and 16-node elements are indeed correct.
- 5.30. Consider Table 5.1 and the case of curved edge distortion. Prove that the terms listed in the column for the 8-, 9-, 12-, and 16-node elements are correct.
- 5.31. Consider the 4/1 isoparametric u/p element shown. Construct all matrices for the evaluation of the stiffness matrix of the element but do not perform any integrations.

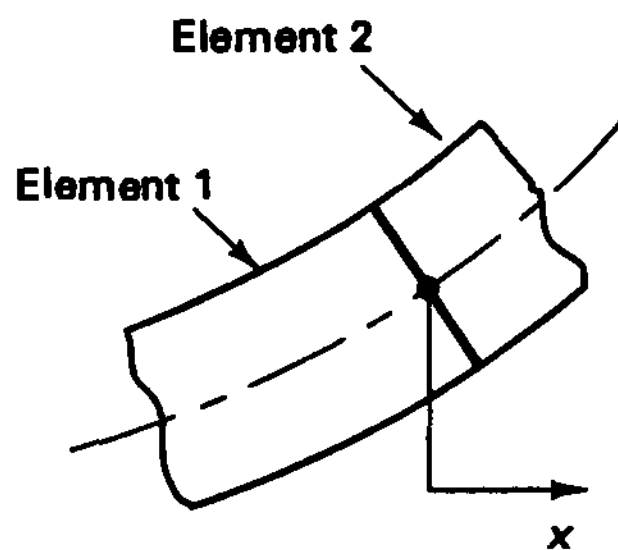
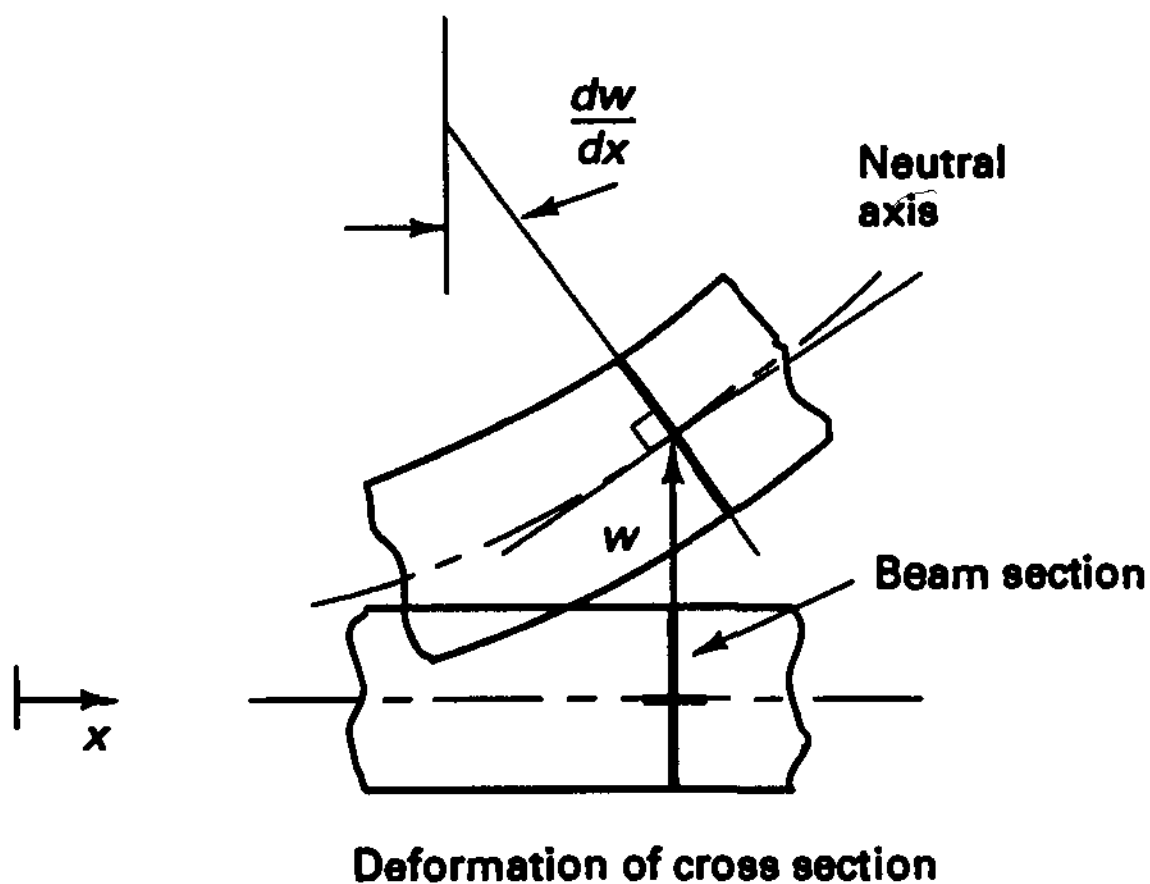


5.4 FORMULATION OF STRUCTURAL ELEMENTS

The concepts of geometry and displacement interpolations that have been employed in the formulation of two- and three-dimensional continuum elements can also be employed in the evaluation of beam, plate, and shell structural element matrices. However, whereas in the formulation of the continuum elements the displacements u , v , w (whichever are applicable) are interpolated in terms of nodal point displacements of the same kind, in the formulation of structural elements, the displacements u , v , and w are interpolated in terms of midsurface displacements and rotations. We will show that this procedure corresponds in essence to a continuum isoparametric element formulation with displacement constraints. In addition, there is of course the major assumption that the stress normal to the midsurface is zero. The structural elements are for these reasons appropriately called *degenerate isoparametric elements*, but frequently we still refer to them simply as *isoparametric elements*.

Considering the formulation of structural elements, we have already discussed briefly in Section 4.2.3 how beam, plate, and shell elements can be formulated using the Bernoulli beam and Kirchhoff plate theory, in which shear deformations are neglected. Using the Kirchhoff theory it is difficult to satisfy interelement continuity on displacements and edge rotations because the plate (or shell) rotations are calculated from the transverse displacements. Furthermore, using an assemblage of flat elements to represent a shell structure, a relatively large number of elements may be required in order to represent the shell geometry to sufficient accuracy.

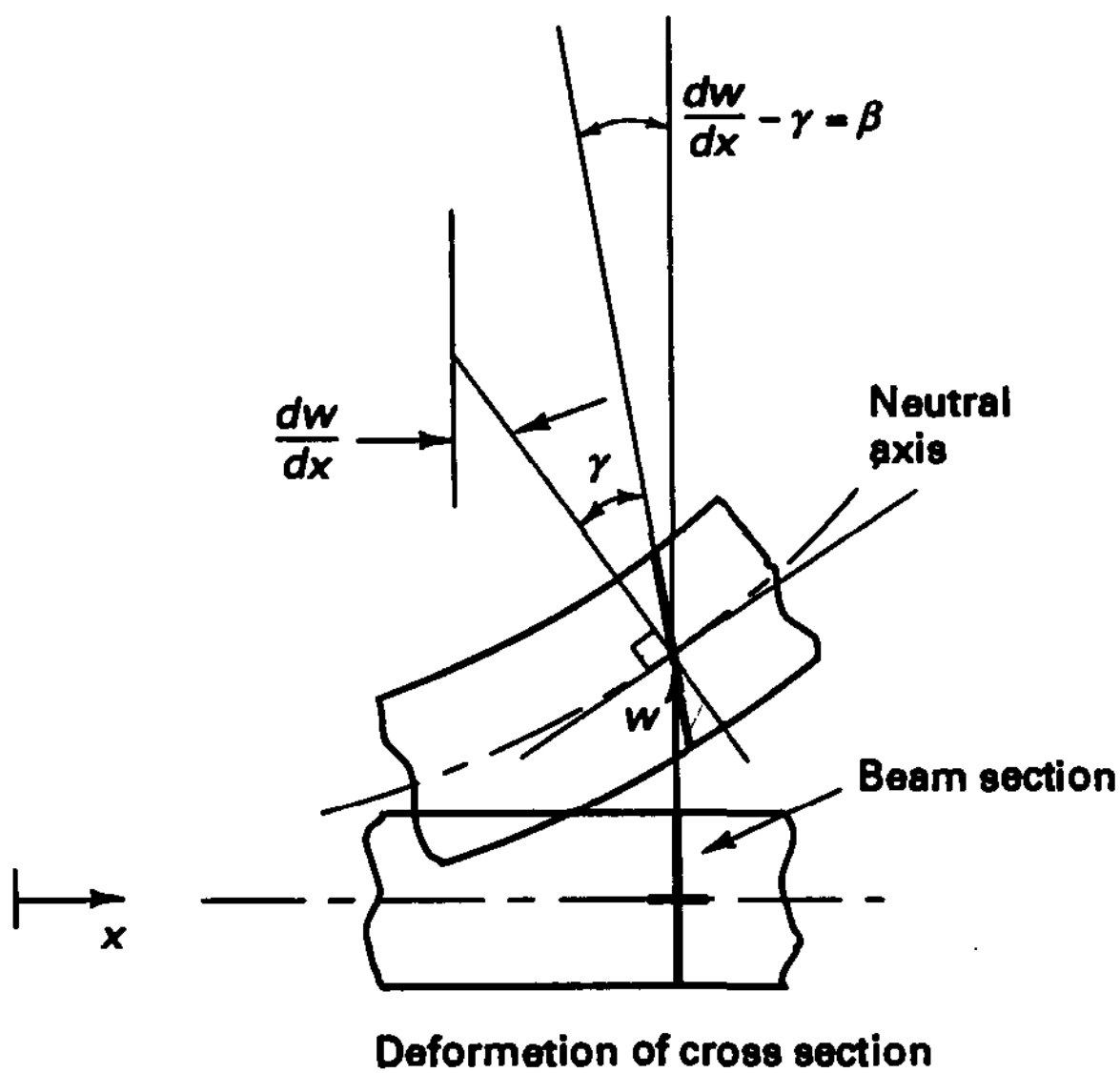
Our objective in this section is to discuss an alternative approach to formulating beam, plate, and shell elements. The basis of this method is a theory that includes the effects of shear deformations. In this theory the displacements and rotations of the midsurface normals are independent variables, and the interelement continuity conditions on these quantities can be satisfied directly, as in the analysis of continua. In addition, if the concepts of isoparametric interpolation are employed, the geometry of curved shell surfaces is interpolated and can be represented to a high degree of accuracy. In the following sections we discuss first the formulation of beam and axisymmetric shell elements, where we can demonstrate in detail the basic principles used, and we then present the formulation of general plate and shell elements.



Boundary conditions between beam elements

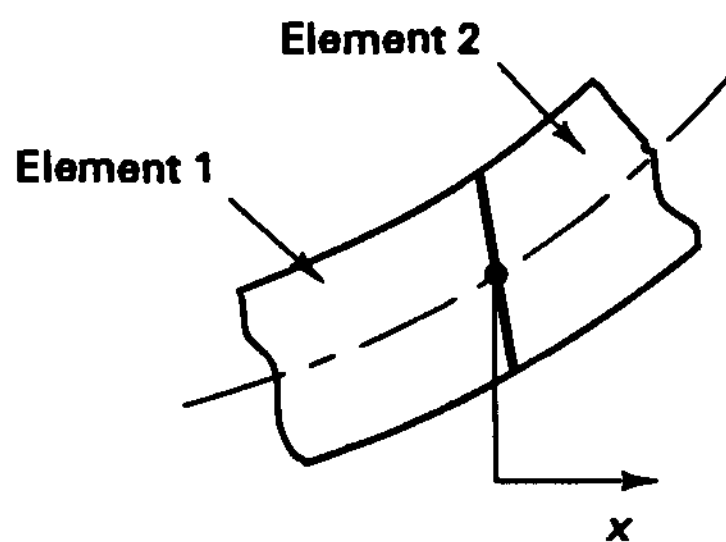
$$w \Big|_{x=0^-} = w \Big|_{x=0^+}; \quad \frac{dw}{dx} \Big|_{x=0^-} = \frac{dw}{dx} \Big|_{x=0^+}$$

(a) Beam deformations excluding shear effect



$$u = -\beta(x)z$$

$$w = w(x)$$



Boundary conditions between beam elements

$$w \Big|_{x=0^-} = w \Big|_{x=0^+}$$

$$\beta \Big|_{x=0^-} = \beta \Big|_{x=0^+}$$

(b) Beam deformations including shear effect

Figure 5.18 Beam deformation assumptions

5.4.1 Beam and Axisymmetric Shell Elements

Let us discuss first some basic assumptions pertaining to the formulation of beam elements. The basic assumption in beam bending analysis excluding shear deformations is that a normal to the midsurface (neutral axis) of the beam remains straight during deformation and that its angular rotation is equal to the slope of the beam midsurface. This kinematic assumption, illustrated in Fig. 5.18(a), corresponds to the Bernoulli beam theory and leads to the well-known beam-bending governing differential equation in which the transverse displacement w is the only variable (see Example 3.20). Therefore, using beam elements formulated with this theory, displacement continuity between elements requires that w and dw/dx be continuous.

Considering now beam bending analysis with the effect of shear deformations, we retain the assumption that a plane section originally normal to the neutral axis remains plane, but because of shear deformations this section does not remain normal to the neutral axis. As illustrated in Fig. 5.18(b), the total rotation of the plane originally normal to the neutral axis of the beam is given by the rotation of the tangent to the neutral axis and the shear deformation,

$$\beta = \frac{dw}{dx} - \gamma \quad (5.56)$$

where γ is a constant shearing strain across the section. This kinematic assumption corresponds to Timoshenko beam theory (see S. H. Crandall, N. C. Dahl, and T. J. Lardner [A]). Since the actual shearing stress and strain vary over the section, the shearing strain γ in (5.56) is an equivalent constant strain on a corresponding shear area A_s ,

$$\tau = \frac{V}{A_s}; \quad \gamma = \frac{\tau}{G}; \quad k = \frac{A_s}{A} \quad (5.57)$$

where V is the shear force at the section being considered. Different assumptions may be used to evaluate a reasonable factor k (see S. Timoshenko and J. N. Goodier [A] and K. Washizu [B]). One simple procedure is to evaluate the shear correction factor using the condition that when acting on A_s , the constant shear stress in (5.57) must yield the same shear strain energy as the actual shearing stress (evaluated from beam theory) acting on the actual cross-sectional area A of the beam. Consider the following example.

EXAMPLE 5.23: Evaluate the shear correction factor k for a beam of rectangular cross section, width b , and depth h .

The shear strain energy \mathcal{U} of the beam per unit length is

$$\mathcal{U} = \int_A \frac{1}{2G} \tau_a^2 dA \quad (a)$$

where τ_a is the actual shear stress, G is the shear modulus, and A is the cross-sectional area, $A = bh$.

In our finite element model, by assumption, the shear strain is constant over the cross-sectional area of the beam [see (5.56)]. Since in reality the shear strain varies over the beam cross section, we want to find an equivalent beam cross-sectional area A_s for our finite element model. This equivalency will be based on equating shear strain energies.

Hence using \mathcal{U} , given in (a), with the actual shear stress distribution, we can calculate A_s from

$$\int_A \frac{1}{2G} \tau_a^2 dA = \int_{A_s} \frac{1}{2G} \left(\frac{V}{A_s} \right)^2 dA_s \quad (b)$$

where V is the total shearing force at the section,

$$V = \int_A \tau_a dA \quad (c)$$

If we use $k = A_s/A$, we obtain from (b),

$$k = \frac{V^2}{A \int_A \tau_a^2 dA}$$

We now use (b) and (c) for the rectangular cross-section beam. Elementary beam theory gives (see S. H. Crandall, N. C. Dahl, and T. J. Lardner [A])

$$\tau_a = \frac{3}{2} \frac{V}{A} \left[\frac{(h/2)^2 - y^2}{(h/2)^2} \right]$$

which gives $k = \frac{5}{6}$.

The finite element formulation of a beam element with the assumption in (5.56) is obtained using the basic virtual work expressions in (4.19) to (4.22). In the following we consider first, for illustrative purposes, the specific formulation of the beam element matrices corresponding to the simple element in Fig. 5.19, and we discuss afterward the formulation of more general three-dimensional beam elements, and the formulation of axisymmetric shell elements.

Two-Dimensional Straight Beam Elements

Figure 5.19 shows the two-dimensional rectangular cross-section beam considered. Using the general expression of the principle of virtual work with the assumptions discussed above we have (see Exercise 5.32)

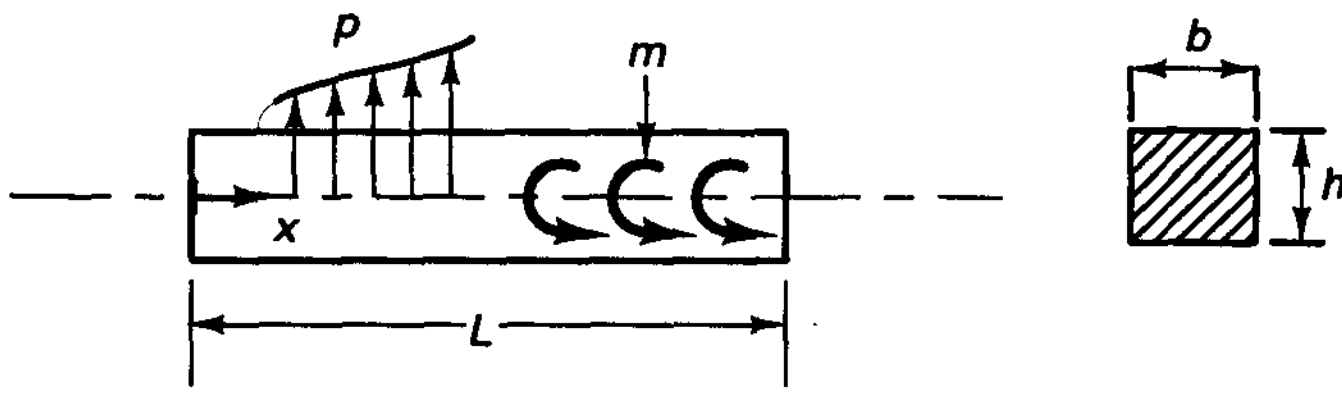
$$EI \int_0^L \left(\frac{d\beta}{dx} \right) \left(\frac{d\bar{\beta}}{dx} \right) dx + GAk \int_0^L \left(\frac{dw}{dx} - \beta \right) \left(\frac{d\bar{w}}{dx} - \bar{\beta} \right) dx = \int_0^L p\bar{w} dx + \int_0^L m\bar{\beta} dx \quad (5.58)$$

where p and m are the transverse and moment loadings per unit length. Using now the interpolations

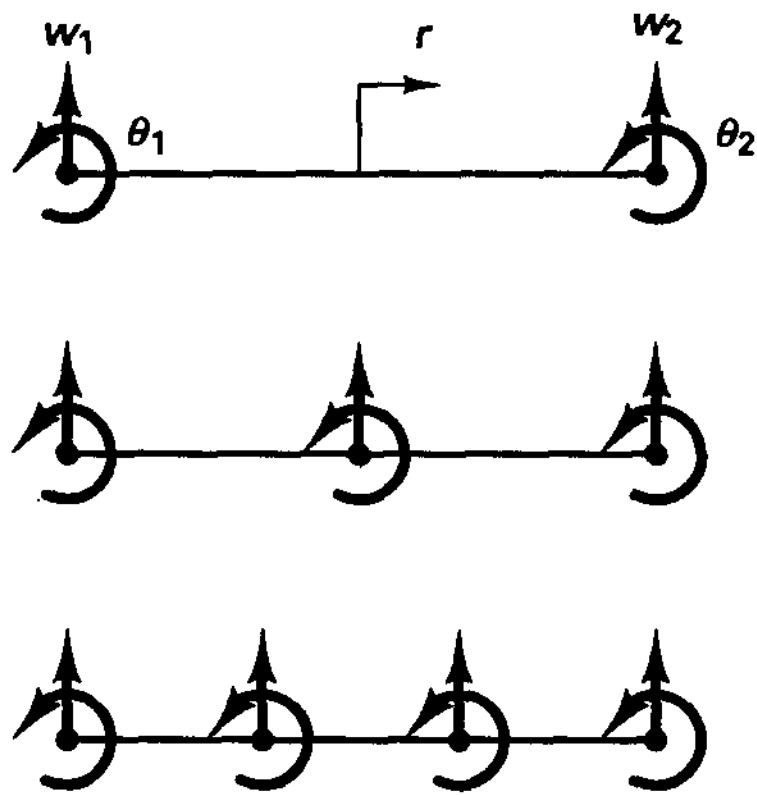
$$w = \sum_{i=1}^q h_i w_i; \quad \beta = \sum_{i=1}^q h_i \theta_i \quad (5.59)$$

where q is equal to the number of nodes used and the h_i are the one-dimensional interpolation functions listed in Fig. 5.3, we can directly employ the concepts of the isoparametric formulations discussed in Section 5.3 to establish all relevant element matrices. Let

$$\begin{aligned} w &= \mathbf{H}_w \hat{\mathbf{u}}; & \beta &= \mathbf{H}_\beta \hat{\mathbf{u}} \\ \frac{\partial w}{\partial x} &= \mathbf{B}_w \hat{\mathbf{u}}; & \frac{\partial \beta}{\partial x} &= \mathbf{B}_\beta \hat{\mathbf{u}} \end{aligned} \quad (5.60)$$



(a) Beam with applied loading
 $E = \text{Young's modulus}; G = \text{shear modulus};$
 $k = \frac{5}{6}; A = hb; I = \frac{bh^3}{12}$



(b) 2-, 3-, and 4-node models; $\theta_i = \beta_i, i = 1, \dots, q$
 (Interpolation functions are given in Fig. 5.3)

Figure 5.19 Formulation of two-dimensional beam element

where

$$\begin{aligned} \hat{\mathbf{u}}^T &= [w_1 \dots w_q \quad \theta_1 \dots \theta_q] \\ \mathbf{H}_w &= [h_1 \dots h_q \quad 0 \dots 0] \\ \mathbf{H}_\beta &= [0 \dots 0 \quad h_1 \dots h_q] \end{aligned} \tag{5.61}$$

and

$$\begin{aligned} \mathbf{B}_w &= J^{-1} \begin{bmatrix} \frac{\partial h_1}{\partial r} & \dots & \frac{\partial h_q}{\partial r} & 0 & \dots & 0 \end{bmatrix} \\ \mathbf{B}_\beta &= J^{-1} \begin{bmatrix} 0 & \dots & 0 & \frac{\partial h_1}{\partial r} & \dots & \frac{\partial h_q}{\partial r} \end{bmatrix} \end{aligned} \tag{5.62}$$

where $J = \partial x / \partial r$; then we have for a single element,

$$\begin{aligned} \mathbf{K} &= EI \int_{-1}^1 \mathbf{B}_\beta^T \mathbf{B}_\beta \det J \, dr + GAk \int_{-1}^1 (\mathbf{B}_w - \mathbf{H}_\beta)^T (\mathbf{B}_w - \mathbf{H}_\beta) \det J \, dr \\ \mathbf{R} &= \int_{-1}^1 \mathbf{H}_w^T p \det J \, dr + \int_{-1}^1 \mathbf{H}_\beta^T m \det J \, dr \end{aligned} \tag{5.63}$$

Also, in dynamic analysis the mass matrix can be calculated using the d'Alembert principle [see (4.23)]; hence,

$$\mathbf{M} = \int_{-1}^1 \begin{bmatrix} \mathbf{H}_w \\ \mathbf{H}_\beta \end{bmatrix}^T \begin{bmatrix} \rho b h & 0 \\ 0 & \frac{\rho b h^3}{12} \end{bmatrix} \begin{bmatrix} \mathbf{H}_w \\ \mathbf{H}_\beta \end{bmatrix} \det J \, dr \tag{5.64}$$

In these evaluations we are using the natural coordinate system of the beam because this is effective in the formulation of more general beam, plate, and shell elements. However, when considering a straight beam of constant cross section, the integrals can also be evaluated efficiently without using the natural coordinate system, as demonstrated in the following example.

EXAMPLE 5.24: Evaluate the detailed expressions for calculation of the stiffness matrix and the load vector of the three-node beam element shown in Fig. E5.24.

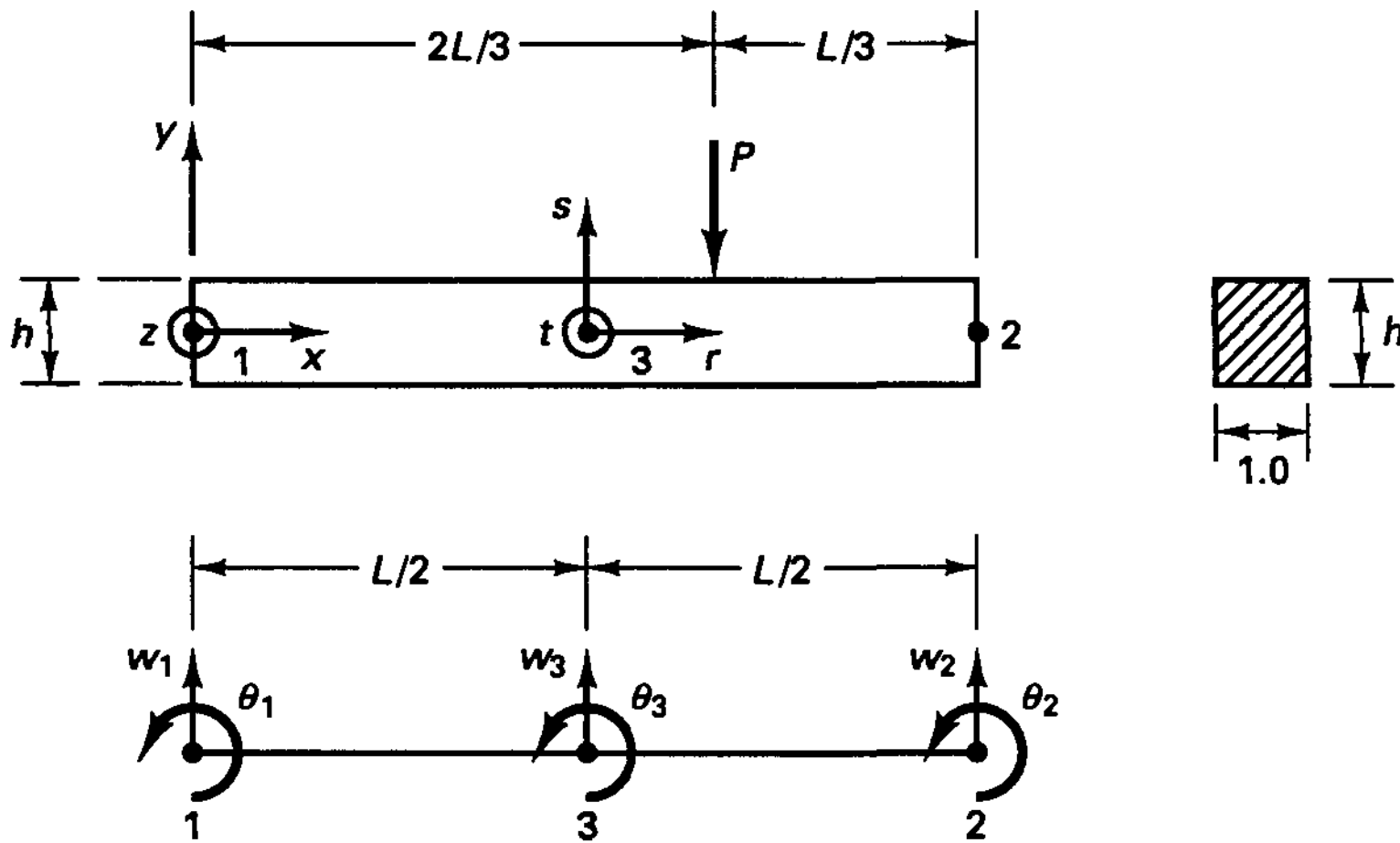


Figure E5.24 Three-node beam element

The interpolation functions to be used are listed in Fig. 5.3. These functions are given in terms of r and yield

$$x = \sum_{i=1}^3 h_i x_i$$

Using $x_1 = 0$, $x_2 = L$, $x_3 = L/2$, we obtain

$$x = \frac{L}{2}(1 + r)$$

Hence, the interpolation functions in terms of x are

$$h_1 = \frac{2x^2}{L^2} - \frac{3x}{L} + 1$$

$$h_2 = \frac{2x^2}{L^2} - \frac{x}{L}$$

$$h_3 = \frac{4x}{L} - \frac{4x^2}{L^2}$$

Using the notation $(\quad)' \equiv \partial/\partial x$ it follows that

$$h'_1 = \frac{4x}{L^2} - \frac{3}{L}$$

$$h'_2 = \frac{4x}{L^2} - \frac{1}{L}$$

$$h'_3 = \frac{4}{L} - \frac{8x}{L^2}$$

Hence, with the degrees of freedom ordered as in (5.61), we have

$$\mathbf{K} = \frac{Eh^3}{12} \int_0^L \begin{bmatrix} 0 \\ 0 \\ 0 \\ h'_1 \\ h'_2 \\ h'_3 \end{bmatrix} [0 \quad 0 \quad 0 \quad h'_1 \quad h'_2 \quad h'_3] dx$$

$$+ \frac{5Gh}{6} \int_0^L \begin{bmatrix} h'_1 \\ h'_2 \\ h'_3 \\ -h_1 \\ -h_2 \\ -h_3 \end{bmatrix} [h'_1 \quad h'_2 \quad h'_3 \quad -h_1 \quad -h_2 \quad -h_3] dx$$

and

$$\mathbf{R}^T = -P[-\frac{1}{9} \quad \frac{2}{9} \quad \frac{8}{9} \quad 0 \quad 0 \quad 0]$$

The element in Fig. 5.19 is a pure displacement-based element (assuming exact integration of all integrals) and can be employed provided three or four nodes are used (and the interior nodes are located at the midpoint and third-points, respectively). However, if the two-node element is employed or the interior nodes of the three- and four-node elements are not located at the midpoint and third-points, respectively, the use of the element cannot be recommended because the shearing deformations are not represented to sufficient accuracy. This deficiency is particularly pronounced when the element is thin.

In order to obtain some insight into the behavior of these elements when the beam becomes thin, we recall that the principle of virtual work is equivalent to the stationarity of the total potential (see Example 4.4). For the beam formulation the total potential is given by

$$\Pi = \frac{EI}{2} \int_0^L \left(\frac{d\beta}{dx}\right)^2 dx + \frac{GAk}{2} \int_0^L \left(\frac{dw}{dx} - \beta\right)^2 dx - \int_0^L pw dx - \int_0^L m\beta dx \quad (5.65)$$

where the first two integrals represent, respectively, the bending and shearing strain energies and the last two integrals represent the potential of the loads.

Let us consider the total potential Π

$$\tilde{\Pi} = \int_0^L \left(\frac{d\beta}{dx}\right)^2 dx + \frac{GAk}{EI} \int_0^L \left(\frac{dw}{dx} - \beta\right)^2 dx \quad (5.66)$$

which is obtained by neglecting the load contributions in (5.65) and dividing by $\frac{1}{2}EI$. The relation in (5.66) shows the relative importance of the bending and shearing contributions to the stiffness matrix of an element, where we note that the factor $G Ak/EI$ in the shearing term can be very large when a thin element is considered. This factor can be interpreted as a penalty number (see Section 3.4.1); i.e., we can write

$$\tilde{\Pi} = \int_0^L \left(\frac{d\beta}{dx}\right)^2 dx + \alpha \int_0^L \left(\frac{dw}{dx} - \beta\right)^2 dx; \quad \alpha = \frac{G Ak}{EI} \tag{5.67}$$

where $\alpha \rightarrow \infty$ as $h \rightarrow 0$. However, this means that as the beam becomes thin, the constraint of zero shear deformations (i.e., $dw/dx = \beta$ with $\gamma = 0$) will be approached.

This argument holds for the actual continuous model which is governed by the stationarity condition of $\tilde{\Pi}$.

Considering now the finite element representation, it is important that the finite element displacement assumptions on β and w admit that for large values of α the shearing

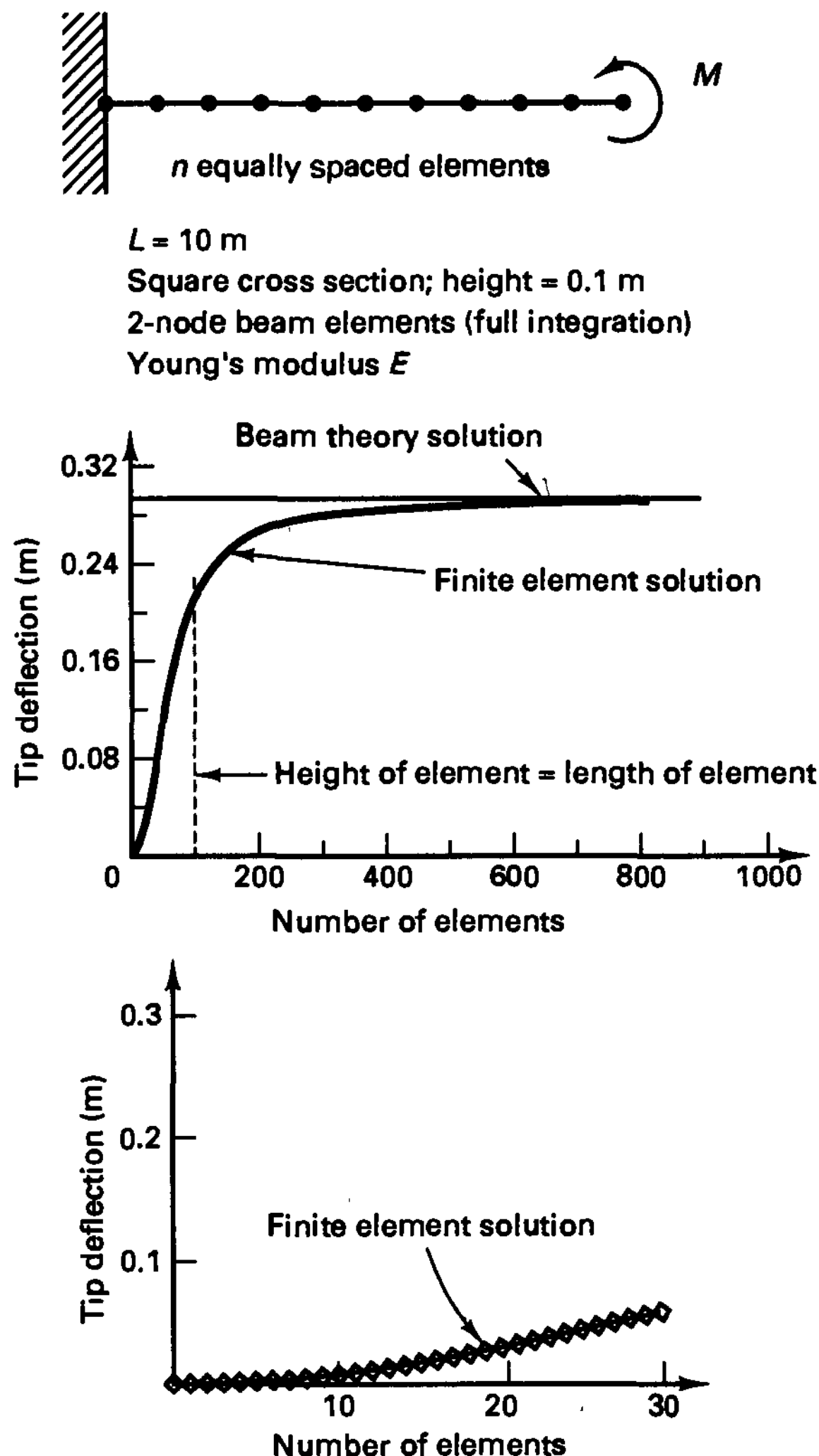


Figure 5.20 Solution of cantilever beam problem; tip deflection as a number of elements used, showing locking of elements

deformations can be small throughout the domain of the element. If by virtue of the assumptions used on w and β the shearing deformations cannot be small—and indeed zero—everywhere, then an erroneous shear strain energy (which can be large compared with the bending energy) is included in the analysis. This error results into much smaller displacements than the exact values when the beam structure analyzed is thin. Hence, in such cases, the finite element models are much too stiff.

This phenomenon is observed when the two-node beam element in Fig. 5.19 is used, which therefore should not be employed in the analysis of thin beam structures, and the conclusion is also applicable to the pure displacement-based low-order plate and shell elements discussed in Section 5.4.2. The very stiff behavior exhibited by the thin elements has been referred to as *element shear locking*. Figure 5.20 shows an example of locking using the two-node displacement-based element. We study the phenomenon of shear locking in the following example (see also Section 4.5.7).

EXAMPLE 5.25: Consider a two-node isoparametric beam element modeling a cantilever beam that is subjected to only a moment end load (see Fig. E5.25). Determine what values of θ_2 , w_2 would be obtained assuming that the shear strain is zero.

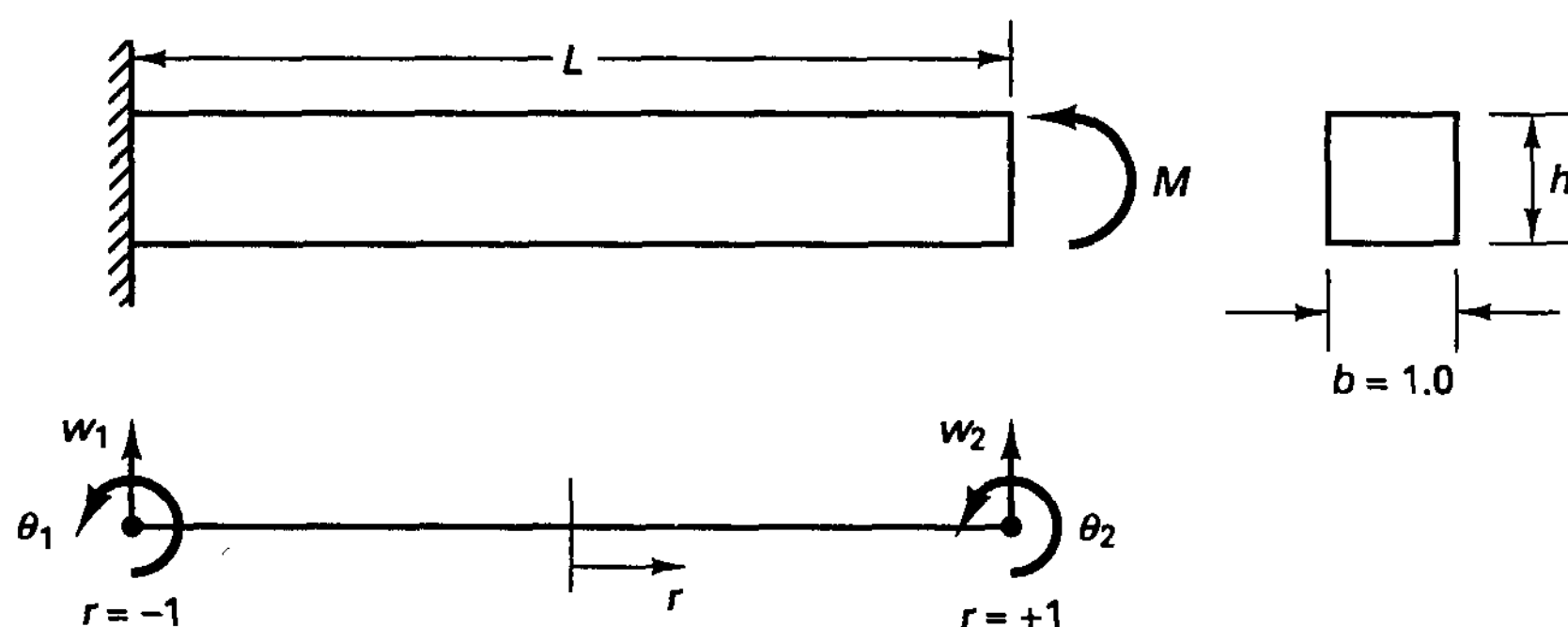


Figure E5.25 Two-node element representing a cantilever beam

The interpolations for w and β , for the given data, are

$$\beta = \frac{1+r}{2} \theta_2$$

$$w = \frac{1+r}{2} w_2$$

Hence, the shearing strain is

$$\gamma = \frac{w_2}{L} - \frac{1+r}{2} \theta_2$$

For an applied moment only, the shearing strain is to be zero. Imposing this condition gives

$$0 = \frac{w_2}{L} - \frac{1+r}{2} \theta_2 \quad (a)$$

However, for this expression to be zero all along the beam (i.e., for any value $-1 \leq r \leq +1$), we clearly must have $w_2 = \theta_2 = 0$. Hence, a zero shear strain in the beam can be reached only when there are no deformations!

Similarly, if we enforce (a) to hold at the two Gauss points $r = \pm 1/\sqrt{3}$, (i.e., if we use two-point Gauss integration), we obtain the two equations,

$$\begin{bmatrix} \frac{1}{L} & -\frac{1 + 1/\sqrt{3}}{2} \\ \frac{1}{L} & -\frac{1 - 1/\sqrt{3}}{2} \end{bmatrix} \begin{bmatrix} w_2 \\ \theta_2 \end{bmatrix} = \begin{bmatrix} 0 \\ 0 \end{bmatrix}$$

Since the coefficient matrix is nonsingular, the only solution is $w_2 = \theta_2 = 0$. This is of course the result obtained before, because setting the linearly varying shear strain equal to zero at two points means imposing a zero shear strain all along the element.

However, we can now also use (a) to investigate what happens when we enforce the shear strain to be zero only at the midpoint of the beam (i. e., at $r = 0$). In this case, (a) gives the relation

$$w_2 = \frac{\theta_2}{2} L \quad (b)$$

Hence, if we were to assume a constant shear strain of value

$$\gamma = \frac{w_2}{L} - \frac{\theta_2}{2}$$

a more attractive element might be obtained. We actually used this assumption in Example 4.30.

Various procedures may be proposed to modify this pure displacement-based beam element formulation—and the formulation of pure displacement-based isoparametric plate bending elements—in order to arrive at efficient nonlocking elements.

The key point of any such formulation is that the resulting element should be reliable and efficient; this means in particular that the element stiffness matrix must not contain any spurious zero energy mode and that the element should have a high predictive capability under general geometric and loading conditions. These requirements are considerably more easy to satisfy with beam elements than with general plate and shell elements.

An effective beam element is obtained by using a mixed interpolation of displacements and transverse shear strains. This mixed interpolation is an application of the more general procedure employed in the formulation of plate bending and shell elements (see Section 5.4.2).

The discussion in Example 5.25 suggests that to satisfy the possibility of a zero transverse shear strain in the element, we may assume for an element with q nodes the interpolations (see also Example 4.30)

$$\left. \begin{aligned} w &= \sum_{i=1}^q h_i w_i \\ \beta &= \sum_{i=1}^q h_i \theta_i \end{aligned} \right\} \quad (5.68)$$

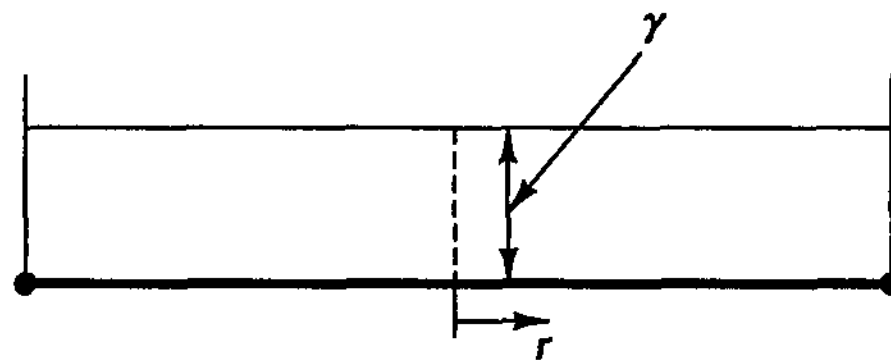
$$\gamma = \sum_{i=1}^{q-1} h_i^* \gamma|_{G_i}^{DI} \quad (5.69)$$

Here the h_i are the displacement and section rotation interpolation functions for q nodes and the h_i^* are the interpolation functions for the transverse shear strains. These functions are

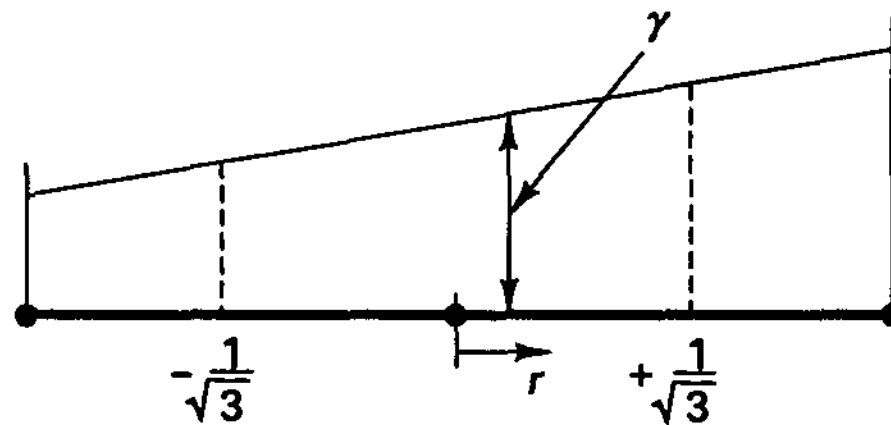
associated with the $(q - 1)$ discrete values $\gamma|_{G_i}^{DI}$, where $\gamma|_{G_i}^{DI}$ is the shear strain at the Gauss point i directly obtained from the displacement/section rotation interpolations (i.e., by displacement interpolation); hence,

$$\gamma|_{G_i}^{DI} = \left(\frac{dw}{dx} - \beta \right) \Big|_{G_i} \tag{5.70}$$

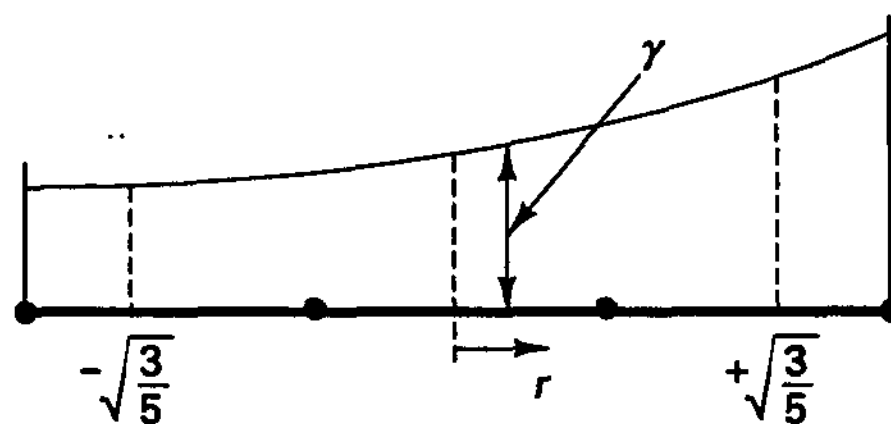
Figure 5.21 shows the shear strain interpolations used for the two-, three-, and four-node beam elements. These mixed interpolated beam elements are very reliable in that they do not lock, show excellent convergence behavior, and of course do not contain any spurious zero energy mode. For the solution of the problem in Fig. 5.20 only a single element needs to be employed to obtain the exact tip displacement and rotation. We can easily prove this result for the two-node element by continuing the analysis presented in Example 5.25, and the three- and four-node elements contain the interpolations of the two-node element and must therefore also give the exact solution. Hence, there is a drastic improvement in element behavior resulting from the use of mixed interpolation.



2-node element, constant γ ; G_1 corresponds to $r = 0$



3-node element, linearly varying γ ; G_1 and G_2 correspond to $r = \pm \frac{1}{\sqrt{3}}$



4-node element, parabolically varying γ ;
 $G_1, G_2,$ and G_3 correspond to $r = \pm \sqrt{\frac{3}{5}}$ and $r = 0$

Figure 5.21 Shear strain interpolations for mixed interpolated beam elements

In addition, there is an attractive computational feature: the stiffness matrices of these elements can be evaluated efficiently by simply integrating the displacement-based model with one-point Gauss integration for the two-node element, two-point Gauss integration for the three-node element, and three-point Gauss integration for the four-node element. Namely, using one-point integration in the evaluation of the two-node element stiffness matrix, the transverse shear strain is assumed to be constant, and the contribution from the bending deformation is still evaluated exactly. A similar argument holds for the three- and four-node elements. This computational approach to evaluating the stiffness matrices of the elements may be called “reduced integration” of the displacement-based element but in fact is actually full integration of the mixed interpolated element. A mathematical analysis of the elements is presented in Section 4.5.7.

General Curved Beam Elements

In the preceding discussion we assumed that the elements considered were straight; hence the formulation was based on equation (5.58). To arrive at a general three-dimensional curved beam element formulation, we proceed in a similar way but now need to interpolate the curved geometry and corresponding beam displacements. With these interpolations a pure displacement-based element is derived that, as for the straight elements, is very stiff and not useful. In the case of straight beam elements only spurious shear strains are generated (always for the two-node element, and for the three- and four-node elements when the interior nodes are not at their natural positions; see Exercise 5.34), but for curved elements also spurious membrane strains are obtained. Hence, a curved element also displays *membrane locking* (see, for example, H. Stolarski and T. Belytschko [A]).

Efficient general beam elements are obtained by the mixed interpolation already introduced. However, now, in the case of general three-dimensional action, the transverse shear strains *and* the bending and membrane strains are interpolated using the functions in Fig. 5.21. These strain interpolations are tied to the nodal point displacements and rotations by evaluating the displacement-based strains and equating them to the assumed strains at the Gauss integration points.

It follows that the mixed interpolated element stiffness matrices can be numerically obtained by evaluating the displacement-based element matrices with Gauss point integration at the points given in Fig. 5.21.

Consider the three-dimensional beam of rectangular cross section in Fig. 5.22, and let us assume first that an accurate representation of the torsional rigidity is not required.

The basic kinematic assumption in the formulation of the element is the same as that employed in the formulation of the two-dimensional element in Fig. 5.19: namely that plane sections originally normal to the centerline axis remain plane and undistorted under deformation but not necessarily normal to this axis. This kinematic assumption does not allow for warping effects in torsion (which we can introduce by additional displacement functions; see Exercise 5.37).

Using the natural coordinates r, s, t , the Cartesian coordinates of a point in the element with q nodal points are then, before and after deformations,

$${}^e x(r, s, t) = \sum_{k=1}^q h_k {}^e x_k + \frac{t}{2} \sum_{k=1}^q a_k h_k {}^e V_{tx}^k + \frac{s}{2} \sum_{k=1}^q b_k h_k {}^e V_{sx}^k$$

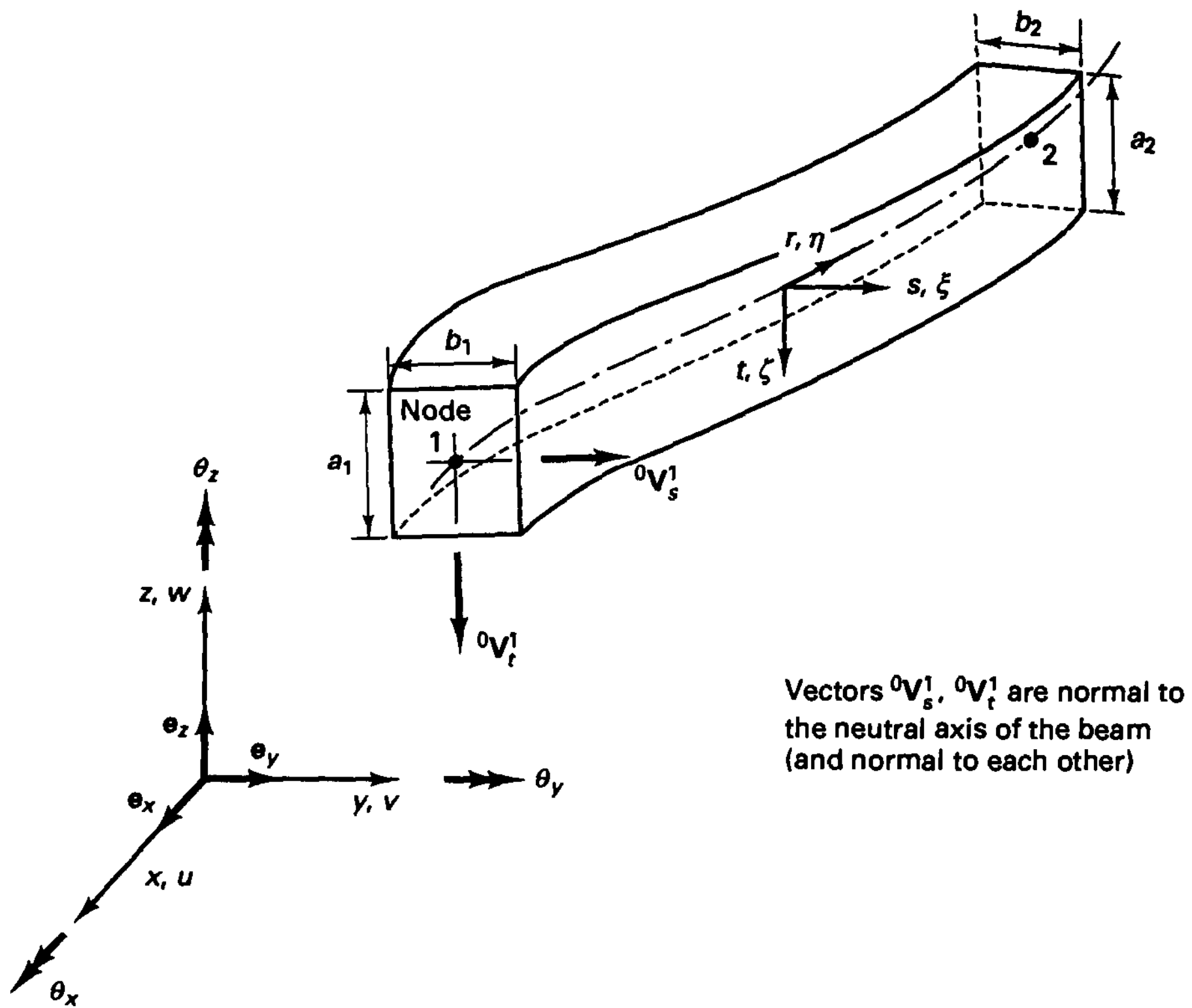


Figure 5.22 Three-dimensional beam element

$${}^\ell y(r, s, t) = \sum_{k=1}^q h_k {}^\ell y_k + \frac{t}{2} \sum_{k=1}^q a_k h_k {}^\ell V_{iy}^k + \frac{s}{2} \sum_{k=1}^q b_k h_k {}^\ell V_{sy}^k \quad (5.71)$$

$${}^\ell z(r, s, t) = \sum_{k=1}^q h_k {}^\ell z_k + \frac{t}{2} \sum_{k=1}^q a_k h_k {}^\ell V_{iz}^k + \frac{s}{2} \sum_{k=1}^q b_k h_k {}^\ell V_{sz}^k$$

where the $h_k(r)$ are the interpolation functions summarized in Fig. 5.3 and

${}^\ell x, {}^\ell y, {}^\ell z$ = Cartesian coordinates of any point in the element

${}^\ell x_k, {}^\ell y_k, {}^\ell z_k$ = Cartesian coordinates of nodal point k

a_k, b_k = cross-sectional dimensions of the beam at nodal point k

${}^\ell V_{ix}^k, {}^\ell V_{iy}^k, {}^\ell V_{iz}^k$ = components of unit vector ${}^\ell V_i^k$ in direction t at nodal point k

${}^\ell V_{sx}^k, {}^\ell V_{sy}^k, {}^\ell V_{sz}^k$ = components of unit vector ${}^\ell V_s^k$ in direction s at nodal point k ; we call ${}^\ell V_i^k$ and ${}^\ell V_s^k$ the normal vectors or director vectors at nodal point k ,

and the left superscript ℓ denotes the configuration of the element; i.e., $\ell = 0$ denotes the original configuration, whereas $\ell = 1$ corresponds to the configuration in the deformed position.

We assume here that the vectors ${}^0\mathbf{V}_s^k, {}^0\mathbf{V}_i^k$ are normal to the neutral axis of the beam and are normal to each other. However, this condition can be relaxed, as is done in the shell element formulation (see Section 5.4.2).

The displacement components at any point of the element are

$$\begin{aligned} u(r, s, t) &= {}^1x - {}^0x \\ v(r, s, t) &= {}^1y - {}^0y \\ w(r, s, t) &= {}^1z - {}^0z \end{aligned} \tag{5.72}$$

and substituting from (5.71), we obtain

$$\begin{aligned} u(r, s, t) &= \sum_{k=1}^q h_k u_k + \frac{t}{2} \sum_{k=1}^q a_k h_k V_{ix}^k + \frac{s}{2} \sum_{k=1}^q b_k h_k V_{sx}^k \\ v(r, s, t) &= \sum_{k=1}^q h_k v_k + \frac{t}{2} \sum_{k=1}^q a_k h_k V_{iy}^k + \frac{s}{2} \sum_{k=1}^q b_k h_k V_{sy}^k \\ w(r, s, t) &= \sum_{k=1}^q h_k w_k + \frac{t}{2} \sum_{k=1}^q a_k h_k V_{iz}^k + \frac{s}{2} \sum_{k=1}^q b_k h_k V_{sz}^k \end{aligned} \tag{5.73}$$

where
$$\mathbf{V}_i^k = {}^1\mathbf{V}_i^k - {}^0\mathbf{V}_i^k; \quad \mathbf{V}_s^k = {}^1\mathbf{V}_s^k - {}^0\mathbf{V}_s^k \tag{5.74}$$

Finally, we express the vectors \mathbf{V}_i^k and \mathbf{V}_s^k in terms of rotations about the Cartesian axes x, y, z :

$$\begin{aligned} \mathbf{V}_i^k &= \boldsymbol{\theta}_k \times {}^0\mathbf{V}_i^k \\ \mathbf{V}_s^k &= \boldsymbol{\theta}_k \times {}^0\mathbf{V}_s^k \end{aligned} \tag{5.75}$$

where $\boldsymbol{\theta}_k$ is a vector listing the nodal point rotations at nodal point k (see Fig. 5.22):

$$\boldsymbol{\theta}_k = \begin{bmatrix} \theta_x^k \\ \theta_y^k \\ \theta_z^k \end{bmatrix} \tag{5.76}$$

Using (5.71) to (5.76), we have all the basic equations necessary to establish the displacement and strain interpolation matrices employed in evaluating the beam element matrices.

The terms in the displacement interpolation matrix \mathbf{H} are obtained by substituting (5.75) into (5.73). To evaluate the strain-displacement matrix, we recognize that for the beam the only strain components of interest are the longitudinal strain $\epsilon_{\eta\eta}$ and transverse shear strains $\gamma_{\eta\xi}$ and $\gamma_{\eta\zeta}$, where $\eta, \xi,$ and ζ are convected (body-attached) coordinates axes (see Fig. 5.22). Thus, we seek a relation of the form

$$\begin{bmatrix} \epsilon_{\eta\eta} \\ \gamma_{\eta\xi} \\ \gamma_{\eta\zeta} \end{bmatrix} = \sum_{k=1}^q \mathbf{B}_k \hat{\mathbf{u}}_k \tag{5.77}$$

where
$$\hat{\mathbf{u}}_k^T = [u_k \ v_k \ w_k \ \theta_x^k \ \theta_y^k \ \theta_z^k] \tag{5.78}$$

and the matrices $\mathbf{B}_k, k = 1, \dots, q$, together constitute the matrix \mathbf{B} ,

$$\mathbf{B} = [\mathbf{B}_1 \ \dots \ \mathbf{B}_q] \tag{5.79}$$

Following the usual procedure of isoparametric finite element formulation, we have, using (5.73),

$$\begin{bmatrix} \frac{\partial u}{\partial r} \\ \frac{\partial u}{\partial s} \\ \frac{\partial u}{\partial t} \end{bmatrix} = \sum_{k=1}^q \begin{bmatrix} \frac{\partial h_k}{\partial r} & [1 & (g)_{1i}^k & (g)_{2i}^k & (g)_{3i}^k] \\ h_k & [0 & (\hat{g})_{1i}^k & (\hat{g})_{2i}^k & (\hat{g})_{3i}^k] \\ h_k & [0 & (\bar{g})_{1i}^k & (\bar{g})_{2i}^k & (\bar{g})_{3i}^k] \end{bmatrix} \begin{bmatrix} u_k \\ \theta_x^k \\ \theta_y^k \\ \theta_z^k \end{bmatrix} \quad (5.80)$$

and the derivatives of v and w are obtained by simply substituting v and w for u . In (5.80) we have $i = 1$ for u , $i = 2$ for v , and $i = 3$ for w , and we employ the notation

$$(\hat{g})^k = \frac{b_k}{2} \begin{bmatrix} 0 & -{}^0V_{sz}^k & {}^0V_{sy}^k \\ {}^0V_{sz}^k & 0 & -{}^0V_{sx}^k \\ -{}^0V_{sy}^k & {}^0V_{sx}^k & 0 \end{bmatrix} \quad (5.81)$$

$$(\bar{g})^k = \frac{a_k}{2} \begin{bmatrix} 0 & -{}^0V_{tz}^k & {}^0V_{ty}^k \\ {}^0V_{tz}^k & 0 & -{}^0V_{tx}^k \\ -{}^0V_{ty}^k & {}^0V_{tx}^k & 0 \end{bmatrix} \quad (5.82)$$

$$(g)_{ij}^k = s(\hat{g})_{ij}^k + t(\bar{g})_{ij}^k \quad (5.83)$$

To obtain the displacement derivatives corresponding to the coordinate axes x , y , and z , we employ the Jacobian transformation

$$\frac{\partial}{\partial \mathbf{x}} = \mathbf{J}^{-1} \frac{\partial}{\partial \mathbf{r}} \quad (5.84)$$

where the Jacobian matrix \mathbf{J} contains the derivatives of the coordinates x , y , and z with respect to the natural coordinates r , s , and t . Substituting from (5.80) into (5.84), we obtain

$$\begin{bmatrix} \frac{\partial u}{\partial x} \\ \frac{\partial u}{\partial y} \\ \frac{\partial u}{\partial z} \end{bmatrix} = \sum_{k=1}^q \begin{bmatrix} J_{11}^{-1} \frac{\partial h_k}{\partial r} & (G1)_{i1}^k & (G2)_{i1}^k & (G3)_{i1}^k \\ J_{21}^{-1} \frac{\partial h_k}{\partial r} & (G1)_{i2}^k & (G2)_{i2}^k & (G3)_{i2}^k \\ J_{31}^{-1} \frac{\partial h_k}{\partial r} & (G1)_{i3}^k & (G2)_{i3}^k & (G3)_{i3}^k \end{bmatrix} \begin{bmatrix} u_k \\ \theta_x^k \\ \theta_y^k \\ \theta_z^k \end{bmatrix} \quad (5.85)$$

and again, the derivatives of v and w are obtained by simply substituting v and w for u . In (5.85) we employ the notation

$$(Gm)_{in}^k = [J_{n1}^{-1}(g)_{mi}^k] \frac{\partial h_k}{\partial r} + [J_{n2}^{-1}(\hat{g})_{mi}^k + J_{n3}^{-1}(\bar{g})_{mi}^k] h_k \quad (5.86)$$

Using the displacement derivatives in (5.85), we can now calculate the elements of the strain-displacement matrix at the element Gauss point by establishing the strain components corresponding to the x , y , z axes and transforming these components to the local strains $\epsilon_{\eta\eta}$, $\gamma_{\eta\xi}$, and $\gamma_{\eta\zeta}$.

The corresponding stress-strain law to be employed in the formulation is (using k as the shear correction factor)

TABLE 5.2 Performance of isoparametric beam elements in the analysis of the problem in Fig. 5.23

(a) $\theta_{\text{finite element}}/\theta_{\text{analytical}}$ at tip of beam, one three-node element solution

h/R	Midnode at $\alpha = 22.5^\circ$		Midnode at $\alpha = 20^\circ$	
	Displacement-based	Mixed interpolated	Displacement-based	Mixed interpolated
0.50	0.92	1.00	0.91	1.00
0.10	0.31	1.00	0.31	1.00
0.01	0.004	1.00	0.005	1.00
0.001	0.00004	1.00	0.00005	1.00

(b) $\theta_{\text{finite element}}/\theta_{\text{analytical}}$ at tip of beam, one four-node element solution

h/R	Internal nodes at $\alpha_1 = 15^\circ, \alpha_2 = 30^\circ$		Internal nodes at $\alpha_1 = 10^\circ, \alpha_2 = 25^\circ$	
	Displacement-based	Mixed interpolated	Displacement-based	Mixed interpolated
0.50	1.00	1.00	0.97	0.997
0.10	0.999	1.00	0.70	0.997
0.01	0.998	1.00	0.37	0.997
0.001	0.998	1.00	0.37	0.997

$$\begin{bmatrix} \tau_{\eta\eta} \\ \tau_{\eta\xi} \\ \tau_{\eta\zeta} \end{bmatrix} = \begin{bmatrix} E & 0 & 0 \\ 0 & Gk & 0 \\ 0 & 0 & Gk \end{bmatrix} \begin{bmatrix} \epsilon_{\eta\eta} \\ \gamma_{\eta\xi} \\ \gamma_{\eta\zeta} \end{bmatrix} \tag{5.87}$$

The stiffness matrix of the element is then obtained by numerical integration, using for the r -integration the Gauss points shown in Fig. 5.21 and for the s - and t -integrations either the Newton-Cotes or Gauss formulas (see Section 5.5).

Table 5.2 illustrates the performance of the mixed interpolated elements in the analysis of the curved cantilever in Fig. 5.23 and shows the efficiency of the elements.

As pointed out already, this element does not include warping effects, which can be significant for the rectangular cross-sectional beam elements and of course for beam ele-

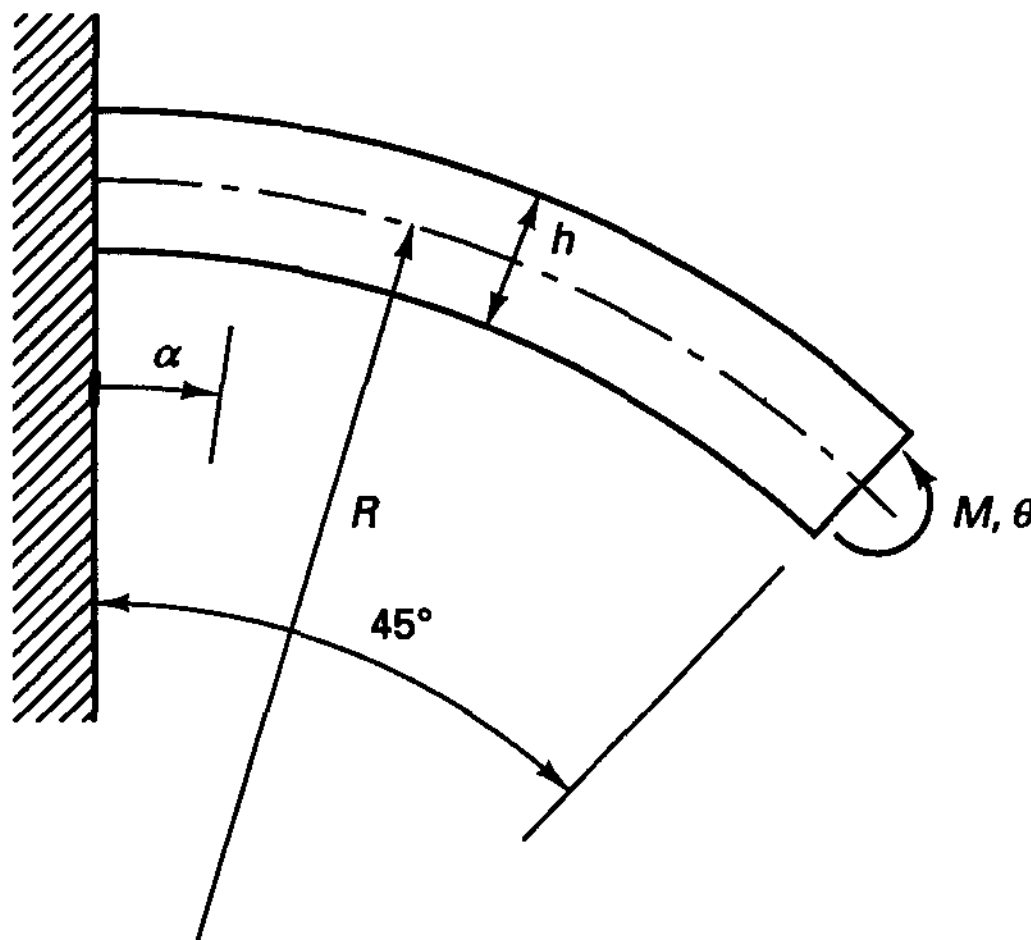


Figure 5.23 Curved cantilever problem to test isoparametric beam elements

ments of general cross sections. Warping displacements can be introduced by adding appropriate displacement interpolations to those given in (5.73). If additional degrees of freedom are also introduced, corresponding to the warping deformations, continuity of warping between elements can be imposed. However, it may be sufficient to allow for “free” warping in each element without enforcing continuity of warping between elements. This is achieved by adding warping deformations to the displacement interpolations and then statically condensing out the intensity of these deformations (see K. J. Bathe and A. B. Chaudhary [A] and Exercise 5.37).

In another application of the general curved beam formulation, the cross section is circular and hollow, that is, a pipe cross section is considered. In this case, ovalization and warping deformations can be important when the element is curved, and once again the displacement interpolations given in (5.73) must be amended. In this case it is important to impose continuity in the ovalization and warping deformations, and for this reason additional nodal degrees of freedom must be introduced (see K. J. Bathe and C. A. Almeida [A]).

Considering the basic formulation in (5.71) to (5.87), we recognize that the element can be arbitrarily curved and that the cross-sectional dimensions can change along its axis. The beam width and height and the location of the element axis are interpolated along the element. In the given formulation, the axis of the element coincides with the element geometric midline, but this is not necessary, and more general elements can be formulated directly (see Exercise 5.38).

In addition to representing a general formulation for linear analysis, this approach is particularly useful for the nonlinear large displacement analysis of beam structures. As discussed in Section 6.5.1, in such analyses initially straight beam elements become curved and distorted, and these deformations can be modeled accurately.

Of course, if linear analysis is pursued and the element is straight and has a constant cross-sectional area, the formulation reduces to the formulation given in (5.56) to (5.70). We illustrate this point in the following example.

EXAMPLE 5.26: Show that the application of the general formulation in (5.71) to (5.87) to the beam element in Fig. E5.24 reduces to the use of (5.58).

For the application of the general relations in (5.71) to (5.87), we refer to Figs. E5.24 and 5.22 and thus have

$${}^0\mathbf{V}_s = \begin{bmatrix} 0 \\ 1 \\ 0 \end{bmatrix}; \quad {}^0\mathbf{V}_t = \begin{bmatrix} 0 \\ 0 \\ 1 \end{bmatrix}; \quad a_k = 1; \quad b_k = h; \quad k = 1, 2, 3$$

Hence, the relations in (5.71) reduce to

$${}^0x = \sum_{k=1}^3 h_k {}^0x_k$$

$${}^0y = \frac{s}{2} h$$

$${}^0z = \frac{t}{2}$$

We next evaluate (5.75) to obtain (see Section 2.4)

$$\mathbf{V}_t^k = \det \begin{bmatrix} \mathbf{e}_x & \mathbf{e}_y & \mathbf{e}_z \\ \theta_x^k & \theta_y^k & \theta_z^k \\ 0 & 0 & 1 \end{bmatrix}$$

or

$$\mathbf{V}_t^k = \theta_y^k \mathbf{e}_x - \theta_x^k \mathbf{e}_y \quad (a)$$

and

$$\mathbf{V}_s^k = \det \begin{bmatrix} \mathbf{e}_x & \mathbf{e}_y & \mathbf{e}_z \\ \theta_x^k & \theta_y^k & \theta_z^k \\ 0 & 1 & 0 \end{bmatrix}$$

or

$$\mathbf{V}_s^k = -\theta_z^k \mathbf{e}_x + \theta_x^k \mathbf{e}_z \quad (b)$$

The relations in (a) and (b) correspond to the three-dimensional action of the beam. We allow rotations only about the z -axis, in which case

$$\mathbf{V}_t^k = \mathbf{0}; \quad \mathbf{V}_s^k = -\theta_z^k \mathbf{e}_x$$

Furthermore, we assume that the nodal points can displace only in the y direction. Hence, (5.73) yields the displacement assumptions

$$u(r, s) = -\frac{sh}{2} \sum_{k=1}^3 h_k \theta_z^k \quad (c)$$

$$v(r) = \sum_{k=1}^3 h_k v_k \quad (d)$$

where we note that u is only a function of r, s and v is only a function of r . These relations are identical to the displacement assumptions used before, but with the more conventional beam displacement notation we identified the transverse displacement and section rotation at a nodal point with w_k and θ_k instead of v_k and θ_z^k .

Now using (5.80), we obtain

$$\begin{bmatrix} \frac{\partial u}{\partial r} \\ \frac{\partial u}{\partial s} \end{bmatrix} = \sum_{k=1}^3 \begin{bmatrix} -\frac{sh}{2} \frac{\partial h_k}{\partial r} \\ -\frac{h}{2} h_k \end{bmatrix} \theta_z^k$$

$$\begin{bmatrix} \frac{\partial v}{\partial r} \\ \frac{\partial v}{\partial s} \end{bmatrix} = \sum_{k=1}^3 \begin{bmatrix} \frac{\partial h_k}{\partial r} \\ 0 \end{bmatrix} v_k$$

These relations could also be directly obtained by differentiating the displacements in (c) and (d). Since

$$\mathbf{J} = \begin{bmatrix} \frac{L}{2} & 0 \\ 0 & \frac{h}{2} \end{bmatrix}; \quad \mathbf{J}^{-1} = \begin{bmatrix} \frac{2}{L} & 0 \\ 0 & \frac{2}{h} \end{bmatrix}$$

we obtain

$$\begin{bmatrix} \frac{\partial u}{\partial x} \\ \frac{\partial u}{\partial y} \end{bmatrix} = \sum_{k=1}^3 \begin{bmatrix} -\frac{h}{2} \frac{2}{L} s \frac{\partial h_k}{\partial r} \\ -h_k \end{bmatrix} \theta_z^k \quad (e)$$

and

$$\begin{bmatrix} \frac{\partial v}{\partial x} \\ \frac{\partial v}{\partial y} \end{bmatrix} = \sum_{k=1}^3 \begin{bmatrix} \frac{2}{L} \frac{\partial h_k}{\partial r} \\ 0 \end{bmatrix} v_k \quad (f)$$

To analyze the response of the beam in Fig E5.24 we now use the principle of virtual work [see (4.7)] with the appropriate strain measures:

$$\int_{-1}^{+1} \int_{-1}^{+1} [\bar{\epsilon}_{xx} \quad \bar{\gamma}_{xy}] \begin{bmatrix} E & 0 \\ 0 & Gk \end{bmatrix} \begin{bmatrix} \epsilon_{xx} \\ \gamma_{xy} \end{bmatrix} \det \mathbf{J} \, ds \, dr = -P\bar{v}|_{r=1/3} \quad (g)$$

where

$$\epsilon_{xx} = \frac{\partial u}{\partial x}; \quad \bar{\epsilon}_{xx} = \frac{\partial \bar{u}}{\partial x}$$

$$\gamma_{xy} = \frac{\partial u}{\partial y} + \frac{\partial v}{\partial x}; \quad \bar{\gamma}_{xy} = \frac{\partial \bar{u}}{\partial y} + \frac{\partial \bar{v}}{\partial x}$$

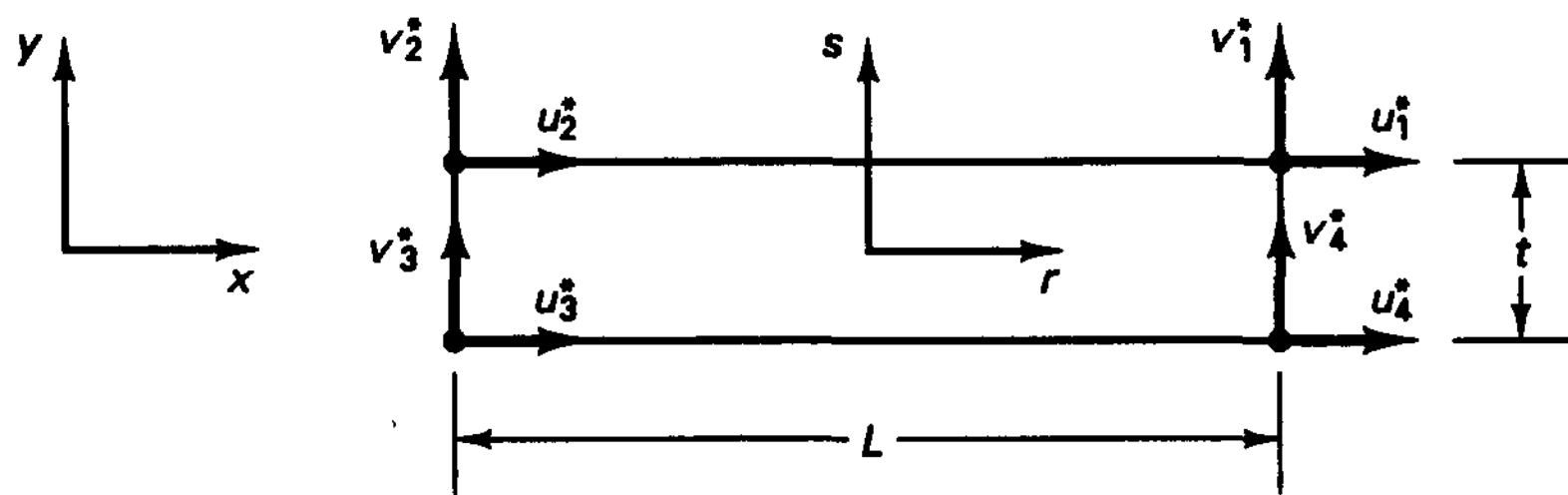
Considering the relations in (e), (f), (g), and (5.58), we recognize that (g) corresponds to (5.58) if we use $\beta \equiv \theta_z$, and $w \equiv v$.

Transition Elements

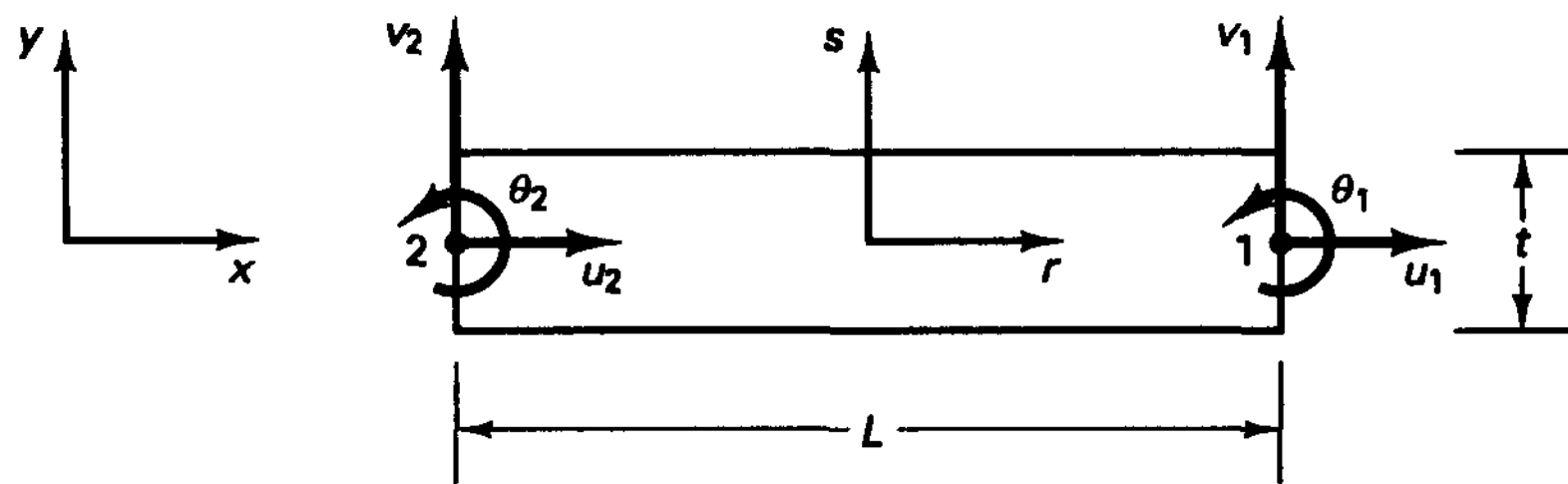
In the preceding discussions, we considered continuum elements and beam elements separately. However, the very close relationship between these elements should be recognized; the only differences are the kinematic assumption that plane sections initially normal to the neutral axis remain plane and the stress assumption that stresses normal to the neutral axis are zero. In the beam formulation presented, the kinematic assumption was incorporated directly in the basic geometry and displacement interpolations and the stress assumption was used in the stress-strain law. Since these two assumptions are the only two basic differences between the beam and continuum elements, it is apparent that the structural element matrices can also be derived from the continuum element matrices by degeneration. Furthermore, elements can be devised that act as transition elements between continuum and structural elements. Consider the following example.

EXAMPLE 5.27: Assume that the strain-displacement matrix of a four-node plane stress element has been derived. Show how the strain-displacement matrix of a two-node beam element can be constructed.

Figure E5.27 shows the plane stress element with its degrees of freedom and the beam element for which we want to establish the strain-displacement matrix. Consider node 2 of the beam element and nodes 2 and 3 of the plane stress element. The entries in the strain-displacement matrix of the plane stress element are



(a) Plane stress element



(b) Beam element

Figure E5.27 Derivation of beam element from plane stress element

$$\mathbf{B}^* = \begin{bmatrix} \dots & -\frac{1}{2L}(1+s) & 0 & -\frac{1}{2L}(1-s) & 0 & \dots \\ \dots & 0 & \frac{1}{2t}(1-r) & 0 & -\frac{1}{2t}(1-r) & \dots \\ \dots & \frac{1}{2t}(1-r) & -\frac{1}{2L}(1+s) & -\frac{1}{2t}(1-r) & -\frac{1}{2L}(1-s) & \dots \end{bmatrix} \quad (a)$$

Using now the beam deformation assumptions, we have the following kinematic constraints:

$$u_2^* = u_2 - \frac{t}{2}\theta_2$$

$$u_3^* = u_2 + \frac{t}{2}\theta_2 \quad (b)$$

$$v_2^* = v_2; \quad v_3^* = v_2$$

These constraints are now substituted to obtain from the elements of \mathbf{B}^* in (a) the elements of the strain-displacement matrix of the beam. Using the rows of \mathbf{B}^* , we have with (b),

$$\begin{aligned}
 -\frac{1}{2L}(1+s)u_2^* - \frac{1}{2L}(1-s)u_3^* &= -\frac{1}{2L}(1+s)\left(u_2 - \frac{t}{2}\theta_2\right) \\
 &\quad - \frac{1}{2L}(1-s)\left(u_2 + \frac{t}{2}\theta_2\right) \quad (c)
 \end{aligned}$$

$$\frac{1}{2t}(1-r)v_2^* - \frac{1}{2t}(1-r)v_3^* = \frac{1}{2t}(1-r)v_2 - \frac{1}{2t}(1-r)v_2 \tag{d}$$

$$\begin{aligned} & \frac{1}{2t}(1-r)u_2^* - \frac{1}{2L}(1+s)v_2^* - \frac{1}{2t}(1-r)u_3^* - \frac{1}{2L}(1-s)v_3^* \\ &= \frac{1}{2t}(1-r)\left(u_2 - \frac{t}{2}\theta_2\right) - \frac{1}{2L}(1+s)v_2 - \frac{1}{2t}(1-r)\left(u_2 + \frac{t}{2}\theta_2\right) - \frac{1}{2L}(1-s)v_2 \end{aligned} \tag{e}$$

The relations on the right-hand side of (c) to (e) comprise the entries of the beam strain-displacement matrix

$$\mathbf{B} = \begin{bmatrix} \dots & \vdots & -\frac{1}{L} & 0 & \frac{t}{2L}s \\ \dots & \vdots & 0 & 0 & 0 \\ \dots & \vdots & 0 & -\frac{1}{L} & -\frac{1}{2}(1-r) \end{bmatrix}$$

$u_2 \quad v_2 \quad \theta_2$
 $\downarrow \quad \downarrow \quad \downarrow$

However, the first- and third-row entries are those that are also obtained using the beam formulation of (5.71) to (5.86). We should note that the zeros in the second row of **B** only express the fact that the strain ϵ_{yy} is not included in the formulation. This strain is actually equal to $-\nu\epsilon_{xx}$ because the stress τ_{yy} is zero. As pointed out earlier, we would use the entries in **B** at $r = 0$.

The formulation of a structural element using the approach discussed in Example 5.27 is computationally inefficient and is certainly not recommended for general analysis. However, it is instructive to study this approach and recognize that the structural element matrices can in principle be obtained from continuum element matrices by imposing the appropriate static and kinematic assumptions. Moreover, this formulation directly suggests the construction of transition elements that can be used in an effective manner to couple structural and continuum elements without the use of constraint equations [see Fig. E5.28(a)]. To demonstrate the formulation of transition elements, we consider in the following example a simple transition beam element.

EXAMPLE 5.28: Construct the displacement and strain-displacement interpolation matrices of the transition element shown in Fig. E5.28.

We define the nodal point displacement vector of the element as

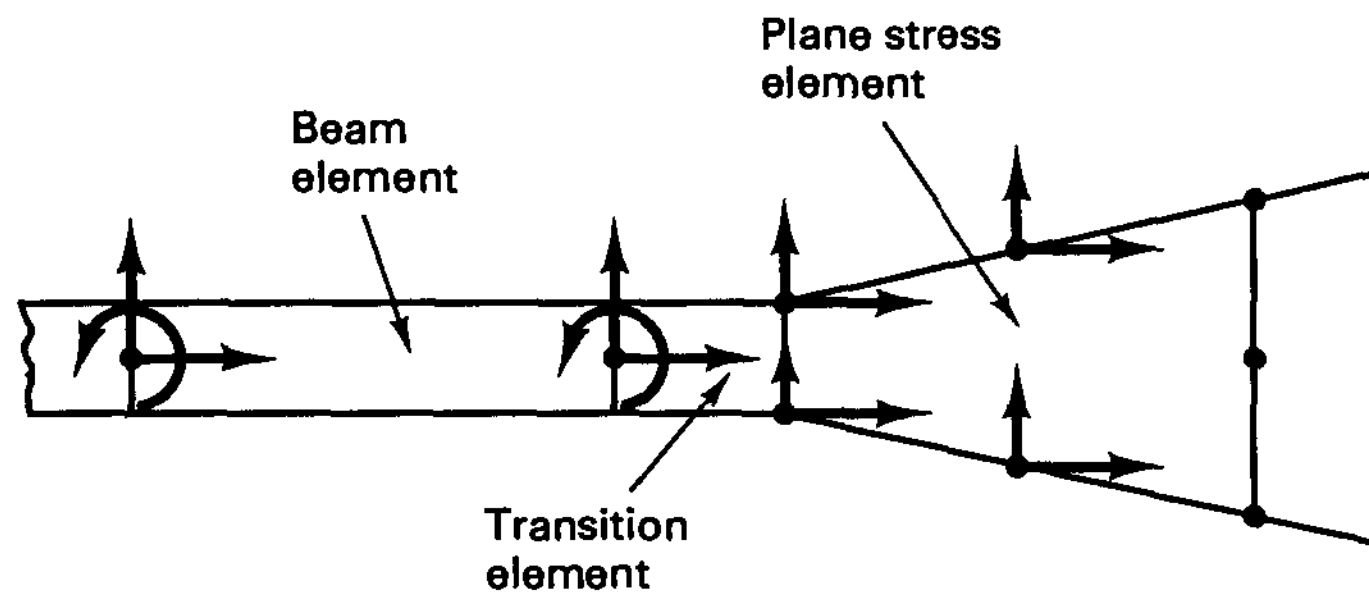
$$\hat{\mathbf{u}}^T = [u_1 \quad v_1 \quad u_2 \quad v_2 \quad u_3 \quad v_3 \quad \theta_3] \tag{a}$$

Since at $r = +1$ we have plane stress element degrees of freedom, the interpolation functions corresponding to nodes 1 and 2 are (see Fig. 5.4)

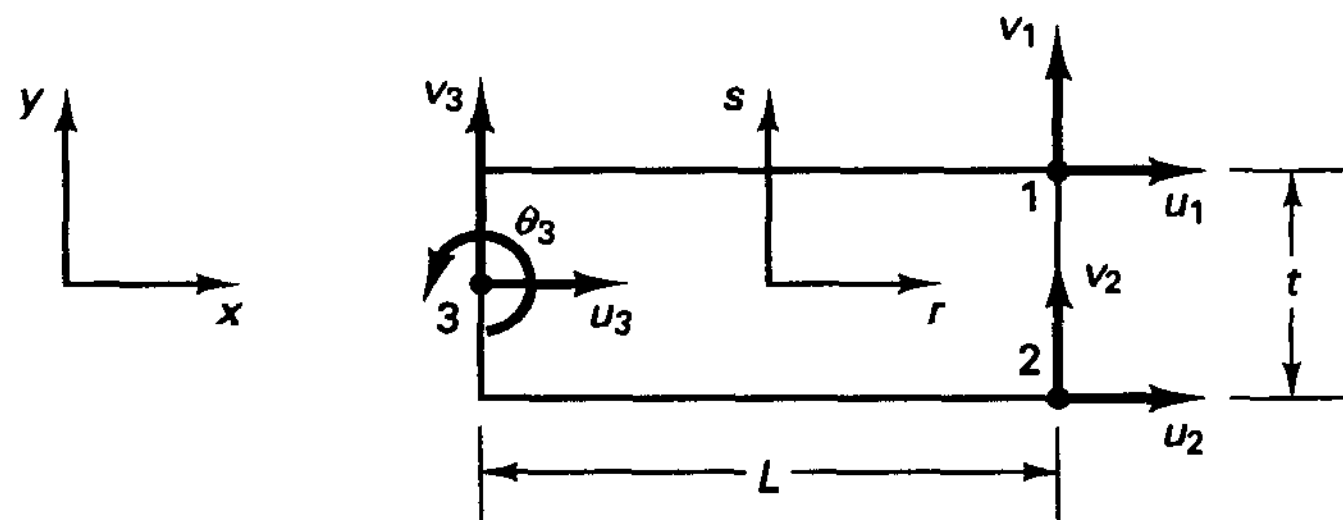
$$h_1 = \frac{1}{4}(1+r)(1+s); \quad h_2 = \frac{1}{4}(1+r)(1-s)$$

Node 3 is a beam node, and the interpolation function is (see Fig. 5.3)

$$h_3 = \frac{1}{2}(1-r)$$



(a) Beam transition element connecting beam and plane stress elements



(b) Transition element

Figure E5.28 Two-dimensional displacement-based beam transition element

The displacements of the element are thus

$$u(r, s) = h_1 u_1 + h_2 u_2 + h_3 u_3 - \frac{t}{2} s h_3 \theta_3$$

Hence, corresponding to the displacement vector in (a) we have

$$\mathbf{H} = \begin{bmatrix} h_1 & 0 & h_2 & 0 & h_3 & 0 & -\frac{t}{2} s h_3 \\ 0 & h_1 & 0 & h_2 & 0 & h_3 & 0 \end{bmatrix}$$

The coordinate interpolation is the same as that of the four-node plane stress element:

$$x(r, s) = \frac{1}{2}(1 + r)L$$

$$y(r, s) = \frac{s}{2}t$$

Hence,

$$\mathbf{J} = \begin{bmatrix} \frac{L}{2} & 0 \\ 0 & \frac{t}{2} \end{bmatrix}; \quad \mathbf{J}^{-1} = \begin{bmatrix} \frac{2}{L} & 0 \\ 0 & \frac{2}{t} \end{bmatrix}$$

Using (5.25), we thus obtain

$$\mathbf{B} = \begin{bmatrix} \frac{1}{2L}(1+s) & 0 & \frac{1}{2L}(1-s) & 0 & -\frac{1}{L} & 0 & \frac{t}{2L}s \\ 0 & \frac{1}{2t}(1+r) & 0 & -\frac{1}{2t}(1+r) & 0 & 0 & 0 \\ \frac{1}{2t}(1+r) & \frac{1}{2L}(1+s) & -\frac{1}{2t}(1+r) & \frac{1}{2L}(1-s) & 0 & -\frac{1}{L} & -\frac{1}{2}(1-r) \end{bmatrix}$$

We may finally note that the last three columns of the \mathbf{B} -matrix could also have been derived as described in Example 5.27.

The isoparametric beam elements presented in this section are an alternative to the classical Hermitian beam elements (see Example 4.16), and we may ask how these types of beam elements compare in efficiency. There is no doubt that in linear analysis of straight, thin beams, the Hermitian elements are usually more effective, since for a cubic displacement description the isoparametric beam element requires twice as many degrees of freedom. However, the isoparametric beam element includes the effects of shear deformations and has the advantages that all displacements are interpolated to the same degree (which for the cubic element results in a cubic axial displacement variation) and that curved geometries can be represented accurately. The element is therefore used efficiently in the analysis of stiffened shells (because the element represents in a natural way the stiffeners for the shell elements discussed in the next section) and as a basis of formulating more complex elements, such as pipe and transition elements. Also, the generality of the formulation with all displacements interpolated to the same degree of variation renders the element efficient in geometric nonlinear analyses (see Section 6.5.1).

Further applications of the general beam formulation given here lie in the use for plane strain situations (see Exercise 5.40) and the development of axisymmetric shell elements.

Axisymmetric Shell Elements

The isoparametric beam element formulation presented above can be directly adapted to the analysis of axisymmetric shells. Figure 5.24 shows a typical three-node element.

In the formulation, the kinematics of the beam element is used as if it were employed in two-dimensional action (i.e., for motion in the x, y plane), but the effects of the hoop strain and stress are also included. Hence, the strain-displacement matrix of the element is the matrix of the beam amended by a row corresponding to the hoop strain u/x . This evaluation is quite analogous to the construction of the \mathbf{B} -matrix of the two-dimensional axisymmetric element when compared with the two-dimensional plane stress element. In that case, also only a row corresponding to the hoop strain was added to the \mathbf{B} -matrix of the plane stress element in order to obtain the \mathbf{B} -matrix for the axisymmetric element. In addition of course the correct stress-strain law needs to be used (allowing for the Poisson effect coupling between the hoop and the r -direction and for the stress to be zero in the s -direction), and the integration is performed corresponding to axisymmetric conditions over 1 radian of the structure (see Example 5.9 and Exercise 5.41). Of course, using the procedures in Example 5.28, transition elements for axisymmetric shell conditions can also be designed (see Exercise 5.42).

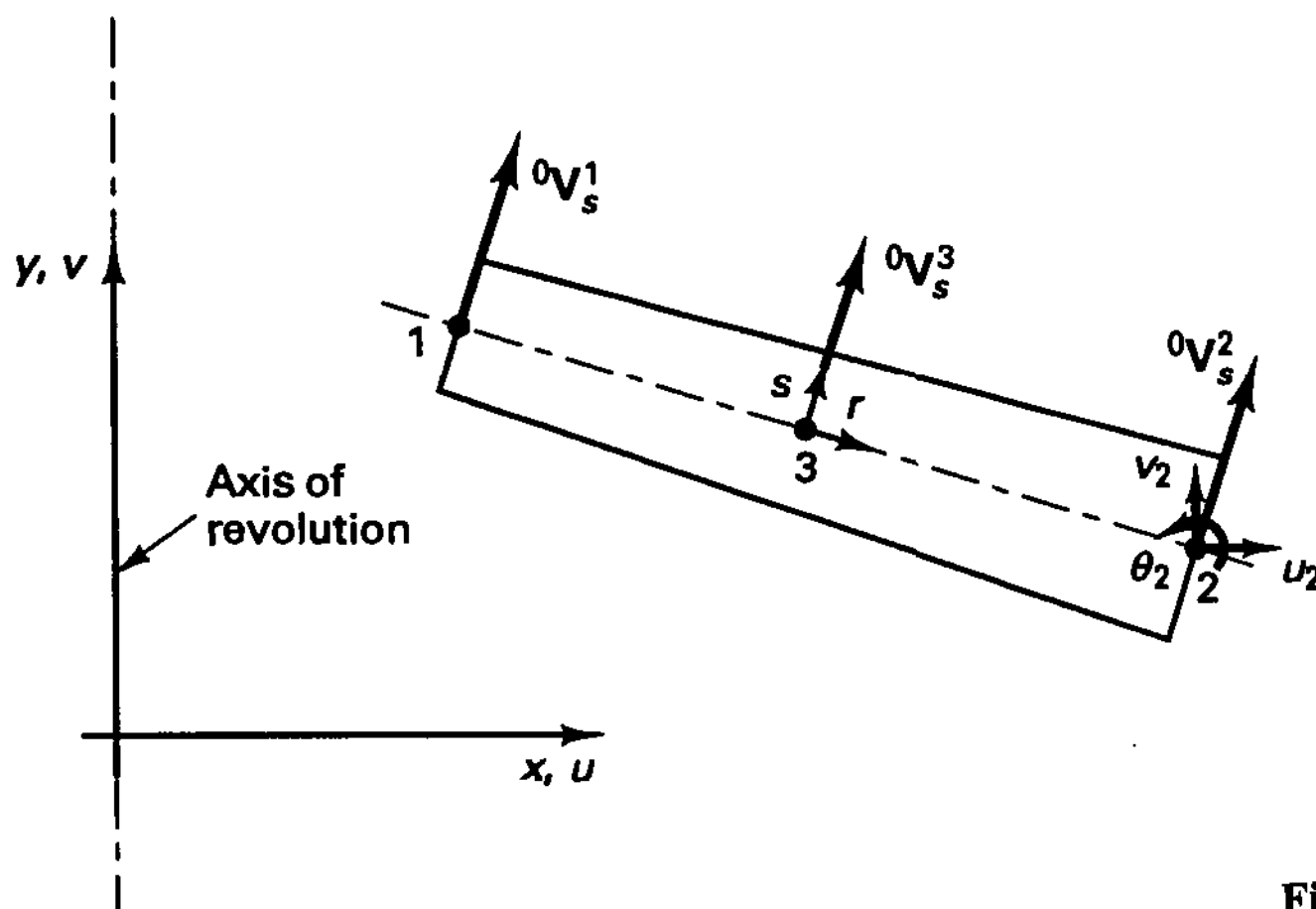


Figure 5.24 Axisymmetric shell element

5.4.2 Plate and General Shell Elements

The procedures we have employed in the previous section to formulate beam elements can also be directly used to establish effective plate and shell elements. In the following presentation we first discuss the formulation of plate elements, and then we proceed to summarize the formulation of general shell elements.

Plate Elements

The plate element formulation is a special case of the general shell element formulation presented later and is based on the theory of plates with transverse shear deformations included. This theory, due to E. Reissner [B] and R. D. Mindlin [A], uses the assumption that particles of the plate originally on a straight line that is normal to the undeformed middle surface remain on a straight line during deformation, but this line is not necessarily normal to the deformed middle surface. With this assumption, the displacement components of a point of coordinates x , y , and z are, in the small displacement bending theory,

$$u = -z\beta_x(x, y); \quad v = -z\beta_y(x, y); \quad w = w(x, y) \quad (5.88)$$

where w is the transverse displacement and β_x and β_y are the rotations of the normal to the undeformed middle surface in the x, z and y, z planes, respectively (see Fig. 5.25). It is instructive to note that in the Kirchhoff plate theory excluding shear deformations, $\beta_x = w_{,x}$ and $\beta_y = w_{,y}$ (and indeed we have selected the convention for β_x and β_y so as to have these Kirchhoff relations).

Considering the plate in Fig. 5.25 the bending strains ϵ_{xx} , ϵ_{yy} , γ_{xy} vary linearly through the plate thickness and are given by the curvatures of the plate using (5.88),

$$\begin{bmatrix} \epsilon_{xx} \\ \epsilon_{yy} \\ \gamma_{xy} \end{bmatrix} = -z \begin{bmatrix} \frac{\partial \beta_x}{\partial x} \\ \frac{\partial \beta_y}{\partial y} \\ \frac{\partial \beta_x}{\partial y} + \frac{\partial \beta_y}{\partial x} \end{bmatrix} \quad (5.89)$$

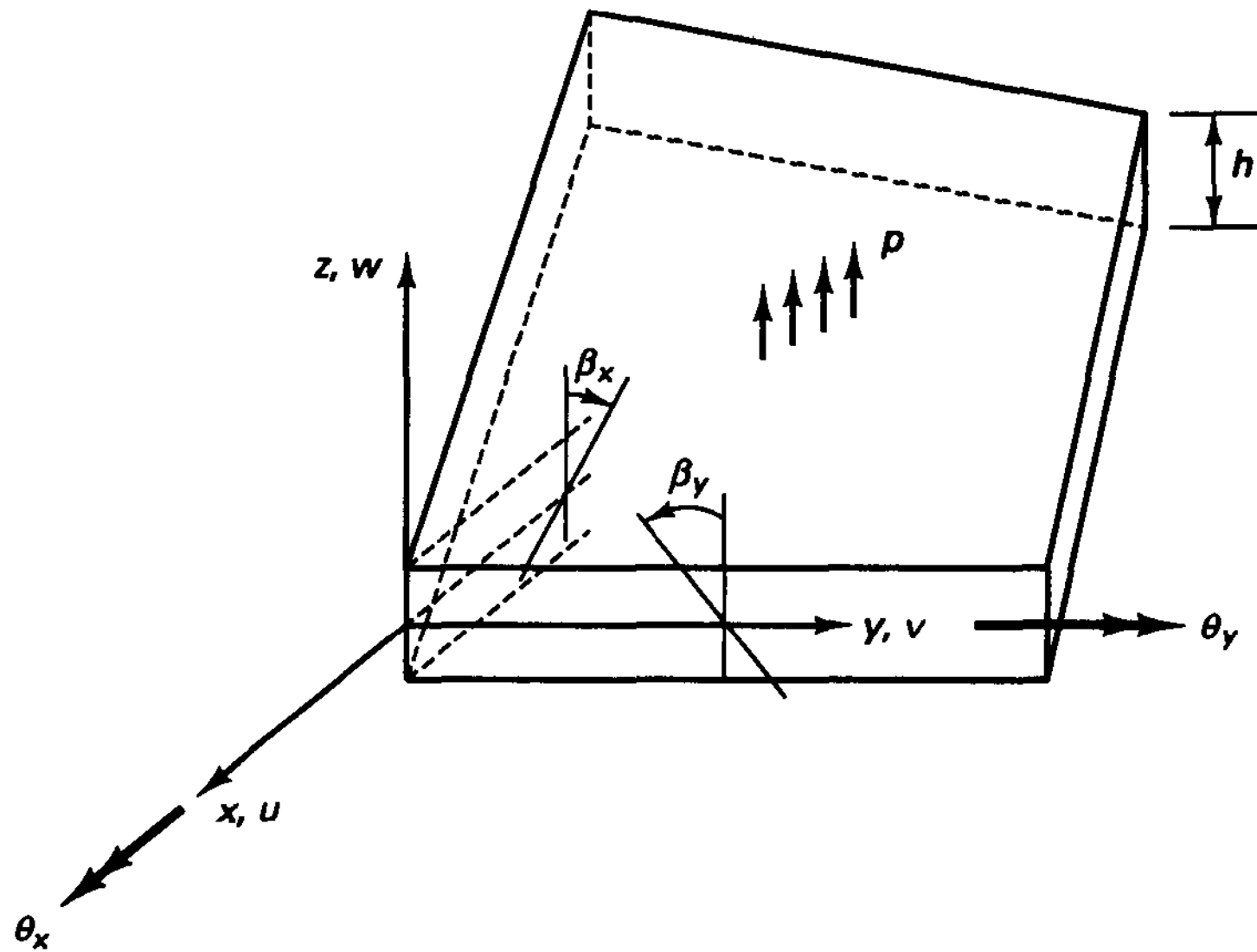


Figure 5.25 Deformation assumptions in analysis of plate including shear deformations

whereas the transverse shear strains are assumed to be constant through the thickness of the plate

$$\begin{bmatrix} \gamma_{xz} \\ \gamma_{yz} \end{bmatrix} = \begin{bmatrix} \frac{\partial w}{\partial x} - \beta_x \\ \frac{\partial w}{\partial y} - \beta_y \end{bmatrix} \tag{5.90}$$

We may note that each transverse shear strain component is of the form (5.56) used in the description of the beam deformations. The state of stress in the plate corresponds to plane stress conditions (i.e., $\tau_{zz} = 0$). For an isotropic material, we can thus write

$$\begin{bmatrix} \tau_{xx} \\ \tau_{yy} \\ \tau_{xy} \end{bmatrix} = -z \frac{E}{1 - \nu^2} \begin{bmatrix} 1 & \nu & 0 \\ \nu & 1 & 0 \\ 0 & 0 & \frac{1 - \nu}{2} \end{bmatrix} \begin{bmatrix} \frac{\partial \beta_x}{\partial x} \\ \frac{\partial \beta_y}{\partial y} \\ \frac{\partial \beta_x}{\partial y} + \frac{\partial \beta_y}{\partial x} \end{bmatrix} \tag{5.91}$$

$$\begin{bmatrix} \tau_{xz} \\ \tau_{yz} \end{bmatrix} = \frac{E}{2(1 + \nu)} \begin{bmatrix} \frac{\partial w}{\partial x} - \beta_x \\ \frac{\partial w}{\partial y} - \beta_y \end{bmatrix} \tag{5.92}$$

To establish the element equilibrium equations we now proceed as in the formulation of the two-dimensional beam element of rectangular cross section [see (5.58) to (5.64)].

Considering the plate, the expression for the principle of virtual work is, with p equal to the transverse loading per unit of the midsurface area A ,

$$\int_A \int_{-h/2}^{h/2} [\bar{\epsilon}_{xx} \quad \bar{\epsilon}_{yy} \quad \bar{\gamma}_{xy}] \begin{bmatrix} \tau_{xx} \\ \tau_{yy} \\ \tau_{xy} \end{bmatrix} dz dA + k \int_A \int_{-h/2}^{h/2} [\bar{\gamma}_{xz} \quad \bar{\gamma}_{yz}] \begin{bmatrix} \tau_{xz} \\ \tau_{yz} \end{bmatrix} dz dA = \int_A \bar{w} p dA \quad (5.93)$$

where the overbar denotes virtual quantities and k is again a constant to account for the actual nonuniformity of the shearing stresses (the value usually used is $\frac{5}{6}$; see Example 5.23). Substituting from (5.89) to (5.92) into (5.93), we thus obtain

$$\int_A \bar{\kappa}^T C_b \kappa dA + \int_A \bar{\gamma}^T C_s \gamma dA = \int_A \bar{w} p dA \quad (5.94)$$

where the internal bending moments and shear forces are $C_b \kappa$ and $C_s \gamma$, respectively, and

$$\kappa = \begin{bmatrix} \frac{\partial \beta_x}{\partial x} \\ \frac{\partial \beta_y}{\partial y} \\ \frac{\partial \beta_x}{\partial y} + \frac{\partial \beta_y}{\partial x} \end{bmatrix}; \quad \gamma = \begin{bmatrix} \frac{\partial w}{\partial x} - \beta_x \\ \frac{\partial w}{\partial y} - \beta_y \end{bmatrix} \quad (5.95)$$

$$(5.96)$$

and

$$C_b = \frac{Eh^3}{12(1-\nu^2)} \begin{bmatrix} 1 & \nu & 0 \\ \nu & 1 & 0 \\ 0 & 0 & \frac{1-\nu}{2} \end{bmatrix}; \quad C_s = \frac{Ehk}{2(1+\nu)} \begin{bmatrix} 1 & 0 \\ 0 & 1 \end{bmatrix} \quad (5.97)$$

Let us note that the variational indicator corresponding to (5.93) is given by (see Example 4.4)

$$\begin{aligned} \Pi = \frac{1}{2} \int_A \int_{-h/2}^{h/2} [\epsilon_{xx} \quad \epsilon_{yy} \quad \gamma_{xy}] \frac{E}{1-\nu^2} \begin{bmatrix} 1 & \nu & 0 \\ \nu & 1 & 0 \\ 0 & 0 & \frac{1-\nu}{2} \end{bmatrix} \begin{bmatrix} \epsilon_{xx} \\ \epsilon_{yy} \\ \gamma_{xy} \end{bmatrix} dz dA \\ + \frac{k}{2} \int_A \int_{-h/2}^{h/2} [\gamma_{xz} \quad \gamma_{yz}] \frac{E}{2(1+\nu)} \begin{bmatrix} \gamma_{xz} \\ \gamma_{yz} \end{bmatrix} dz dA - \int_A w p dA \end{aligned} \quad (5.98)$$

with the strains given by (5.89) and (5.90). The principle of virtual work corresponds to invoking $\delta\Pi = 0$ with respect to the transverse displacement w and section rotations β_x and β_y .

We emphasize that in this theory w , β_x , and β_y are independent variables. Hence, in the finite element discretization using the displacement method, we need to enforce inter-element continuity only on w , β_x , and β_y and not on any derivatives thereof, which can readily be achieved in the same way as in the isoparametric finite element analysis of solids.

Let us consider the pure displacement discretization first. As in the analysis of beams, the pure displacement discretization will not yield efficient lower-order elements but does provide the basis for the mixed interpolation that we shall discuss afterward.

In the pure displacement discretization we use

$$\begin{aligned}
 w &= \sum_{i=1}^q h_i w_i; & \beta_x &= -\sum_{i=1}^q h_i \theta_y^i \\
 \beta_y &= \sum_{i=1}^q h_i \theta_x^i
 \end{aligned}
 \tag{5.99}$$

where the h_i are the interpolation functions and q is the number of nodes of the element. With these interpolations we can now proceed in the usual way, and all concepts pertaining to the isoparametric finite elements discussed earlier are directly applicable. For example, some interpolation functions applicable to the formulation of plate elements are listed in Fig. 5.4, and triangular elements can be established as discussed in Section 5.3.2. Since the interpolation functions are given in terms of the isoparametric coordinates r, s , we can also directly calculate the matrices of plate elements that are curved in their plane (to model, for example, a circular plate).

We demonstrate the formulation of a simple four-node element in the following example.

EXAMPLE 5.29: Derive the expressions used in the evaluation of the stiffness matrix of the four-node plate element shown in Fig. E5.29.

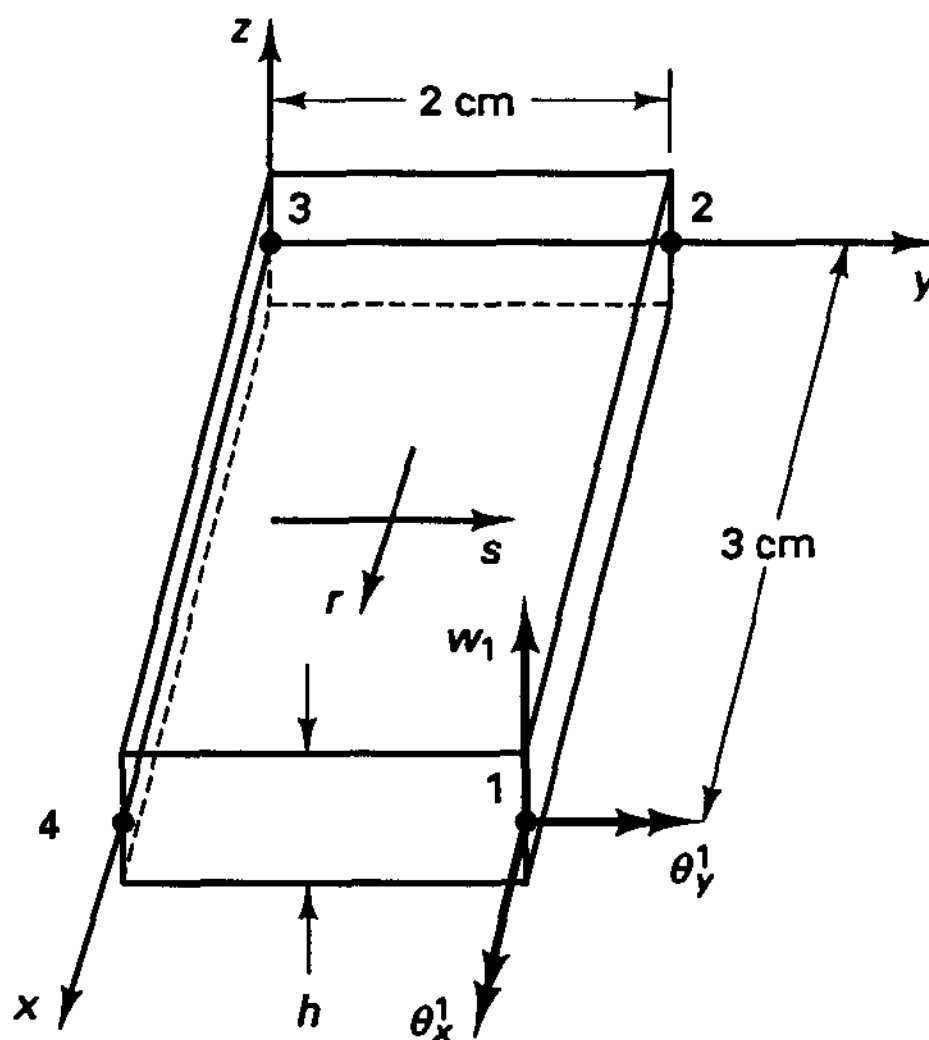


Figure E5.29 A four-node plate element

The calculations are very similar to those performed in the formulation of the two-dimensional plane stress element in Example 5.5.

For the element in Fig. E5.29 we have (see Example 5.3)

$$\mathbf{J} = \begin{bmatrix} \frac{3}{2} & 0 \\ 0 & 1 \end{bmatrix}$$

and then, using the interpolation functions defined in Fig. 5.4,

$$\begin{bmatrix} \frac{\partial w}{\partial x} \\ \frac{\partial w}{\partial y} \end{bmatrix} = \frac{1}{4} \begin{bmatrix} \frac{2}{3} & 0 \\ 0 & 1 \end{bmatrix} \begin{bmatrix} (1+s) & -(1+s) & -(1-s) & (1-s) \\ (1+r) & (1-r) & -(1-r) & -(1+r) \end{bmatrix} \begin{bmatrix} w_1 \\ w_2 \\ w_3 \\ w_4 \end{bmatrix}$$

with similar expressions for the derivatives of β_x and β_y . Thus, if we use the following notation,

$$\kappa(r, s) = \mathbf{B}_\kappa \hat{\mathbf{u}}$$

$$\gamma(r, s) = \mathbf{B}_\gamma \hat{\mathbf{u}}$$

$$w(r, s) = \mathbf{H}_w \hat{\mathbf{u}}$$

where

$$\hat{\mathbf{u}}^T = [w_1 \quad \theta_x^1 \quad \theta_y^1; w_2 \quad \dots \quad \theta_y^4]$$

we have

$$\mathbf{B}_\kappa = \begin{bmatrix} 0 & 0 & -\frac{1}{6}(1+s) & \dots & -\frac{1}{6}(1-s) \\ 0 & \frac{1}{4}(1+r) & 0 & \dots & 0 \\ 0 & \frac{1}{6}(1+s) & -\frac{1}{4}(1+r) & \dots & \frac{1}{4}(1+r) \end{bmatrix}$$

$$\mathbf{B}_\gamma = \begin{bmatrix} \frac{1}{6}(1+s) & 0 & \frac{1}{4}(1+r)(1+s) & \dots & \frac{1}{4}(1+r)(1-s) \\ \frac{1}{4}(1+r) & -\frac{1}{4}(1+r)(1+s) & 0 & \dots & 0 \end{bmatrix}$$

$$\mathbf{H}_w = \frac{1}{4} [(1+r)(1+s) \quad 0 \quad 0 \quad \dots \quad 0]$$

The element stiffness matrix is then

$$\mathbf{K} = \frac{3}{2} \int_{-1}^{+1} \int_{-1}^{+1} (\mathbf{B}_\kappa^T \mathbf{C}_b \mathbf{B}_\kappa + \mathbf{B}_\gamma^T \mathbf{C}_s \mathbf{B}_\gamma) dr ds \quad (a)$$

and the consistent load vector is

$$\mathbf{R}_s = \frac{3}{2} \int_{-1}^{+1} \int_{-1}^{+1} \mathbf{H}_w^T p dr ds \quad (b)$$

where the integrals in (a) and (b) could be evaluated in closed form but are usually evaluated using numerical integration (see Section 5.5).

This pure displacement-based plate element formulation is of value only when higher-order elements are employed. Indeed, the least order of interpolation that should be used is a cubic interpolation, which results in a 16-node quadrilateral element and a 10-node triangular element. However, even these high-order elements still do not display a good predictive capability, particularly when the elements are geometrically distorted and used for stress predictions (see, for example, M. L. Bucelem and K. J. Bathe [A]).

As in the formulation of isoparametric beam elements, the basic difficulty is that spurious shear stresses are predicted with the displacement-based elements. These spurious shear stresses result in a strong artificial stiffening of the elements as the thickness/length ratio decreases. This effect of shear locking is more pronounced for a low-order element and when the elements are geometrically distorted because, simply, the error in the shear stresses is then larger.

To arrive at efficient and reliable plate bending elements, the pure displacement-based formulation must be extended, and a successful approach is to use a mixed interpolation of transverse displacement, section rotations, and transverse shear strains.

We should note here that in the above discussion, we assumed that the integrals for the computation of the element matrices (stiffness and mass matrices and load vectors) are evaluated accurately; hence, throughout our discussion we assumed and shall continue to assume that the error in the numerical integration (that usually is performed in practice; see Section 5.5) is small and certainly does not change the character of the element matrices. A number of authors have advocated the use of simple reduced integration to alleviate the shear locking problem. We discuss such techniques briefly in Section 5.5.6.

In the following we present a family of plate bending elements that have a good mathematical basis and are reliable and efficient. These elements are referred to as the MITC n elements, where n refers to the number of element nodes and $n = 4, 9, 16$ for the quadrilateral and $n = 7, 12$ for the triangular elements (here MITC stands for *mixed interpolation of tensorial components*), (see K. J. Bathe, M. L. Bucelem, and F. Brezzi [A]). Let us consider the MITC4 element in detail and give the basic interpolations for the other elements in tabular form.

An important feature of the MITC element formulation is the use of tensorial components of shear strains so as to render the resulting element relatively distortion-insensitive. Figure 5.26 shows a generic four-node element with the coordinate systems used.

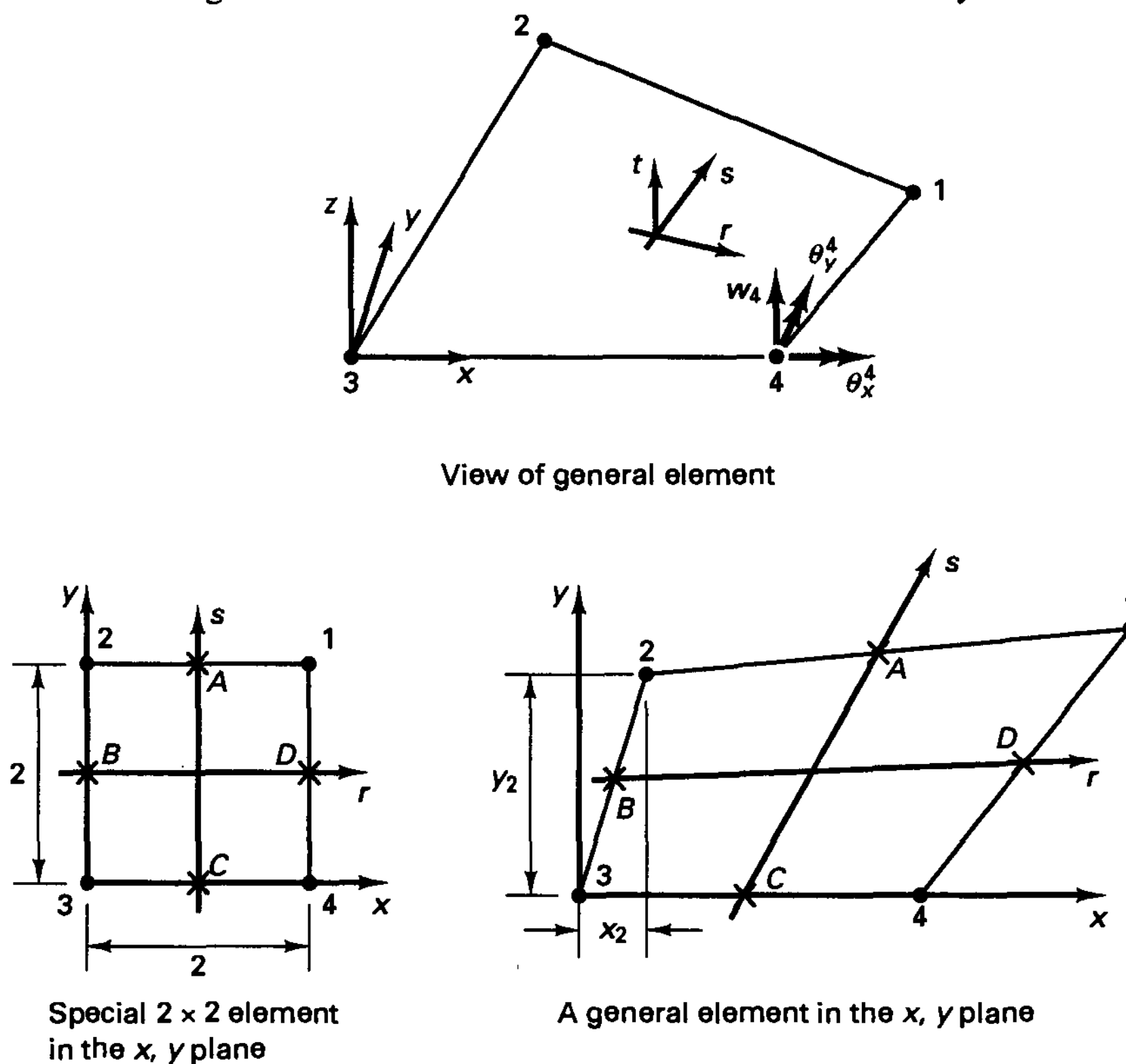


Figure 5.26 Conventions used in formulation of four-node plate bending element

To circumvent the shear locking problem, we formulate the element stiffness matrix by including the bending and shear effects through different interpolations. For the section curvatures in (5.95) we use the same interpolation as in the displacement-based method, as evaluated using (5.99), but we proceed differently in evaluating the transverse shear strains.

Consider first the MITC4 element when it is of geometry 2×2 (for which the x, y coordinates could be taken to be equal to the r, s isoparametric coordinates). For this element we use the interpolation (see K. J. Bathe and E. N. Dvorkin [A])

$$\begin{aligned}\gamma_{rz} &= \frac{1}{2}(1 + s)\gamma_{rz}^A + \frac{1}{2}(1 - s)\gamma_{rz}^C \\ \gamma_{sz} &= \frac{1}{2}(1 + r)\gamma_{sz}^D + \frac{1}{2}(1 - r)\gamma_{sz}^B\end{aligned}\quad (5.100)$$

where $\gamma_{rz}^A, \gamma_{rz}^C, \gamma_{sz}^D$, and γ_{sz}^B are the (physical) shear strains at points A, B, C , and D evaluated by the displacement and section rotations in (5.99). Hence,

$$\begin{aligned}\gamma_{rz} &= \frac{1}{2}(1 + s)\left(\frac{w_1 - w_2}{2} + \frac{\theta_y^1 + \theta_y^2}{2}\right) + \frac{1}{2}(1 - s)\left(\frac{w_4 - w_3}{2} + \frac{\theta_y^4 + \theta_y^3}{2}\right) \\ \gamma_{sz} &= \frac{1}{2}(1 + r)\left(\frac{w_1 - w_4}{2} - \frac{\theta_x^1 + \theta_x^4}{2}\right) + \frac{1}{2}(1 - r)\left(\frac{w_2 - w_3}{2} - \frac{\theta_x^2 + \theta_x^3}{2}\right)\end{aligned}\quad (5.101)$$

With these interpolations given, all strain-displacement interpolation matrices can be directly constructed and the stiffness matrix is formulated in the standard manner. Of course, the same procedure can also be directly employed for any rectangular element.

Considering next the case of a general quadrilateral four-node element, we use the same basic idea of interpolating the transverse shear strains, but—using the interpolation in (5.100)—we interpolate the covariant tensor components measured in the r, s, z coordinate system. In this way we are directly taking account of the element distortion (from the 2×2 geometry). Proceeding in this way with the tensor shear strain components, we obtain (see Example 5.30) the following expressions for the γ_{xz} and γ_{yz} shear strains:

$$\begin{aligned}\gamma_{xz} &= \gamma_{rz} \sin \beta - \gamma_{sz} \sin \alpha \\ \gamma_{yz} &= -\gamma_{rz} \cos \beta + \gamma_{sz} \cos \alpha\end{aligned}\quad (5.102)$$

where α and β are the angles between the r and x axes and s and x axes, respectively, and

$$\begin{aligned}\gamma_{rz} &= \frac{\sqrt{(C_x + rB_x)^2 + (C_y + rB_y)^2}}{8 \det \mathbf{J}} \\ &\quad \left\{ (1 + s) \left[\frac{w_1 - w_2}{2} + \frac{x_1 - x_2}{4}(\theta_y^1 + \theta_y^2) - \frac{y_1 - y_2}{4}(\theta_x^1 + \theta_x^2) \right] \right. \\ &\quad \left. + (1 - s) \left[\frac{w_4 - w_3}{2} + \frac{x_4 - x_3}{4}(\theta_y^4 + \theta_y^3) - \frac{y_4 - y_3}{4}(\theta_x^4 + \theta_x^3) \right] \right\} \\ \gamma_{sz} &= \frac{\sqrt{(A_x + sB_x)^2 + (A_y + sB_y)^2}}{8 \det \mathbf{J}} \\ &\quad \left\{ (1 + r) \left[\frac{w_1 - w_4}{2} + \frac{x_1 - x_4}{4}(\theta_y^1 + \theta_y^4) - \frac{y_1 - y_4}{4}(\theta_x^1 + \theta_x^4) \right] \right. \\ &\quad \left. + (1 - r) \left[\frac{w_2 - w_3}{2} + \frac{x_2 - x_3}{4}(\theta_y^2 + \theta_y^3) - \frac{y_2 - y_3}{4}(\theta_x^2 + \theta_x^3) \right] \right\}\end{aligned}\quad (5.103)$$

In equations (5.103) we have

$$\det \mathbf{J} = \det \begin{bmatrix} \frac{\partial x}{\partial r} & \frac{\partial y}{\partial r} \\ \frac{\partial x}{\partial s} & \frac{\partial y}{\partial s} \end{bmatrix}\quad (5.104)$$

and

$$\begin{aligned}
 A_x &= x_1 - x_2 - x_3 + x_4 \\
 B_x &= x_1 - x_2 + x_3 - x_4 \\
 C_x &= x_1 + x_2 - x_3 - x_4 \\
 A_y &= y_1 - y_2 - y_3 + y_4 \\
 B_y &= y_1 - y_2 + y_3 - y_4 \\
 C_y &= y_1 + y_2 - y_3 - y_4
 \end{aligned}
 \tag{5.105}$$

We further consider the above relationships in the following example.

EXAMPLE 5.30: Derive the transverse shear strain interpolations of the general MITC4 plate bending element.

In the natural coordinate system of the plate bending element, the covariant base vectors are defined as

$$\begin{aligned}
 \mathbf{g}_r &= \frac{\partial \mathbf{x}}{\partial r}; & \mathbf{g}_s &= \frac{\partial \mathbf{x}}{\partial s} \\
 \mathbf{g}_z &= \frac{h}{2} \mathbf{e}_z
 \end{aligned}
 \tag{a}$$

where \mathbf{x} is the vector of coordinates, and $\mathbf{e}_x, \mathbf{e}_y, \mathbf{e}_z$ are the base vectors of the Cartesian system.

Let us recall that in the natural coordinate system, the strain tensor can be expressed using covariant tensor components and contravariant base vectors (see Section 2.4)

$$\epsilon = \tilde{\epsilon}_{ij} \mathbf{g}^i \mathbf{g}^j; \quad i, j \equiv r, s, z$$

where the tilde (\sim) indicates that the tensor components are measured in the natural coordinate system.

To obtain the shear tensor components we now use the equivalent of (5.100),

$$\tilde{\epsilon}_{rz} = \frac{1}{2}(1 + s)\tilde{\epsilon}_{rz}^A + \frac{1}{2}(1 - s)\tilde{\epsilon}_{rz}^C \tag{b}$$

$$\tilde{\epsilon}_{sz} = \frac{1}{2}(1 + r)\tilde{\epsilon}_{sz}^D + \frac{1}{2}(1 - r)\tilde{\epsilon}_{sz}^B \tag{c}$$

where $\tilde{\epsilon}_{rz}^A, \tilde{\epsilon}_{rz}^C, \tilde{\epsilon}_{sz}^D,$ and $\tilde{\epsilon}_{sz}^B$ are the shear tensor components at points A, B, C, and D evaluated from the displacement interpolations. To obtain these components we use the linear terms of the general relation for the strain components in terms of the base vectors (see Example 2.28),

$${}^1_0 \tilde{\epsilon}_{ij} = \frac{1}{2} [{}^1 \mathbf{g}_i \cdot {}^1 \mathbf{g}_j - {}^0 \mathbf{g}_i \cdot {}^0 \mathbf{g}_j]$$

where the left superscript of the base vectors is equal to 1 for the deformed configuration and equal to 0 for the initial configuration. Substituting from (5.99) and (a), we obtain

$$\tilde{\epsilon}_{rz}^A = \frac{1}{4} \left[\frac{h}{2}(w_1 - w_2) + \frac{h}{4}(x_1 - x_2)(\theta_y^1 + \theta_y^2) - \frac{h}{4}(y_1 - y_2)(\theta_x^1 + \theta_x^2) \right]$$

and

$$\tilde{\epsilon}_{rz}^C = \frac{1}{4} \left[\frac{h}{2}(w_4 - w_3) + \frac{h}{4}(x_4 - x_3)(\theta_y^4 + \theta_y^3) - \frac{h}{4}(y_4 - y_3)(\theta_x^4 + \theta_x^3) \right]$$

Therefore, using (b), we obtain

$$\begin{aligned}\bar{\epsilon}_{rz} = & \frac{1}{8}(1+s) \left[\frac{h}{2}(w_1 - w_2) + \frac{h}{4}(x_1 - x_2)(\theta_y^1 + \theta_y^2) - \frac{h}{4}(y_1 - y_2)(\theta_x^1 + \theta_x^2) \right] \\ & + \frac{1}{8}(1-s) \left[\frac{h}{2}(w_4 - w_3) + \frac{h}{4}(x_4 - x_3)(\theta_y^4 + \theta_y^3) - \frac{h}{4}(y_4 - y_3)(\theta_x^4 + \theta_x^3) \right]\end{aligned}$$

and in the same way, using (c),

$$\begin{aligned}\bar{\epsilon}_{sz} = & \frac{1}{8}(1+r) \left[\frac{h}{2}(w_1 - w_4) + \frac{h}{4}(x_1 - x_4)(\theta_y^1 + \theta_y^4) - \frac{h}{4}(y_1 - y_4)(\theta_x^1 + \theta_x^4) \right] \\ & + \frac{1}{8}(1-r) \left[\frac{h}{2}(w_2 - w_3) + \frac{h}{4}(x_2 - x_3)(\theta_y^2 + \theta_y^3) - \frac{h}{4}(y_2 - y_3)(\theta_x^2 + \theta_x^3) \right]\end{aligned}$$

Next we use

$$\bar{\epsilon}_{ij} \mathbf{g}^i \mathbf{g}^j = \epsilon_{kl} \mathbf{e}_k \mathbf{e}_l \quad (d)$$

where the ϵ_{kl} are the components of the strain tensor measured in the Cartesian coordinate system. From (d) we obtain

$$\begin{aligned}\gamma_{xz} &= 2\bar{\epsilon}_{rz}(\mathbf{g}^r \cdot \mathbf{e}_x)(\mathbf{g}^z \cdot \mathbf{e}_z) + 2\bar{\epsilon}_{sz}(\mathbf{g}^s \cdot \mathbf{e}_x)(\mathbf{g}^z \cdot \mathbf{e}_z) \\ \gamma_{yz} &= 2\bar{\epsilon}_{rz}(\mathbf{g}^r \cdot \mathbf{e}_y)(\mathbf{g}^z \cdot \mathbf{e}_z) + 2\bar{\epsilon}_{sz}(\mathbf{g}^s \cdot \mathbf{e}_y)(\mathbf{g}^z \cdot \mathbf{e}_z)\end{aligned} \quad (e)$$

However (using the standard procedure described in Section 2.4),

$$\begin{aligned}\mathbf{g}^r &= \sqrt{g^{rr}} (\sin \beta \mathbf{e}_x - \cos \beta \mathbf{e}_y) \\ \mathbf{g}^s &= \sqrt{g^{ss}} (-\sin \alpha \mathbf{e}_x + \cos \alpha \mathbf{e}_y) \\ \mathbf{g}^z &= \sqrt{g^{zz}} \mathbf{e}_z\end{aligned}$$

where α and β are the angles between the r and x axes and s and x axes, respectively, and

$$\begin{aligned}g^{rr} &= \frac{(C_x + rB_x)^2 + (C_y + rB_y)^2}{16(\det \mathbf{J})^2} \\ g^{ss} &= \frac{(A_x + sB_x)^2 + (A_y + sB_y)^2}{16(\det \mathbf{J})^2}\end{aligned}$$

where A_x , B_x , C_x , A_y , B_y , and C_y are defined in (5.105) and

$$g^{zz} = \frac{4}{h^2}$$

Substituting into (e), the relations in (5.102) are obtained.

The MITC4 plate bending element is in rectangular or parallelogram geometric configurations identical or closely related to other four-node plate bending elements (see T. J. R. Hughes and T. E. Tezduyar [A] and R. H. MacNeal [A]). However, an important attribute of the MITC plate element is that it is a special case of a general shell element for linear and nonlinear analysis. Specifically, the use of covariant strain interpolations gives the element a relatively high predictive capability even when it is used with angular geometric distortions as shown in Fig. 5.31 (see also K. J. Bathe and E. N. Dvorkin [A]). In practice, elements with angular distortions are of course widely used.

Some observations pertaining to the MITC4 element are the following.

The element behaves like the two-node mixed interpolated isoparametric beam element (discussed in the previous section) when used in the analysis of two-dimensional beam action.

The element can be derived from the Hu-Washizu variational principle (see Example 4.30).

The element passes the patch test (for an analytical proof see K. J. Bathe and E. N. Dvorkin [B]).

A mathematical convergence analysis for the transverse displacement and section rotations has been provided by K. J. Bathe and F. Brezzi [A] (assuming uniform meshes, i.e., that the element assemblage consists of square elements of sides h).

This analysis gives the results

$$\|\boldsymbol{\beta} - \boldsymbol{\beta}_h\|_1 \leq c_1 h \quad ; \quad \|\nabla w - \nabla w_h\|_0 \leq c_2 h \quad (5.106)$$

where $\boldsymbol{\beta}$ and w are the exact solutions, $\boldsymbol{\beta}_h$ and w_h are the finite element solutions corresponding to a mesh of elements with sides h , and c_1, c_2 are constants independent of h . A convergence analysis of the transverse shear strains gave the result that the L^2 -norm of the error is not bounded independent of the plate thickness (see F. Brezzi, M. Fortin, and R. Stenberg [A]).

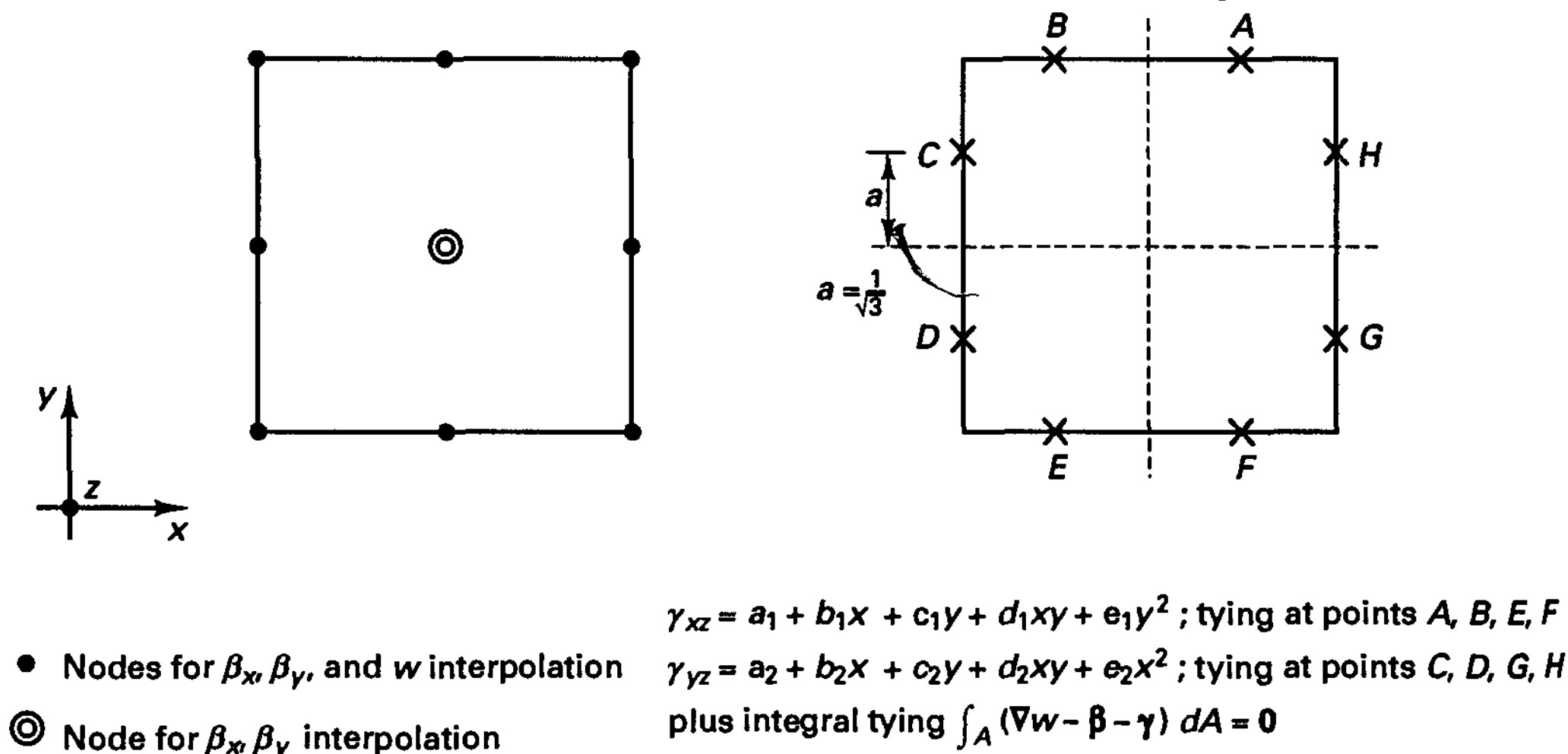
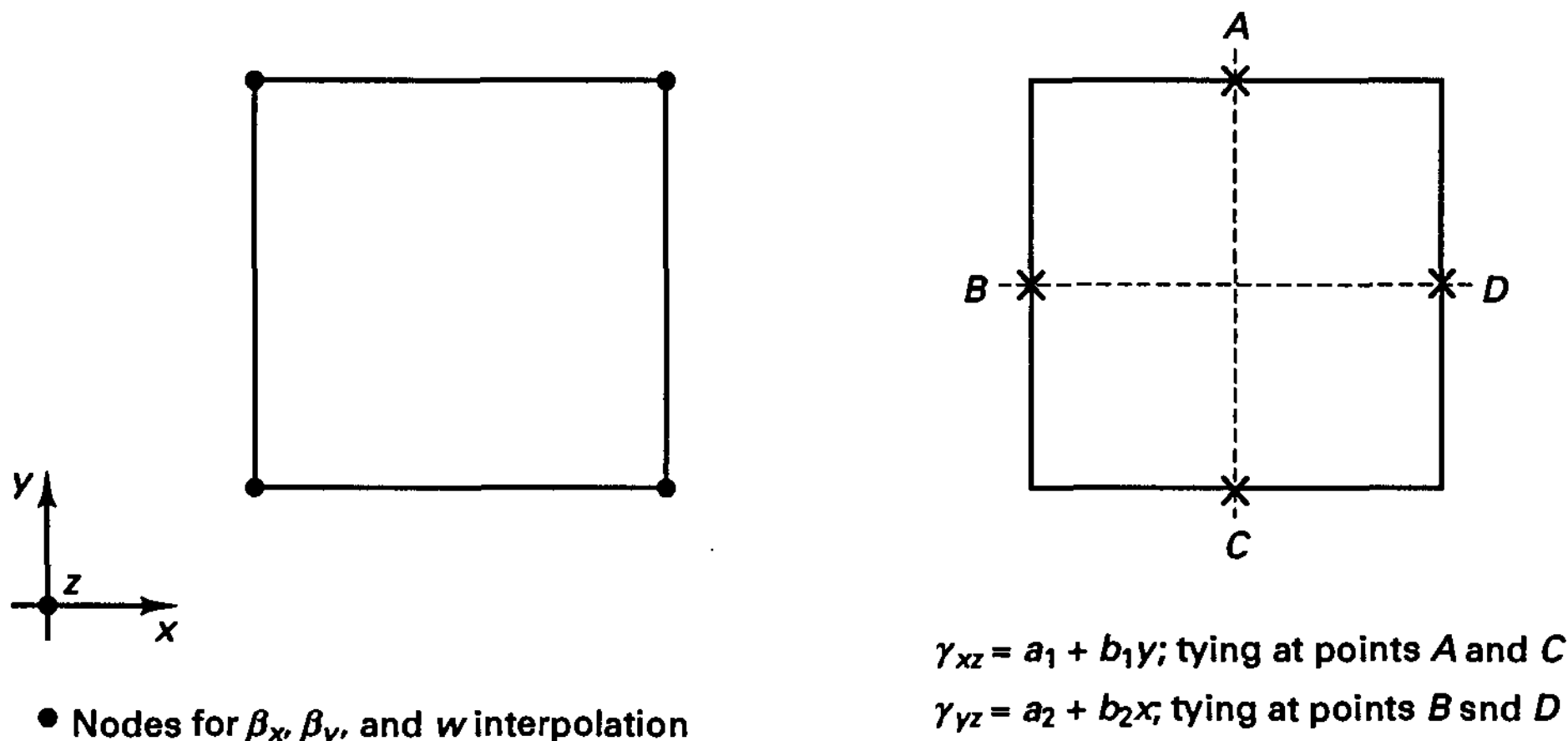
The essence of the results of these analytical convergence studies is also seen in practice for uniform and distorted meshes. The element predicts the transverse displacements and bending strains quite well, but the transverse shear strain predictions may not be satisfactory, particularly when very thin plates are analyzed.

A most important observation in the mathematical analysis of the MITC4 element was that this element, in its mathematical basis, is an analog of the 4/1 element of the u/p element family presented in Section 4.4.3: in the u/p formulation the displacements and pressure are interpolated to satisfy the constraint of (almost) incompressibility, $e_v = 0$, whereas in the MITC4 element formulation the transverse displacement, section rotations and transverse shear strains are interpolated to satisfy the thin plate condition, $\boldsymbol{\gamma} = \mathbf{0}$. This analogy between the incompressibility constraint in solid mechanics and the zero transverse shear strain constraint in the Reissner-Mindlin plate theory resulted in the development of a mathematical basis aimed at the construction of new plate bending elements (see K. J. Bathe and F. Brezzi [B]). Since these elements are all based on the mixed interpolation of the transverse displacement, section rotations and transverse shear strains and for general geometries use the tensorial components (as for the MITC4 element), we refer to these elements as MITC elements with n nodes (i.e., MITC n elements).

The basic difficulty is choosing the orders of interpolations of transverse displacement, section rotations, and transverse shear strains which *together* result in nonlocking behavior and optimal convergence of the element. The mathematical considerations for choosing the appropriate interpolations were summarized by K. J. Bathe and F. Brezzi [B], K. J. Bathe, M. L. Bucelem, and F. Brezzi [A], and F. Brezzi, K. J. Bathe, and M. Fortin [A], who presented the elements in Fig. 5.27 as well as additional ones, and also gave numerical results.

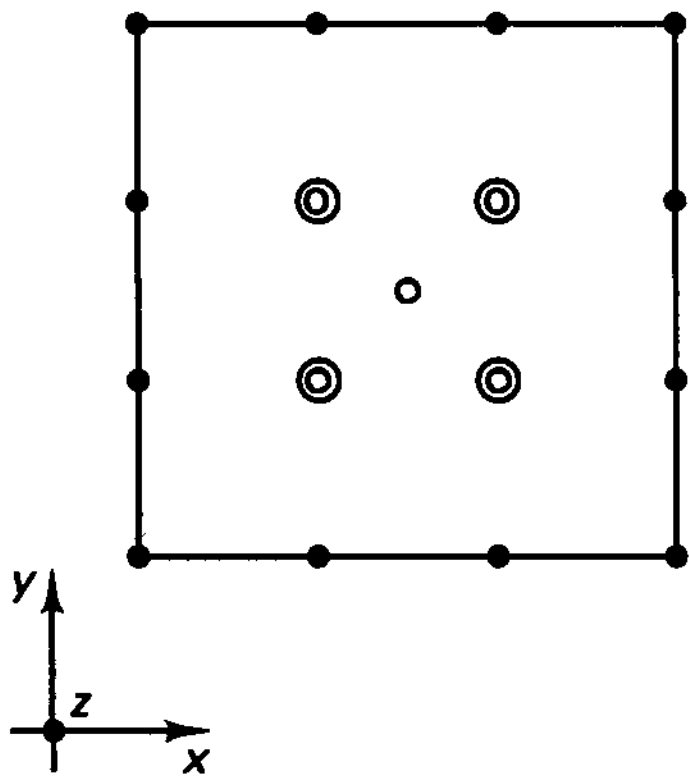
Figure 5.27 and Table 5.3 summarize the interpolations of 9- and 16-node quadrilateral elements and 7- and 12-node triangular elements and give the rates of convergence. In Fig. 5.27 the interpolations are given for the elements in geometrically nondistorted form, and we use tensorial components, as for the MITC4 element, to generalize the interpolations to geometrically distorted elements. Let us illustrate the use of the interpolations given in Fig. 5.27 in an example.

MITC4 element: 4 nodes for interpolation of section rotations and transverse displacement (2 × 2 Gauss integration)

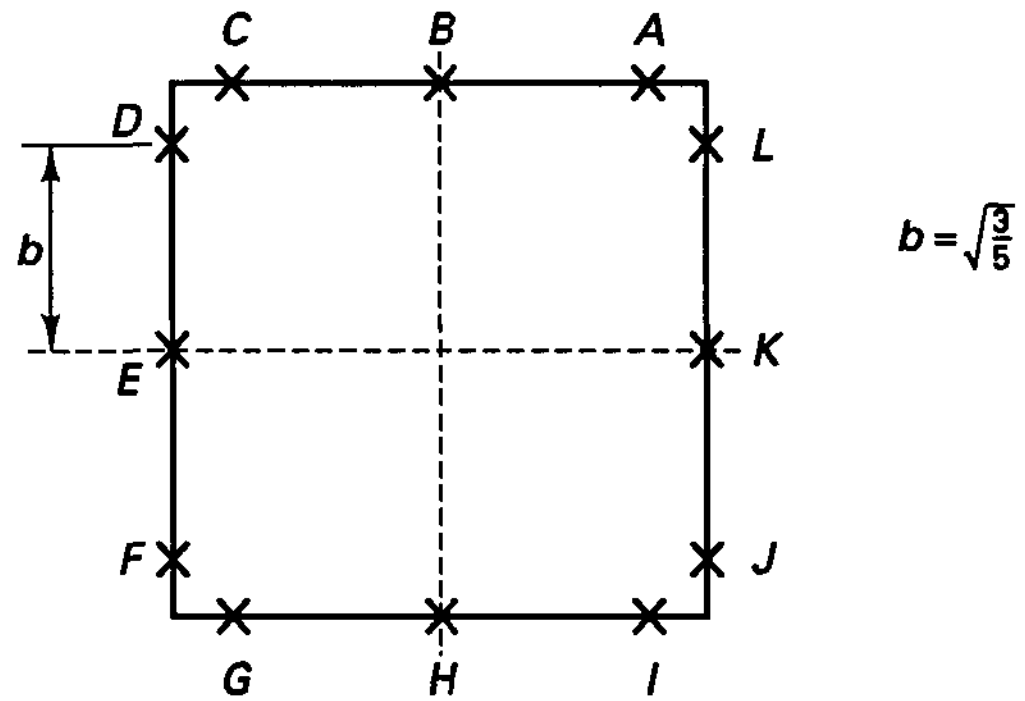


MITC16 element:

16 nodes for interpolation of section rotations and 13 nodes for interpolation of transverse displacement (4 × 4 Gauss integration)



- Nodes for $\beta_x, \beta_y,$ and w interpolation
- ⊙ Nodes for β_x, β_y interpolation
- Node for w interpolation



$$\gamma_{xz} = a_1 + b_1x + c_1y + d_1x^2 + e_1xy + f_1y^2 + g_1x^2y + h_1xy^2 + i_1y^3;$$

tying at points A, B, C, G, H, I;

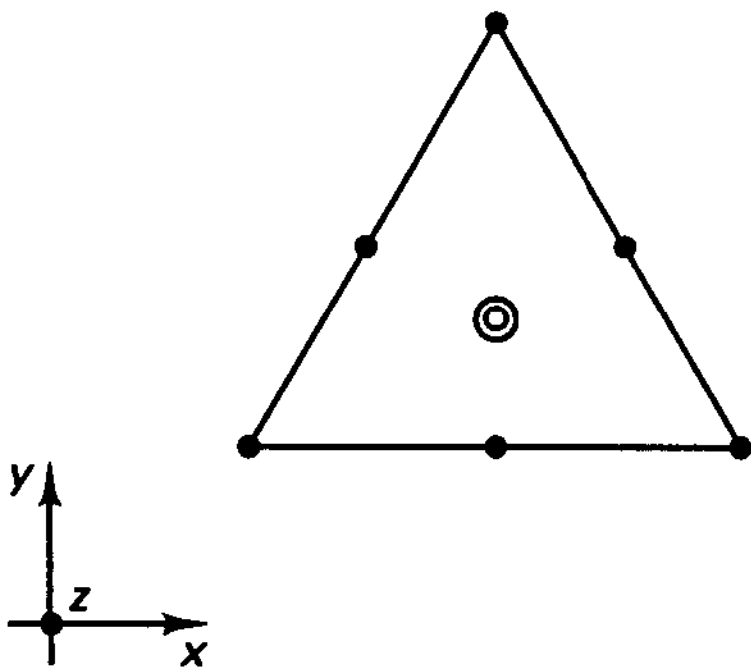
$$\gamma_{yz} = a_2 + b_2x + c_2y + d_2x^2 + e_2xy + f_2y^2 + g_2x^2y + h_2xy^2 + i_2x^3;$$

tying at points D, E, F, J, K, L;

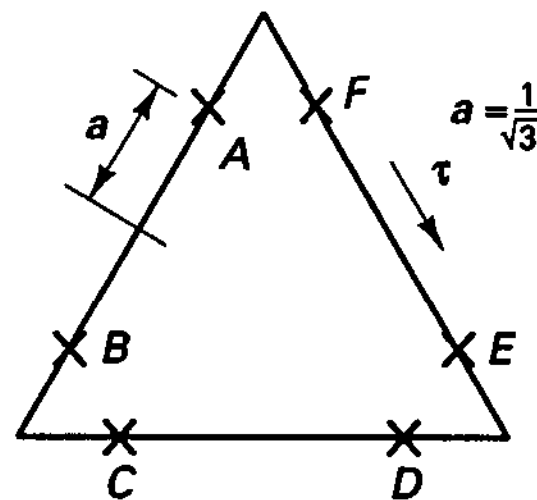
plus integral tying $\int_A (\nabla w - \beta - \gamma) dA = \int_A (\nabla w - \beta - \gamma)x dA = \int_A (\nabla w - \beta - \gamma)y dA = 0$

MITC7 element:

7 nodes for interpolation of section rotations and 6 nodes for interpolation of transverse displacement (7-point Gauss integration)



- Nodes for $\beta_x, \beta_y,$ and w interpolation
- ⊙ Node for β_x, β_y interpolation



$$\gamma_{xz} = a_1 + b_1x + c_1y + y(dx + ey);$$

$$\gamma_{yz} = a_2 + b_2x + c_2y - x(dx + ey);$$

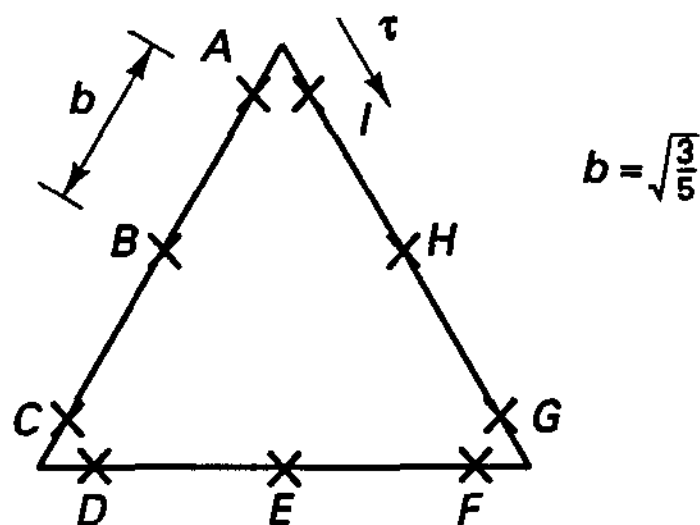
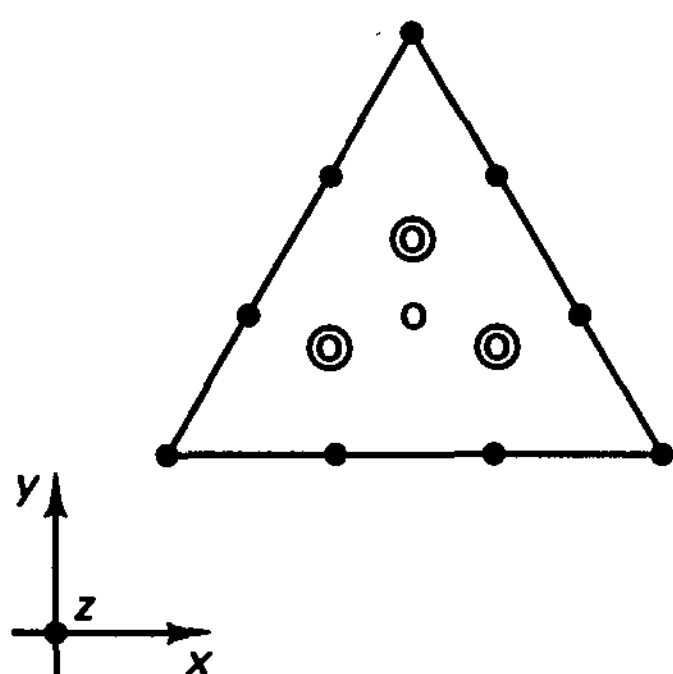
tying of $\gamma \cdot \tau$ at A, B, C, D, E, F

plus integral tying $\int_A (\nabla w - \beta - \gamma) dA = 0$

Figure 5.27 (continued)

MITC12 element:

12 nodes for interpolation of section rotations and 10 nodes for interpolation of transverse displacement (13-point Gauss integration)



- Nodes for $\beta_x, \beta_y,$ and w interpolation
- ⊙ Nodes for β_x, β_y interpolation
- Node for w interpolation

$$\gamma_{xz} = a_1 + b_1x + c_1y + d_1x^2 + e_1xy + f_1y^2 + y(gx^2 + hxy + iy^2);$$

$$\gamma_{yz} = a_2 + b_2x + c_2y + d_2x^2 + e_2xy + f_2y^2 - x(gx^2 + hxy + iy^2);$$

tying of $\gamma \cdot \tau$ at points A, B, C, D, E, F, G, H, I

$$\text{plus integral tying } \int_A (\nabla w - \beta - \gamma) dA = \int_A (\nabla w - \beta - \gamma)x dA = \int_A (\nabla w - \beta - \gamma)y dA = 0$$

Figure 5.27 (continued)

TABLE 5.3 Interpolation spaces and theoretically predicted error estimates for plate bending elements

Element	Spaces used for section rotations and transverse displacement [†]	Error estimates
MITC4	$\beta_h \in Q_1 \times Q_1$ $w_h \in Q_1$	$\ \beta - \beta_h\ _1 \leq ch$ $\ \nabla w - \nabla w_h\ _0 \leq ch$
MITC9	$\beta_h \in Q_2 \times Q_2$ $w_h \in Q_2 \cap P_3$	$\ \beta - \beta_h\ _1 \leq ch^2$ $\ \nabla w - \nabla w_h\ _0 \leq ch^2$
MITC16	$\beta_h \in Q_3 \times Q_3$ $w_h \in Q_3 \cap P_4$	$\ \beta - \beta_h\ _1 \leq ch^3$ $\ \nabla w - \nabla w_h\ _0 \leq ch^3$
MITC7	$\beta_h \in (P_2 \oplus \{L_1L_2L_3\}) \times (P_2 \oplus \{L_1L_2L_3\})$ $w_h \in P_2$	$\ \beta - \beta_h\ _1 \leq ch^2$ $\ \nabla w - \nabla w_h\ _0 \leq ch^2$
MITC12	$\beta_h \in (P_3 \oplus \{L_1L_2L_3\}P_1) \times (P_3 \oplus \{L_1L_2L_3\}P_1)$ $w_h \in P_3$	$\ \beta - \beta_h\ _1 \leq ch^3$ $\ \nabla w - \nabla w_h\ _0 \leq ch^3$

[†] For notation used, see Section 4.3.

EXAMPLE 5.31: Show how to establish the strain interpolation matrices for the stiffness matrix of the MITC9 element shown in Fig. E5.31.

The geometry of the element is the same as for the four-node element considered in Fig. E5.29; hence the Jacobian matrix is the same.

Since the transverse displacements are determined by the eight-node interpolations, which are given in Fig. 5.4, we have

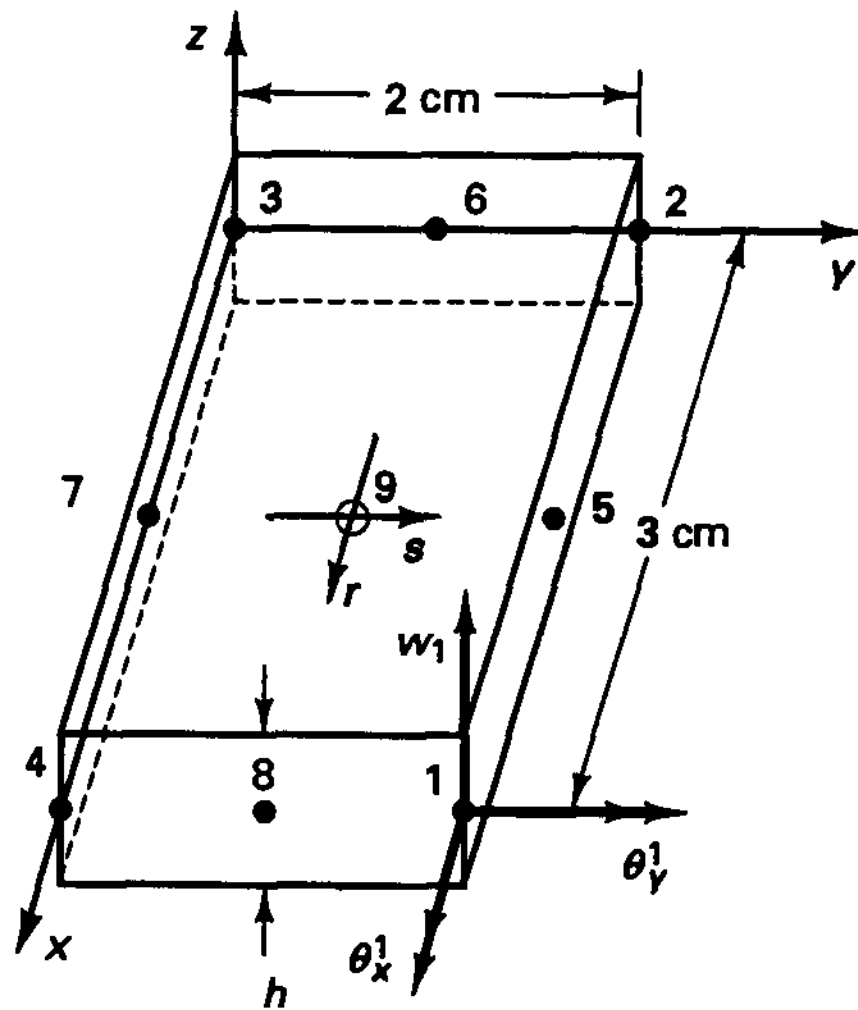


Figure E5.31 A nine-node plate bending element

$$\begin{bmatrix} \frac{\partial w}{\partial x} \\ \frac{\partial w}{\partial y} \end{bmatrix} = \frac{1}{4} \begin{bmatrix} \frac{2}{3} & 0 \\ 0 & 1 \end{bmatrix} \begin{bmatrix} (1+2r)(1+s) - (1-s^2) & | & \dots \\ (1+2s)(1+r) - (1-r^2) & | & \dots \end{bmatrix} \begin{bmatrix} w_1 \\ w_2 \\ \vdots \\ w_8 \end{bmatrix} \quad (a)$$

The section rotations are determined by the nine-node interpolation functions, which are also given in Fig. 5.4, and we have

$$\begin{bmatrix} \frac{\partial \beta_x}{\partial x} \\ \frac{\partial \beta_x}{\partial y} \end{bmatrix} = -\frac{1}{4} \begin{bmatrix} \frac{2}{3} & 0 \\ 0 & 1 \end{bmatrix} \begin{bmatrix} (1+2r)(1+s) - (1+2r)(1-s^2) & | & \dots \\ (1+2s)(1+r) - (1+2s)(1-r^2) & | & \dots \end{bmatrix} \begin{bmatrix} \theta_y^1 \\ \theta_y^2 \\ \vdots \\ \theta_y^8 \end{bmatrix} \quad (b)$$

$$\begin{bmatrix} \frac{\partial \beta_y}{\partial x} \\ \frac{\partial \beta_y}{\partial y} \end{bmatrix} = \frac{1}{4} \begin{bmatrix} \frac{2}{3} & 0 \\ 0 & 1 \end{bmatrix} \begin{bmatrix} (1+2r)(1+s) - (1+2r)(1-s^2) & | & \dots \\ (1+2s)(1+r) - (1+2s)(1-r^2) & | & \dots \end{bmatrix} \begin{bmatrix} \theta_x^1 \\ \theta_x^2 \\ \vdots \\ \theta_x^8 \end{bmatrix} \quad (c)$$

Let us use the following ordering of nodal point displacements and rotations

$$\hat{\mathbf{u}}^T = [w_1 \quad \theta_x^1 \quad \theta_y^1 \quad | \quad \dots \quad | \quad w_8 \quad \theta_x^8 \quad \theta_y^8 \quad | \quad \theta_x^9 \quad \theta_y^9]$$

The transverse displacement interpolation matrix \mathbf{H}_w is then given by

$$\mathbf{H}_w = [h_1 \quad 0 \quad 0 \quad | \quad h_2 \quad 0 \quad 0 \quad | \quad \dots \quad | \quad h_8 \quad 0 \quad 0 \quad | \quad 0 \quad 0]$$

where the h_1 to h_8 are given in Fig. 5.4 and correspond to an eight-node element.

The curvature interpolation matrix \mathbf{B}_κ is obtained directly from the relations (b) and (c),

$$\mathbf{B}_\kappa = \begin{bmatrix} 0 & & 0 \\ 0 & \frac{1}{4}[(1+2s)(1+r) - (1+2s)(1-r^2)] & \\ 0 & \frac{1}{6}[(1+2r)(1+s) - (1+2r)(1-s^2)] & \\ & & -\frac{1}{6}[(1+2r)(1+s) - (1+2r)(1-s^2)] & | & \dots \\ & & 0 & | & \dots \\ & & -\frac{1}{4}[(1+2s)(1+r) - (1+2s)(1-r^2)] & | & \dots \end{bmatrix}$$

The transverse shear strain interpolation matrix is obtained from the shear interpolation given in Fig. 5.27 and the tying procedure indicated in the same figure. Hence,

$$\mathbf{B}_\gamma = \begin{bmatrix} 1 & r & s & rs & s^2 & | & 0 & 0 & 0 & 0 & 0 \\ 0 & 0 & 0 & 0 & 0 & | & 1 & r & s & rs & r^2 \end{bmatrix} \boldsymbol{\alpha} \tag{e}$$

where $\boldsymbol{\alpha}^T = [a_1 \quad b_1 \quad c_1 \quad d_1 \quad e_1 \quad | \quad a_2 \quad b_2 \quad c_2 \quad d_2 \quad e_2]$

The values in the vector $\boldsymbol{\alpha}$ are expressed in terms of the nodal point displacements and rotations using the tying relations. For example, since point A is at $x = \frac{3}{2}[1 + 1/\sqrt{3}]$, $y = 2$, we have

$$\begin{aligned} \gamma_{xz}|_A &= a_1 + b_1\left(\frac{3}{2}\right)\left(1 + \frac{1}{\sqrt{3}}\right) + c_1(2) + d_2(3)\left(1 + \frac{1}{\sqrt{3}}\right) + e_1(4) \\ &= \left(\frac{\partial w}{\partial x} - \beta_x\right)\Big|_{\text{at } r=1/\sqrt{3}, s=1} \end{aligned} \tag{f}$$

Of course, $\partial w/\partial x$ is given by (a) and the section rotation β_x is given by (5.99) with the h_i corresponding to nine nodes.

Using all 10 tying relations in Fig. 5.27 as in (f), we can solve for the entries in (e) in terms of the nodal point displacements and rotations.

The numerical performance of the MITC n elements has been published by K. J. Bathe, M. L. Bucelem, and F. Brezzi [A]. However, let us briefly note that

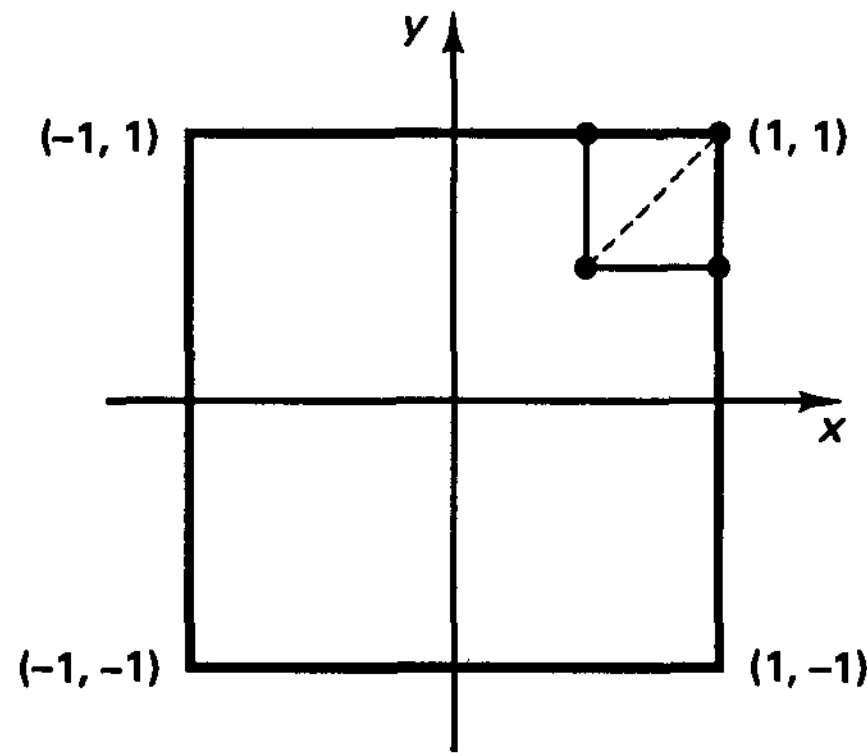
The element matrices are all evaluated using full numerical Gauss integration (see Fig. 5.27).

The elements do not contain any spurious zero energy modes.

The elements pass the pure bending patch test (see Fig. 4.18).

To illustrate the performance of the elements and introduce a valuable test problem consider Figs. 5.28 to 5.32. In Fig. 5.28 the test problem is stated. We note that the transverse displacement and the section rotations are prescribed along the complete boundary of the square plate and that in this problem there are no boundary layers (as encountered in practical analyses; see B. Häggblad and K. J. Bathe [A]). Therefore, the numerically calculated orders of convergence should be close to the analytically predicted values. Figure 5.29 shows results obtained using uniform meshes, and these results compare well with the analytically predicted behavior (these predictions assume uniform meshes). Figures 5.30 and 5.31 show results obtained using a sequence of quasi-uniform⁶ meshes, and we observe that the orders of convergence are not drastically affected by the element distortions. Finally, the convergence of the transverse shear strains, as predicted numerically, is shown in Fig. 5.32. In these specific finite element solutions the shear strains are predicted with surprisingly high orders of convergence (which in general of course cannot be expected).

⁶For the definition of a sequence of quasi-uniform meshes, see Section 5.3.3.



- (a) Square plate considered in ad hoc plate bending problem; transverse loading $p = 0$, nonzero boundary conditions. A typical 4-node element is shown. The dashed line indicates the subdivision used for the triangular element meshes; $h = 2/N$, where $N =$ number of elements per side.
- (b) Exact transverse displacement and rotations: $w = \sin kx e^{ky} + \sin k e^{-k}$; $\theta_x = k \sin kx e^{ky}$; $\theta_y = -k \cos kx e^{ky}$
- (c) Test problem: Prescribe the functional values of w , θ_x , and θ_y on the complete boundary and $p = 0$, calculate interior values; k is a chosen constant; we use $k = 5$

Figure 5.28 Ad-hoc test problem for plate bending elements

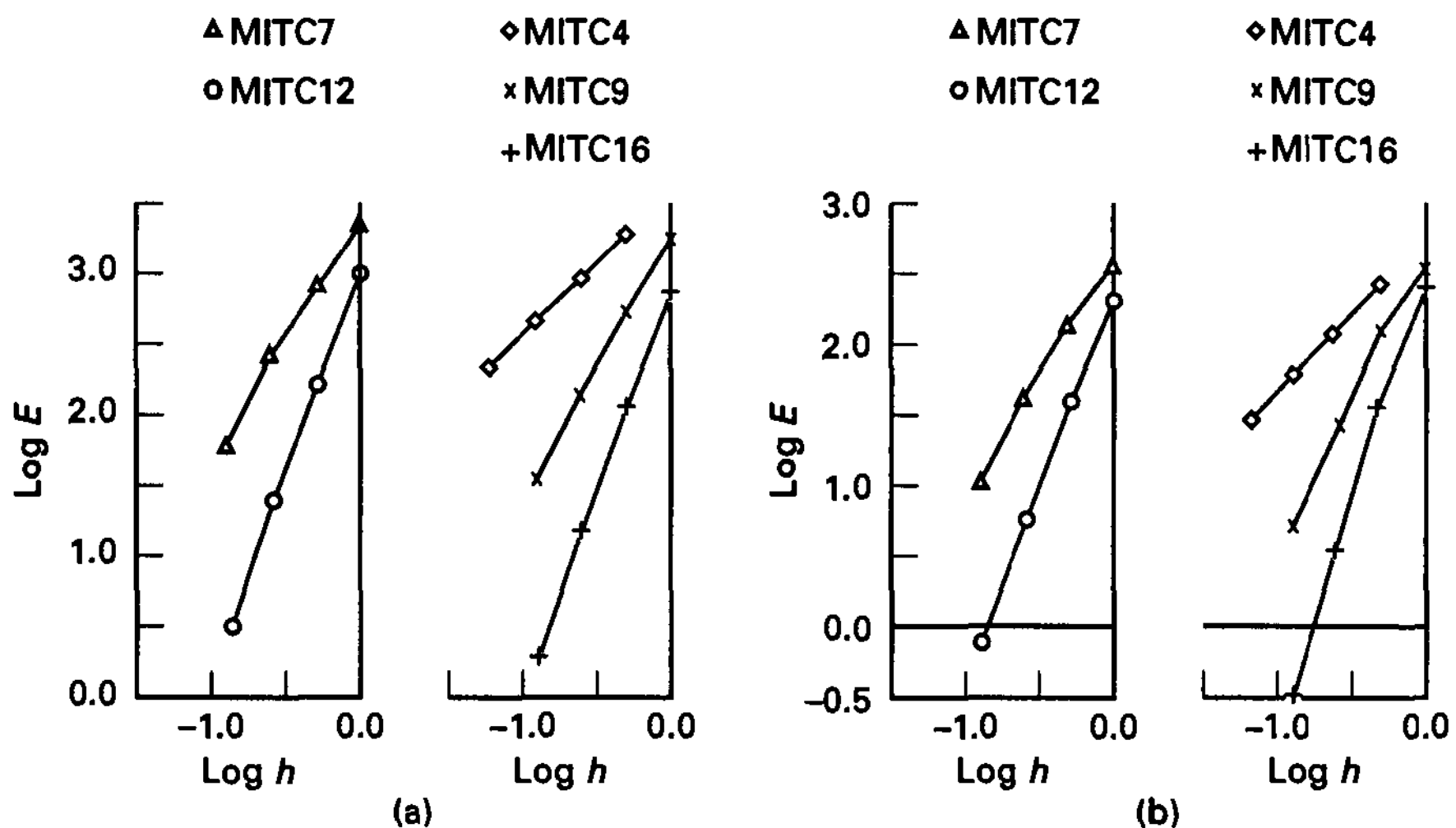


Figure 5.29 (s) Convergence of section rotations in analysis of ad-hoc problem using uniform meshes. The error measure is $E = \|\beta - \beta_h\|_1$. (b) Convergence of gradient of vertical displacement in analysis of ad-hoc problem using uniform meshes. The error measure is $E = \|\nabla w - \nabla w_h\|_0$.

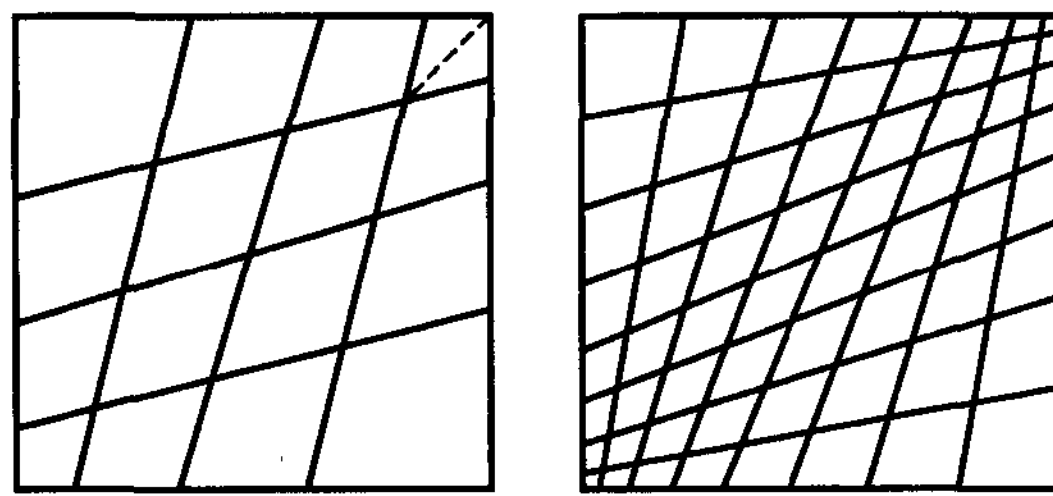


Figure 5.30 Two typical distorted meshes used in analysis of ad-hoc problem.-----, indicates the subdivision used for the triangular element meshes.

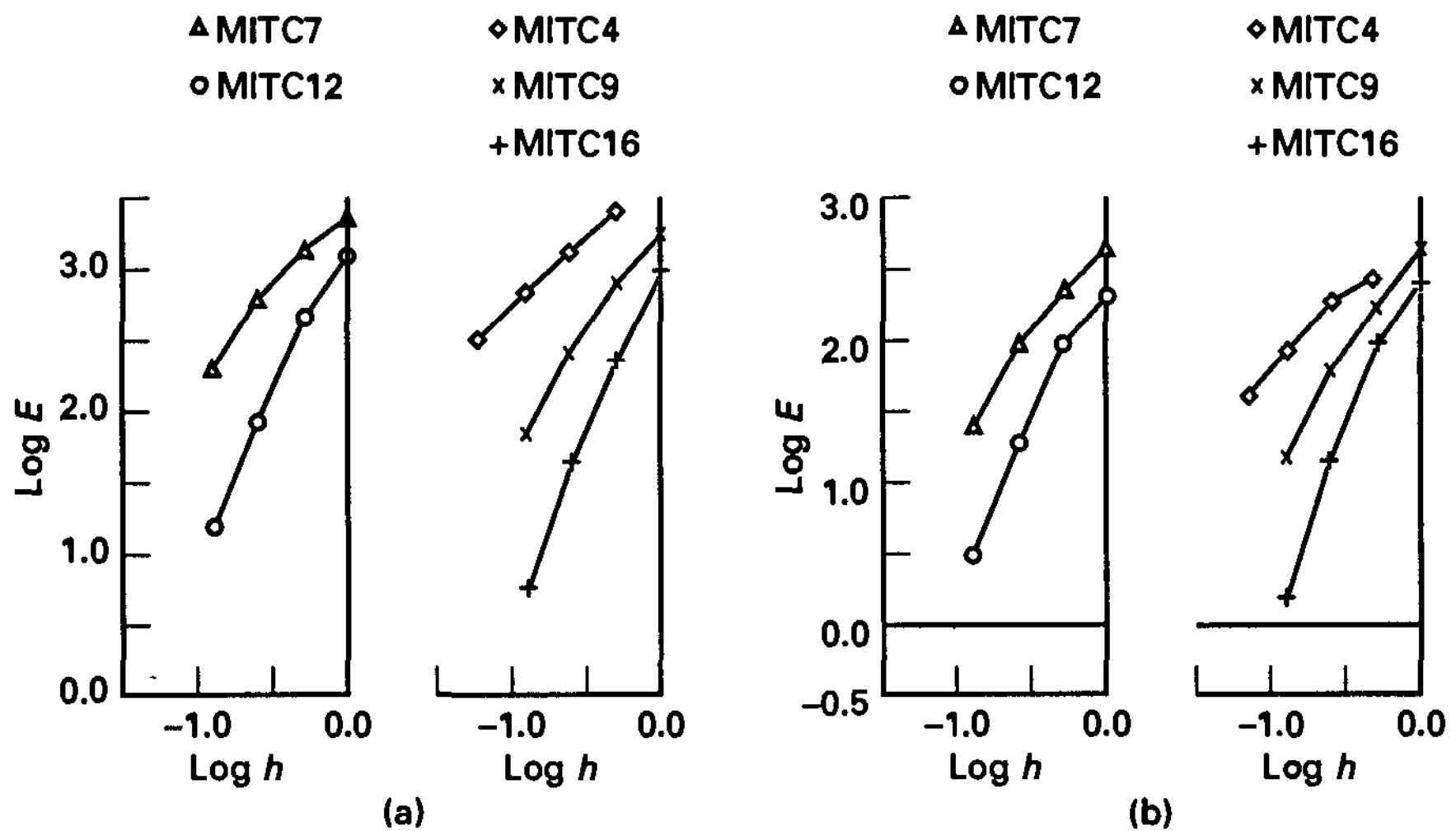


Figure 5.31 (a) Convergence of section rotations in analysis of ad-hoc problem using distorted meshes. The error measure is $E = \|\boldsymbol{\beta} - \boldsymbol{\beta}_h\|_1$. (b) Convergence of gradient of vertical displacement in analysis of ad-hoc problem using distorted meshes. The error measure is $E = \|\nabla w - \nabla w_h\|_0$.

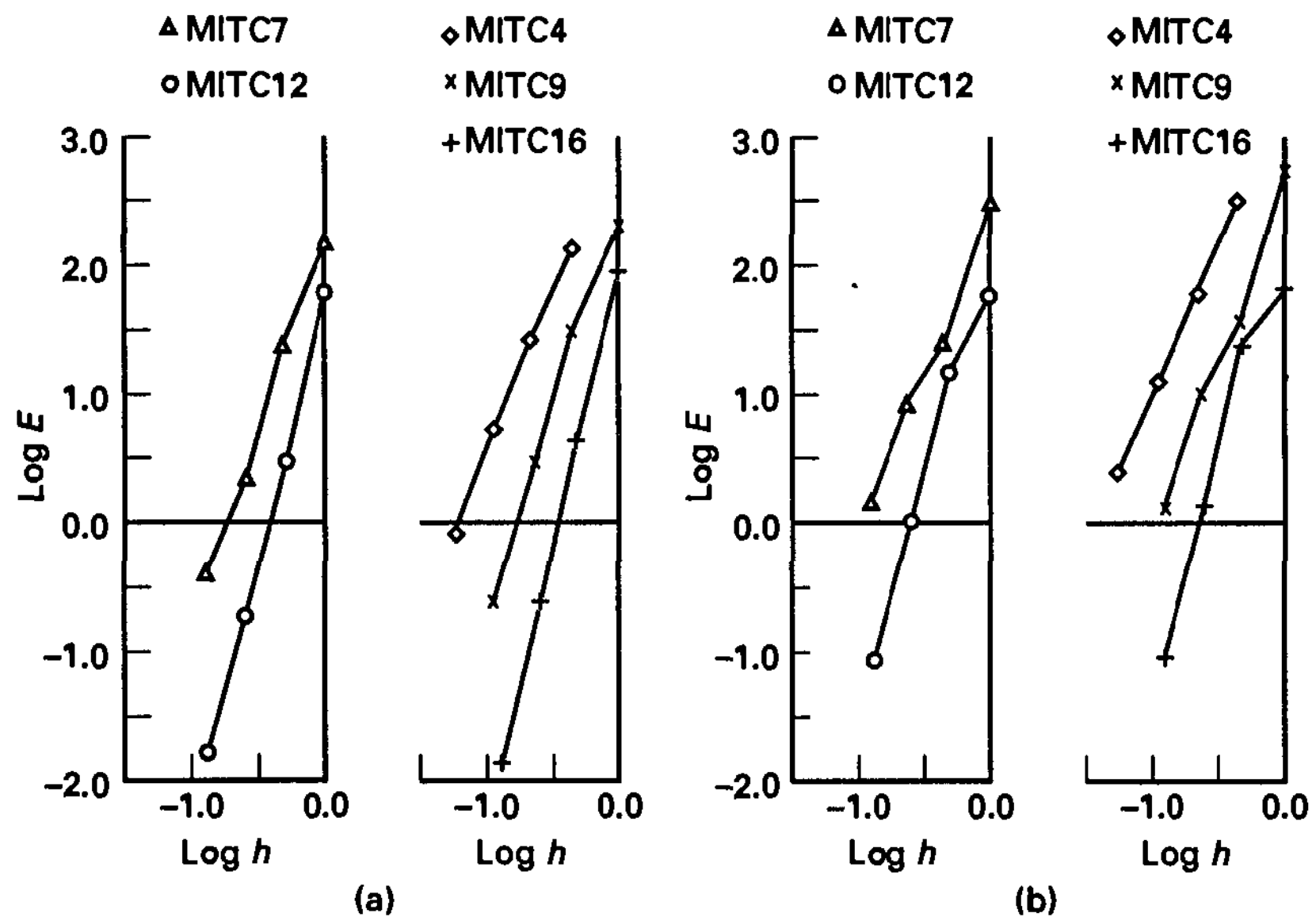


Figure 5.32 Convergence of transverse shear strains in analysis of ad-hoc problem. The error measure is $E = \|\boldsymbol{\gamma} - \boldsymbol{\gamma}_h\|_0$. (a) Uniform meshes. (b) Distorted meshes.

General Shell Elements

Let us consider next the formulation of general shell elements that can be used to analyze very complex shell geometries and stress distributions. For this objective we need to generalize the preceding plate element formulation approach, much in the same way as we generalized the isoparametric beam element formulation from straight two-dimensional to curved three-dimensional beams. As in the case of the formulation of beam elements (see Section 5.4.1), we consider the displacement interpolation which leads to a pure displacement-based element (see S. Ahmad, B. M. Irons, and O. C. Zienkiewicz [A]), and we then modify the formulation so as to not exhibit shear and membrane locking.

The displacement interpolation is obtained by considering the geometry interpolation. Consider a general shell element with a variable number of nodes, q . Figure 5.33 shows a nine-node element for which $q = 9$. Using the natural coordinates r, s , and t , the Cartesian coordinates of a point in the element with q nodal points are, before and after deformations,

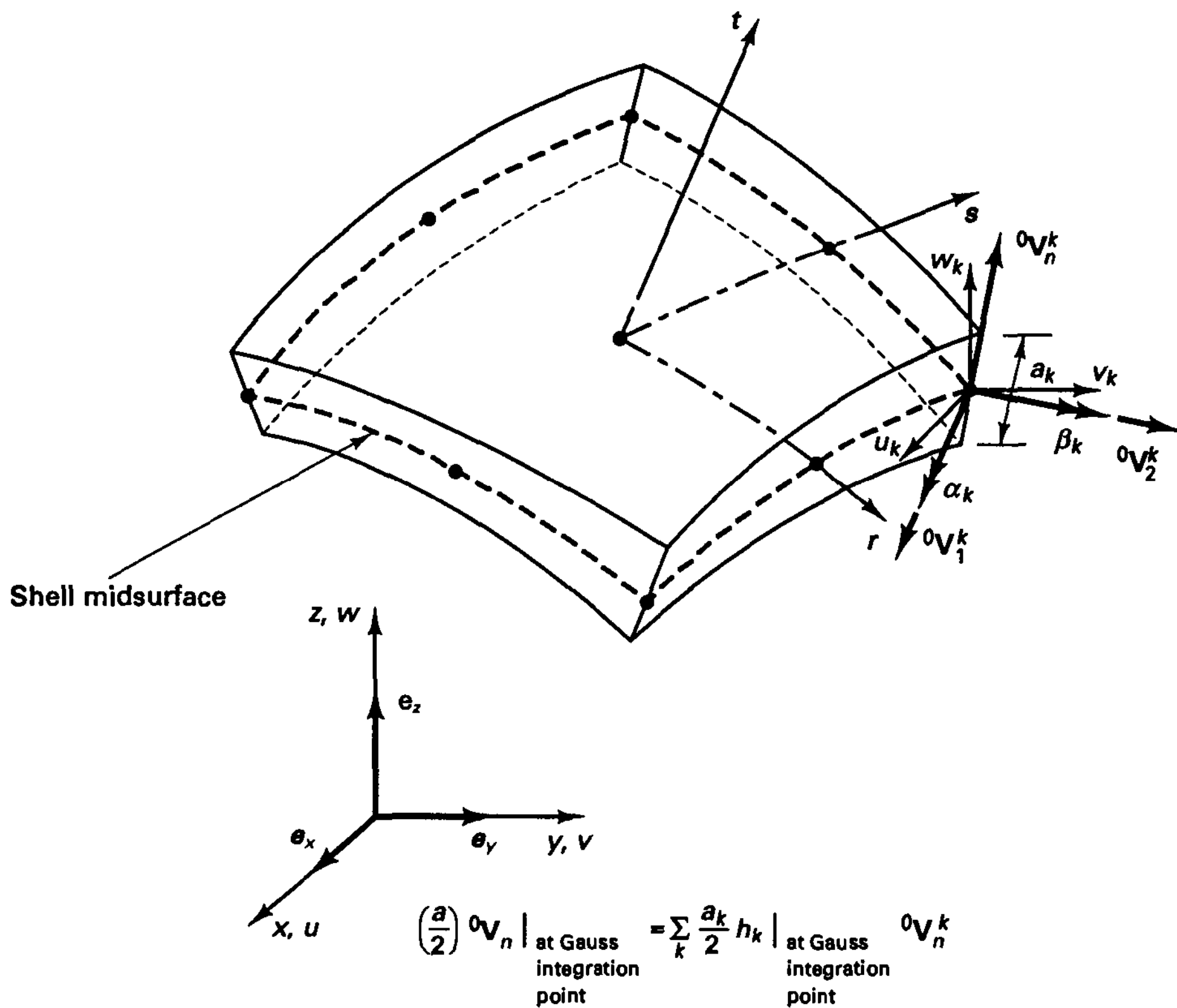


Figure 5.33 Nine-node shell element; also, definition of orthogonal $\bar{r}, \bar{s}, \bar{t}$ axes for constitutive relations

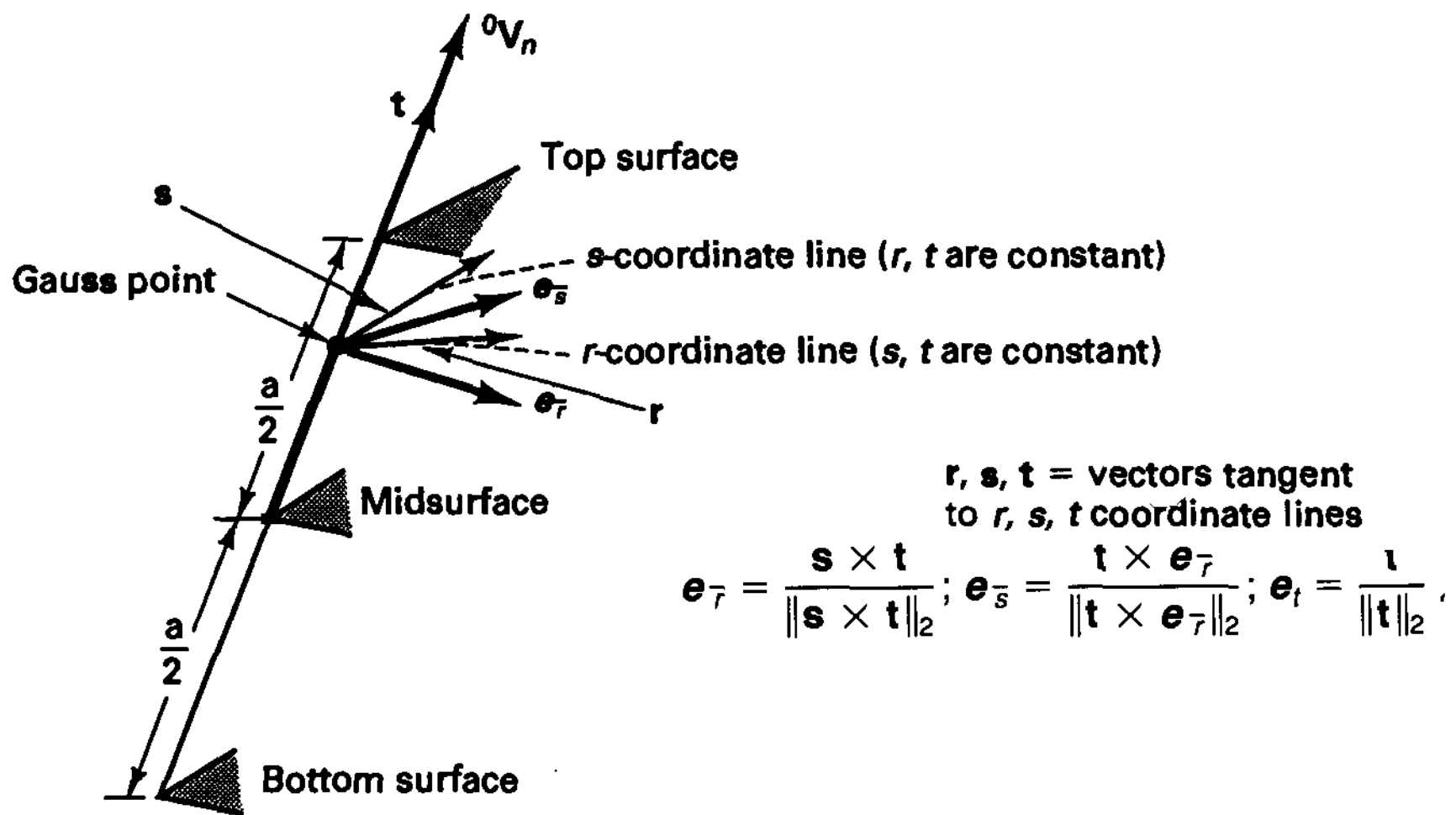


Figure 5.33 (continued)

$$\begin{aligned}
 {}^\ell x(r, s, t) &= \sum_{k=1}^q h_k {}^\ell x_k + \frac{t}{2} \sum_{k=1}^q a_k h_k {}^\ell V_{nx}^k \\
 {}^\ell y(r, s, t) &= \sum_{k=1}^q h_k {}^\ell y_k + \frac{t}{2} \sum_{k=1}^q a_k h_k {}^\ell V_{ny}^k \\
 {}^\ell z(r, s, t) &= \sum_{k=1}^q h_k {}^\ell z_k + \frac{t}{2} \sum_{k=1}^q a_k h_k {}^\ell V_{nz}^k
 \end{aligned} \tag{5.107}$$

where the $h_k(r, s)$ are the interpolation functions summarized in Fig. 5.4 and

${}^\ell x, {}^\ell y, {}^\ell z =$ Cartesian coordinates of any point in the element

${}^\ell x_k, {}^\ell y_k, {}^\ell z_k =$ Cartesian coordinates of nodal point k

$a_k =$ thickness of shell in t direction at nodal point k

${}^\ell V_{nx}^k, {}^\ell V_{ny}^k, {}^\ell V_{nz}^k =$ components of unit vector ${}^\ell V_n^k$ “normal” to the shell midsurface in direction t at nodal point k ; we call ${}^\ell V_n^k$ the normal vector⁷ or, more appropriately, the director vector, at nodal point k

and the left superscript ℓ denotes, as in the general beam formulation, the configuration of the element; i.e., $\ell = 0$ and 1 denote the original and final configurations of the shell element. Hence, using (5.107), the displacement components are

$$\begin{aligned}
 u(r, s, t) &= \sum_{k=1}^q h_k u_k + \frac{t}{2} \sum_{k=1}^q a_k h_k V_{nx}^k \\
 v(r, s, t) &= \sum_{k=1}^q h_k v_k + \frac{t}{2} \sum_{k=1}^q a_k h_k V_{ny}^k \\
 w(r, s, t) &= \sum_{k=1}^q h_k w_k + \frac{t}{2} \sum_{k=1}^q a_k h_k V_{nz}^k
 \end{aligned} \tag{5.108}$$

⁷ We call ${}^\ell V_n^k$ the normal vector although it may not be exactly normal to the midsurface of the shell in the original configuration (see Example 5.32), and in the final configuration (e.g., because of shear deformations).

where \mathbf{V}_n^k stores the increments in the direction cosines of ${}^0\mathbf{V}_n^k$,

$$\mathbf{V}_n^k = {}^1\mathbf{V}_n^k - {}^0\mathbf{V}_n^k \quad (5.109)$$

The components of \mathbf{V}_n^k can be expressed in terms of rotations at the nodal point k ; however, there is no unique way of proceeding. An efficient way is to define two unit vectors ${}^0\mathbf{V}_1^k$ and ${}^0\mathbf{V}_2^k$ that are orthogonal to ${}^0\mathbf{V}_n^k$:

$${}^0\mathbf{V}_1^k = \frac{\mathbf{e}_y \times {}^0\mathbf{V}_n^k}{\|\mathbf{e}_y \times {}^0\mathbf{V}_n^k\|_2} \quad (5.110a)$$

where \mathbf{e}_y is a unit vector in the direction of the y -axis. (For the special case ${}^0\mathbf{V}_n^k$ parallel to \mathbf{e}_y , we may simply use ${}^0\mathbf{V}_1^k$ equal to \mathbf{e}_z .) We can now obtain ${}^0\mathbf{V}_2^k$,

$${}^0\mathbf{V}_2^k = {}^0\mathbf{V}_n^k \times {}^0\mathbf{V}_1^k \quad (5.110b)$$

Let α_k and β_k be the rotations of the director vector ${}^0\mathbf{V}_n^k$ about the vectors ${}^0\mathbf{V}_1^k$ and ${}^0\mathbf{V}_2^k$. We then have, because α_k and β_k are small angles,

$$\mathbf{V}_n^k = -{}^0\mathbf{V}_2^k \alpha_k + {}^0\mathbf{V}_1^k \beta_k \quad (5.111)$$

This relationship can readily be proven when ${}^0\mathbf{V}_1 = \mathbf{e}_x$, ${}^0\mathbf{V}_2 = \mathbf{e}_y$ and ${}^0\mathbf{V}_n = \mathbf{e}_z$, but since these vectors are tensors, the relationship must also hold in general (see Section 2.4). Substituting from (5.111) into (5.108), we thus obtain

$$\begin{aligned} u(r, s, t) &= \sum_{k=1}^q h_k u_k + \frac{t}{2} \sum_{k=1}^q a_k h_k (-{}^0V_{2x}^k \alpha_k + {}^0V_{1x}^k \beta_k) \\ v(r, s, t) &= \sum_{k=1}^q h_k v_k + \frac{t}{2} \sum_{k=1}^q a_k h_k (-{}^0V_{2y}^k \alpha_k + {}^0V_{1y}^k \beta_k) \\ w(r, s, t) &= \sum_{k=1}^q h_k w_k + \frac{t}{2} \sum_{k=1}^q a_k h_k (-{}^0V_{2z}^k \alpha_k + {}^0V_{1z}^k \beta_k) \end{aligned} \quad (5.112)$$

With the element displacements and coordinates defined in (5.112) and (5.107) we can now proceed as usual to evaluate the element matrices of a pure displacement-based element. The entries in the displacement interpolation matrix \mathbf{H} of the shell element are given in (5.112), and the entries in the strain-displacement interpolation matrix can be calculated using the procedures already described in the formulation of the beam element (see Section 5.4.1).

To evaluate the strain-displacement matrix, we obtain from (5.112),

$$\begin{bmatrix} \frac{\partial u}{\partial r} \\ \frac{\partial u}{\partial s} \\ \frac{\partial u}{\partial t} \end{bmatrix} = \sum_{k=1}^q \begin{bmatrix} \frac{\partial h_k}{\partial r} [1 & tg_{1x}^k & tg_{2x}^k] \\ \frac{\partial h_k}{\partial s} [1 & tg_{1x}^k & tg_{2x}^k] \\ h_k [0 & g_{1x}^k & g_{2x}^k] \end{bmatrix} \begin{bmatrix} u_k \\ \alpha_k \\ \beta_k \end{bmatrix} \quad (5.113)$$

and the derivatives of v and w are given by simply substituting for u and x the variables v , y and w , z , respectively. In (5.113) we use the notation

$$\mathbf{g}_1^k = -\frac{1}{2}a_k {}^0\mathbf{V}_2^k; \quad \mathbf{g}_2^k = \frac{1}{2}a_k {}^0\mathbf{V}_1^k \quad (5.114)$$

To obtain the displacement derivatives corresponding to the Cartesian coordinates x, y, z , we use the standard transformation

$$\frac{\partial}{\partial \mathbf{x}} = \mathbf{J}^{-1} \frac{\partial}{\partial \mathbf{r}} \tag{5.115}$$

where the Jacobian matrix \mathbf{J} contains the derivatives of the coordinates x, y, z with respect to the natural coordinates r, s, t . Substituting from (5.113) into (5.115), we obtain

$$\begin{bmatrix} \frac{\partial u}{\partial x} \\ \frac{\partial u}{\partial y} \\ \frac{\partial u}{\partial z} \end{bmatrix} = \sum_{k=1}^q \begin{bmatrix} \frac{\partial h_k}{\partial x} & g_{1x}^k G_x^k & g_{2x}^k G_x^k \\ \frac{\partial h_k}{\partial y} & g_{1y}^k G_y^k & g_{2y}^k G_y^k \\ \frac{\partial h_k}{\partial z} & g_{1z}^k G_z^k & g_{2z}^k G_z^k \end{bmatrix} \begin{bmatrix} u_k \\ \alpha_k \\ \beta_k \end{bmatrix} \tag{5.116}$$

and the derivatives of v and w are obtained in an analogous manner. In (5.116) we have

$$\begin{aligned} \frac{\partial h_k}{\partial x} &= J_{11}^{-1} \frac{\partial h_k}{\partial r} + J_{12}^{-1} \frac{\partial h_k}{\partial s} \\ G_x^k &= t \left(J_{11}^{-1} \frac{\partial h_k}{\partial r} + J_{12}^{-1} \frac{\partial h_k}{\partial s} \right) + J_{13}^{-1} h_k \end{aligned} \tag{5.117}$$

where J_{ij}^{-1} is element (i, j) of \mathbf{J}^{-1} , and so on.

With the displacement derivatives defined in (5.116) we now directly assemble the strain-displacement matrix \mathbf{B} of a shell element. Assuming that the rows in this matrix correspond to all six global Cartesian strain components, $\epsilon_{xx}, \epsilon_{yy}, \dots, \gamma_{zx}$, the entries in \mathbf{B} are constructed in the usual way (see Section 5.3), but then the stress-strain law must contain the shell assumption that the stress normal to the shell surface is zero. We impose that the stress in the direction of the vector is zero. Thus, if $\boldsymbol{\tau}$ and $\boldsymbol{\epsilon}$ store the Cartesian stress and strain components, we use

$$\boldsymbol{\tau} = \mathbf{C}_{sh} \boldsymbol{\epsilon} \tag{5.118}$$

where

$$\begin{aligned} \boldsymbol{\tau}^T &= [\tau_{xx} \quad \tau_{yy} \quad \tau_{zz} \quad \tau_{xy} \quad \tau_{yz} \quad \tau_{zx}] \\ \boldsymbol{\epsilon}^T &= [\epsilon_{xx} \quad \epsilon_{yy} \quad \epsilon_{zz} \quad \gamma_{xy} \quad \gamma_{yz} \quad \gamma_{zx}] \\ \mathbf{C}_{sh} &= \mathbf{Q}_{sh}^T \left(\frac{E}{1-\nu^2} \begin{bmatrix} 1 & \nu & 0 & 0 & 0 & 0 \\ & 1 & 0 & 0 & 0 & 0 \\ & & 0 & 0 & 0 & 0 \\ & & & \frac{1-\nu}{2} & 0 & 0 \\ \text{Symmetric} & & & & k \frac{1-\nu}{2} & 0 \\ & & & & & k \frac{1-\nu}{2} \end{bmatrix} \right) \mathbf{Q}_{sh} \end{aligned} \tag{5.119}$$

and \mathbf{Q}_{sh} represents a matrix that transforms the stress-strain law from an \bar{r}, \bar{s}, t Cartesian shell-aligned coordinate system to the global Cartesian coordinate system. The elements of

the matrix \mathbf{Q}_{sh} are obtained from the direction cosines of the \bar{r}, \bar{s}, t coordinate axes measured in the x, y, z coordinate directions,

$$\mathbf{Q}_{sh} = \begin{bmatrix} l_1^2 & m_1^2 & n_1^2 & l_1 m_1 & m_1 n_1 & n_1 l_1 \\ l_2^2 & m_2^2 & n_2^2 & l_2 m_2 & m_2 n_2 & n_2 l_2 \\ l_3^2 & m_3^2 & n_3^2 & l_3 m_3 & m_3 n_3 & n_3 l_3 \\ 2l_1 l_2 & 2m_1 m_2 & 2n_1 n_2 & l_1 m_2 + l_2 m_1 & m_1 n_2 + m_2 n_1 & n_1 l_2 + n_2 l_1 \\ 2l_2 l_3 & 2m_2 m_3 & 2n_2 n_3 & l_2 m_3 + l_3 m_2 & m_2 n_3 + m_3 n_2 & n_2 l_3 + n_3 l_2 \\ 2l_3 l_1 & 2m_3 m_1 & 2n_3 n_1 & l_3 m_1 + l_1 m_3 & m_3 n_1 + m_1 n_3 & n_3 l_1 + n_1 l_3 \end{bmatrix} \quad (5.120)$$

where

$$\begin{aligned} l_1 &= \cos(\mathbf{e}_x, \mathbf{e}_{\bar{r}}); & m_1 &= \cos(\mathbf{e}_y, \mathbf{e}_{\bar{r}}); & n_1 &= \cos(\mathbf{e}_z, \mathbf{e}_{\bar{r}}) \\ l_2 &= \cos(\mathbf{e}_x, \mathbf{e}_{\bar{s}}); & m_2 &= \cos(\mathbf{e}_y, \mathbf{e}_{\bar{s}}); & n_2 &= \cos(\mathbf{e}_z, \mathbf{e}_{\bar{s}}) \\ l_3 &= \cos(\mathbf{e}_x, \mathbf{e}_t); & m_3 &= \cos(\mathbf{e}_y, \mathbf{e}_t); & n_3 &= \cos(\mathbf{e}_z, \mathbf{e}_t) \end{aligned} \quad (5.121)$$

and the relation in (5.119) corresponds to a fourth-order tensor transformation as described in Section 2.4.

It follows that in the analysis of a general shell the matrix \mathbf{Q}_{sh} may have to be evaluated anew at each integration point that is employed in the numerical integration of the stiffness matrix (see Section 5.5). However, when special shells are considered and, in particular, when a plate is analyzed, the transformation matrix and the stress-strain matrix \mathbf{C}_{sh} need only be evaluated at specific points and can then be employed repetitively. For example, in the analysis of an assemblage of flat plates, the stress-strain matrix \mathbf{C}_{sh} needs to be calculated only once for each flat structural part.

In the above formulation the strain-displacement matrix is formulated corresponding to the Cartesian strain components, which can be directly established using the derivatives in (5.116). Alternatively, we could calculate the strain components corresponding to coordinate axes aligned with the shell element midsurface and establish a strain-displacement matrix for these strain components, as we did in the formulation of the general beam element in Section 5.4.1. The relative computational efficiency of these two approaches depends on whether it is more effective to transform the strain components (which always differ at the integration points) or to transform the stress-strain law.

It is instructive to compare this shell element formulation with a formulation in which flat elements with a superimposed plate bending and membrane stress behavior are employed (see Section 4.2.3). To identify the differences, assume that the general shell element is used as a flat element in the modeling of a shell; then the stiffness matrix of this element could also be obtained by superimposing the plate bending stiffness matrix derived in (5.94) to (5.99) (see Example 5.29) and the plane stress stiffness matrix discussed in Section 5.3.1. Thus, in this case, the general shell element reduces to a plate bending element *plus* a plane stress element, but a computational difference lies in the fact that these element matrices are calculated by integrating numerically only in the r - s element midplanes, whereas in the shell element stiffness calculation numerical integration is also performed in the t -direction (unless the general formulation is modified for this special case).

We illustrate some of the above relations in the following example.

EXAMPLE 5.32: Consider the four-node shell element shown in Fig. E5.32.

- (a) Develop the entries in the displacement interpolation matrix.
- (b) Calculate the thickness at the midpoint of the element and give the direction in which this thickness is measured.

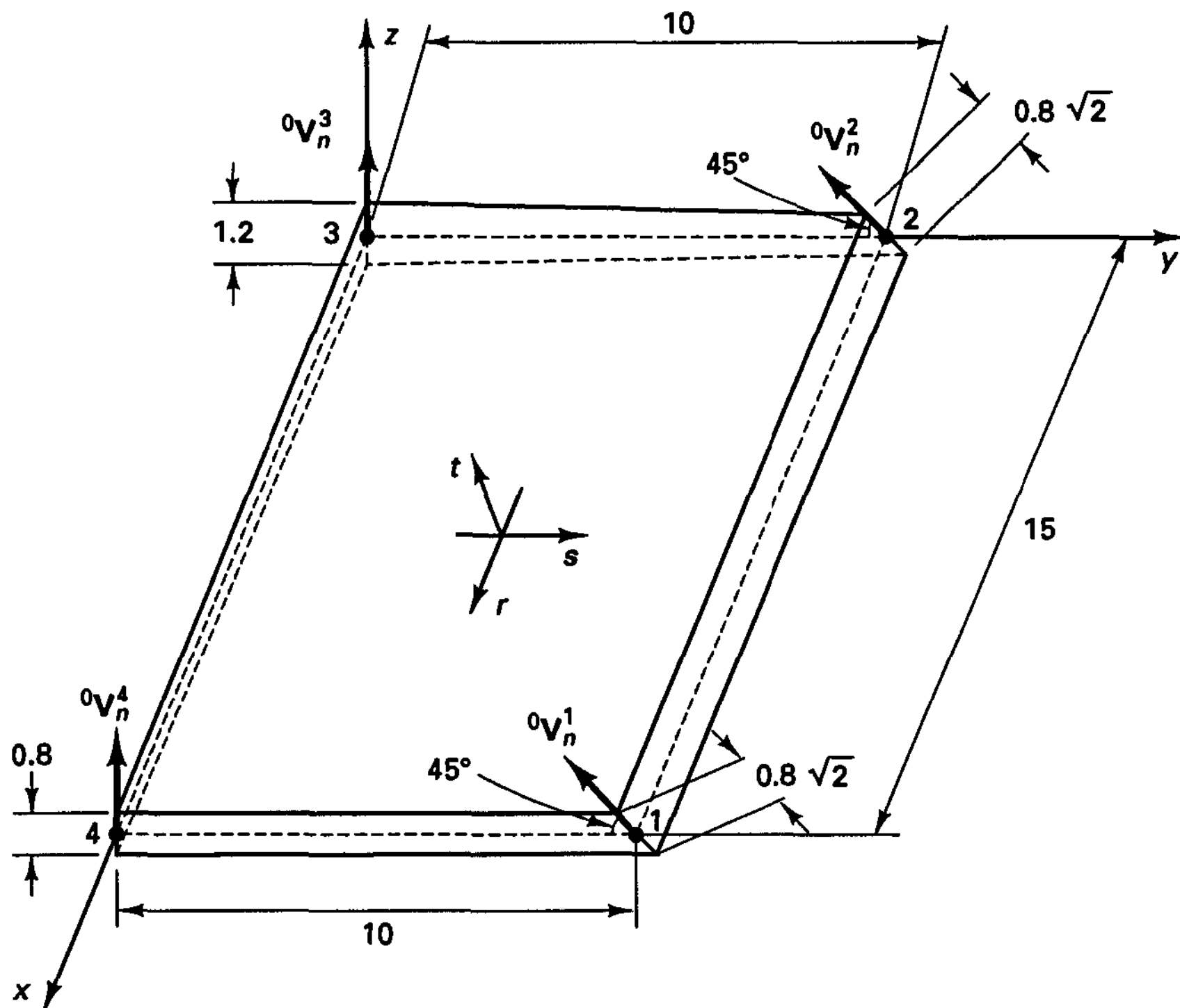


Figure E5.32 Four-node shell element

The shell element considered has varying thickness but in some respects can be compared with the plate element in Example 5.29.

The displacement interpolation matrix \mathbf{H} is given by the relations in (5.112). The functions h_k are those of a four-node two-dimensional element (see Fig. 5.4 and Example 5.29). The director vectors ${}^0\mathbf{V}_n^k$ are given by the geometry of the element:

$${}^0\mathbf{V}_n^1 = \begin{bmatrix} 0 \\ -1/\sqrt{2} \\ 1/\sqrt{2} \end{bmatrix}; \quad {}^0\mathbf{V}_n^2 = \begin{bmatrix} 0 \\ -1/\sqrt{2} \\ 1/\sqrt{2} \end{bmatrix}; \quad {}^0\mathbf{V}_n^3 = \begin{bmatrix} 0 \\ 0 \\ 1 \end{bmatrix}; \quad {}^0\mathbf{V}_n^4 = \begin{bmatrix} 0 \\ 0 \\ 1 \end{bmatrix}$$

Hence,

$${}^0\mathbf{V}_1^1 = {}^0\mathbf{V}_1^2 = {}^0\mathbf{V}_1^3 = {}^0\mathbf{V}_1^4 = \begin{bmatrix} 1 \\ 0 \\ 0 \end{bmatrix}$$

$${}^0\mathbf{V}_2^1 = {}^0\mathbf{V}_2^2 = \begin{bmatrix} 0 \\ 1/\sqrt{2} \\ 1/\sqrt{2} \end{bmatrix}; \quad {}^0\mathbf{V}_2^3 = {}^0\mathbf{V}_2^4 = \begin{bmatrix} 0 \\ 1 \\ 0 \end{bmatrix}$$

Also, $a_1 = a_2 = 0.8\sqrt{2}; \quad a_3 = 1.2; \quad a_4 = 0.8$

The above expressions give all entries in (5.112).

To evaluate the thickness at the element midpoint and the direction in which the thickness is measured, we use the relation

$$\left(\frac{a}{2}\right) {}^0\mathbf{V}_n \Big|_{\text{midpoint}} = \sum_{k=1}^4 \frac{a_k}{2} h_k \Big|_{r=s=0} {}^0\mathbf{V}_n^k$$

where a is the thickness and the director vector ${}^0\mathbf{V}_n$ gives the direction sought. This expression gives

$$\frac{a}{2} {}^0\mathbf{V}_n = \frac{0.8\sqrt{2}}{4} \begin{bmatrix} 0 \\ -1/\sqrt{2} \\ 1/\sqrt{2} \end{bmatrix} + \frac{1.2}{8} \begin{bmatrix} 0 \\ 0 \\ 1 \end{bmatrix} + \frac{0.8}{8} \begin{bmatrix} 0 \\ 0 \\ 1 \end{bmatrix} = \begin{bmatrix} 0 \\ -0.2 \\ 0.45 \end{bmatrix}$$

which gives ${}^0\mathbf{V}_n = \begin{bmatrix} 0.0 \\ -0.406 \\ 0.914 \end{bmatrix}; \quad a = 0.985$

This shell element formulation clearly has an important attribute, namely, that any geometric shape of a shell can be directly represented. The generality is further increased if the formulation is extended to transition elements (similar to the extension for the isoparametric beam element discussed in Section 5.4.1). Figure 5.34 shows how shell transition

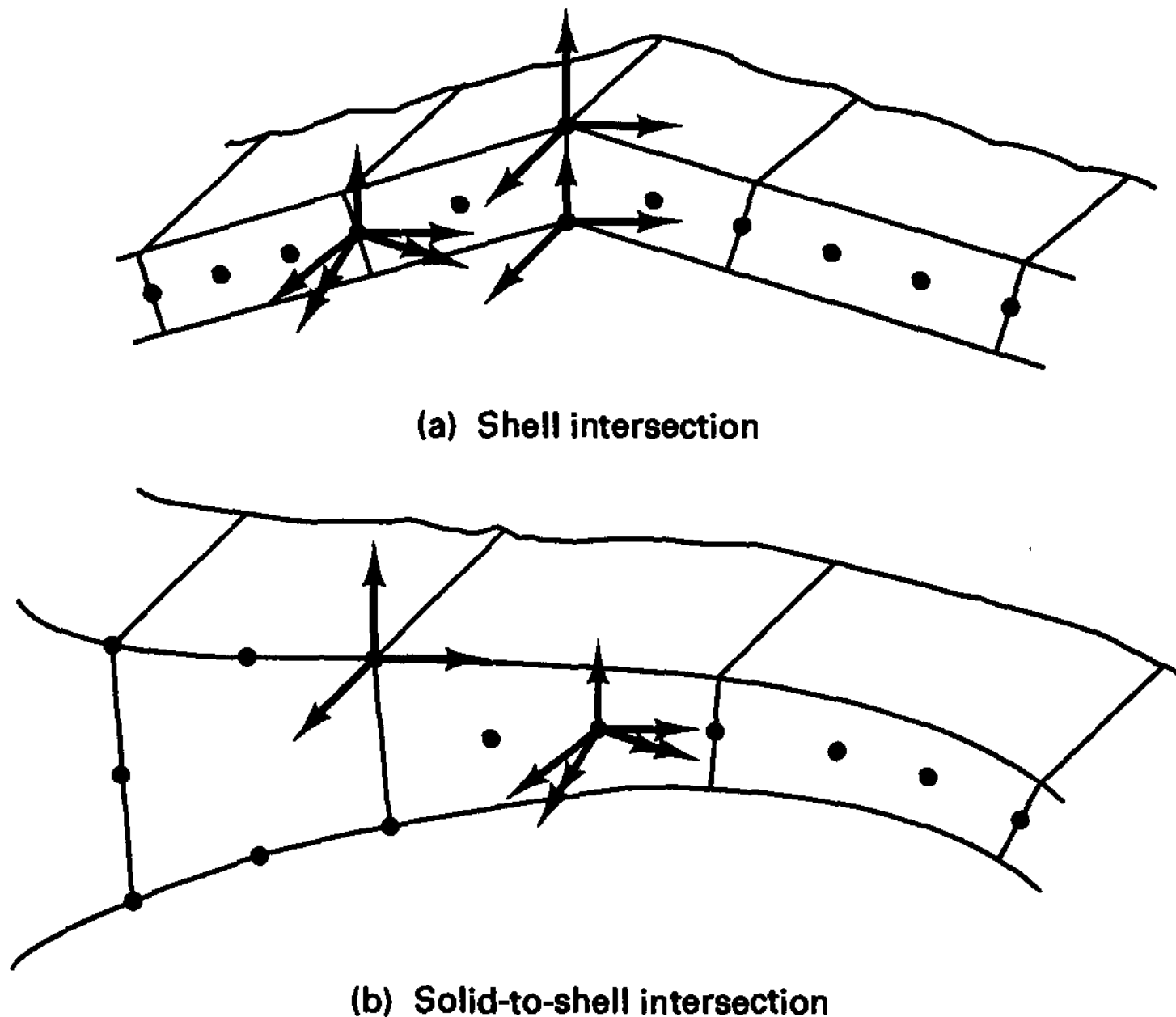


Figure 5.34 Use of shell transition elements

elements can be used to model shell intersections and shell-to-solid transitions using compatible element idealizations without the use of special constraint equations. The features of generality and accuracy in the modeling of a shell structure can be especially important in the material and geometric nonlinear analysis of shell structures, since particularly in such analyses shell geometries must be accounted for accurately. We discuss the extension of the formulation to general nonlinear analysis in Section 6.5.2.

The pure displacement-based formulation has, as in the case of displacement-based isoparametric beam elements, the disadvantage that the lower-order elements lock as a result of spurious shear strains, and when the elements are curved, also because of spurious membrane strains. Indeed, the least order of interpolation that should be used is a cubic interpolation of displacements (and geometry) leading to 16-node quadrilateral and 10-node triangular shell elements. But even these elements, when geometrically distorted, show some shear and membrane locking (for these reasons the MITC16 and MITC12 plate bending elements are presented in Fig. 5.27). To circumvent the locking behavior, a mixed interpolation is used, and the use of tensorial components as proposed by E. N. Dvorkin and K. J. Bathe [A] and K. J. Bathe and E. N. Dvorkin [B] is particularly attractive.

The first step in the mixed interpolation is to write the complete strain tensor at an integration point as

$$\epsilon = \underbrace{\tilde{\epsilon}_{rr} \mathbf{g}^r \mathbf{g}^r + \tilde{\epsilon}_{ss} \mathbf{g}^s \mathbf{g}^s + \tilde{\epsilon}_{rs} (\mathbf{g}^r \mathbf{g}^s + \mathbf{g}^s \mathbf{g}^r)}_{\text{in-layer strains}} + \underbrace{\tilde{\epsilon}_{rt} (\mathbf{g}^r \mathbf{g}^t + \mathbf{g}^t \mathbf{g}^r) + \tilde{\epsilon}_{st} (\mathbf{g}^s \mathbf{g}^t + \mathbf{g}^t \mathbf{g}^s)}_{\text{transverse shear strains}} \quad (5.122)$$

where the $\tilde{\epsilon}_{rr}, \tilde{\epsilon}_{ss}, \dots$, are the covariant strain components corresponding to the base vectors

$$\mathbf{g}_r = \frac{\partial \mathbf{x}}{\partial r}; \quad \mathbf{g}_s = \frac{\partial \mathbf{x}}{\partial s}; \quad \mathbf{g}_t = \frac{\partial \mathbf{x}}{\partial t} \quad (5.123)$$

$$\mathbf{x} = \begin{bmatrix} x \\ y \\ z \end{bmatrix}$$

and the $\mathbf{g}^r, \mathbf{g}^s, \mathbf{g}^t$ are the corresponding contravariant base vectors (see Section 2.4). We note that if we use indicial notation with $i = 1, 2, 3$ corresponding to $r, s,$ and $t,$ respectively, and $r_1 = r, r_2 = s, r_3 = t,$ we can define

$${}^0 \mathbf{g}_i = \frac{\partial \mathbf{x}}{\partial r_i}; \quad {}^1 \mathbf{g}_i = \frac{\partial (\mathbf{x} + \mathbf{u})}{\partial r_i} \quad (5.124)$$

and then the covariant Green-Lagrange strain tensor components are

$${}^1 \tilde{\epsilon}_{ij} = \frac{1}{2} ({}^1 \mathbf{g}_i \cdot {}^1 \mathbf{g}_j - {}^0 \mathbf{g}_i \cdot {}^0 \mathbf{g}_j) \quad (5.125)$$

The strain components in (5.118) are the linear Cartesian components of the strain tensor given by (5.125) (see Example 2.28).

In the mixed interpolation, the objective is to interpolate the in-layer and transverse shear strain components independently and tie these interpolations to the usual displacement interpolations. The result is that the stiffness matrix is then obtained corresponding to only the same nodal point variables (displacements and section rotations) as are used for the displacement-based elements. Of course, the key is to choose in-layer and transverse

shear strain component interpolations, for the displacement interpolations used, such that the resulting element has an optimal predictive capability.

An attractive four-node element is the MITC4 shell element proposed by E. N. Dvorkin and K. J. Bathe [A] for which the in-layer strains are computed from the displacement interpolations (since the element is not curved and membrane locking is not present in the displacement-based element) and the covariant transverse shear strain components are interpolated and tied to the displacement interpolations as discussed for the plate element [see (5.101)]. The element performs quite well in out-of-plane bending (the plate bending) action, and also in in-plane (the membrane) action if the incompatible modes as discussed in Example 4.28 are added to the basic four-node element displacement interpolations.

A significantly better predictive capability is obtained with higher-order elements, and Fig. 5.35 shows the interpolations and tying points used for the 9-node and 16-node elements proposed by M. L. Bucelem and K. J. Bathe [A]. These elements are referred to as MITC9 and MITC16 shell elements.

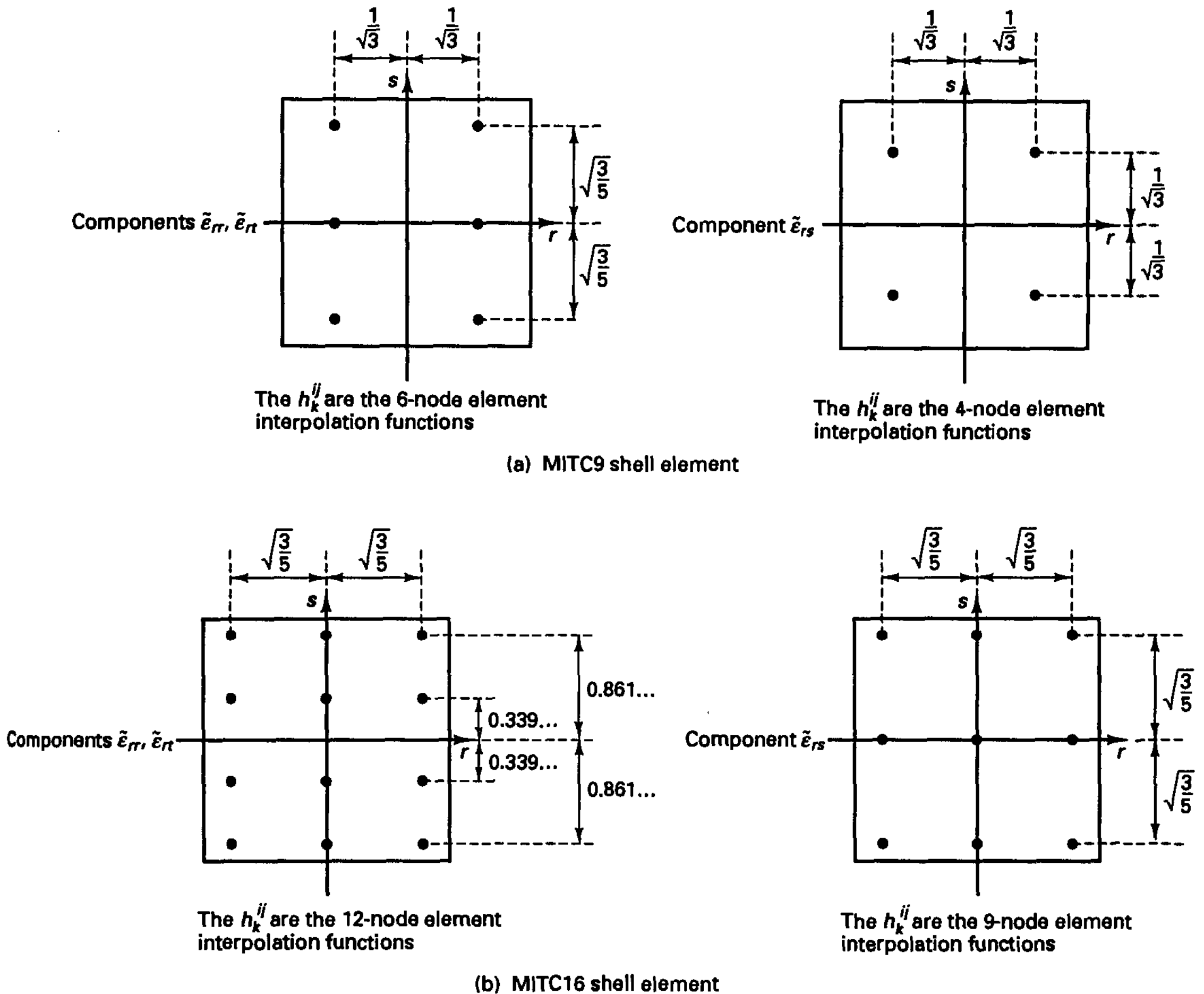


Figure 5.35 MITC shell elements; interpolations of strain components and tying points

Following our earlier discussion of the mixed interpolation of plate elements, in the formulation of these shell elements we use

$$\tilde{\epsilon}_{ij} = \sum_{k=1}^{n_{ij}} h_k^{\tilde{u}} \mathbf{B}_{ij}^{\text{DI}}|_k \hat{\mathbf{u}} \tag{5.126}$$

where n_{ij} denotes the number of tying points used for the strain component considered, $h_k^{\tilde{u}}$ is the interpolation function corresponding to the tying point k , and $\mathbf{B}_{ij}^{\text{DI}}|_k \hat{\mathbf{u}}$ is the strain component evaluated at the tying point k by the displacement assumption (by displacement interpolation). Note that with (5.126) only point tying and no integral tying (as in the higher-order MITC plate elements) is performed.

Unfortunately, a mathematical analysis of the MITC9 and MITC16 shell elements, as achieved for the plate elements summarized in Fig. 5.27, is not yet available, although some valuable insight has been gained by the work of J. Pitkäranta [A]. Hence, the formulation of the shell elements is so far based on the mathematical and physical insight available from the formulations and analyses of beam and plate elements, intuition to represent shell behavior accurately, and well-chosen numerical tests.

Of course, the MITC shell elements presented here do not contain any spurious zero energy modes. Also, the membrane and pure bending patch tests are passed by these elements. A further valuable test is the analysis of the problem in Fig. 5.36. This test tells whether an element locks (as a result of spurious membrane or shear stresses) and indicates how sensitive the element predictive capability is when the curved element is geometrically distorted in the model of a curved shell. Table 5.4 gives the analysis results of the problem in Fig. 5.36 and shows the good performance of the MITC9 and MITC16 elements.

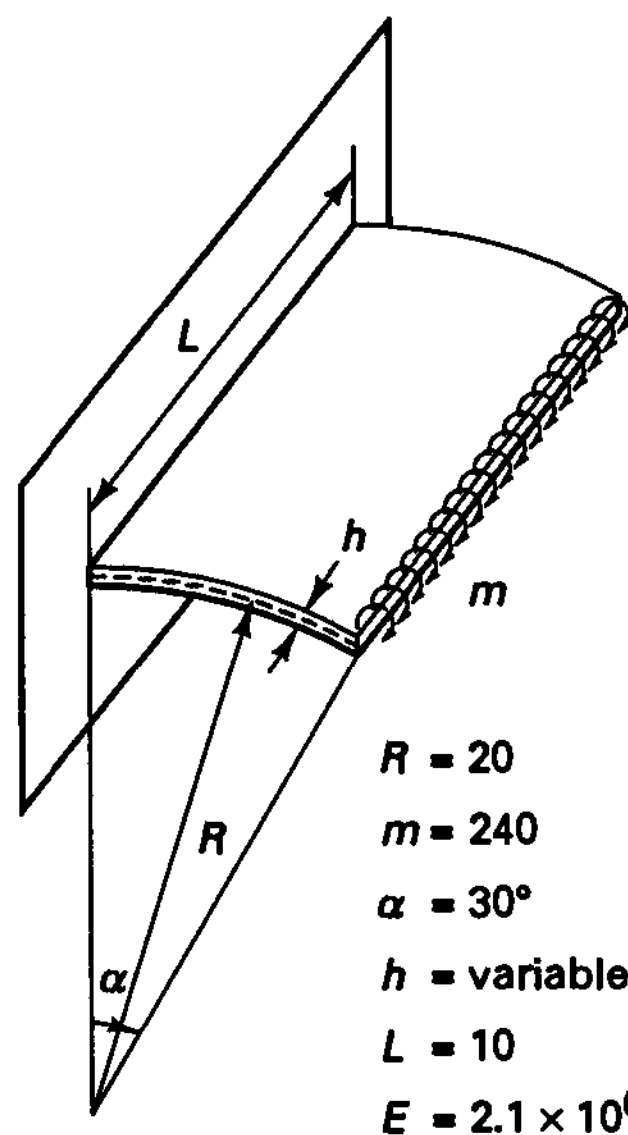
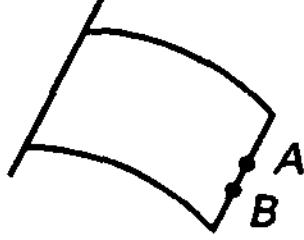
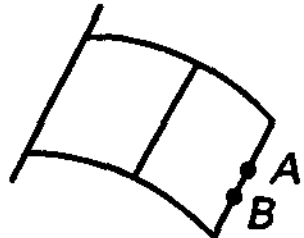
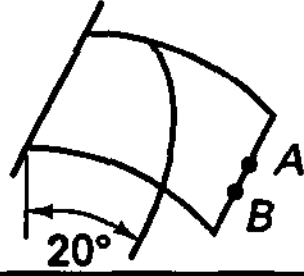
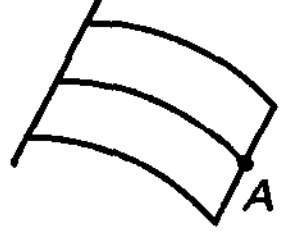
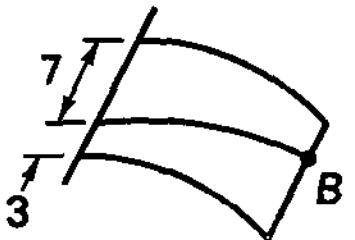


Figure 5.36 Curved cantilever problem to test curved shell elements

Additional numerical results using the MITC9 and MITC16 shell elements are given by M. L. Bucalem and K. J. Bathe [A]; similarly formulated elements have been presented by H. C. Huang and E. Hinton [A], K. C. Park and G. M. Stanley [A], and J. Jang and P. M. Pinsky [A].

TABLE 5.4 Performance of MITC9 and MITC16 shell elements in the analysis of the problem in Fig. 5.36

Mesh	h/R	θ_{FE}/θ_{AN}	
		MITC9 shell element (results at point A) [†]	MITC16 shell element (results at point B) [‡]
	1/100	0.9995	1.0001
	1/1000	0.9995	1.0001
	1/100000	0.9995	1.0001
	1/100	1.0000	1.0000
	1/1000	1.0000	1.0000
	1/100000	1.0000	0.9999
	1/100	0.9956	0.9975
	1/1000	0.9913	0.9796
	1/100000	0.9883	0.9318
	1/100	0.9995	1.0001
	1/1000	0.9995	1.0001
	1/100000	0.9995	1.0001
	1/100	0.9995	1.0000
	1/1000	0.9995	1.0001
	1/100000	0.9995	1.0001

[†] A is the middle of the edge.
[‡] B is the third point of the edge.

Boundary Conditions

The plate elements presented in this section are based on Reissner-Mindlin plate theory, in which the transverse displacement and section rotations are independent variables. This assumption is fundamentally different from the kinematic assumption used in Kirchhoff plate theory, in which the transverse displacement is the only independent variable. Hence, whereas in Kirchhoff plate theory all boundary conditions are written only in terms of the transverse displacement (and of course its derivatives), in the Reissner-Mindlin theory all boundary conditions are written in terms of the transverse displacement and the section rotations (and their derivatives). Since the section rotations are used as additional kinematic variables, the actual physical condition of a support can also be modeled more accurately.

As an example, consider the support conditions at the edge of the thin structure shown in Fig. 5.37. If this structure were modeled as a three-dimensional continuum, the element idealization might be as shown in Fig. 5.38(a), and then the boundary conditions would be

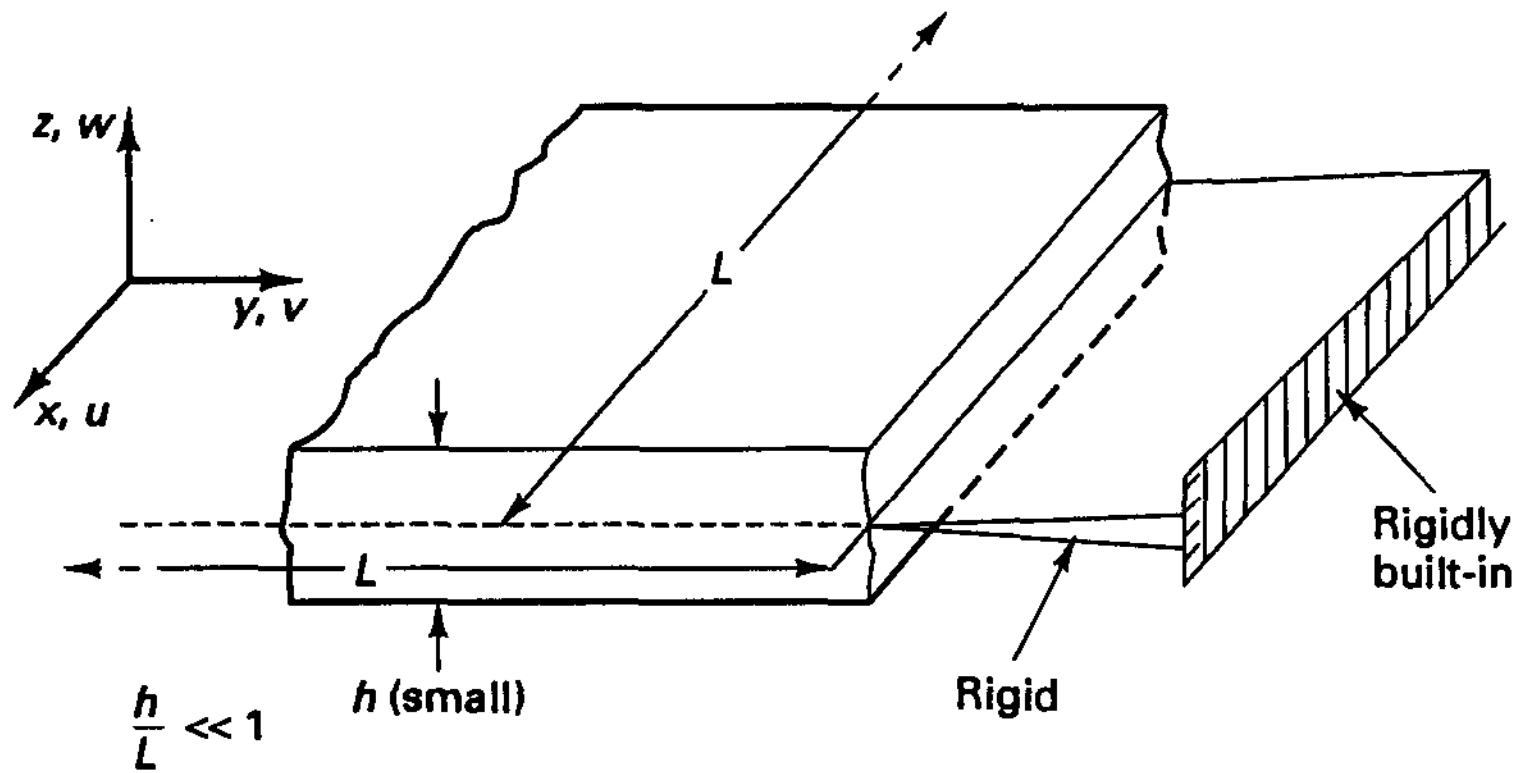


Figure 5.37 Knife-edge support for thin structure

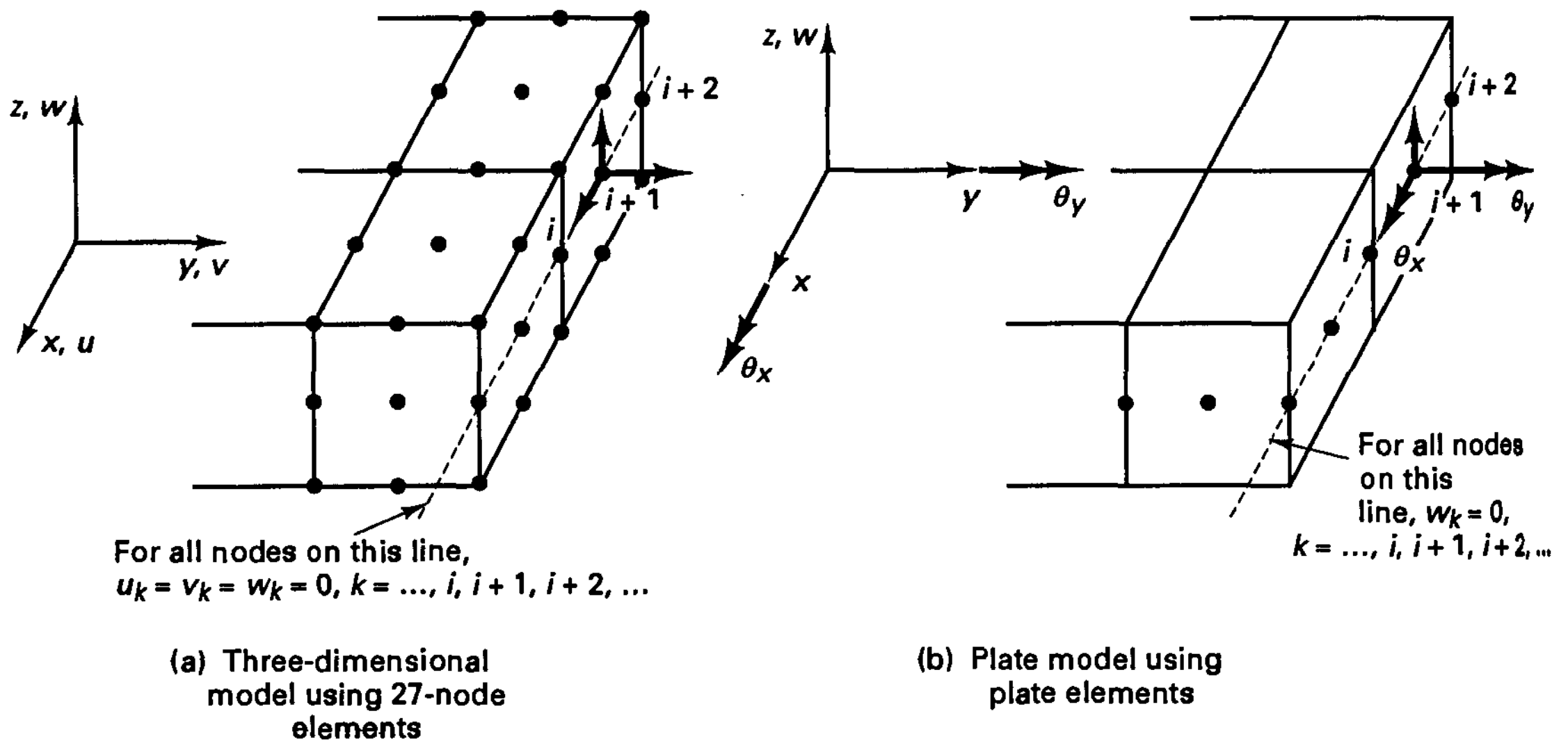


Figure 5.38 Three-dimensional and plate models for problem in Fig. 5.37

those given in the figure. Of course, such a model would be inefficient and impractical because the finite element discretization would have to be very fine for an accurate solution (recall that the three-dimensional elements would display the shear locking phenomenon).

Employing Reissner-Mindlin plate theory, the thin structure is represented using the assumptions given in (5.88) and Fig. 5.25. The boundary conditions are that the transverse displacement is restrained to zero but the section rotations are free; see Fig. 5.38(b). Surely, these conditions represent the physical situation as closely as possible consistent with the assumptions of the theory.

We note, on the other hand, that using Kirchhoff plate theory, the transverse displacement and edge rotation given by $\partial w / \partial x$ would both be zero, and therefore the finite element model would also have to impose $\theta_y = 0$. Hence, in summary, the edge conditions in Fig. 5.37 would be modeled as follows in a finite element solution.

Using three-dimensional elements:

$$\text{on the edge: } u = v = w = 0 \quad (5.127)$$

Using Reissner-Mindlin plate theory-based elements (e.g., the MITC elements in Fig. 5.27):

$$\text{on the edge: } w = 0; \quad \theta_x \text{ and } \theta_y \text{ are left free} \quad (5.128)$$

Using Kirchhoff plate theory-based elements (e.g., the elements in Example 4.18):

$$\text{on the edge: } w = \theta_y = 0; \quad \theta_x \text{ is left free} \quad (5.129)$$

where in Kirchhoff plate theory,

$$\theta_y = -\frac{\partial w}{\partial x} \quad (5.130)$$

Of course, we could also visualize a physical support condition that, in addition to the rigid knife-edge support in Fig. 5.37, prevents the section rotation β_x . In this case we also would set θ_y to zero when using the Reissner-Mindlin plate theory-based elements, and we would set all u -displacements on the face of the plate equal to zero when using the three-dimensional elements.

The boundary condition in (5.128) is referred to as the “soft” boundary condition for a simple support, whereas when θ_y is also set to zero, the boundary condition is of the “hard” type. Similar possibilities also exist when the plate edge is “clamped”, i.e., when the edge is also restrained against the rotation θ_x . In this case we clearly have $w = 0$ and $\theta_x = 0$ on the plate edge. However, again a choice exists regarding θ_y : in the soft boundary condition θ_y is left free, and in the hard boundary condition $\theta_y = 0$. In practice, we usually use the soft boundary conditions, but of course, depending on the actual physical situation, the hard boundary condition is also employed.

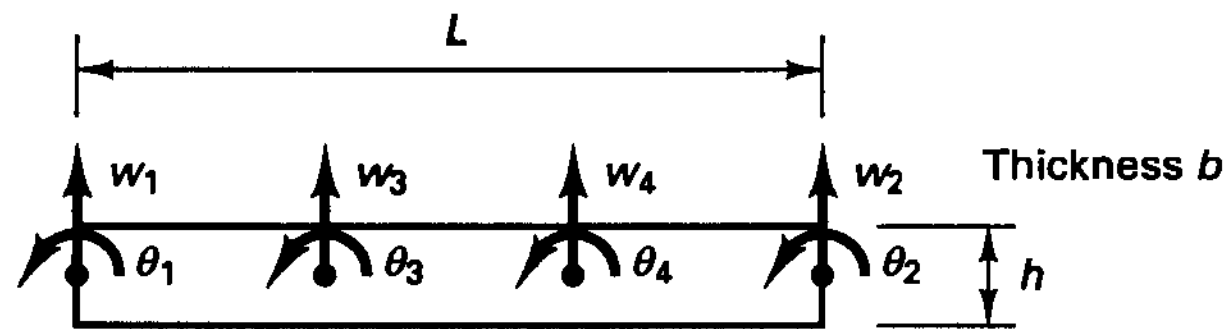
The important point is that when the Reissner-Mindlin plate theory-based elements are used, the boundary conditions on the transverse displacement and rotations are not necessarily the same as when Kirchhoff plate theory is being used and must be chosen to model appropriately the actual physical situation.

The same observations hold of course for the use of the shell elements presented earlier, for which the section rotations are also independent variables (and are not given by the derivatives of the transverse displacement).

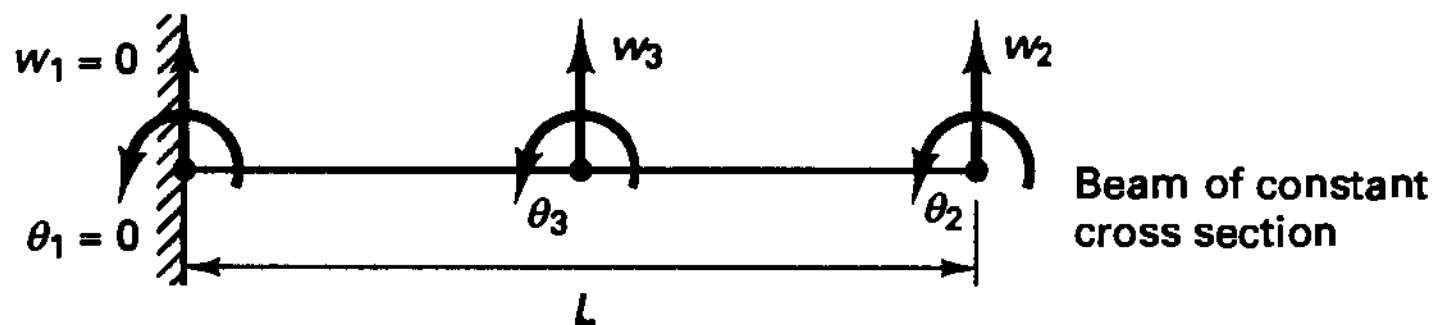
Since the Reissner-Mindlin theory contains more variables for describing the plate behavior than the Kirchhoff theory, various interesting questions arise regarding a comparison of these theories and the convergence of results based on the Reissner-Mindlin theory to those based on the Kirchhoff theory. These questions have been addressed, for example, by K. O. Friedrichs and R. F. Dressler [A], E. Reissner [C], B. Häggblad and K. J. Bathe [A], and D. N. Arnold and R. S. Falk [A]. A main result is that when the Reissner-Mindlin theory is used, boundary layers along plate edges develop for specific boundary conditions when the thickness/length ratio of the plate becomes very small. These boundary layers represent the actual physical situation more realistically than the Kirchhoff plate theory does. Hence, the plate and shell elements presented in this section are not only attractive for computational reasons but can also be used to represent the actual situations in nature more accurately. Some numerical results and comparisons using the Kirchhoff and Reissner-Mindlin plate theories are given by B. Häggblad and K. J. Bathe [A] and K. J. Bathe, N. S. Lee, and M. L. Bucelem [A].

5.4.3 Exercises

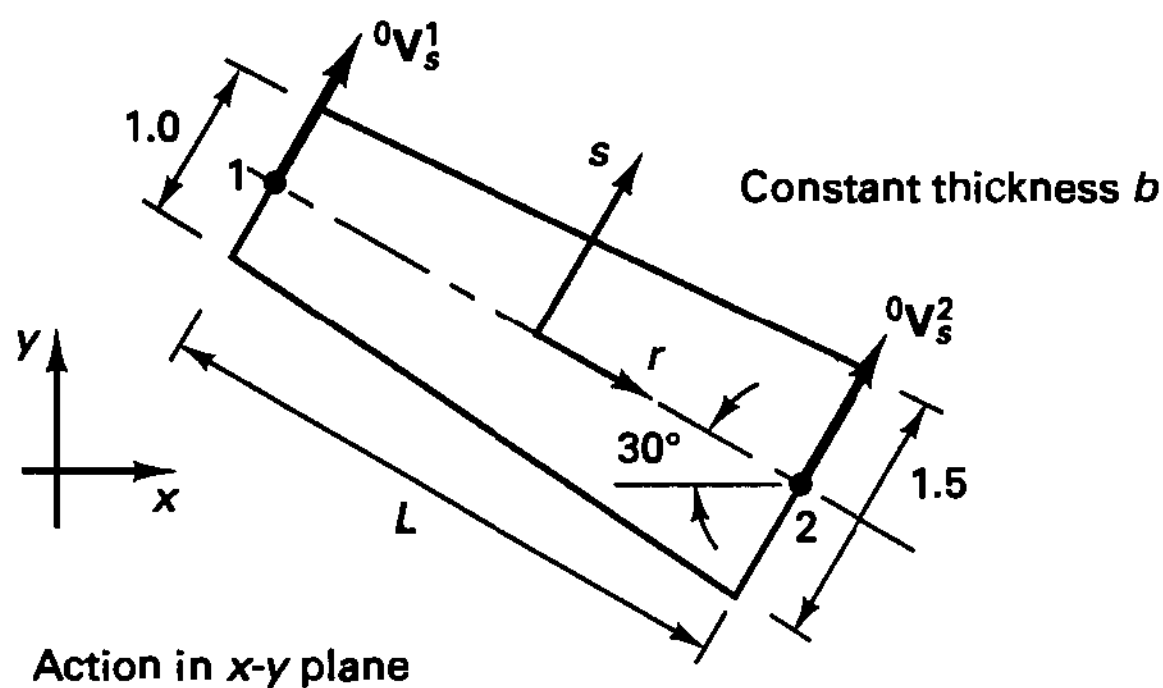
- 5.32. Consider the beam of constant cross-sectional area in Fig. 5.19. Derive from (4.7), using the assumptions in Fig. 5.18, the virtual work expression in (5.58).
- 5.33. Consider the cubic displacement-based isoparametric beam element shown. Construct all matrices needed for the evaluation of the stiffness and mass matrices (but do not perform any integrations to evaluate these matrices).



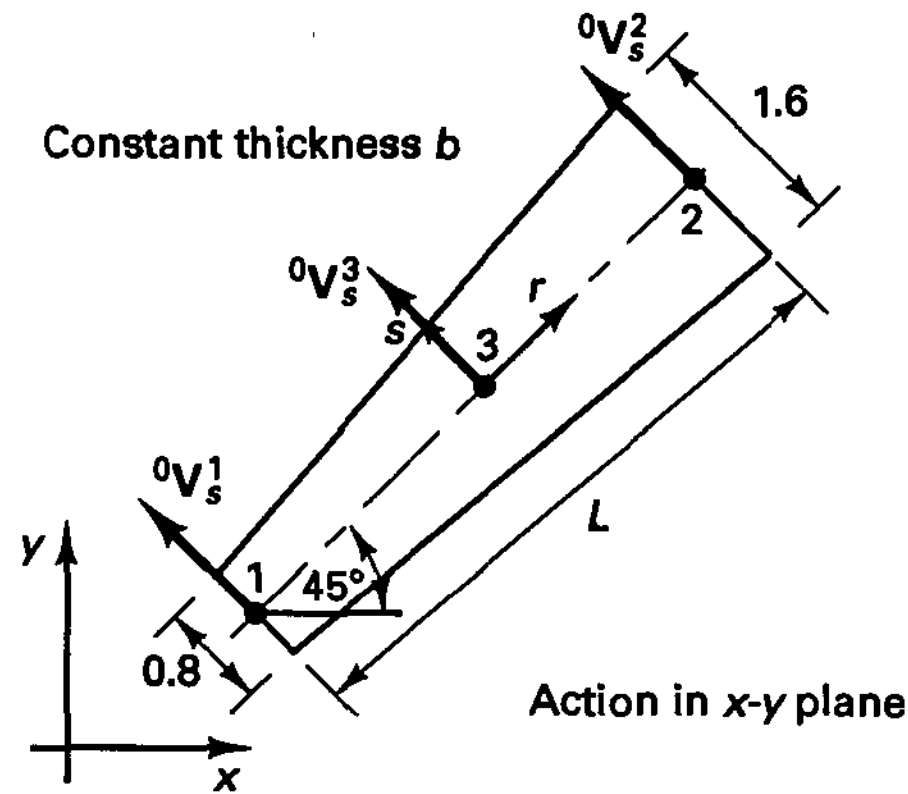
- 5.34. Consider the 3-node isoparametric displacement-based beam element used to model the cantilever beam problem in Fig. 5.20. Show analytically that excellent results are obtained when node 3 is placed exactly at the midlength of the beam, but that the results deteriorate when this node is shifted from that position.



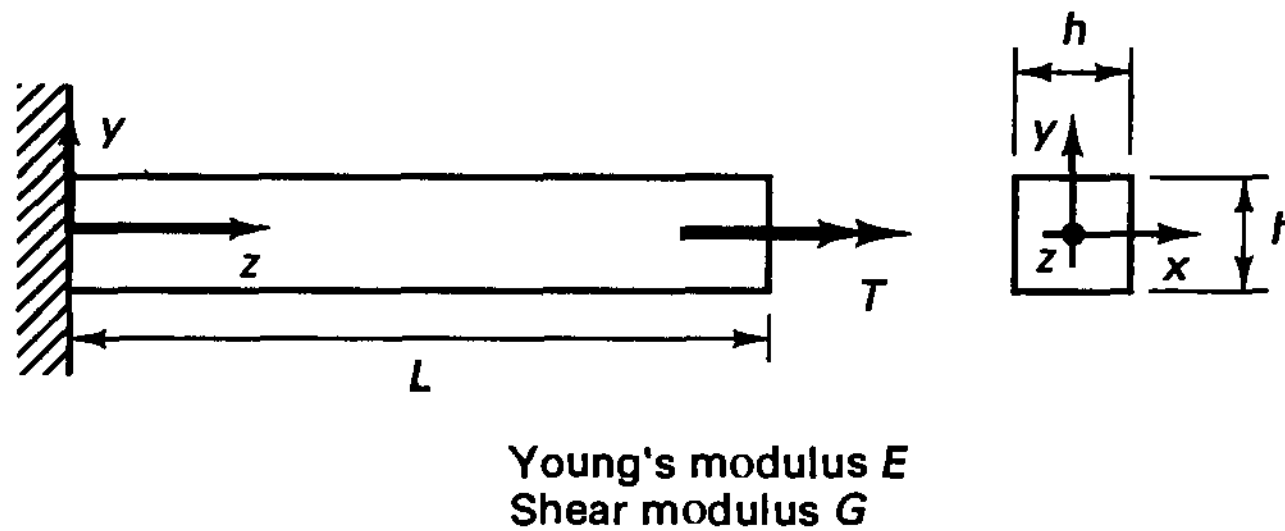
- 5.35. Consider the two-node beam element shown. Specialize the expressions (5.71) to (5.86) to this case.



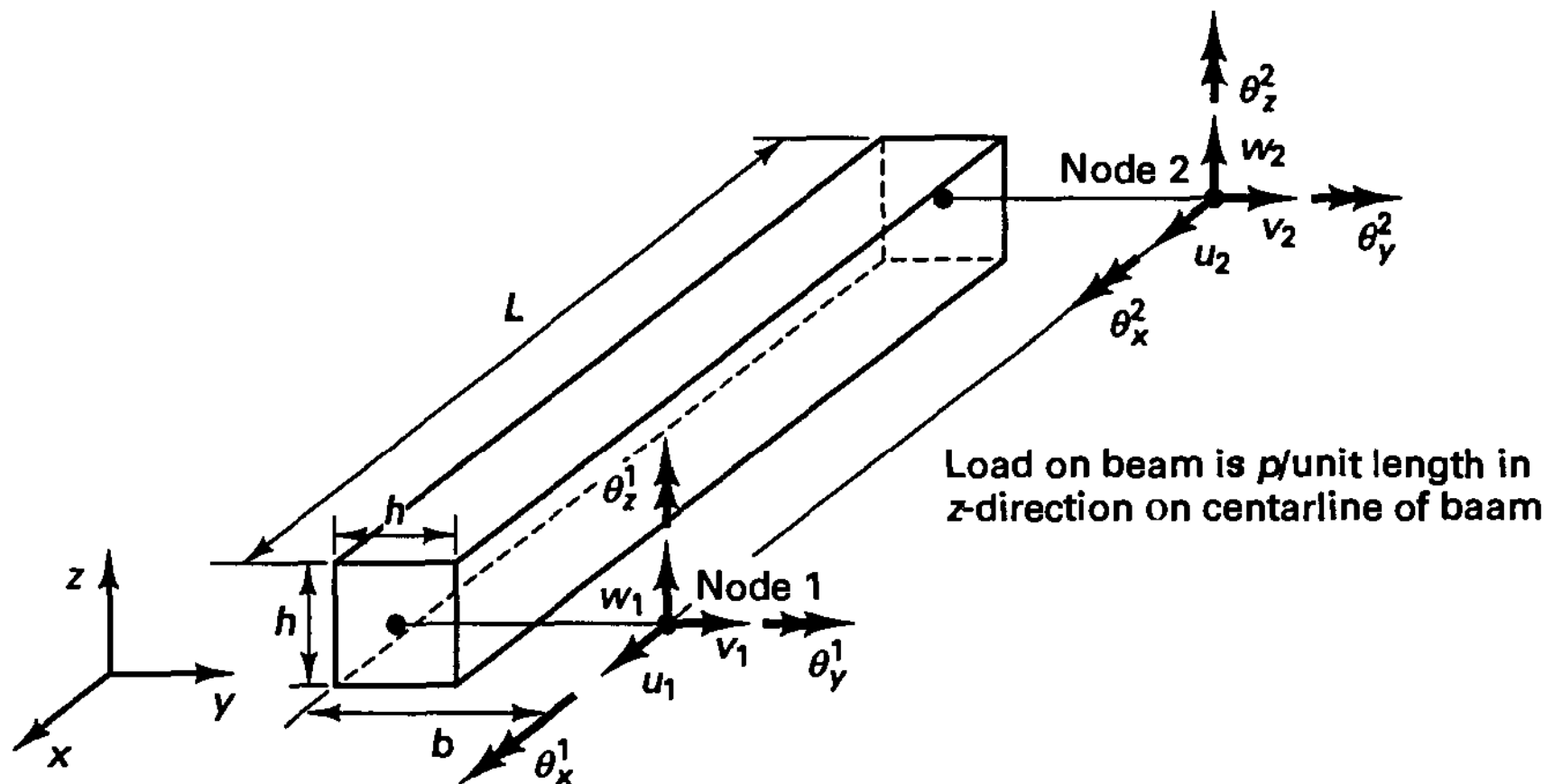
5.36. Consider the three-node beam element shown. Specialize the expressions (5.71) to (5.86) to this case.



5.37. Consider the cantilever beam shown. Idealize this structure by one two-node mixed interpolated beam element and analyze the response. First, neglect warping effects. Next, introduce warping displacements using the warping displacement function $w_w = xy(x^2 - y^2)$ and assuming a linear variation in warping along the element axis.



5.38. Consider the two-node mixed interpolated beam element shown. Derive all expressions needed to calculate the stiffness matrix, mass matrix, and nodal force vector for the degrees of freedom indicated. However, do not perform any integrations.



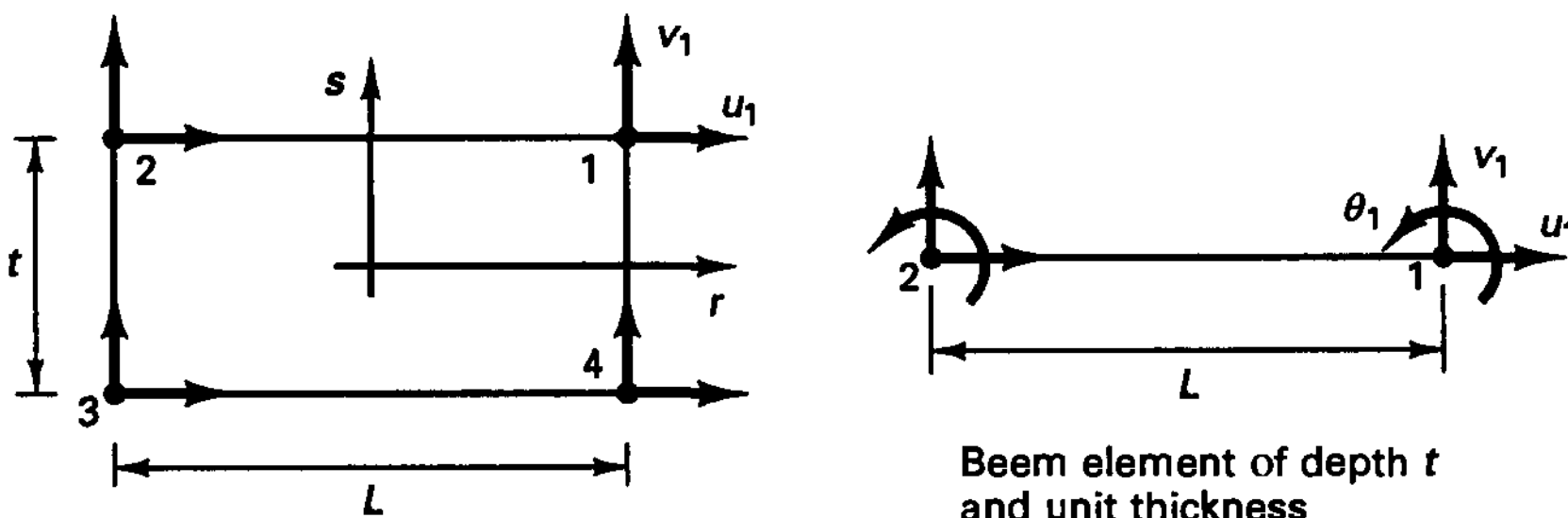
5.39. Consider the plane stress element shown and evaluate the strain-displacement matrix of this element (called \mathbf{B}_{pl}).

Also consider the two-node displacement-based isoparametric beam element shown and evaluate the strain-displacement matrix (called \mathbf{B}_b).

Derive from \mathbf{B}_{pl} , using the appropriate kinematic constraints, the strain-displacement matrix of the degenerated plane stress element (called $\tilde{\mathbf{B}}_{pl}$) for the degrees of freedom used in the beam element. Show explicitly that

$$\int_V \mathbf{B}_b^T \mathbf{C}_b \mathbf{B}_b dV = \int_V \tilde{\mathbf{B}}_{pl}^T \tilde{\mathbf{C}} \tilde{\mathbf{B}}_{pl} dV$$

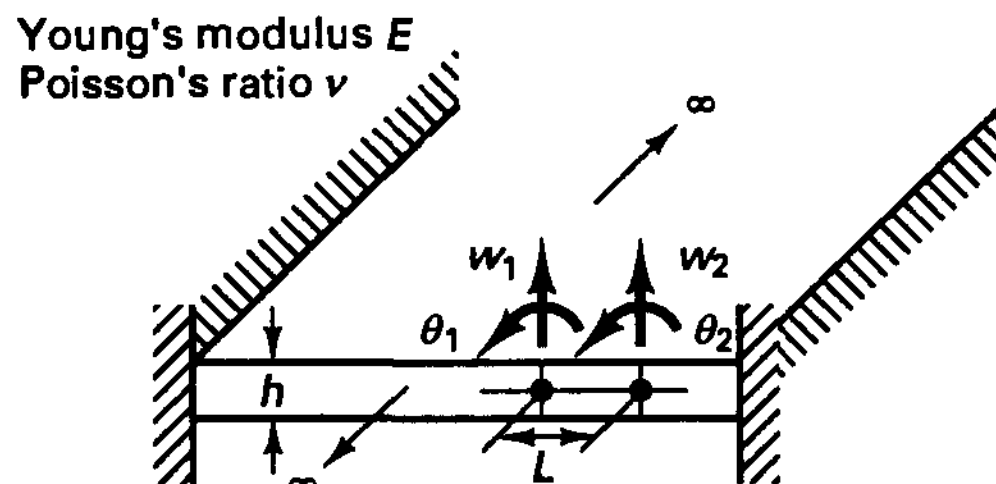
with \mathbf{C}_b and $\tilde{\mathbf{C}}$ to be determined by you.



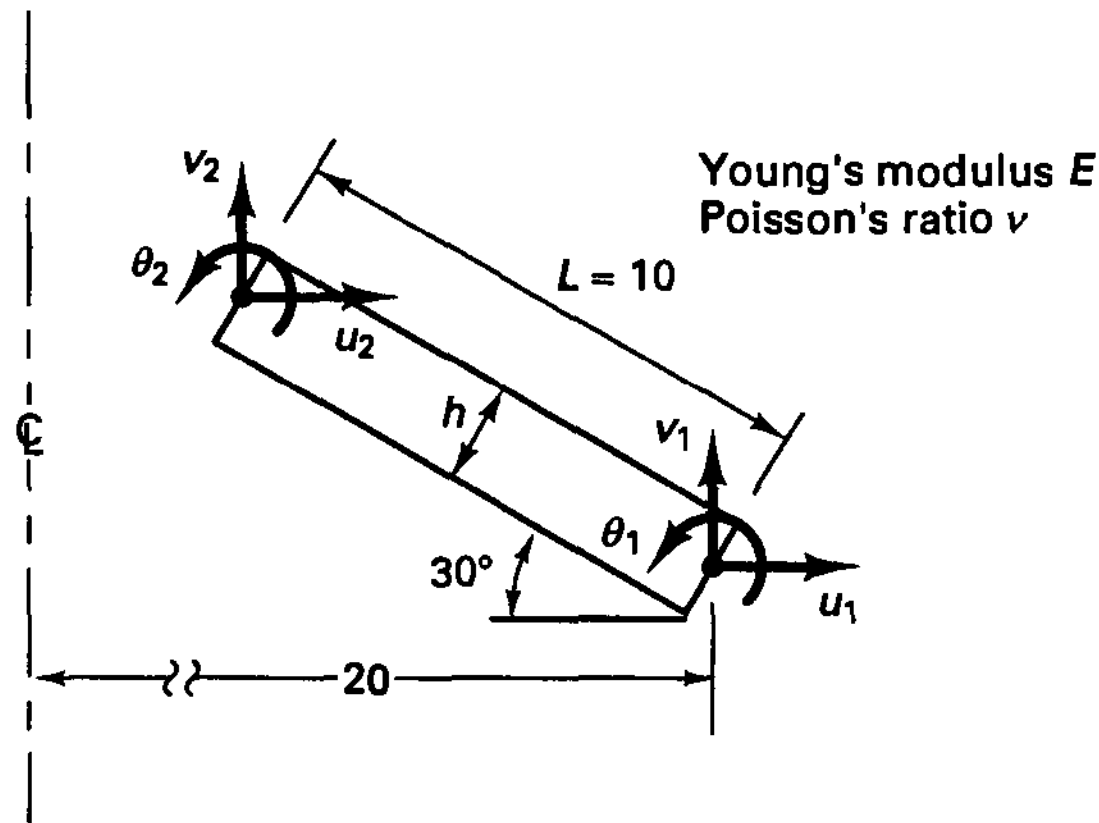
Plane stress element (unit thickness)
Young's modulus E
Poisson's ratio ν

Beam element of depth t and unit thickness

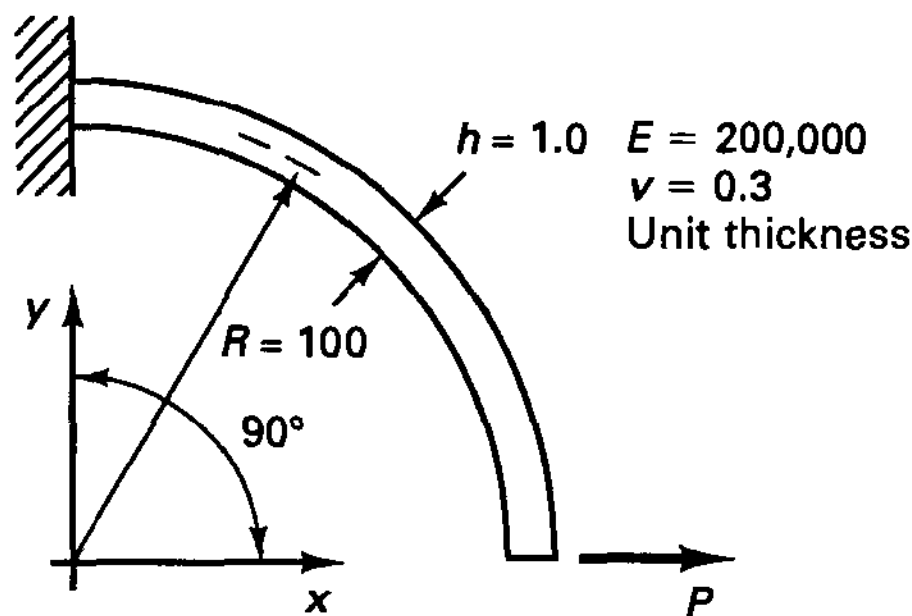
5.40. Consider the problem of an infinitely long, thin plate, rigidly clamped on two sides as shown. Calculate the stiffness matrix of a two-node plane strain beam element to be used to analyze the plate. [Use the mixed interpolation of (5.68) and (5.69).]



5.41. Consider the axisymmetric shell element shown. Construct the strain-displacement matrix assuming mixed interpolation with a constant transverse shear strain. Also, establish the corresponding stress-strain matrix to be used in the evaluation of the stiffness matrix.

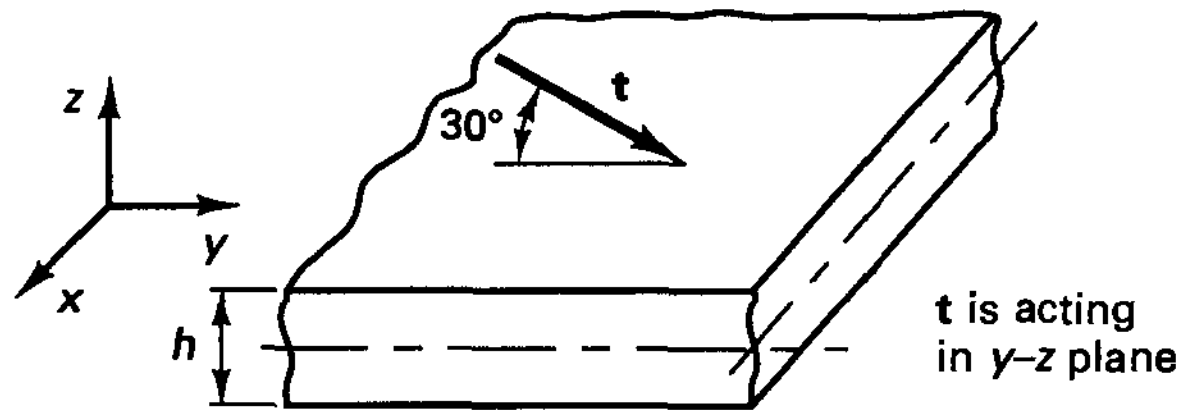


- 5.42. Assume that in Example 5.28 axisymmetric conditions are being considered. Construct the strain-displacement matrix of the transition element. Assume that the axis of revolution, i.e. the y axis, is at distance R from node 3.
- 5.43. Use a computer program to analyze the curved beam shown for the deformations and internal stresses.
- (a) Use displacement-based discretizations of, first, four-node plane stress elements, and then, eight-node plane stress elements.
 - (b) Use discretizations of, first, two-node beam elements, and then, three-node beam elements. Compare the calculated solutions with the analytical solution and increase the fineness of your meshes until an accurate solution is obtained.



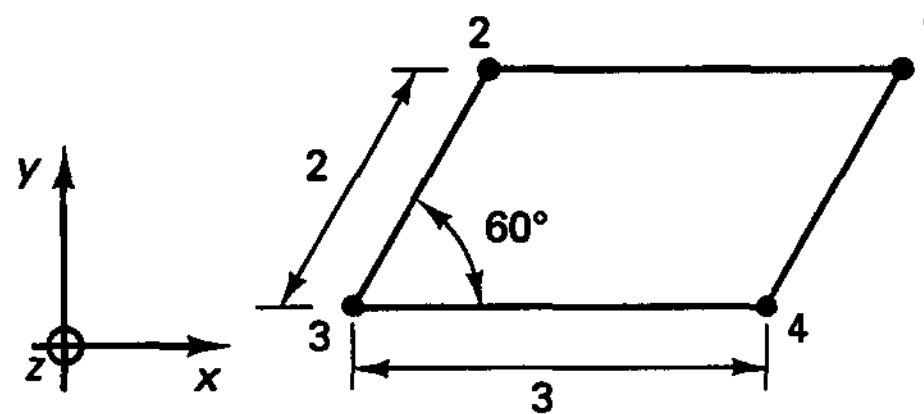
- 5.44. Perform the analysis in Exercise 5.43 but assume axisymmetric conditions; i.e., assume that the figure in Exercise 5.43 shows the cross section of an axisymmetric shell with the centerline at $x = 0$, and that P is a line load per unit length.
- 5.45. Consider the four-node plate bending element in Example 5.29. Assume that $w_1 = 0.1$ and $\theta_y^1 = 0.01$ and that all other nodal point displacements and rotations are zero. Plot the curvatures κ and transverse shear strains γ as a function of r, s over the midsurface of the element.

5.46. Consider the four-node plate bending element in Example 5.29. Assume that the element is loaded on its top surface with the constant traction shown. Calculate the consistent nodal point forces and moments.



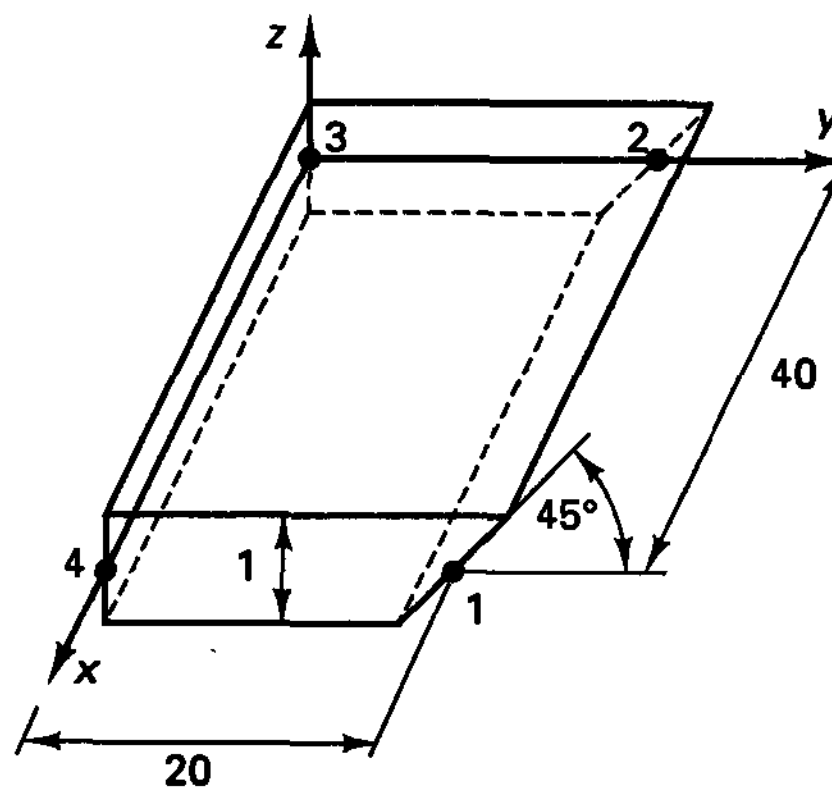
$$\mathbf{t} = \begin{bmatrix} 0 \\ \sqrt{3}/2 \\ -1/2 \end{bmatrix} \quad \text{force per unit area}$$

5.47. Establish the transverse shear strain interpolation matrix \mathbf{B}_γ of the parallelogram-shaped MITC4 element shown.



5.48. Consider the formulation of the MITC4 element and Example 4.30. Show that the MITC4 element formulation can be derived from the Hu-Washizu variational principle.

5.49. Consider the four-node shell element shown and develop the geometry and displacement interpolations (5.107) and (5.112).



5.50. Show explicitly that using the general shell element formulation in (5.107) to (5.118) for a flat element is equivalent to the superposition of the Reissner-Mindlin plate element formulation in (5.88) to (5.99) and the plane stress membrane element formulation in Section 5.3.1.

5.51. Use a computer program to solve the problem shown in Fig. 5.36 with curved shell elements. First, use a single element, and then, use two geometrically distorted elements for the structure to study the element distortion sensitivity.

5.52. Consider the following Kirchhoff plate theory boundary conditions at the edge of a plate:

$$w = 0; \quad \frac{\partial w}{\partial x} = \frac{\partial w}{\partial y} = 0 \tag{a}$$

Establish a corresponding reasonable choice of boundary conditions for the Reissner-Mindlin plate theory. Also, discuss and illustrate graphically that the boundary conditions in (a) do not uniquely determine the boundary conditions for the Reissner-Mindlin plate theory.

5.5 NUMERICAL INTEGRATION

An important aspect of isoparametric and related finite element analysis is the required numerical integration. The required matrix integrals in the finite element calculations have been written as

$$\int \mathbf{F}(r) dr; \int \mathbf{F}(r, s) dr ds; \int \mathbf{F}(r, s, t) dr ds dt \tag{5.131}$$

in the one-, two-, and three-dimensional cases, respectively. It was stated that these integrals are in practice evaluated numerically using

$$\left. \begin{aligned} \int \mathbf{F}(r) dr &= \sum_i \alpha_i \mathbf{F}(r_i) + \mathbf{R}_n \\ \int \mathbf{F}(r, s) dr ds &= \sum_{i,j} \alpha_{ij} \mathbf{F}(r_i, s_j) + \mathbf{R}_n \\ \int \mathbf{F}(r, s, t) dr ds dt &= \sum_{i,j,k} \alpha_{ijk} \mathbf{F}(r_i, s_j, t_k) + \mathbf{R}_n \end{aligned} \right\} \tag{5.132}$$

where the summations extend over all i, j , and k specified, the α_i, α_{ij} , and α_{ijk} are weighting factors, and $\mathbf{F}(r_i), \mathbf{F}(r_i, s_j)$, and $\mathbf{F}(r_i, s_j, t_k)$ are the matrices $\mathbf{F}(r), \mathbf{F}(r, s)$, and $\mathbf{F}(r, s, t)$ evaluated at the points specified in the arguments. The matrices \mathbf{R}_n are error matrices, which in practice are usually not evaluated. Therefore, we use

$$\left. \begin{aligned} \int \mathbf{F}(r) dr &= \sum_i \alpha_i \mathbf{F}(r_i) \\ \int \mathbf{F}(r, s) dr ds &= \sum_{i,j} \alpha_{ij} \mathbf{F}(r_i, s_j) \\ \int \mathbf{F}(r, s, t) dr ds dt &= \sum_{i,j,k} \alpha_{ijk} \mathbf{F}(r_i, s_j, t_k) \end{aligned} \right\} \tag{5.133}$$

The purpose in this section is to present the theory and practical implications of numerical integrations. An important point is the integration accuracy that is needed, i.e., the number of integration points required in the element formation.

As presented above, in finite element analysis we integrate matrices, which means that each element of the matrix considered is integrated individually. Hence, for the derivation

of the numerical integration formulas we can consider a typical element of a matrix, which we denote as F .

Consider the one-dimensional case first, i.e., the integration of $\int_a^b F(r) dr$. In an isoparametric element calculation we would actually have $a = -1$ and $b = +1$.

The numerical integration of $\int_a^b F(r) dr$ is essentially based on passing a polynomial $\psi(r)$ through given values of $F(r)$ and then using $\int_a^b \psi(r) dr$ as an approximation to $\int_a^b F(r) dr$. The number of evaluations of $F(r)$ and the positions of the sampling points in the interval from a to b determine how well $\psi(r)$ approximates $F(r)$ and hence the error of the numerical integration (see, for example, C. E. Fröberg [A]).

5.5.1 Interpolation Using a Polynomial

Assume that $F(r)$ has been evaluated at the $(n + 1)$ distinct points r_0, r_1, \dots, r_n to obtain F_0, F_1, \dots, F_n , respectively, and that a polynomial $\psi(r)$ is to be passed through these data. Then there is a unique polynomial $\psi(r)$ given as

$$\psi(r) = a_0 + a_1 r + a_2 r^2 + \dots + a_n r^n \tag{5.134}$$

Using the condition $\psi(r) = F(r)$ at the $(n + 1)$ interpolating points, we have

$$\mathbf{F} = \mathbf{V} \mathbf{a} \tag{5.135}$$

where

$$\mathbf{F} = \begin{bmatrix} F_0 \\ F_1 \\ \vdots \\ F_n \end{bmatrix}; \quad \mathbf{a} = \begin{bmatrix} a_0 \\ a_1 \\ \vdots \\ a_n \end{bmatrix} \tag{5.136}$$

and \mathbf{V} is the *Vandermonde matrix*,

$$\mathbf{V} = \begin{bmatrix} 1 & r_0 & r_0^2 & \dots & r_0^n \\ 1 & r_1 & r_1^2 & \dots & r_1^n \\ \vdots & \vdots & \vdots & \dots & \vdots \\ 1 & r_n & r_n^2 & \dots & r_n^n \end{bmatrix} \tag{5.137}$$

Since $\det \mathbf{V} \neq 0$, provided that the r_i are distinct points, we have a unique solution for \mathbf{a} .

However, a more convenient way to obtain $\psi(r)$ is to use *Lagrangian interpolation*. First, we recall that the $(n + 1)$ functions $1, r, r^2, \dots, r^n$ form an $(n + 1)$ -dimensional vector space, say V_n , in which $\psi(r)$ is an element (see Section 2.3). Since the coordinates $a_0, a_1, a_2, \dots, a_n$ of $\psi(r)$ are relatively difficult to evaluate using (5.135), we seek a different basis for the space V_n in which the coordinates of $\psi(r)$ are more easily evaluated. This basis is provided by the fundamental polynomials of Lagrangian interpolation, given as

$$l_j(r) = \frac{(r - r_0)(r - r_1) \dots (r - r_{j-1})(r - r_{j+1}) \dots (r - r_n)}{(r_j - r_0)(r_j - r_1) \dots (r_j - r_{j-1})(r_j - r_{j+1}) \dots (r_j - r_n)} \tag{5.138}$$

where

$$l_j(r_i) = \delta_{ij} \tag{5.139}$$

where δ_{ij} is the Kronecker delta; i.e., $\delta_{ij} = 1$ for $i = j$, and $\delta_{ij} = 0$ for $i \neq j$. Using the property in (5.139), the coordinates of the base vectors are simply the values of $F(r)$, and the polynomial $\psi(r)$ is

$$\psi(r) = F_0 l_0(r) + F_1 l_1(r) + \cdots + F_n l_n(r) \tag{5.140}$$

EXAMPLE 5.33: Establish the interpolating polynomial $\psi(r)$ for the function $F(r) = 2^r - r$ when the data at the points $r = 0, 1,$ and 3 are used. In this case $r_0 = 0, r_1 = 1, r_2 = 3,$ and $F_0 = 1, F_1 = 1, F_2 = 5.$

In the first approach we use the relation in (5.135) to calculate the unknown coefficients $a_0, a_1,$ and a_2 of the polynomial $\psi(r) = a_0 + a_1 r + a_2 r^2.$ In this case we have

$$\begin{bmatrix} 1 & 0 & 0 \\ 1 & 1 & 1 \\ 1 & 3 & 9 \end{bmatrix} \begin{bmatrix} a_0 \\ a_1 \\ a_2 \end{bmatrix} = \begin{bmatrix} 1 \\ 1 \\ 5 \end{bmatrix}$$

The solution gives $a_0 = 1, a_1 = -\frac{2}{3}, a_2 = \frac{2}{3},$ and therefore $\psi(r) = 1 - \frac{2}{3}r + \frac{2}{3}r^2.$

If Lagrangian interpolation is employed, we use the relation in (5.140) which in this case gives

$$\psi(r) = (1) \frac{(r-1)(r-3)}{(-1)(-3)} + (1) \frac{(r)(r-3)}{(1)(-2)} + (5) \frac{(r)(r-1)}{(3)(2)}$$

or, as before,

$$\psi(r) = 1 - \frac{2}{3}r + \frac{2}{3}r^2$$

5.5.2 The Newton-Cotes Formulas (One-Dimensional Integration)

Having established an interpolating polynomial $\psi(r),$ we can now obtain an approximation to the integral $\int_a^b F(r) dr.$ In Newton-Cotes integration, it is assumed that the sampling points of F are spaced at equal distances, and we define

$$r_0 = a; \quad r_n = b; \quad h = \frac{b-a}{n} \tag{5.141}$$

Using Lagrangian interpolation to obtain $\psi(r)$ as an approximation to $F(r),$ we have

$$\int_a^b F(r) dr = \sum_{i=0}^n \left[\int_a^b l_i(r) dr \right] F_i + R_n \tag{5.142}$$

or, evaluated,

$$\int_a^b F(r) dr = (b-a) \sum_{i=0}^n C_i^n F_i + R_n \tag{5.143}$$

where R_n is the remainder and the C_i^n are the *Newton-Cotes constants* for numerical integration with n intervals.

The Newton-Cotes constants and corresponding remainder terms are summarized in Table 5.5 for $n = 1$ to $6.$ The cases $n = 1$ and $n = 2$ are the well-known *trapezoidal rule* and *Simpson formula.* We note that the formulas for $n = 3$ and $n = 5$ have the same order of accuracy as the formulas for $n = 2$ and $n = 4,$ respectively. For this reason, the even formulas with $n = 2$ and $n = 4$ are used in practice.

TABLE 5.5 Newton-Cotes numbers and error estimates

Number of intervals n	C_0^n	C_1^n	C_2^n	C_3^n	C_4^n	C_5^n	C_6^n	Upper bound on error R_n as a function of the derivative of F
1	$\frac{1}{2}$	$\frac{1}{2}$						$10^{-1}(b-a)^3 F''(r)$
2	$\frac{1}{6}$	$\frac{4}{6}$	$\frac{1}{6}$					$10^{-3}(b-a)^5 F^{IV}(r)$
3	$\frac{1}{8}$	$\frac{3}{8}$	$\frac{3}{8}$	$\frac{1}{8}$				$10^{-3}(b-a)^5 F^{IV}(r)$
4	$\frac{7}{90}$	$\frac{32}{90}$	$\frac{12}{90}$	$\frac{32}{90}$	$\frac{7}{90}$			$10^{-6}(b-a)^7 F^{VI}(r)$
5	$\frac{19}{288}$	$\frac{75}{288}$	$\frac{50}{288}$	$\frac{50}{288}$	$\frac{75}{288}$	$\frac{19}{288}$		$10^{-6}(b-a)^7 F^{VI}(r)$
6	$\frac{41}{840}$	$\frac{216}{840}$	$\frac{27}{840}$	$\frac{272}{840}$	$\frac{27}{840}$	$\frac{216}{840}$	$\frac{41}{840}$	$10^{-9}(b-a)^9 F^{VIII}(r)$

EXAMPLE 5.34: Evaluate the Newton-Cotes constants when the interpolating polynomial is of order 2; i.e., $\psi(r)$ is a parabola.

In this case we have

$$\int_a^b F(r) dr \doteq \int_a^b \left[F_0 \frac{(r-r_1)(r-r_2)}{(r_0-r_1)(r_0-r_2)} + F_1 \frac{(r-r_0)(r-r_2)}{(r_1-r_0)(r_1-r_2)} + F_2 \frac{(r-r_0)(r-r_1)}{(r_2-r_0)(r_2-r_1)} \right] dr$$

Using $r_0 = a$, $r_1 = a + h$, $r_2 = a + 2h$, where $h = (b-a)/2$, the evaluation of the integral gives

$$\int_a^b F(r) dr \doteq \frac{b-a}{6} (F_0 + 4F_1 + F_2)$$

Hence the Newton-Cotes constants are as given in Table 5.5 for the case $n = 2$.

EXAMPLE 5.35: Use Simpson's rule to integrate $\int_0^3 (2^r - r) dr$.

In this case $n = 2$ and $h = \frac{3}{2}$. Therefore, $r_0 = 0$, $r_1 = \frac{3}{2}$, $r_2 = 3$, and $F_0 = 1$, $F_1 = 1.328427$, $F_2 = 5$, and we obtain

$$\int_0^3 (2^r - r) dr \doteq \frac{3}{6} [(1)(1) + (4)(1.328427) + (1)(5)]$$

or
$$\int_0^3 (2^r - r) dr \doteq 5.656854$$

The exact result is
$$\int_0^3 (2^r - r) dr = 5.598868$$

Hence the error is
$$R = 0.057986$$

However, using the upper bound value on the error, we have

$$R < \frac{(3-0)^5}{1000} (\ln 2)^4 (2^r) = 0.448743$$

To obtain greater accuracy in the integration using the Newton-Cotes formulas we need to employ a smaller interval h , i.e., include more evaluations of the function to be integrated. Then we have the choice between two different strategies: we may use a higher-order Newton-Cotes formula or, alternatively, employ the lower-order formula in a repeated manner, in which case the integration procedure is referred to as a *composite formula*. Consider the following example.

EXAMPLE 5.36: Increase the accuracy of the integration in Example 5.35 by using half the interval spacing.

In this case we have $h = \frac{3}{4}$, and the required function values are $F_0 = 1$, $F_1 = 0.931792$, $F_2 = 1.328427$, $F_3 = 2.506828$, and $F_4 = 5$. The choice now lies between using the higher-order Newton-Cotes formula with $n = 4$ or applying the Simpson's rule twice, i.e., to the first two intervals and then to the second two intervals. Using the Newton-Cotes formula with $n = 4$, we obtain

$$\int_0^3 (2^r - r) dr \doteq \frac{3}{90}(7F_0 + 32F_1 + 12F_2 + 32F_3 + 7F_4)$$

Hence,
$$\int_0^3 (2^r - r) dr \doteq 5.599232$$

On the other hand, using Simpson's rule twice, we have

$$\int_0^3 (2^r - r) dr = \int_0^{3/2} (2^r - r) dr + \int_{3/2}^3 (2^r - r) dr$$

The integration is performed using

$$\int_0^{3/2} (2^r - r) dr \doteq \frac{\frac{3}{2} - 0}{6}(F_0 + 4F_1 + F_2)$$

where F_0 , F_1 , and F_2 are the function values at $r = 0$, $r = \frac{3}{4}$, and $r = \frac{3}{2}$, respectively; i.e.,

$$F_0 = 1; \quad F_1 = 0.931792; \quad F_2 = 1.328427$$

Hence we use
$$\int_0^{3/2} (2^r - r) dr \doteq 1.513899 \tag{a}$$

Next we need to evaluate

$$\int_{3/2}^3 (2^r - r) dr \doteq \frac{3 - \frac{3}{2}}{6}(F_0 + 4F_1 + F_2)$$

where F_0 , F_1 , and F_2 are the function values at $r = \frac{3}{2}$, $r = \frac{9}{4}$, and $r = 3$, respectively,

$$F_0 = 1.328427; \quad F_1 = 2.506828; \quad F_2 = 5$$

Hence we have
$$\int_{3/2}^3 (2^r - r) dr \doteq 4.088935 \tag{b}$$

Adding the results in (a) and (b), we obtain

$$\int_0^3 (2^r - r) dr \doteq 5.602834$$

The use of a composite formula has a number of advantages over the application of high-order Newton-Cotes formulas. A composite formula, such as the repetitive use of Simpson's rule, is easy to employ. Convergence is ensured as the interval of sampling decreases, and, in practice, a sampling interval could be used that varies from one application of the basic formula to the next. This is particularly advantageous when there are discontinuities in the function to be integrated. For these reasons, in practice, composite formulas are commonly used.

EXAMPLE 5.37: Use a composite formula that employs Simpson's rule to evaluate the integral $\int_{-1}^{+13} F(r) dr$ of the function $F(r)$ in Fig. E5.37.

This function is best integrated by considering three intervals of integration, as follows:

$$\int_{-1}^{13} F dr = \int_{-1}^2 (r^3 + 3) dr + \int_2^9 [10 + (r - 1)^{1/3}] dr + \int_9^{13} \left[\frac{1}{128} (13 - r)^5 + 4 \right] dr$$

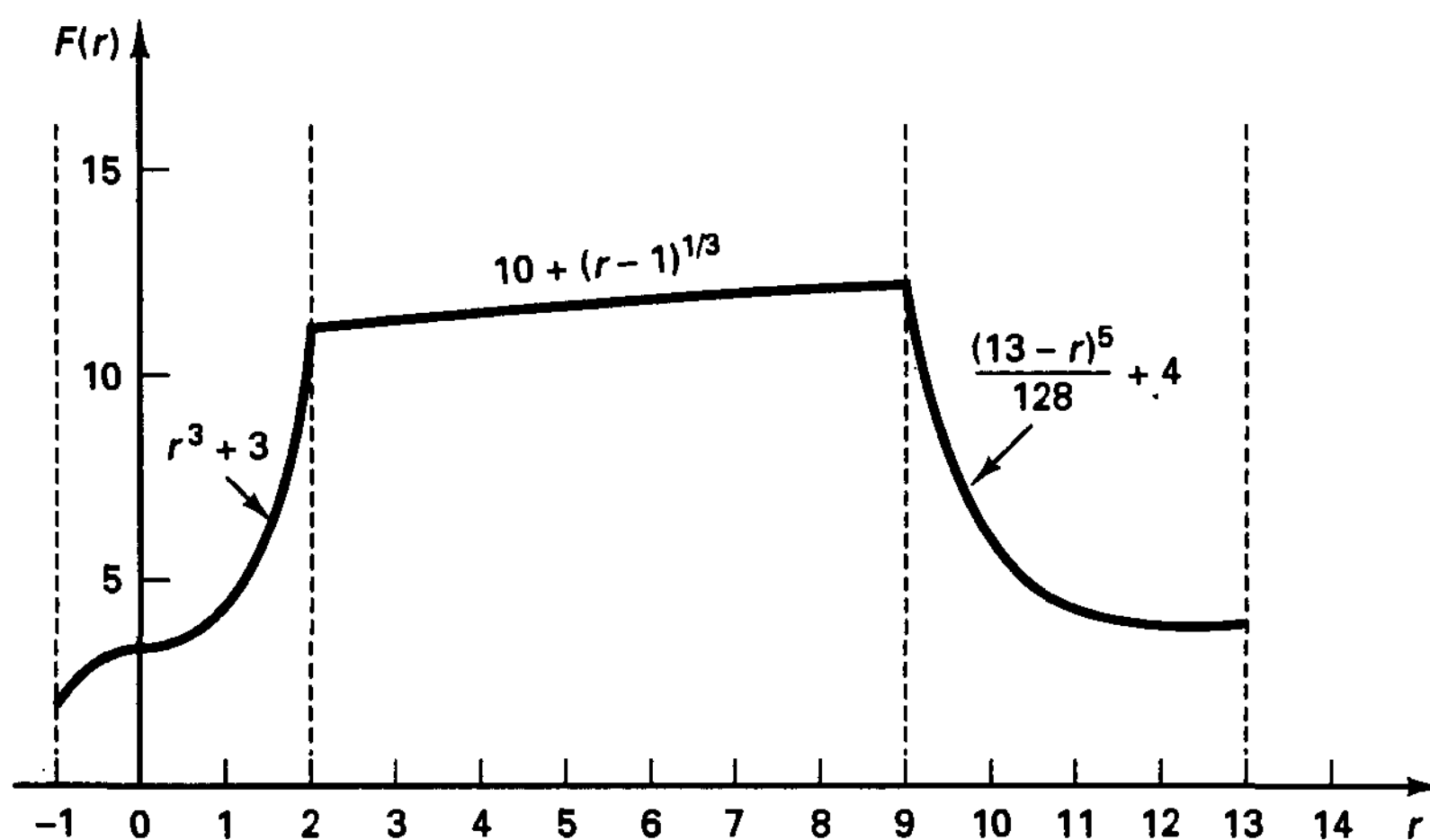


Figure E5.37 Function $F(r)$

We evaluate each of the three integrals using Simpson's rule and have

$$\int_{-1}^2 (r^3 + 3) dr = \frac{2 - (-1)}{6} [(1)(2) + (4)(3.125) + (1)(11)]$$

or
$$\int_{-1}^2 (r^3 + 3) dr = 12.75$$

$$\int_2^9 [10 + (r - 1)^{1/3}] dr \doteq \frac{9 - 2}{6} [(1)(11) + (4)(11.650964) + (1)(12)]$$

or
$$\int_2^9 [10 + (r - 1)^{1/3}] dr \doteq 81.204498$$

$$\int_9^{13} \left[\frac{1}{128} (13 - r)^5 + 4 \right] dr \doteq \frac{13 - 9}{6} [(1)(12) + (4)(4.25) + (1)(4)]$$

or
$$\int_9^{13} \left[\frac{1}{128} (13 - r)^5 + 4 \right] dr \doteq 22$$

$$\begin{aligned} \text{Hence,} \quad & \int_{-1}^{13} F dr \doteq 12.75 + 81.204498 + 22 \\ \text{or} \quad & \int_{-1}^{13} F dr \doteq 115.954498 \end{aligned}$$

5.5.3 The Gauss Formulas (One-Dimensional Integration)

The basic integration schemes that we have considered so far use equally spaced sampling points, although the basic methods could be employed to construct procedures that allow the interval of sampling to be varied; i.e., the composite formulas have been introduced. The methods discussed so far are effective when measurements of an unknown function to be integrated have been taken at certain intervals. However, in the integration of finite element matrices, a subroutine is called to evaluate the unknown function F at given points, and these points may be anywhere on the element. No additional difficulties arise if the sampling points are not equally spaced. Therefore, it seems natural to try to improve the accuracy that can be obtained for a given number of function evaluations by also optimizing the positions of the sampling points. A very important numerical intergration procedure in which both the positions of the sampling points and the weights have been optimized is *Gauss quadrature*. The basic assumption in Gauss numerical integration is that

$$\int_a^b F(r) dr = \alpha_1 F(r_1) + \alpha_2 F(r_2) + \dots + \alpha_n F(r_n) + R_n \tag{5.144}$$

where both the weights $\alpha_1, \dots, \alpha_n$ and the sampling points r_1, \dots, r_n are variables. It should be recalled that in the derivation of the Newton-Cotes formulas, only the weights were unknown, and they were determined from the integration of a polynomial $\psi(r)$ that passed through equally spaced sampling points of the function $F(r)$. We now also calculate the positions of the sampling points and therefore have $2n$ unknowns to determine a higher-order integration scheme.

In analogy with the derivation of the Newton-Cotes formulas, we use an interpolating polynomial $\psi(r)$ of the form given in (5.140),

$$\psi(r) = \sum_{j=1}^n F_j l_j(r) \tag{5.145}$$

where n samplings points are now considered, r_1, \dots, r_n , which are still unknown. For the determination of the values r_1, \dots, r_n , we define a function $P(r)$,

$$P(r) = (r - r_1)(r - r_2) \dots (r - r_n) \tag{5.146}$$

which is a polynomial of order n . We note that $P(r) = 0$ at the sampling points r_1, \dots, r_n . Therefore, we can write

$$F(r) = \psi(r) + P(r)(\beta_0 + \beta_1 r + \beta_2 r^2 + \dots) \tag{5.147}$$

Integrating $F(r)$, we obtain

$$\int_a^b F(r) dr = \sum_{j=1}^n F_j \left[\int_a^b l_j(r) dr \right] + \sum_{j=0}^{\infty} \beta_j \left[\int_a^b r^j P(r) dr \right] \tag{5.148}$$

where it should be noted that in the first integral on the right in (5.148), functions of order $(n - 1)$ and lower are integrated, and in the second integral the functions that are integrated are of order n and higher. The unknown values $r_j, j = 1, 2, \dots, n$, can now be determined using the conditions

$$\int_a^b P(r)r^k dr = 0 \quad k = 0, 1, 2, \dots, n - 1 \tag{5.149}$$

Then, since the polynomial $\psi(r)$ passes through n sampling points of $F(r)$, and $P(r)$ vanishes at these points, the conditions in (5.149) mean that the required integral $\int_a^b F(r) dr$ is approximated by integrating a polynomial of order $(2n - 1)$ instead of $F(r)$.

In summary, using the Newton-Cotes formulas, we use $(n + 1)$ equally spaced sampling points and integrate exactly a polynomial of order at most n . On the other hand, in Gauss quadrature we require n unequally spaced sampling points and integrate exactly a polynomial of order at most $(2n - 1)$. Polynomials of orders less than n and $(2n - 1)$, respectively, for the two cases are also integrated exactly.

To determine the sampling points and the integration weights, we realize that they depend on the interval a to b . However, to make the calculations general, we consider a natural interval from -1 to $+1$ and deduce the sampling points and weights for any interval. Namely, if r_i is a sampling point and α_i is the weight for the interval -1 to $+1$, the corresponding sampling point and weight in the integration from a to b are

$$\frac{a + b}{2} + \frac{b - a}{2} r_i \quad \text{and} \quad \frac{b - a}{2} \alpha_i$$

respectively.

Hence, consider an interval from -1 to $+1$. The sampling points are determined from (5.149) with $a = -1$ and $b = +1$. To calculate the integration weights we substitute for $F(r)$ in (5.144) the interpolating polynomial $\psi(r)$ from (5.145) and perform the integration. It should be noted that because the sampling points have been determined, the polynomial $\psi(r)$ is known, and hence

$$\alpha_j = \int_{-1}^{+1} l_j(r) dr; \quad j = 1, 2, \dots, n \tag{5.150}$$

TABLE 5.6 Sampling points and weights in Gauss-Legendre numerical integration (interval -1 to $+1$)

n	r_i			α_i		
1	0.	(15 zeros)		2.	(15 zeros)	
2	± 0.57735	02691	89626	1.00000	00000	00000
3	± 0.77459	66692	41483	0.55555	55555	55556
	0.00000	00000	00000	0.88888	88888	88889
4	± 0.86113	63115	94053	0.34785	48451	37454
	± 0.33998	10435	84856	0.65214	51548	62546
5	± 0.90617	98459	38664	0.23692	68850	56189
	± 0.53846	93101	05683	0.47862	86704	99366
	0.00000	00000	00000	0.56888	88888	88889
6	± 0.93246	95142	03152	0.17132	44923	79170
	± 0.66120	93864	66265	0.36076	15730	48139
	± 0.23861	91860	83197	0.46791	39345	72691

The sampling points and weights for the interval -1 to $+1$ have been published by A. N. Lowan, N. Davids, and A. Levenson [A] and are reproduced in Table 5.6 for $n = 1$ to 6.

The coefficients in Table 5.6 can be calculated directly using (5.149) and (5.150) (see Example 5.38). However, for larger n the solution becomes cumbersome, and it is expedient to use Legendre polynomials to solve for the coefficients, which are thus referred to as Gauss-Legendre coefficients.

EXAMPLE 5.38: Derive the sampling points and weights for two-point Gauss quadrature. In this case $P(r) = (r - r_1)(r - r_2)$ and (5.149) gives the two equations

$$\int_{-1}^{+1} (r - r_1)(r - r_2) dr = 0$$

$$\int_{-1}^{+1} (r - r_1)(r - r_2)r dr = 0$$

Solving, we obtain $r_1 r_2 = -\frac{1}{3}$

and $r_1 + r_2 = 0$

Hence $r_1 = -\frac{1}{\sqrt{3}}; \quad r_2 = +\frac{1}{\sqrt{3}}$

The corresponding weights are obtained using (5.150), which in this case gives

$$\alpha_1 = \int_{-1}^{+1} \frac{r - r_2}{r_1 - r_2} dr$$

$$\alpha_2 = \int_{-1}^{+1} \frac{r - r_1}{r_2 - r_1} dr$$

Since $r_2 = -r_1$, we obtain $\alpha_1 = \alpha_2 = 1.0$.

EXAMPLE 5.39: Use two-point Gauss quadrature to evaluate the integral $\int_0^3 (2^r - r) dr$ considered in Examples 5.35 and 5.36.

Using two-point Gauss quadrature, we obtain from (5.144),

$$\int_0^3 (2^r - r) dr \doteq \alpha_1 F(r_1) + \alpha_2 F(r_2) \tag{a}$$

where α_1, α_2 and r_1, r_2 are weights and sampling points, respectively. Since the interval is from 0 to 3, we need to determine the values α_1, α_2, r_1 , and r_2 from the values given in Table 5.6,

$$\alpha_1 = \frac{3}{2}(1); \quad \alpha_2 = \frac{3}{2}(1)$$

$$r_1 = \frac{3}{2}\left(1 - \frac{1}{\sqrt{3}}\right); \quad r_2 = \frac{3}{2}\left(1 + \frac{1}{\sqrt{3}}\right)$$

where $1/\sqrt{3} = 0.5773502692$. Thus,

$$F(r_1) = 0.91785978; \quad F(r_2) = 2.78916389$$

and (a) gives $\int_0^3 (2^r - r) dr \doteq 5.56053551$

The Gauss-Legendre integration procedure is commonly used in isoparametric finite element analysis. However, it should be noted that other integration schemes, in which both the weights and sampling positions are varied to obtain maximum accuracy, have also been derived (see C. E. Fröberg [A] and A. H. Stroud and D. Secrest [A]).

5.5.4 Integrations in Two and Three Dimensions

So far we have considered the integration of a one-dimensional function $F(r)$. However, two- and three-dimensional integrals need to be evaluated in two- and three-dimensional finite element analyses. In the evaluation of rectangular elements, we can apply the above one-dimensional integration formulas successively in each direction.⁸ As in the analytical evaluation of multidimensional integrals, in this procedure, successively, the innermost integral is evaluated by keeping the variables corresponding to the other integrals constant. Therefore, we have for a two-dimensional integral,

$$\int_{-1}^{+1} \int_{-1}^{+1} F(r, s) dr ds = \sum_i \alpha_i \int_{-1}^{+1} F(r_i, s) ds \tag{5.151}$$

or
$$\int_{-1}^{+1} \int_{-1}^{+1} F(r, s) dr ds = \sum_{i,j} \alpha_i \alpha_j F(r_i, s_j) \tag{5.152}$$

and corresponding to (5.133), $\alpha_{ij} = \alpha_i \alpha_j$, where α_i and α_j are the integration weights for one-dimensional integration. Similarly, for a three-dimensional integral,

$$\int_{-1}^{+1} \int_{-1}^{+1} \int_{-1}^{+1} F(r, s, t) dr ds dt = \sum_{i,j,k} \alpha_i \alpha_j \alpha_k F(r_i, s_j, t_k) \tag{5.153}$$

and $\alpha_{ijk} = \alpha_i \alpha_j \alpha_k$. We should note that it is not necessary in the numerical integration to use the same quadrature rule in the two or three dimensions; i.e., we can employ different numerical integration schemes in the r , s , and t directions.

EXAMPLE 5.40: Given that the (i, j) th element of a stiffness matrix \mathbf{K} is $\int_{-1}^{+1} \int_{-1}^{+1} r^2 s^2 dr ds$. Evaluate the integral $\int_{-1}^{+1} \int_{-1}^{+1} r^2 s^2 dr ds$ using (1) Simpson's rule in both r and s , (2) Gauss quadrature in both r and s , and (3) Gauss quadrature in r and Simpson's rule in s .

1. Using Simpson's rule, we have

$$\begin{aligned} \int_{-1}^{+1} \int_{-1}^{+1} r^2 s^2 dr ds &= \int_{-1}^{+1} \frac{1}{3} [(1)(1) + (4)(0) + (1)(1)] s^2 ds \\ &= \int_{-1}^{+1} \frac{2}{3} s^2 ds = \frac{1}{3} \left[(1) \left(\frac{2}{3} \right) + (4)(0) + (1) \left(\frac{2}{3} \right) \right] = \frac{4}{9} \end{aligned}$$

2. Using two-point Gauss quadrature, we have

$$\begin{aligned} \int_{-1}^{+1} \int_{-1}^{+1} r^2 s^2 dr ds &= \int_{-1}^{+1} \left[(1) \left(\frac{1}{\sqrt{3}} \right)^2 + (1) \left(\frac{1}{\sqrt{3}} \right)^2 \right] s^2 ds \\ &= \int_{-1}^{+1} \frac{2}{3} s^2 ds = \frac{2}{3} \left[(1) \left(\frac{1}{\sqrt{3}} \right)^2 + (1) \left(\frac{1}{\sqrt{3}} \right)^2 \right] = \frac{4}{9} \end{aligned}$$

⁸ This results in much generality of the integration, but for special cases somewhat less costly procedures can be designed (see B. M. Irons [C]).

3. Finally, using Gauss quadrature in r and Simpson's rule in s , we have

$$\begin{aligned} \int_{-1}^{+1} \int_{-1}^{+1} \left[(1) \left(\frac{1}{\sqrt{3}} \right)^2 + (1) \left(\frac{1}{\sqrt{3}} \right)^2 \right] s^2 ds \\ = \int_{-1}^{+1} \frac{2}{3} s^2 ds = \frac{1}{3} \left[(1) \left(\frac{2}{3} \right) + (4)(0) + (1) \left(\frac{2}{3} \right) \right] = \frac{4}{9} \end{aligned}$$

We should note that these numerical integrations are exact because both integration schemes, i.e., Simpson's rule and two-point Gauss quadrature, integrate a parabola exactly.

The above procedure is directly applicable to the evaluation of matrices of quadrilateral elements in which all integration limits are -1 to $+1$. Hence, in the evaluation of a two-dimensional finite element, the integrations can be carried out for each entry of the stiffness and mass matrices and load vectors as illustrated in Example 5.40. Based on the information given in Table 5.6, some common Gauss quadrature rules for two-dimensional analysis are summarized in Table 5.7.

Considering next the evaluation of triangular and tetrahedral element matrices, however, the procedure given in Example 5.40 is not applicable directly because now the integration limits involve the variables themselves. A great deal of research has been spent on the development of suitable integration formulas for triangular domains, and here, too, formulas of the Newton-Cotes type (see P. Silvester [A]) and of the Gauss quadrature type are available (see P. C. Hammer, O. J. Marlowe, and A. H. Stroud [A] and G. R. Cowper [A]). As in the integration over quadrilateral domains, the Gauss quadrature rules are in general more efficient because they yield a higher integration accuracy for the same number of evaluations. Table 5.8 lists the integration stations and integration weights of the Gauss integration formulas published by G. R. Cowper [A].

5.5.5 Appropriate Order of Numerical Integration

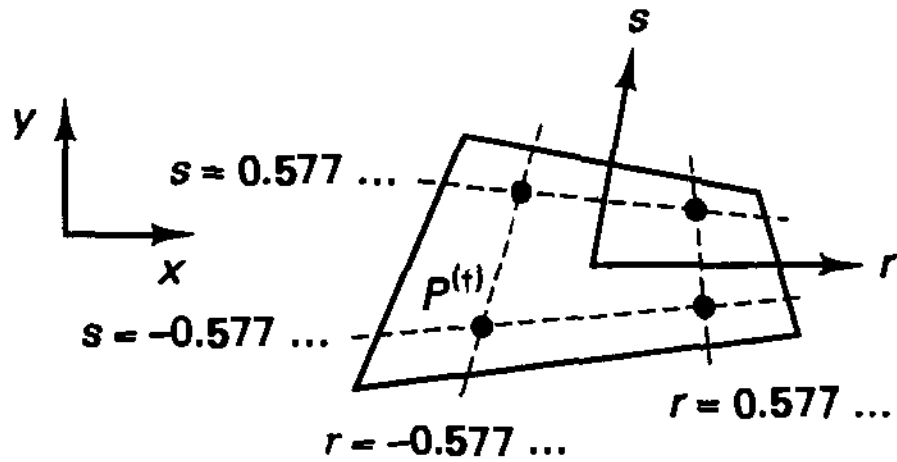
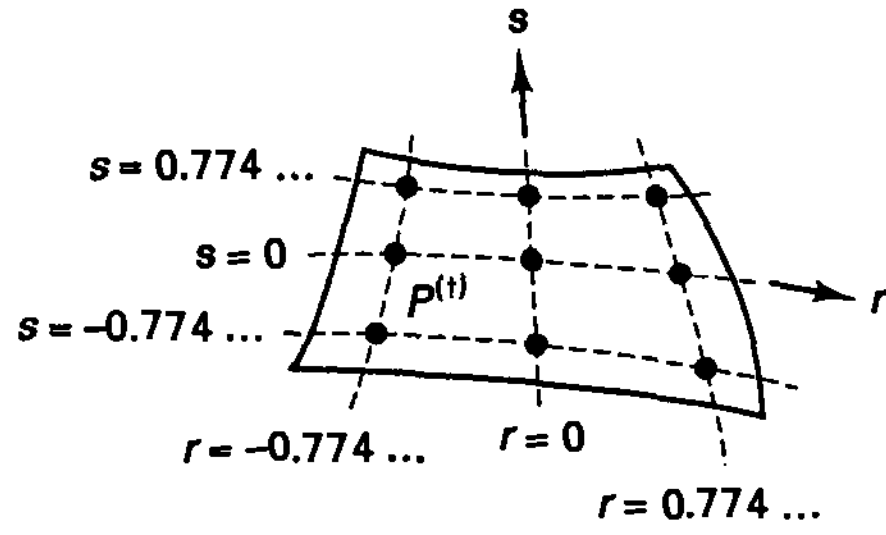
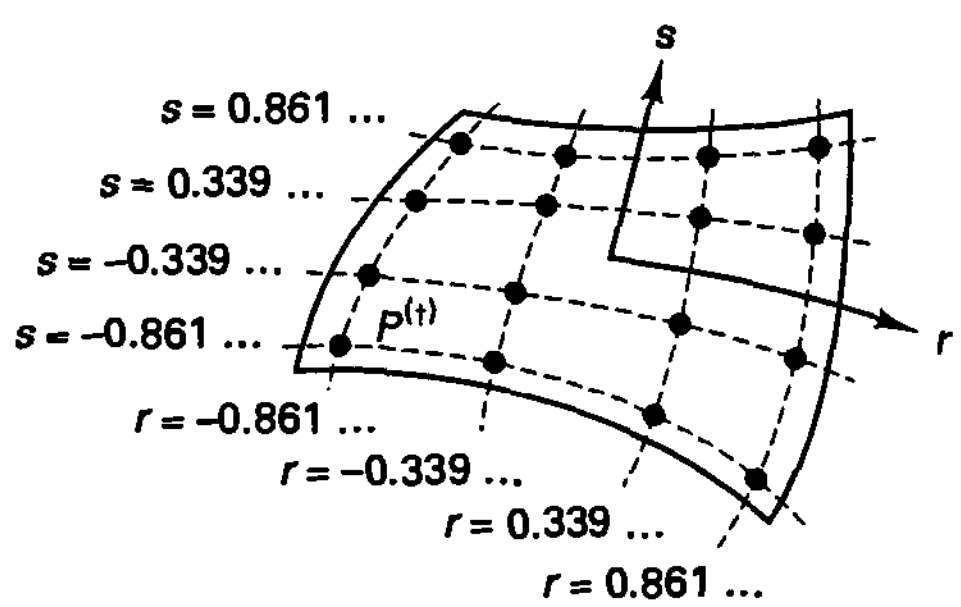
In the practical use of the numerical integration procedures presented in the previous section, basically two questions arise, namely, what kind of integration scheme to use, and what order to select. We pointed out that in using the Newton-Cotes formulas, $(n + 1)$ function evaluations are required to integrate without error a polynomial of order n . On the other hand, if Gauss quadrature is used, a polynomial of order $(2n - 1)$ is integrated exactly with only n function evaluations. In each case of course any polynomial of lower order than n and $(2n - 1)$, respectively, is also integrated exactly.

In finite element analysis a large number of function evaluations directly increases the cost of analysis, and the use of Gauss quadrature is attractive. However, the Newton-Cotes formulas may be efficient in nonlinear analysis for the reasons discussed in Section 6.8.4.

Having selected a numerical integration scheme, the order of numerical integration to be used in the evaluation of the various finite element integrals needs to be determined. The choice of the order of numerical integration is important in practice because, first, the cost of analysis increases when a higher-order integration is employed, and second, using a different integration order, the results can be affected by a very large amount. These considerations are particularly important in three-dimensional analysis.

The matrices to be evaluated by numerical integration are the stiffness matrix \mathbf{K} , the mass matrix \mathbf{M} , the body force vector \mathbf{R}_B , the initial stress vector \mathbf{R}_I , and the surface load

TABLE 5.7 Gauss numerical integrations over quadrilateral domains

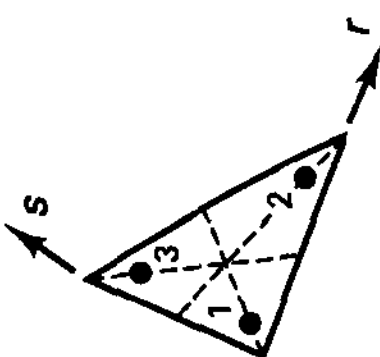
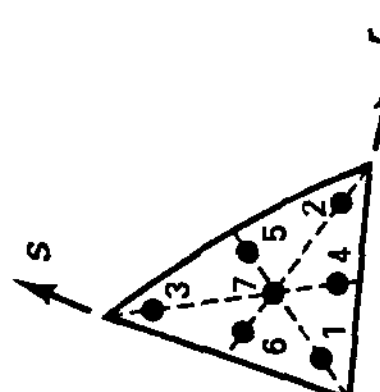
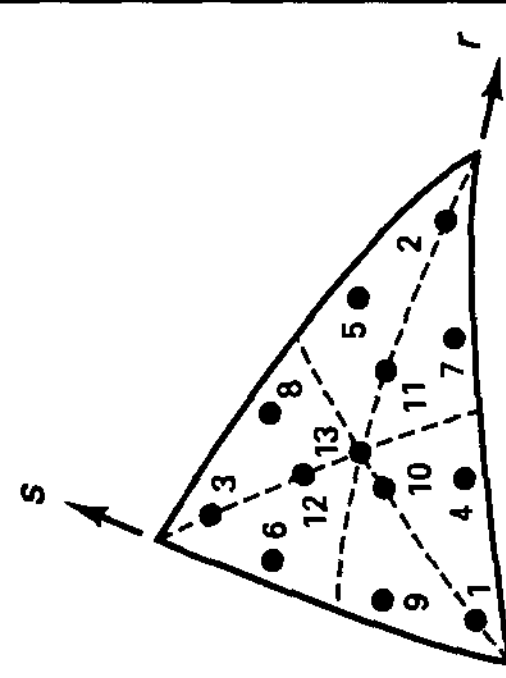
Integration order	Degree of precision	Location of integration points
2×2	3	
3×3	5	
4×4	7	

^(†)The location of any integration point in the x, y coordinate system is given by: $x_p = \sum_i h_i(r_p, s_p)x_i$ and $y_p = \sum_i h_i(r_p, s_p)y_i$. The integration weights are given in Table 5.6 using (5.152).

vector \mathbf{R}_S . In general, the appropriate integration order depends on the matrix that is evaluated and the specific finite element being considered. To demonstrate the important aspects, consider the Gauss numerical integration order required to evaluate the matrices of the continuum and structural elements discussed in Sections 5.3 and 5.4.

A first observation in the selection of the order of numerical integration is that, in theory, if a high enough order is used, all matrices will be evaluated very accurately. On the other hand, using too low an order of integration, the matrices may be evaluated very inaccurately and, in fact, the problem solution may not be possible. For example, consider an element stiffness matrix. If the order of numerical integration is too low, the matrix can have a larger number of zero eigenvalues than the number of physical rigid body modes. Hence, for a successful solution of the equilibrium equations alone, it would be necessary

TABLE 5.8 Gauss numerical integrations over triangular domains [$\iint F dr ds = \frac{1}{2} \sum w_i F(r_i, s_i)$]

Integration order	Degree of precision	Integration points	r-coordinates	s-coordinates	Weights
3-point	2		$r_1 = 0.16666$ $r_2 = 0.66666$ $r_3 = r_1$	$s_1 = r_1$ $s_2 = r_1$ $s_3 = r_2$	$w_1 = 0.33333$ $w_2 = w_1$ $w_3 = w_1$
7-point	5		$r_1 = 0.10128$ $r_2 = 0.79742$ $r_3 = r_1$ $r_4 = 0.47014$ $r_5 = r_4$ $r_6 = 0.05971$ $r_7 = 0.33333$	$s_1 = r_1$ $s_2 = r_1$ $s_3 = r_2$ $s_4 = r_6$ $s_5 = r_4$ $s_6 = r_4$ $s_7 = r_7$	$w_1 = 0.12593$ $w_2 = w_1$ $w_3 = w_1$ $w_4 = 0.13239$ $w_5 = w_4$ $w_6 = w_4$ $w_7 = 0.225$
13-point	7		$r_1 = 0.06513$ $r_2 = 0.86973$ $r_3 = r_1$ $r_4 = 0.31286$ $r_5 = 0.63844$ $r_6 = 0.04869$ $r_7 = r_5$ $r_8 = r_4$ $r_9 = r_6$ $r_{10} = 0.26034$ $r_{11} = 0.47930$ $r_{12} = r_{10}$ $r_{13} = 0.33333$	$s_1 = r_1$ $s_2 = r_1$ $s_3 = r_2$ $s_4 = r_6$ $s_5 = r_4$ $s_6 = r_5$ $s_7 = r_6$ $s_8 = r_5$ $s_9 = r_4$ $s_{10} = r_{10}$ $s_{11} = r_{10}$ $s_{12} = r_{11}$ $s_{13} = r_{13}$	$w_1 = 0.05334$ $w_2 = w_1$ $w_3 = w_1$ $w_4 = 0.07711$ $w_5 = w_4$ $w_6 = w_4$ $w_7 = w_4$ $w_8 = w_4$ $w_9 = w_4$ $w_{10} = 0.17561$ $w_{11} = w_{10}$ $w_{12} = w_{10}$ $w_{13} = -0.14957$

that the deformation modes corresponding to all zero eigenvalues of the element be properly restrained in the assemblage of finite elements because otherwise the structure stiffness matrix would be singular. A simple example is the evaluation of the stiffness matrix of a three-node truss element. If one-point Gauss numerical integration is used, the row and column corresponding to the degree of freedom at the midnode of the element are null vectors, which may result in a structure stiffness matrix that is singular. Therefore, the integration order should in general be higher than a certain limit.

The integration order required to evaluate a specific element matrix accurately can be determined by studying the order of the function to be integrated. In the case of the stiffness matrix, we need to evaluate

$$\mathbf{K} = \int_V \mathbf{B}^T \mathbf{C} \mathbf{B} \det \mathbf{J} dV \tag{5.154}$$

where \mathbf{C} is a constant material property matrix, \mathbf{B} is the strain-displacement matrix in the natural coordinate system r, s, t , $\det \mathbf{J}$ is the determinant of the Jacobian transforming local (or global) to natural coordinates (see Section 5.3), and the integration is performed over the element volume in the natural coordinate system. The matrix function \mathbf{F} to be integrated is, therefore,

$$\mathbf{F} = \mathbf{B}^T \mathbf{C} \mathbf{B} \det \mathbf{J} \tag{5.155}$$

The matrices \mathbf{J} and \mathbf{B} have been defined in Sections 5.3 and 5.4.

A case for which the order of the variables in \mathbf{F} can be evaluated with relative ease arises when the four-node two-dimensional element studied in Example 5.5 is used as a rectangular or parallelogram element. It is instructive to consider this case in detail because the procedure of evaluating the required integration order is displayed clearly.

EXAMPLE 5.41: Evaluate the required Gauss numerical integration order for the calculation of the stiffness matrix of a four-node displacement-based rectangular element.

The integration order to be used depends on the order of the variables r and s in \mathbf{F} defined in (5.155). For a rectangular element with sides $2a$ and $2b$, we can write

$$x = ar; y = bs$$

and consequently the Jacobian matrix \mathbf{J} is

$$\mathbf{J} = \begin{bmatrix} a & 0 \\ 0 & b \end{bmatrix}$$

Since the elements of \mathbf{J} are constant, referring to the information given in Example 5.5, the elements of the strain-displacement matrix \mathbf{B} are therefore functions of r or s only. But the determinant of \mathbf{J} is also constant; hence,

$$\mathbf{F} = f(r^2, rs, s^2)$$

where f denotes “function of.”

Using two-point Gauss numerical integration in the r and s directions, all functions in r and s involving at most cubic terms are integrated without error; e.g., for integration order n , the order of r and s integrated exactly is $(2n - 1)$. Hence, two-point Gauss integration is adequate.

Note that the Jacobian matrix \mathbf{J} is also constant for a four-node parallelogram element; hence, the same derivation and result are applicable.

In an analogous manner, the required integration order to evaluate exactly (or very accurately) the stiffness matrices, mass matrices, and element load vectors of other elements can be assessed. In this context it should be noted that the Jacobian matrix is not constant for nonrectangular and nonparallelogram element shapes, which may mean that a very high integration order might be required to evaluate the element matrices to high accuracy.

In the above example, a displacement-based element was considered, but we should emphasize that, of course, the same numerical integration schemes are also used in the evaluation of the element matrices of mixed formulations. Hence, in mixed formulations the required integration order must also be identified using the procedure just discussed (see Exercise 5.57).

In studying which integration order to use for geometrically distorted elements, we recognize that it is frequently not necessary to calculate the matrices to very high precision using a very high order of numerical integration. Namely, the change in the matrix entries (and their effects) due to using an order of l instead of $(l - 1)$ may be negligible. Hence, we need to ask what order of integration is generally sufficient, and we present the following guideline.

We recommend that *full numerical integration*⁹ always be used for a displacement-based or mixed finite element formulation, where we define “full” numerical integration as the order that gives the exact matrices (i.e., the analytically integrated values) when the elements are geometrically undistorted. Table 5.9 lists this order for elements used in two-dimensional analyses.


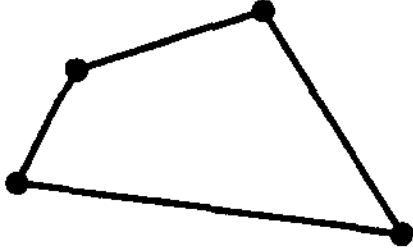
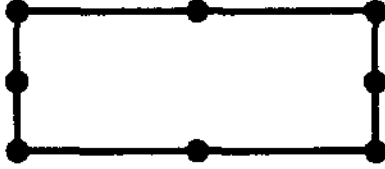
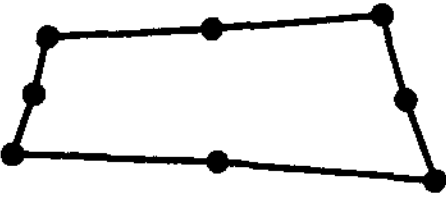
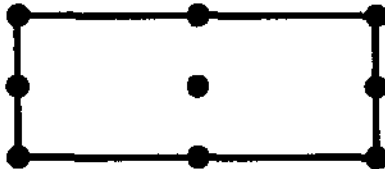
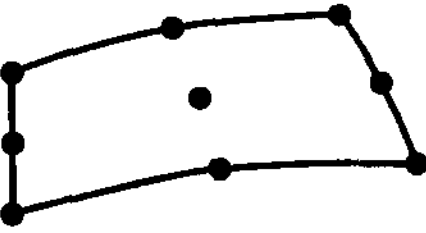
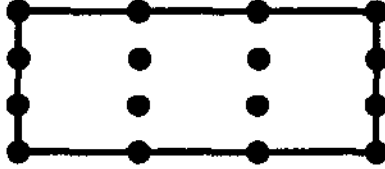
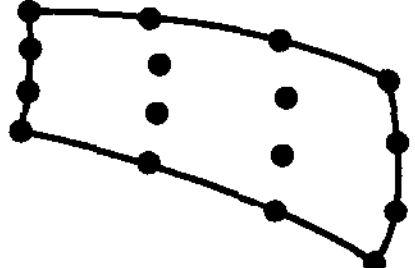
Using this integration order for a geometrically distorted element will not yield the exactly integrated element matrices. The analysis is, however, reliable because the numerical integration errors are acceptably small assuming of course reasonable geometric distortions. Indeed, as shown by P. G. Ciarlet [A], if the geometric distortions are not excessive and are such that in exact integration the full order of convergence is still obtained (with the provisions discussed in Section 5.3.3), then that same order of convergence is also obtained using the full numerical integration recommended here. Hence, in that case, the order of numerical integration recommended in Table 5.9 does not result in a reduction of the order of convergence. On the other hand, if the element geometric distortions are very large, and in nonlinear analysis of course, a higher integration order may be appropriate (see Section 6.8.4).

Figure 5.39 shows some results obtained in the solution of the ad-hoc test problem described in Fig. 4.12. These results were obtained using sequences of distorted, quasi-uniform meshes. Figure 5.39(a) describes the geometric distortions used, and Fig. 5.39(b) and (c) show the convergence results obtained with the eight-node and nine-node elements using the Gauss integration order in Table 5.9. These results show that the order of convergence (the slopes of the graphed curves when h is small) is approximately 4 in all cases (as is theoretically predicted). However, the actual value of the error for a given value of h is larger when the elements are distorted. That is, the constant c in (4.102) increases as the elements are distorted.

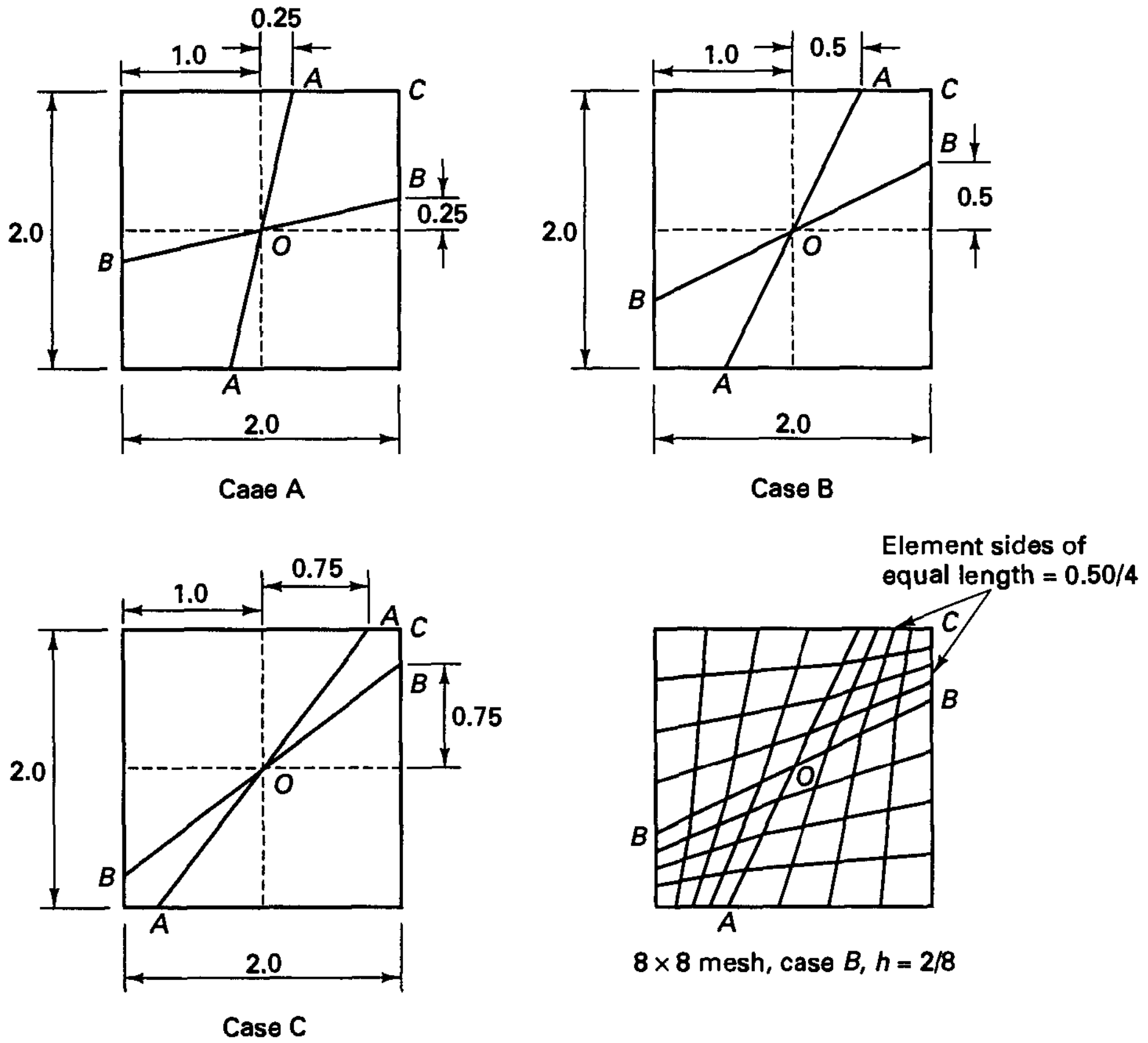
The reason for recommending the numerical integration orders in Table 5.9 is that the *reliability of the finite element procedures is of utmost concern* (see Section 1.3), and if an

⁹In Section 5.5.6 we briefly discuss “reduced” numerical integration, which is the counterpart of full numerical integration.

TABLE 5.9 Recommended full Gauss numerical integration orders for the evaluation of isoparametric displacement-based element matrices (use of Table 5.7)

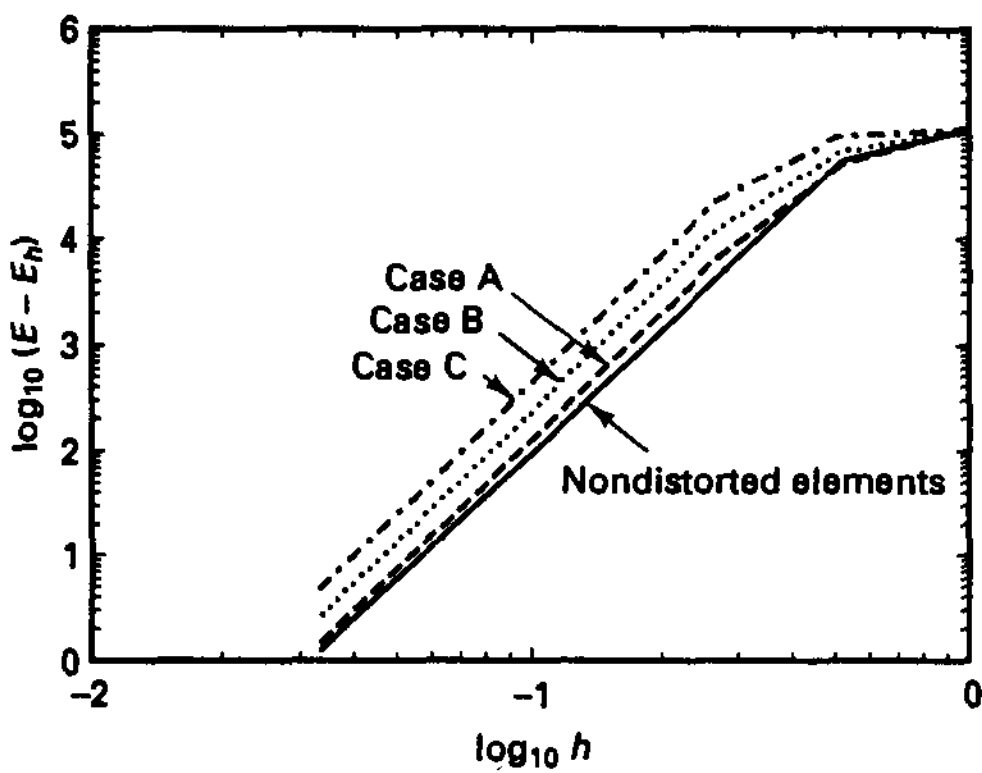
	Two-dimensional elements (plane stress, plane strain and axisymmetric conditions)	Integration order
4-node		2 × 2
4-node distorted		2 × 2
8-node		3 × 3
8-node distorted		3 × 3
9-node		3 × 3
9-node distorted		3 × 3
16-node		4 × 4
16-node distorted		4 × 4

(Note: In axisymmetric analysis, the hoop strain effect is in all cases not integrated exactly, but with sufficient accuracy.)

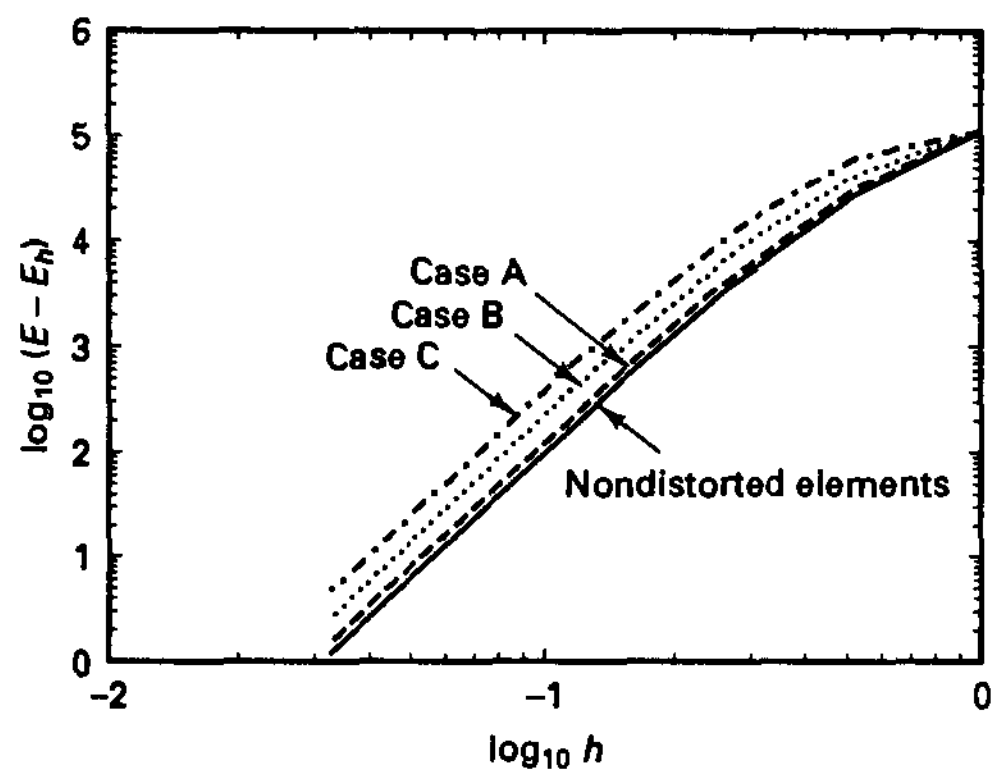


The lines AA and BB are drawn, and then the sides AC , CB , BO , OA are subdivided into equal lengths to form the elements in the domain $ACBO$. Similarly for the other three domains.

(a) Distortions used



(b) Results using 8-node elements



(c) Results using 9-node elements

Figure 5.39 Solution of test problem of Fig. 4.12 with geometrically distorted elements, and the Gauss integration order of Table 5.9. $E = a(\mathbf{u}, \mathbf{u})$, $E_h = a(\mathbf{u}_h, \mathbf{u}_h)$

integration order lower than the “full” order is used (for a displacement-based or a mixed formulation), the analysis is in general unreliable.

An interesting case is the rectangular two-dimensional plane stress eight-node displacement-based isoparametric element evaluated with 2×2 Gauss integration. This integration order yields an element stiffness matrix with one spurious zero energy mode (see Exercise 5.56); that is, the element matrix not only has three zero eigenvalues (corresponding to the physical rigid body motions) but also has one additional zero eigenvalue that is purely a result of using too low an order of integration. Figure 5.40 shows a very simple analysis case using a single eight-node element with 2×2 Gauss integration in which the model is unstable; that is, if the solution is obtained, the calculated nodal point displacements are very large and have no resemblance to the correct solution.¹⁰ In this simple analysis it is readily seen that the eight-node element using 2×2 Gauss integration is inadequate, and it can be argued that in more complex analysis the (single) spurious zero energy mode is usually adequately restrained in an assemblage of elements. However, in a large, complex model, in general, elements with spurious zero energy modes in an uncontrolled manner improve the overall solution results, introduce large errors, or result in an unstable solution.

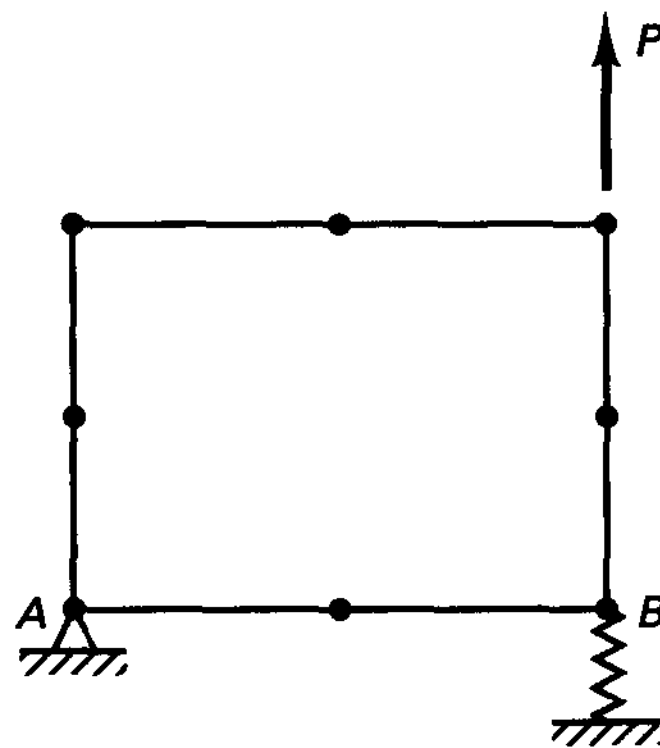


Figure 5.40 Eight-node plane stress element supported at B by a spring. Analysis unstable with 2×2 Gauss integration.

As an example, let us consider the dynamic analysis of the cantilever bracket shown in Fig. 5.41 and use the nine-node displacement-based element with 2×2 Gauss integration, in which case each element stiffness matrix has three spurious zero energy modes. We have considered this bracket already in Fig. 4.20, but with two pin supports instead of the fixed condition used now. (As noted there, the 16-element model of the pin-supported bracket using 2×2 Gauss integration for the element stiffness matrices was unstable). The frequency solution of the 16-element mesh of nine-node displacement-based elements representing the clamped cantilever bracket gives the results listed in Table 5.10. This table shows that the use of 2×2 Gauss integration (referred to as reduced integration; see Section 5.5.6) does not result in a spurious zero energy mode of the complete model (because the bracket is clamped at its left end) but in one *spurious nonzero* energy mode that is part of the predicted smallest six frequencies. Such modes of no physical reality—which we refer to also as “phantom” modes—can introduce uncontrolled errors into a

¹⁰ In exact arithmetic the stiffness matrix is singular, but because of round-off errors in the computations a solution is usually obtained.

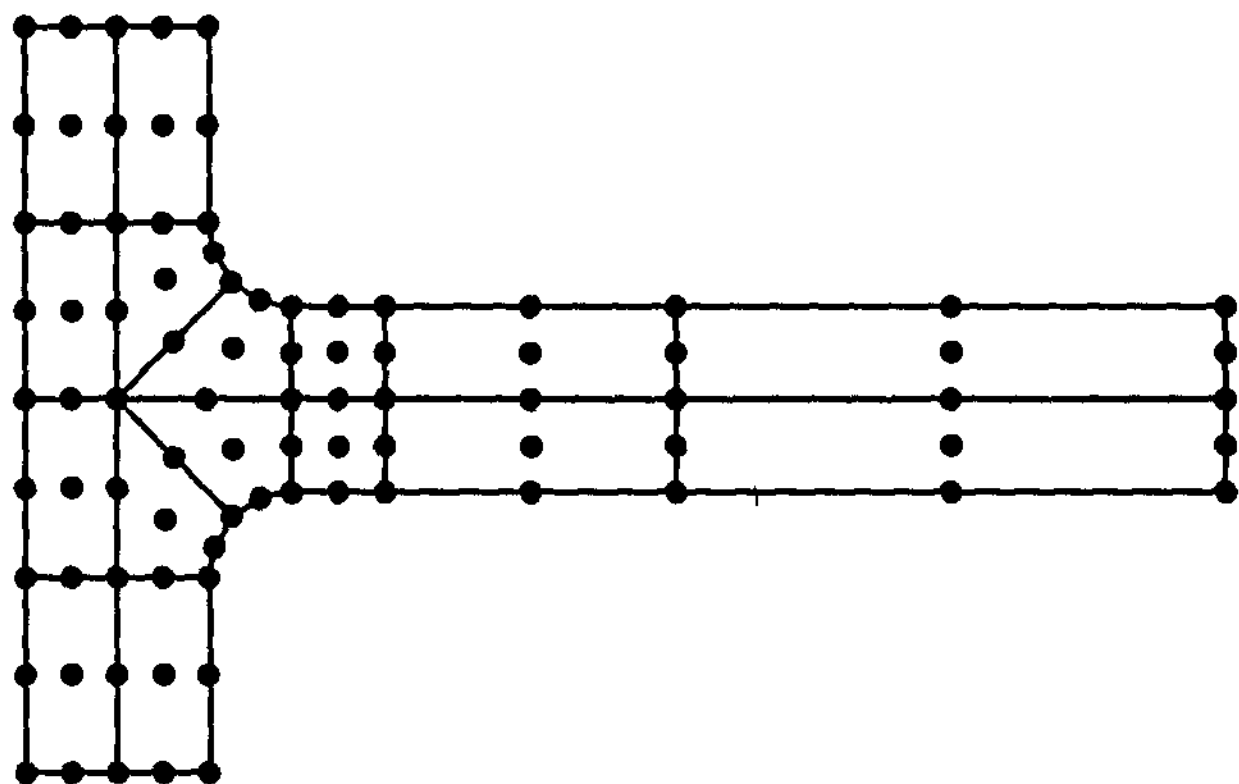
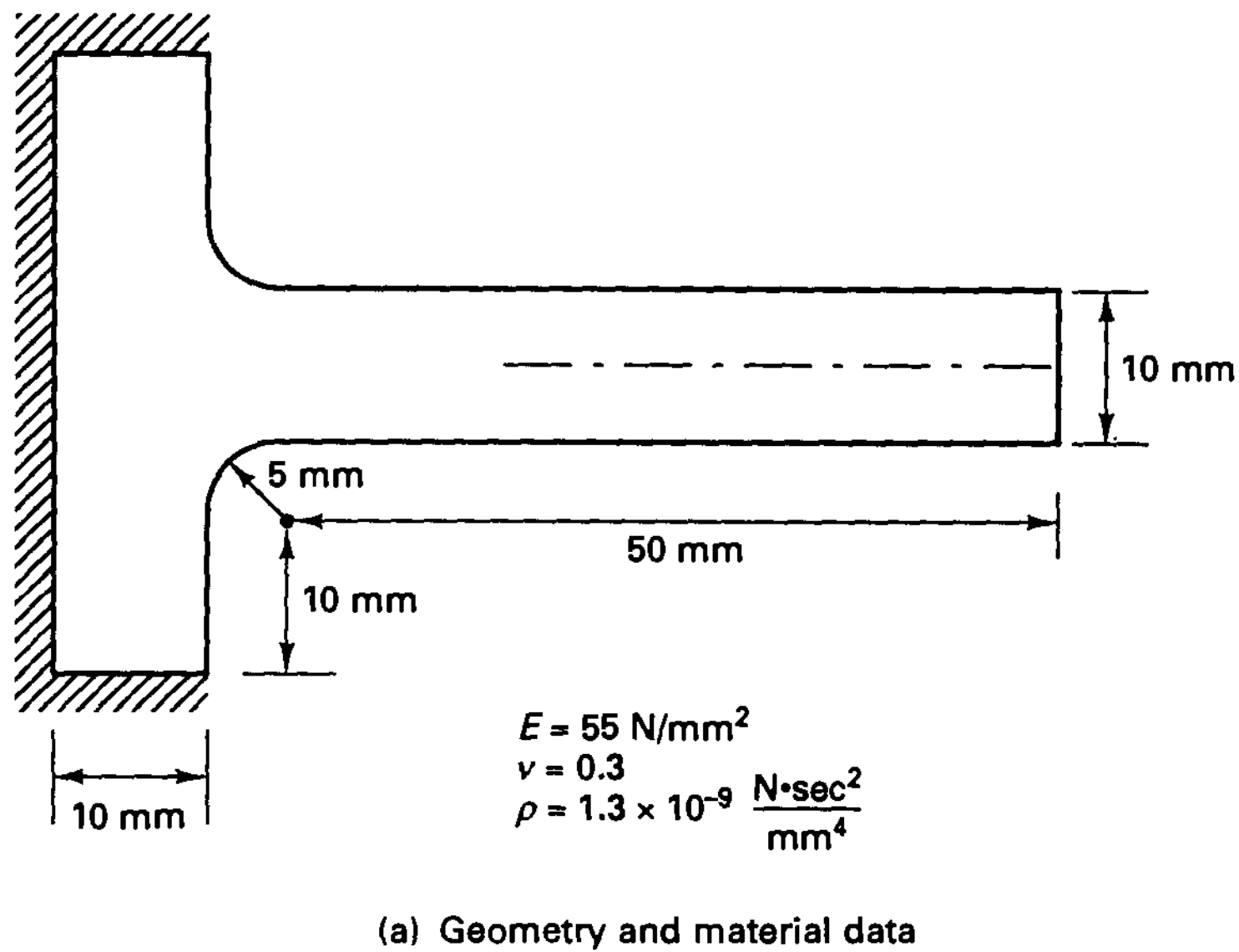


Figure 5.41 Frequency solution of clamped cantilever bracket

dynamic step-by-step solution¹¹ that may not be easily detectable, and even if these errors are detected, the analysis would require additional solution attempts all of which may result in extensive and undesirable numerical experimentation.

For these reasons any element with a spurious zero energy mode should not be used in engineering practice, in linear or in nonlinear analysis, and we therefore do not discuss such elements in this book. However, we should mention that to prevent the deleterious effects of spurious modes, significant research efforts have been conducted to control their

¹¹ The mode shapes of phantom frequencies may indicate that the response is not physical, but in a dynamic step-by-step solution, the frequencies and mode shapes are normally not calculated.

TABLE 5.10 *Smallest six frequencies (in Hz) of the 16-element mesh in Fig. 5.41(b) using a consistent mass matrix[†]*

Mode number	16-element model		16 × 64 element model, [‡] 3 × 3 Gauss integration
	3 × 3 Gauss integration	2 × 2 Gauss integration	
1	112.4	110.5	110.6
2	634.5	617.8	606.4
3	906.9	905.5	905.2
4	1548	958.4 [§]	1441
5	2654	1528	2345
6	2691	2602	2664

[†]The element consistent mass matrices are always integrated using 3 × 3 Gauss integration.

[‡]We include the results using a fine mesh (with 64 elements replacing each nine-node element of the 16-element mesh) for comparison purposes.

[§]Spurious i.e., phantom mode.

behavior (see, for example, T. Belytschko, W. K. Liu, J. S.-J. Ong, and D. Lam [A] and T. J. R. Hughes [A]).

In the above discussion we focused attention on the evaluation of the element stiffness matrices. Considering the element force vectors, it is usually good practice to employ the same integration scheme and the same order of integration as for the stiffness matrices. For the evaluation of an element mass matrix, it should be recognized that for a lumped mass matrix only the volume of the element needs to be evaluated correctly and for the consistent mass matrix the order given in Table 5.9 is usually appropriate. However, special cases exist in which for the sufficiently accurate evaluation of a consistent mass matrix a higher-order integration may be necessary than in the calculation of the stiffness matrix.

EXAMPLE 5.42: Evaluate the stiffness and mass matrices and the body force vector of element 2 in Example 4.5 using Gauss numerical integration.

The expressions to be integrated have been derived in Example 4.5,

$$\mathbf{K} = E \int_0^{80} \left(1 + \frac{x}{40}\right)^2 \begin{bmatrix} -\frac{1}{80} \\ 1 \\ \frac{1}{80} \end{bmatrix} \begin{bmatrix} -\frac{1}{80} & \frac{1}{80} \end{bmatrix} dx \quad (\text{a})$$

$$\mathbf{M} = \rho \int_0^{80} \left(1 + \frac{x}{40}\right)^2 \begin{bmatrix} 1 - \frac{x}{80} \\ \frac{x}{80} \end{bmatrix} \begin{bmatrix} \left(1 - \frac{x}{80}\right) & \frac{x}{80} \end{bmatrix} dx \quad (\text{b})$$

$$\mathbf{R}_B = \frac{1}{10} \int_0^{80} \left(1 + \frac{x}{40}\right)^2 \begin{bmatrix} 1 - \frac{x}{80} \\ \frac{x}{80} \end{bmatrix} dx \quad (\text{c})$$

The expressions in (a) and (c) are integrated exactly with two-point integration, whereas the evaluation of the integral in (b) requires three-point integration. A higher-order integration is required in the evaluation of the mass matrix because this matrix is obtained from the displacement interpolation functions, whereas the stiffness matrix is calculated using derivatives of the displacement functions.

Using one-, two-, and three-point Gauss integration to evaluate (a), (b), and (c) we obtain
One-point integration:

$$\mathbf{K} = \frac{12E}{240} \begin{bmatrix} 1 & -1 \\ -1 & 1 \end{bmatrix}; \quad \mathbf{M} = \frac{\rho}{6} \begin{bmatrix} 480 & 480 \\ 480 & 480 \end{bmatrix}; \quad \mathbf{R}_B = \frac{1}{6} \begin{bmatrix} 96 \\ 96 \end{bmatrix}$$

Two-point integration:

$$\mathbf{K} = \frac{13E}{240} \begin{bmatrix} 1 & -1 \\ -1 & 1 \end{bmatrix}; \quad \mathbf{M} = \frac{\rho}{6} \begin{bmatrix} 373.3 & 346.7 \\ 346.7 & 1013.3 \end{bmatrix}; \quad \mathbf{R}_B = \frac{1}{6} \begin{bmatrix} 72 \\ 136 \end{bmatrix}$$

Three-point integration:

$$\mathbf{K} = \frac{13E}{240} \begin{bmatrix} 1 & -1 \\ -1 & 1 \end{bmatrix}; \quad \mathbf{M} = \frac{\rho}{6} \begin{bmatrix} 384 & 336 \\ 336 & 1024 \end{bmatrix}; \quad \mathbf{R}_B = \frac{1}{6} \begin{bmatrix} 72 \\ 136 \end{bmatrix}$$

It is interesting to note that with too low an order of integration the total mass of the element and the total load to which the element is subjected are not taken fully into account.

Table 5.9 summarizes the results of an analysis for the appropriate integration orders in the evaluation of the stiffness matrices of two-dimensional elements. Of course, the information given in the table is also valuable in deducing appropriate orders of integration for the calculation of the matrices of other elements.

EXAMPLE 5.43: Discuss the required integration order for the evaluation of the MITC9 plate and isoparametric three-dimensional elements shown in Fig. E5.43.

Consider the plate element first. The integration in the r, s plane corresponds in essence to the evaluation of the nine-node element in Table 5.9. In general, this integration order of 3×3 will also be effective when the element is used in distorted form.

The required integration order for the evaluation of the stiffness matrix of the three-dimensional solid element can also be deduced from the information given in Table 5.9. The displacements vary linearly in the r direction; hence, two-point integration is sufficient. In the

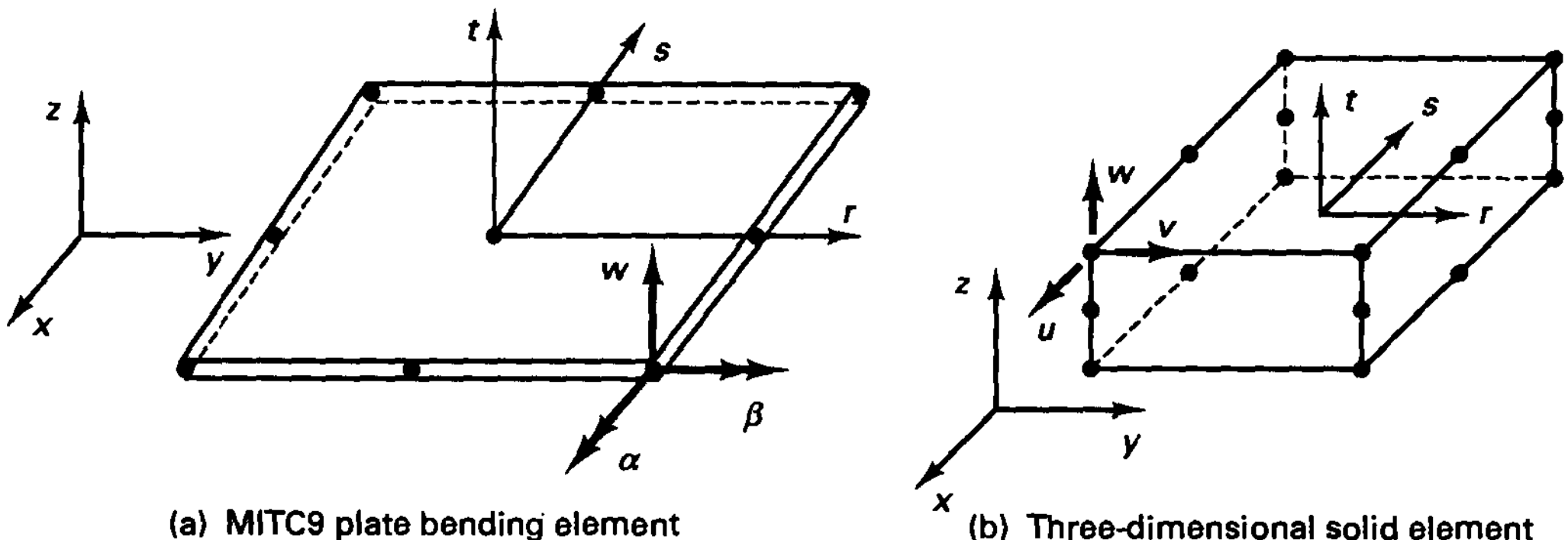


Figure E5.43 Elements considered in Example 5.43

t, s planes, i.e., at r equal to constants, the element displacements correspond to those of the eight-node element in Table 5.9. Hence, $2 \times 3 \times 3$ Gauss integration is required to evaluate the element stiffness matrix exactly.

5.5.6 Reduced and Selective Integration

Table 5.9 gives the recommended Gauss numerical integration orders for two-dimensional isoparametric displacement-based elements, and the recommended orders for other elements can be deduced (see Example 5.43). With these integration orders (referred to as “full” integration), the element matrices of geometrically undistorted elements are evaluated exactly, whereas for geometrically distorted elements a sufficiently accurate approximation is obtained (unless the geometric distortions are very large, in which case a higher integration order is recommended).

However, in view of our discussion in Section 4.3.4, we recall that the displacement formulation of finite element analysis yields a strain energy smaller than the exact strain energy of the mathematical/mechanical model being considered, and physically, a displacement formulation results in overestimating the system stiffness. Therefore, we may expect that by not evaluating the displacement-based element stiffness matrices accurately in the numerical integration, better overall solution results can be obtained. This should be the case if the error in the numerical integration compensates *appropriately* for the overestimation of structural stiffness due to the finite element discretization. In other words, a reduction in the order of the numerical integration from the order that is required to evaluate the element stiffness matrices exactly (for geometrically undistorted elements) may be expected to lead to improved results. When such a reduction in the order of numerical integration is used, we refer to the procedure as *reduced integration*. For example, the use of 2×2 Gauss integration (although not recommended for use in practice; see Section 5.5.5) for the nine-node isoparametric element stiffness matrix corresponds to a reduced integration. In addition to merely using a *reduced* integration order, *selective* integration may also be considered, in which case different strain terms are integrated with different orders of integration. In these cases of reduced and selective numerical integration the specific integration scheme should be regarded as an integral part of the element formulation.

The key question as to whether a reduced and/or selectively integrated element can be recommended for practical use is: Has the element formulation (using the specific integration procedure) been sufficiently tested and analyzed for its stability and convergence? If tractable, a mathematical stability and convergence analysis is of course most desirable.

A natural first step in such an analysis is to view the reduced and/or selectively integrated element as a mixed element (see D. S. Malkus and T. J. R. Hughes [A]). (An example is the two-node mixed interpolated beam element in Section 5.4.1 further mentioned below.) Once the exact equivalence between the reduced and/or selectively integrated element and a mixed formulation has been identified, the second step is to analyze the mixed formulation for stability and convergence and in this way obtain a deep understanding of the element based on the reduced/selective integration.

Since there are many possibilities for assumptions in mixed formulations, it is natural to assume that there exists a mixed formulation that is equivalent to the reduced/selective integrated element and seek that formulation for analysis purposes. However, the mere fact

that *in general* reduced/selectively integrated elements can be regarded as mixed formulations does not justify the use of reduced integration because of course not every mixed formulation represents a reliable and efficient finite element scheme. Rather, *this equivalence* (with the details to be identified in each specific case) *only points toward an approach for the analysis of reduced/selectively integrated elements.*

It also follows that *once a complete equivalence has been identified, we can consider the reduced/selective integration as merely an effective way to accurately calculate the finite element matrices of the mixed formulation,* and we adopt here this view and interpretation of reduced and selective integration.

A relatively simple example is the isoparametric two-node beam element based on one-point (r -direction) Gauss integration. In Example 4.30 and Section 5.4.1 we showed that this element is completely equivalent to the beam element obtained using the Hu-Washizu variational principle with linearly varying transverse displacement w , section rotation β , and a constant shear strain γ within each element. The stability and convergence of the element were considered in Section 4.5.7 where we showed that the ellipticity and inf-sup conditions are satisfied.

Let us consider the following additional example to emphasize these observations.

EXAMPLE 5.44: A simple triangular plate bending element can be derived using the isoparametric displacement formulation in Section 5.4.2 but integrating the stiffness matrix terms with one-point integration. This integration evaluates the stiffness matrix terms corresponding to bending exactly, whereas the terms corresponding to the transverse shear are integrated approximately. Hence, the element stiffness matrix is based on reduced integration (or we may also say selective integration because only the shear terms are not integrated exactly).

Derive a variational formulation and the stiffness matrix for this element.

The element and its variational formulation have been presented by J.-L. Batoz, K. J. Bathe, and L. W. Ho [A]. We note that the element is a natural development when we are aware of the success of the one-point integrated isoparametric beam element (see Example 4.30 and Sections 4.5.7 and 5.4.1). This beam element has a strong variational basis, the mathematical analysis ensures good convergence properties, and computationally the element is simple and effective.

For the development of the variational basis of this plate element, we note that the one-point integration implicitly assumes a constant transverse shear strain (as in the isoparametric one-point integrated two-node beam element). Referring to Example 4.30, we can therefore directly establish the variational indicator for the plate element as

$$\tilde{\Pi}_{HR}^* = \int_A \left(\frac{1}{2} \boldsymbol{\kappa}^T \mathbf{C}_b \boldsymbol{\kappa} + \boldsymbol{\gamma}^T \mathbf{C}_s \boldsymbol{\gamma}^{AS} - \frac{1}{2} \boldsymbol{\gamma}^{AS T} \mathbf{C}_s \boldsymbol{\gamma}^{AS} \right) dA - \int_A w p dA + \text{boundary terms} \quad (a)$$

where $\boldsymbol{\kappa}$, \mathbf{C}_b , $\boldsymbol{\gamma}$, \mathbf{C}_s have been defined in (5.95) to (5.97) and $\boldsymbol{\gamma}^{AS}$ contains the assumed transverse shear strains

$$\boldsymbol{\gamma}^{AS} = \begin{bmatrix} \gamma_{xz}^{AS} \\ \gamma_{yz}^{AS} \end{bmatrix} = \text{constant}$$

The relation in (a) is a modified Hellinger-Reissner functional. Substituting the interpolations for w , β_x , and β_y into $\boldsymbol{\kappa}$ and $\boldsymbol{\gamma}$, integrating over the element midsurface area A , and invoking the stationarity of $\tilde{\Pi}_{HR}^*$ with respect to the nodal point variables $\hat{\mathbf{u}}$,

$$\hat{\mathbf{u}} = \begin{bmatrix} w_1 \\ \theta_x^1 \\ \theta_y^1 \\ \vdots \\ \theta_y^3 \end{bmatrix}$$

and $\boldsymbol{\gamma}^{AS}$, we obtain

$$\begin{bmatrix} \mathbf{K}_b & \mathbf{G}^T \\ \mathbf{G} & -\mathbf{D} \end{bmatrix} \begin{bmatrix} \hat{\mathbf{u}} \\ \boldsymbol{\gamma}^{AS} \end{bmatrix} = \begin{bmatrix} \mathbf{R} \\ \mathbf{0} \end{bmatrix}$$

where

$$\mathbf{K}_b = \int_A \mathbf{B}_b^T \mathbf{C}_b \mathbf{B}_b dA$$

$$\mathbf{D} = \int_A \mathbf{C}_s dA = A \mathbf{C}_s$$

$$\mathbf{G} = \mathbf{C}_s \int_A \mathbf{B}_s dA$$

and \mathbf{B}_b and \mathbf{B}_s are strain-displacement matrices,

$$\boldsymbol{\kappa} = \mathbf{B}_b \hat{\mathbf{u}}$$

$$\boldsymbol{\gamma} = \mathbf{B}_s \hat{\mathbf{u}}$$

Using static condensation, we obtain the stiffness matrix of the element with respect to the nodal point variables only,

$$\mathbf{K} = \mathbf{K}_b + \mathbf{G}^T \mathbf{D}^{-1} \mathbf{G}$$

As we discussed in Section 5.4.2, the pure displacement-based isoparametric plate element (i.e., using full numerical integration for the bending and transverse shear terms in the displacement-based stiffness matrix) is much too stiff (displays the shear locking phenomenon). The presentation in Example 5.44 shows that the one-point integrated element has a variational basis quite analogous to the basis of the one-point integrated isoparametric beam element. However, whereas the beam element is reliable and effective, the plate element stiffness matrix in Example 5.44 has a spurious zero eigenvalue and hence the element is unreliable and should not be used in practice (as was pointed out by J.-L. Batoz, K. J. Bathe, and L. W. Ho [A]).

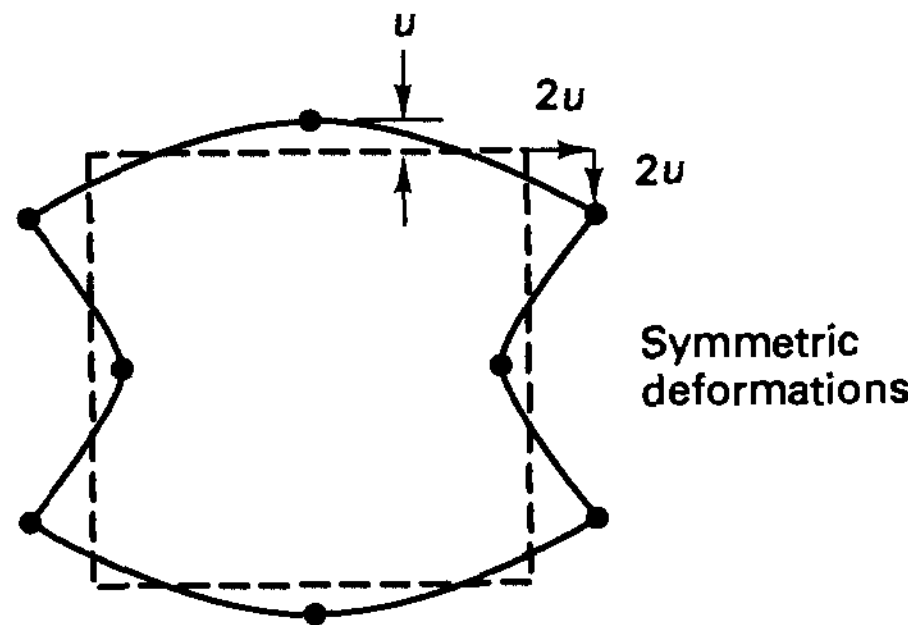
The important point of this example is that a variational basis of an element might well exist, but whether the element is useful and effective can of course be determined only by a deeper analysis of the formulation.

The equivalence between a certain isoparametric reduced or selectively integrated displacement-based element and a mixed formulation may also hold only for specific geometric element shapes and may also no longer be valid when nonisotropic material laws (or geometric nonlinearities) are introduced. An analysis of the effects of each of these conditions should then be performed.

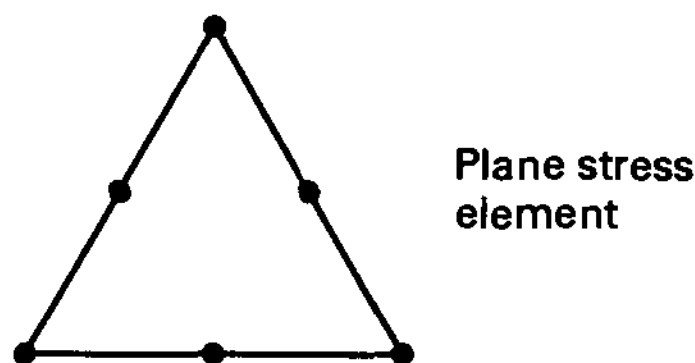
5.5.7 Exercises

- 5.53. Evaluate the Newton-Cotes constants when the interpolating polynomial is of order 3, i.e., $\psi(r)$ is a cubic.
- 5.54. Derive the sampling points and weights for three-point Gauss integration.

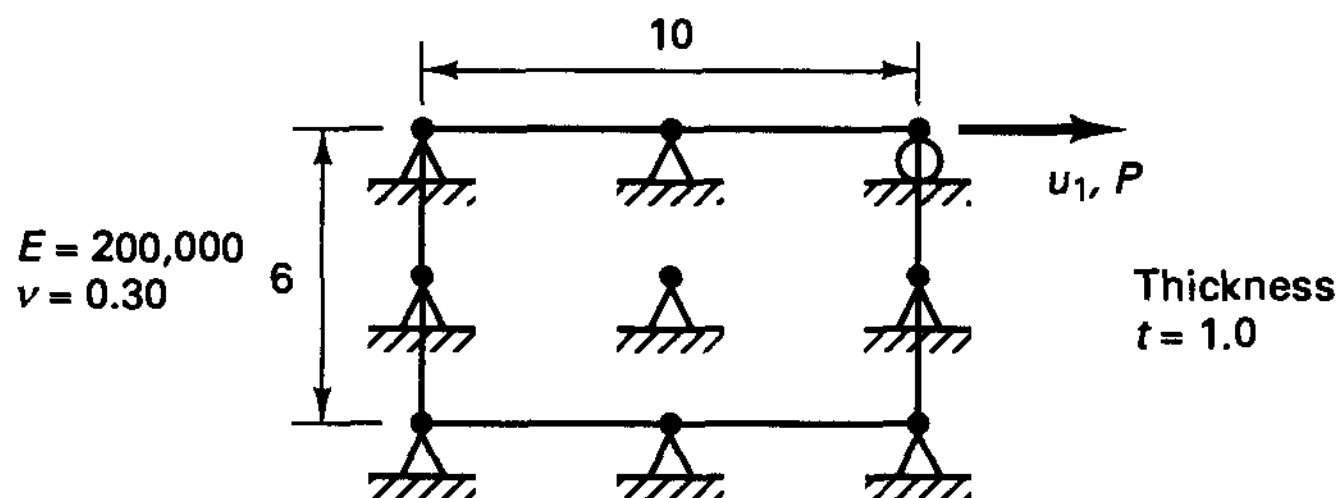
- 5.55. Show that 3×3 Gauss numerical integration is sufficient to calculate the stiffness and mass matrices of a nine-node geometrically undistorted displacement-based element for axisymmetric analysis.
- 5.56. Show that 2×2 Gauss integration of the stiffness matrix of the eight-node plane stress displacement-based square element results in the spurious zero energy mode shown. (*Hint:* You need to show that $\mathbf{B}\hat{\mathbf{u}} = \mathbf{0}$ for the given displacements.)



- 5.57. Consider the $9/3$ u/p element and show that 3×3 Gauss integration of a geometrically undistorted element gives the exact stiffness matrix. Also, show that 2×2 Gauss integration is not adequate.
- 5.58. Identify the required integration order for full integration of the stiffness matrix of the six-node displacement-based triangular element when using the Gauss integration in Table 5.8.



- 5.59. Consider the nine-node plane stress element shown. All nodal point displacements are fixed except that u_1 is free. Calculate the displacement u_1 due to the load P .
- (a) Use analytical integration to evaluate the stiffness coefficient.
- (b) Use 1×1 , 2×2 , and 3×3 Gauss numerical integration to evaluate the stiffness coefficient. Compare your results.



- 5.60. Consider the evaluation of lumped mass matrices for the elements shown in Table 5.9. Determine suitable Gauss integration orders for the evaluation of these matrices.

- 5.61. Consider the plate bending element formulation in Example 5.29. Assume that the element stiffness matrix is evaluated with one-point Gauss integration. Show that this element has spurious zero energy modes.¹²
- 5.62. Consider the plate bending element formulation in Example 5.29 and assume that the bending strain energy is evaluated with 2×2 Gauss integration and the shear strain energy is evaluated with one-point Gauss integration. Show that this element has spurious zero energy modes.¹²

5.6 COMPUTER PROGRAM IMPLEMENTATION OF ISOPARAMETRIC FINITE ELEMENTS

In Section 5.3 we discussed the isoparametric finite element formulation and gave the specific expressions needed in the calculation of four-node plane stress (or plane strain) elements (see Example 5.5). An important advantage of isoparametric element evaluations is the similarity between the calculations of different elements. For example, the calculation of three-dimensional elements is a relatively simple extension from the calculation of two-dimensional elements. Also, in one subroutine, elements with a variety of nodal point configurations can be calculated if an algorithm for selecting the appropriate interpolation functions is used (see Section 5.3).

The purpose of this section is to provide an actual computer program for the calculation of the stiffness matrix of four-node isoparametric elements. In essence, SUBROUTINE QUADS is the computer program implementation of the procedures presented in Example 5.5. In addition to plane stress and plane strain, axisymmetric conditions can be considered. It is believed that by showing the actual program implementation of the element, the relative ease of implementing isoparametric elements is best demonstrated. The input and output variables and the flow of the program are described by means of comment lines.

```

SUBROUTINE QUADS (NEL, ITYPE, NINT, THIC, YM, PR, XX, S, IOUT)          QUA00001
C . . . . . QUA00002
C . . . . . QUA00003
C . . . . . QUA00004
C . . . . . QUA00005
C .   P R O G R A M
C .   TO CALCULATE ISOPARAMETRIC QUADRILATERAL ELEMENT STIFFNESS . QUA00006
C .   MATRIX FOR AXISYMMETRIC, PLANE STRESS, AND PLANE STRAIN . QUA00007
C .   CONDITIONS . QUA00008
C . . . . . QUA00009
C .   - - INPUT VARIABLES - - . QUA00010
C .   NEL           = NUMBER OF ELEMENT . QUA00011
C .   ITYPE        = ELEMENT TYPE . QUA00012
C .               EQ.0 = AXISYMMETRIC . QUA00013
C .               EQ.1 = PLANE STRAIN . QUA00014
C .               EQ.2 = PLANE STRESS . QUA00015
C .   NINT         = GAUSS NUMERICAL INTEGRATION ORDER . QUA00016
C .   THIC        = THICKNESS OF ELEMENT . QUA00017
C .   YM          = YOUNG'S MODULUS . QUA00018
C .   PR          = POISSON'S RATIO . QUA00019
C .   XX(2,4)     = ELEMENT NODE COORDINATES . QUA00020
C .   S(8,8)      = STORAGE FOR STIFFNESS MATRIX . QUA00021
C .   IOUT        = UNIT NUMBER USED FOR OUTPUT . QUA00022
C . . . . . QUA00023

```

¹²Note that these elements should therefore not be used in practice (see Section 5.5.5).


```
C          C A L C U L A T E   E L E M E N T   S T I F F N E S S              QUA00092
C                                                                QUA00093
20 DO 30 I=1,8                                                    QUA00094
   DO 30 J=1,8                                                    QUA00095
30 S(I,J)=0.                                                       QUA00096
   IST=3                                                           QUA00097
   IF (ITYPE.EQ.0) IST=4                                          QUA00098
   DO 80 LX=1,NINT                                                QUA00099
   RI=XG(LX,NINT)                                                 QUA00100
   DO 80 LY=1,NINT                                                QUA00101
   SI=XG(LY,NINT)                                                 QUA00102
C                                                                QUA00103
C          E V A L U A T E   D E R I V A T I V E   O P E R A T O R   B   A N D   T H E   J A C O B I A N   D E T E R M I N A N T   D E T
C                                                                QUA00104
C          C A L L   S T D M   ( X X , B , D E T , R I , S I , X B A R , N E L , I T Y P E , I O U T )
C                                                                QUA00105
C                                                                QUA00106
C          A D D   C O N T R I B U T I O N   T O   E L E M E N T   S T I F F N E S S
C                                                                QUA00107
C                                                                QUA00108
C                                                                QUA00109
   IF (ITYPE.GT.0) XBAR=THIC                                       QUA00110
   WT=WGT(LX,NINT)*WGT(LY,NINT)*XBAR*DET                          QUA00111
   DO 70 J=1,8                                                     QUA00112
   DO 40 K=1,IST                                                   QUA00113
   DB(K)=0.0                                                       QUA00114
   DO 40 L=1,IST                                                  QUA00115
40 DB(K)=DB(K) + D(K,L)*B(L,J)                                     QUA00116
   DO 60 I=J,8                                                     QUA00117
   STIFF=0.0                                                       QUA00118
   DO 50 L=1,IST                                                  QUA00119
50 STIFF=STIFF + B(L,I)*DB(L)                                     QUA00120
60 S(I,J)=S(I,J) + STIFF*WT                                       QUA00121
70 CONTINUE                                                        QUA00122
80 CONTINUE                                                        QUA00123
C                                                                QUA00124
C          D O 90 J=1,8                                             QUA00125
   D O 90 I=J,8                                                    QUA00126
90 S(J,I)=S(I,J)                                                  QUA00127
C                                                                QUA00128
C          R E T U R N                                             QUA00129
C                                                                QUA00130
C          E N D                                                 QUA00131
C          S U B R O U T I N E   S T D M   ( X X , B , D E T , R , S , X B A R , N E L , I T Y P E , I O U T )
C                                                                QUA00132
C                                                                QUA00133
C . . . . . QUA00134
C . . . . . QUA00135
C . . . . . QUA00136
C . P R O G R A M . QUA00137
C .   T O   E V A L U A T E   T H E   S T R A I N - D I S P L A C E M E N T   T R A N S F O R M A T I O N   M A T R I X   B . QUA00137
C .   A T   P O I N T   ( R , S )   F O R   A   Q U A D R I L A T E R A L   E L E M E N T . QUA00138
C . . . . . QUA00139
C . . . . . QUA00140
C . . . . . QUA00141
C . . . . . QUA00142
C . . . . . QUA00143
C . . . . . QUA00144
C . . . . . QUA00145
C . . . . . QUA00146
C . . . . . QUA00147
C . . . . . QUA00148
C . . . . . QUA00149
C . . . . . QUA00150
C . . . . . QUA00151
C . . . . . QUA00152
C . . . . . QUA00153
C . . . . . QUA00154
C . . . . . QUA00155
C . . . . . QUA00156
C . . . . . QUA00157
C . . . . . QUA00158
C . . . . . QUA00159
C . . . . . QUA00160
C . . . . . QUA00161
C . . . . . QUA00162
C . . . . . QUA00163
C . . . . . QUA00163

C          I M P L I C I T   D O U B L E   P R E C I S I O N   ( A - H , O - Z )
C          D I M E N S I O N   X X ( 2 , 4 ) , B ( 4 , 8 ) , H ( 4 ) , P ( 2 , 4 ) , X J ( 2 , 2 ) , X J I ( 2 , 2 )

C          R P = 1.0 + R
C          S P = 1.0 + S
C          R M = 1.0 - R
C          S M = 1.0 - S

C          I N T E R P O L A T I O N   F U N C T I O N S

C          H ( 1 ) = 0.25* R P * S P
C          H ( 2 ) = 0.25* R M * S P
C          H ( 3 ) = 0.25* R M * S M
C          H ( 4 ) = 0.25* R P * S M

C          N A T U R A L   C O O R D I N A T E   D E R I V A T I V E S   O F   T H E   I N T E R P O L A T I O N   F U N C T I O N S

C          1.   W I T H   R E S P E C T   T O   R

C          P ( 1 , 1 ) = 0.25* S P
C          P ( 1 , 2 ) = - P ( 1 , 1 )
C          P ( 1 , 3 ) = - 0.25* S M
C          P ( 1 , 4 ) = - P ( 1 , 3 )
```

```

C          QUA00164
C          2. WITH RESPECT TO S          QUA00165
C          QUA00166
C          P(2,1) = 0.25* RP             QUA00167
C          P(2,2) = 0.25* RM             QUA00168
C          P(2,3) = - P(2,2)            QUA00169
C          P(2,4) = - P(2,1)            QUA00170
C          QUA00171
C          EVALUATE THE JACOBIAN MATRIX AT POINT (R,S) QUA00172
C          QUA00173
C          10 DO 30 I=1,2                 QUA00174
C          DO 30 J=1,2                     QUA00175
C          DUM = 0.0                       QUA00176
C          DO 20 K=1,4                     QUA00177
C          20 DUM=DUM + P(I,K)*XX(J,K)     QUA00178
C          30 XJ(I,J)=DUM                  QUA00179
C          QUA00180
C          COMPUTE THE DETERMINANT OF THE JACOBIAN MATRIX AT POINT (R,S) QUA00181
C          QUA00182
C          DET = XJ(1,1)* XJ(2,2) - XJ(2,1)* XJ(1,2) QUA00183
C          IF (DET.GT.0.00000001) GO TO 40 QUA00184
C          WRITE (IOUT,2000) NEL          QUA00185
C          GO TO 800                       QUA00186
C          QUA00187
C          COMPUTE INVERSE OF THE JACOBIAN MATRIX QUA00188
C          QUA00189
C          40 DUM=1./DET                   QUA00190
C          XJI(1,1) = XJ(2,2)* DUM        QUA00191
C          XJI(1,2) =-XJ(1,2)* DUM       QUA00192
C          XJI(2,1) =-XJ(2,1)* DUM       QUA00193
C          XJI(2,2) = XJ(1,1)* DUM       QUA00194
C          QUA00195
C          EVALUATE GLOBAL DERIVATIVE OPERATOR B QUA00196
C          QUA00197
C          K2=0                             QUA00198
C          DO 60 K=1,4                       QUA00199
C          K2=K2 + 2                          QUA00200
C          B(1,K2-1) = 0.                    QUA00201
C          B(1,K2 ) = 0.                      QUA00202
C          B(2,K2-1) = 0.                    QUA00203
C          B(2,K2 ) = 0.                      QUA00204
C          DO 50 I=1,2                         QUA00205
C          B(1,K2-1) = B(1,K2-1) + XJI(1,I) * P(I,K) QUA00206
C          50 B(2,K2 ) = B(2,K2 ) + XJI(2,I) * P(I,K) QUA00207
C          B(3,K2 ) = B(1,K2-1)              QUA00208
C          60 B(3,K2-1) = B(2,K2 )          QUA00209
C          QUA00210
C          IN CASE OF PLANE STRAIN OR PLANE STRESS ANALYSIS DO NOT INCLUDE QUA00211
C          THE NORMAL STRAIN COMPONENT      QUA00212
C          QUA00213
C          IF (ITYPE.GT.0) GO TO 900        QUA00214
C          QUA00215
C          COMPUTE THE RADIUS AT POINT (R,S) QUA00216
C          QUA00217
C          XBAR=0.0                           QUA00218
C          DO 70 K=1,4                         QUA00219
C          70 XBAR=XBAR + H(K)*XX(1,K)      QUA00220
C          QUA00221
C          EVALUATE THE HOOP STRAIN-DISPLACEMENT RELATION QUA00222
C          QUA00223
C          IF (XBAR.GT.0.00000001) GO TO 90 QUA00224
C          QUA00225
C          FOR THE CASE OF ZERO RADIUS EQUATE RADIAL TO HOOP STRAIN QUA00226
C          QUA00227
C          DO 80 K=1,8                         QUA00228
C          80 B(4,K)=B(1,K)                  QUA00229
C          GO TO 900                          QUA00230
C          QUA00231
C          NON-ZERO RADIUS                   QUA00232
C          QUA00233

```

```
90 DUM=1./XBAR      QUA00234
   K2=0             QUA00235
   DO 100 K=1,4     QUA00236
   K2=K2 + 2       QUA00237
   B(4,K2 ) = 0.   QUA00238
100 B(4,K2-1) = H(K)*DUM QUA00239
   GO TO 900       QUA00240
C                 QUA00241
800 STOP          QUA00242
900 RETURN        QUA00243
C                 QUA00244
2000 FORMAT (//,' *** ERROR *** ', QUA00245
1      ' ZERO OR NEGATIVE JACOBIAN DETERMINANT FOR ELEMENT (',I8,')') QUA00246
C                 QUA00247
   END            QUA00248
```